Study of star cluster populations in the Magellanic Clouds

A thesis

submitted for the degree of

Doctor of Philosophy

in

The Department of Physics,

Pondicherry University,

Puducherry - 605 014, India

by

Prasanta Kumar Nayak

Indian Institute of Astrophysics,

Bangalore - 560 034, India

August 2019

Study of star cluster populations in the Magellanic Clouds

Prasanta Kumar Nayak
Indian Institute of Astrophysics

Indian Institute of Astrophysics
Bangalore - 560 034, India

Title of the thesis	:	**Study of star cluster populations in the Magellanic Clouds**
Name of the author	:	**Prasanta Kumar Nayak**
Address	:	Indian Institute of Astrophysics II Block, Koramangala Bangalore - 560 034, India
Email	:	prasanta@iiap.res.in
Name of the supervisor	:	**Prof. Annapurni Subramaniam**
Address	:	Indian Institute of Astrophysics II Block, Koramangala Bangalore - 560 034, India
Email	:	purni@iiap.res.in

Declaration of Authorship

I hereby declare that the matter contained in this thesis is the result of the investigations carried out by me at the Indian Institute of Astrophysics, Bangalore, under the supervision of Prof. Annapurni Subramaniam. This work has not been submitted for the award of any other degree, diploma, associateship, fellowship, etc. of any other university or institute.

Signed: _____

Date: _____

Certificate

This is to certify that the thesis titled **'Study of star cluster populations in the Magellanic Clouds'** submitted to the Pondicherry University by Mr. Prasanta Kumar Nayak for the award of the degree of Doctor of Philosophy, is based on the results of the investigations carried out by him under my supervision and guidance, at the Indian Institute of Astrophysics. This thesis has not been submitted for the award of any other degree, diploma, associateship, fellowship, etc. of any other university or institute.

Signed:

Date:

List of Publications

1. **Nayak, P. K.**, Subramaniam, A., Choudhury, S., Indu, G. and Sagar, R., 2016, "Star clusters in the Magellanic Clouds - I. Parametrization and classification of 1072 clusters in the LMC", *Mon. Not. Roy. Astron. Soc.*, 463, 14461461. [arXiv:1608.06389]

2. **Nayak, P. K.**, Subramaniam, A., Choudhury, S. and Sagar, R., 2018, "Star clusters in the Magellanic Clouds. II. Age-dating, classification, and spatio-temporal distribution of the SMC clusters", *Astron. Astrophys.*, 616, A187. [arXiv:1804.00635]

3. **Nayak, P. K.** and Subramaniam, A., 2018, "Methods to identify Star Clusters in the Large Magellanic Cloud (LMC)", *Mapana Journal of Sciences*, Vol. 17, No. 1, page 57−73

Presentations

1. Poster presentation in the *Astronomical Society of India meeting 2016 (ASI:2016)* held at the University of Kashmir, Srinagar, Kashmir, India, during 10-13 May 2016.

2. Oral presentation in the international conference *Star Clusters: From Infancy to Teenagehood* held at Max-Planck Haus, Heidelberg, Germany, during 8-12 August 2016.

3. Oral presentation in the conference *Star and Planet Formation: Insights and Intricacies* held at IIST, Thiruvananthapuram, Kerala, India, during 5-7 December 2016.

4. Poster presentation in the *Astronomical Society of India meeting 2017 (ASI:2017)* held at B. M. Birla Auditorium, Jaipur, Rajasthan, India, during 6-10 March 2017.

Acknowledgements

My PhD research works could not have been carried out without the support of many people. I want to express my sincere gratitude to everyone who helped me to complete the work.

I am immensely thankful to Prof. Annapurni Subramaniam for her guidance, continuous support and encouragement. I have always been inspired by her enthusiasm and positive approach towards scientific problems. She has repeatedly helped me in academic, non-academic and personal problems throughout the stint of my PhD. I would like to thank Samyaday, Indu and Smitha help and guidance to carry out my research work. I extend my gratitude to Chayan, Sneha and Sindhu for helping me in learning astronomical tools and having engrossing scientific discussions. I also thank Paul KT, Blesson, Shruthi, Bryan, Koshy, Vikrant, Sharmila, Deepthi. I thank to all the project students worked under Prof. Annapurni. They helped me to understand basic physics and explore new frontiers. I am very much thankful to be part of such a big research group with variety of research work. I acknowledge all the discussions held in the weekly meetings. I am thankful to Prof. Ram Sagar for giving valuable comments on my thesis.

I wish to thank my collaborators Maria-Rosa L. Cioni and Cameron Bell for their valuable suggestions and inputs. I would also take this opportunity to thank my doctoral committee members Prof. R. T. Gangadhara, Prof. Aruna Goswami and Prof. KVP Lata for their help and suggestions.

I feel obliged to the Director, the Dean and the Board of Graduate Studies (BGS) for giving me the opportunity to work in this institute and providing all the facilities required for my research work. I thank to the librarian for helping me to access necessary books and journals. I would like to thank Dr. Baba Varghese, Ashok, Fayaz, Anish and other staffs of ′Data Center′ for their help in computer

and internet related issues. Many thanks to Administrative Officer, Personnel Officer, Accounts Officers and all other administrative staff for their timely help in the administrative related work. I thank the supervisors, cooks and other staff members of Bhaskara for taking care during my stay.

I am fortunate to have friends like Avrajit, Rubinur, Priyanka, Suman and Seniors like Samyaday and Sajal, who are always there to stand by with me. I am happy to thank my seniors Tanmoy, Sudip, Nancy, Susmitha, Honey, Abhijit, Vaibhav, Subham, Joice, Mayuresh, Prasanna S and Prasanna D for helping me in administrative as well as thesis related work. I wish to express my thanks to my colleages and juniors Amit, Anirban, Samrat, Dipanweeta, Tridib, Athira, Bhoomika, Deepak, Prerna, Panini, Priya, Raghubar, Ramya, Ritesh, Sandeep, Annu, Ambily, Anshu, Anwesh, Aritra, Ekta, Hemanth, Indrani, Joby, Jyothi, Mageshwaran, Megha, Nirmal, Partha, Pavana, Piyali, Mayuresh, Satabdwa, Sreekanth, Manoj, Varun, Deshmukh, Phanindra, Subhamay, Suman Saha, Sonith, Tanya, Kshama, Shejeela, Meenakshi, Keyuri, Abha, Brajesh, Kanhaiya, Asish Raj, Arun Surya, Avinash Surendran, Tanve, Rubel. I thank Rakesh and Avinash for helping me in learning programming languages. I am grateful to Eshita who helped me a lot in studying to pass the IIA entrance examination and interview to fullfill my dream of pursuing research in astrophysics.

I like to thank school teachers Mr. Ananta Metya, Mr. Biplob Bhattacharya, Mrs. Mallika Nayak for those wonderful classes at Nabin Manua I.C. High School. I also want to express my gratitude towards my school teacher Mr. Subrata Burai, who first introduced me to the beauty of the world of astronomy and kept me motivating to carry out research work in astrophysics. I thank my school friends Gopal, Abhijit, Samar, Sambhu, Kartik, Tapas, Tufan, Sisir, Moumita, Ashalata, Manideep, Sourav, Adwaitya, Bishnu Maji, Sanat, Bishnu for creating great memories.

I express my gratitude to the course work instructors Prof. Joseph Samuel, Prof. Seetha, Prof. Prabhavati Chingangbam, Prof Tarundeep Saini, Prof. U. S. Kamath, Prof. S. P. Rajaguru, Prof. Prateek Sharma, Prof. Avinash Despande, Prof. Biswajit Paul, Prof. Shreedhar, Prof. Shiv Shethi for teaching me the basics of astrophysics. I thank Sourav, Prasun, Varun and Harsha for their help during course work. I express my deepest gratitude to Prof. Ram Sagar for taking special classes at IIA and Kavalur, which played an indispensable role in understanding the basic as well as nuances of optical astronomy.

I thank Prof. Arup Roy, Prof. Satadal Bhattacharya, Prof. Rabindranath Sasmal, Prof. Upendranath Nandi, Jaydip Mitra, Jayeeta Chowdhury who taught physics in a lively and exciting manner during my B.Sc. in Scottish Church College. I also wish to thank the laboratory assistant Jagadish Da for helping me to learn the experiments. I would like to thank my B.Sc. friends Piyush, Alakesh, Soumi, Sudesna, Debolina, Emroj, Ayan, Biswawjit, Soumi Mullik, Rome, Saptaswa, Somnath Sarkar, Tuhin for their invaluable friendship.

I would like to thank Prof. Somnath Bharatdwaj, Prof. A.K. Singh and Prof. S.P. Khastagir for their excellent teaching during my M.Sc at IIT Kharagpur. I thank my M.Sc. project guide Prof. Prasanta Kumar Dutta, who helped me a lot in both academically and non-academically. I thank Srimanta, Avrajit, Sayan, Suvrakanti, Jagannath, Bappa, Krishna, Prantika, Arindam, Kousik, Alapan, Soumalya, Prahlad, Sourav, Arpita, Nabhanila, Sudeshna, Anish Aviram, Ghanashyam for the amazing time I spent with them.

At last but not the least, I would like to thank my parents, uncles, grandparents and other family members for their continuous support and blessings to pursue my research career. I am also grateful to my brother Susanta and sister Maduri for their love and affection.

Data usage

In this thesis work, we have used both ground and space based data obtained from various resources. I acknowledge data usage from different resources. I would like thank all the team members for making the data available.

Major part of the thesis work has been done using third phase archived data obtained from 1.3 m Warsaw telescope located at the Las Campanas Observatory, Chile, operated by the Carnegie Institute of Washington under the collaborative project, Optical Gravitational Lensing Experiment (OGLE) between the astronomers of Carnegie Institute of Washington and Polish astronomers. I thank the OGLE team for releasing the data in the public domain.

This thesis uses the data from the *AstroSat* mission of the Indian Space Research Organization (ISRO), archived at the Indian Space Science Data Centre (ISSDC) which is a result of collaboration between IIA, Bengaluru, IUCAA, Pune, TIFR, Mumbai, several centres of ISRO, and CSA.

We have used DAOphot catalogue (version V10.0) based on observations made with the NASA/ESA Hubble Space Telescope, and obtained from the Hubble Legacy Archive, which is a collaboration between the Space Telescope Science Institute (STScI/NASA), the Space Telescope European Coordinating Facility (ST-ECF/ESA) and the Canadian Astronomy Data Centre (CADC/NRC/CSA).

We have also made use the advantage of the space based large sky survey data obtained from Global Astrometric Interferometer for Astrophysics (*Gaia*). We used the catalogue available after second data released of *Gaia* mission (*Gaia*-DR2). This work has made use of data from the European Space Agency (ESA) mission

Gaia (`https://www.cosmos.esa.int/gaia`), processed by the *Gaia* Data Processing and Analysis Consortium (DPAC, `https://www.cosmos.esa.int/web/gaia/dpac/consortium`). Funding for the DPAC has been provided by national institutions, in particular the institutions participating in the *Gaia* Multilateral Agreement.

Ground based data from VISTA Magellanic Survey has also been used in the thesis. The observations were obtained with Visible and Infrared Survey Telescope for Astronomy (VISTA) at the Paranal Observatory under program ID 179.B-2003.

We thank the Cambridge Astronomy Survey Unit (CASU) and the Wide Field Astronomy Unit (WFAU) in Edinburgh for providing calibrated data products under the support of the Science and Technology Facility Council (STFC).

Dedicated to
my family

Abstract

The Magellanic Clouds (MCs), neighbouring galaxies to the Milky Way (MW), consist of a pair of irregular type of galaxies : Large Magellanic Cloud (LMC) and Small Magellanic Cloud (SMC). The recent proper motion study of MCs suggested that they are interacting with each other, as well as with the MW. The Magellanic Bridge connecting both Clouds and the Magellanic Stream are the witnesses to these interactions. The interactions between the MCs could have triggered star formation in both the galaxies, which can be confirmed by studying formation and evolution history of star clusters in the MCs. Proximity of MCs and their location at high galactic latitude enables us to resolve their individual populations as well as detect faint stellar populations within them using ground based telescopes under good seeing conditions. Though $\sim$4000 clusters in the MCs have been catalogued, studies suggest the catalogue is still incomplete. Therefore, it is necessary to age-date the identified clusters, including the less massive clusters, to understand the demographics of cluster formation and their correlation in the L&SMC.

In this study, we estimated parameters (age and reddening) of a large number of clusters to understand demographics of cluster formation and signatures of interactions using the Optical Gravitational Experiment III data. We developed a semi-automated method and parameterized more than 1200 clusters to produce two online catalogues. The new tool developed and implemented to characterize $\sim$ 1200 star clusters in the MCs will be useful to age-date the star cluster population when large survey data of MCs get published in the future. We also classified these clusters and grouped them into 5 groups, based on their mass and strength(total number of cluster members). In our sample, 90% of the SMC clusters and 80% of the LMC clusters studied here belong to the open cluster like population in our Galaxy, with mass $<$ 1700 $M_{\odot}$, suggesting similar population of clusters in these three galaxies. We found that both the clouds

have gone through a recent burst of cluster formation at $\sim$125 Myr ago. We suggest the most recent interaction between the Clouds around 100-250 Myr ago could have triggered the cluster formation. We find evidence for an outside to inside propagation of cluster formation in the LMC, whereas the cluster formation is found to propagate from South-West to North-east in the SMC. The bar region of the LMC is found to have formed clusters in the age range 60-250 Myr ago, suggesting that the LMC bar was active in the recent past. We estimated stellar mass function (MF) and total mass of 66 LMC clusters, as well as the cluster mass function in the LMC. The peak value of the slope, -2.26 ± 0.44 is similar to Salpeter's initial MF slope value (-2.35) for the Solar neighbourhood.

Recent studies reveal that, a good number of massive intermediate age ($\sim$ a few Gyr old) star clusters ($>$50%) in the LMC have multiple populations and/or extended main-sequence turn-off (MSTO) stars. These cannot be explained by photometric errors or stellar binarity, whereas age spread and effects due to stellar evolution, such as stellar rotation are the suggested possibilities. This topic has received a lot of attention in the recent years, where most of the studies were focused on star clusters in the LMC and in the optical wavelengths. Here we studied Kron 3, an intermediate age rich star cluster, located in the southern SMC. We used multi-wavelength data from ultraviolet (UV) to infrared to study the stellar population in Kron 3. We used the near-UV observations made using the UltraViolet Imaging Telescope (UVIT) on $AstroSat$ (the first Indian space observatory) for this study. The combined data from UVIT, HST, $Gaia$ and VISTA help us to derive the radius of the cluster and identify an extended red clump population in the field de-contaminated CMD. Analysis using three different methods suggest a large spread in metallicity among the red clump stars as the possible reason for the extended red clump population. Kron 3 is thus one of the younger clusters in the SMC to show multiple population and detailed high resolution spectroscopic studies are needed to confirm this result. This study demonstrated the advantage of superior resolution UVIT data in the near-UV pass-band in addressing metallicity differences among stars in a cluster.

Contents

List of Figures

List of Tables

Abbreviations

NASA	**N**ational **A**eronautics and **S**pace **A**dministration
NOAO	**N**ational **O**ptical **A**stronomy **O**bservatory
HST	**H**ubble **S**pace **T**elescope
UVIT	**U**ltra-**V**iolet **I**maging **T**elescope
OGLE	**O**ptical **G**ravitational **L**ensing **E**xperiment
VISTA	**V**isible and **I**nfrared **S**urvey **T**elescope for **A**stronomy
VMC	**V**ISTA **M**agellanic **S**urvey
Gaia	**G**lobal **A**strometric **I**nterferometer for **A**strophysics
APOD	**A**stronomy **P**icture **O**f the **D**ay
ESA	**E**uropean **S**pace **A**gency
CCD	**C**harge **C**oupled **D**evice
$M_\odot$	Solar **M**ass

Chapter 1

Introduction

The Magellanic Clouds (MCs) consist of a pair of galaxies that are visible from the Southern Hemisphere. The two galaxies are the Large Magellanic Cloud (LMC) and the Small Magellanic Cloud (SMC), which are located at a distance of $\sim$ 50 kpc (Saha *et al.* 2010) and 60 kpc (Storm *et al.* 2004) respectively. The LMC and SMC are smaller, and less massive as compared to our own Galaxy, with a stellar mass of $\sim 10^{10}$ $M_{\odot}$ and 10^{9} $M_{\odot}$ (van der Marel *et al.* 2009) respectively. Morphologically they are categorized as irregular type galaxies. The MCs are gas rich and metal poor (Z=0.008 (Piatti and Geisler 2013) for the LMC, and 0.004 (Piatti 2012c) for the SMC) as compared to the Milky Way (MW, Z=0.02), and have active star-forming regions. Their proximity and location at high galactic latitude enables us to resolve individual stars as well as to detect faint stellar populations within them. It is well known that the MCs are interacting with each other, as well as with the MW (Westerlund 1997). The interaction is supported by the presence of the Magellanic Bridge and the Magellanic Stream (Putman *et al.* 2003) which connect the two galaxies.

FIGURE 1.1: Figure shows the optical image of the LMC (left) and SMC (right). Image credit: APOD

The Clouds are characteristically different from the MW in terms of chemical composition, which has made the study of star clusters in the MCs popular in order to understand cluster formation and stellar evolution in low metallicity environments. Star clusters of various ages found in both the Clouds present themselves as tools to study stellar evolution of a large range of stellar mass, at different metallicities. The cluster formation history helps us to understand the star formation history in these galaxies. As the star as well as cluster formation could be triggered as a result of interactions, the cluster formation history helps us to trace the history of interaction between the Clouds and the Galaxy. There have been extensive studies of star clusters in the MCs such as Olszewski *et al.* (1991); Pietrzynski and Udalski (2000); Grocholski *et al.* (2006); Glatt *et al.* (2010); Palma *et al.* (2016). These studies have brought out not only the diversity of cluster population in the MCs, but also the importance of their studies to understand the fundamentals of stellar evolution.

The MCs are irregular low mass galaxies which provide very different dynamical environments, when compared to the spiral disk of the MW. Formation, evolution as well as survival of star clusters, all of which have strong dependency on the environment, are therefore important topics to be addressed. There does not exist a clear cut dichotomy between massive globular clusters and less massive open clusters in the MCs, as it does in our Galaxy. Due to their interaction among

themselves and with the MW, these two galaxies are subjected to tidal forces which influences the star and cluster formation. As systems like the MCs are numerous in distant clusters of galaxies, where study of spatially resolved stars is impossible, these two galaxies located in our backyard, thus provide a unique opportunity to study resolved stellar population of star clusters in dynamically diverse environments.

Recent studies show that, a good number of massive intermediate age ($\sim$ a few Gyr) star clusters (>50%) in the LMC have multiple populations and/or extended main-sequence turn-off stars. These cannot be explained by photometric errors or stellar binarity (e.g. Milone *et al.* (2009)), whereas spread in age and effects due to stellar evolution, such as stellar rotation are suggested as possible reasons. This topic has received a lot of attention in the recent years, where most of the studies were focused on star clusters in the LMC and in the optical wavelengths.

This is the era of large surveys, which are important in achieving multi-wavelength studies of stellar populations. A good number of survey data are available for the MCs and these are ideal databases to carry out systematic studies with large sky coverage. The *Gaia* DR2, which was released recently holds a lot of potential to study star clusters as well as stellar population in the MCs, along with the archival HST data for crowded regions. India recently launched its first space observatory, *AstroSat* in September 2015. The Ultraviolet Imaging Telescope (UVIT) is one of the instruments on-board the *AstroSat*. The UVIT has a resolution better than 1."5 in the near and far UV. UV is ideal to study hotter population in star clusters and helps in discriminating differences in chemical composition among the stars. We make use of the above mentioned data sets to conduct a comprehensive study of star clusters in the MCs.

1.1 Star clusters

Stars in a cluster are generally assumed to be born from the same material, at about same time and also located at the same distance. The sizes of star clusters range from a few pc to few tens of pc in diameter, very small compared to the distances to the clusters (> 100 pc). Also stars in a cluster are formed from a single molecular cloud in a time scale of a few million years. Hence the above assumption of all stars being coeval in a star cluster is very true for clusters with ages >100 Myr. In the case of very young clusters whose ages are less than 10 Myr, where formation time scale is comparable to the age of the clusters, the assumption of having same age will not be valid. The only parameter which differs between stars in a cluster is their stellar mass. All the stars in a cluster suffer from similar interstellar absorption and reddening due to co-location of stars at the same distance, which can be corrected to estimate their fundamental parameters such as luminosity and effective temperature (T_{eff}) of each and every star in a cluster. Star clusters are thus ideal tools to study the relative properties of stars within a cluster as a function of mass. Star clusters are thus ideal test beds to learn stellar evolution as well as to test the stellar evolutionary models.

Star clusters help us to understand the structure and evolution of the galaxies. Since characteristics of star clusters depend upon the environment of the host galaxy, study of star clusters helps us to understand star formation history (SFH), structure, formation and evolution of the host galaxy. Using star clusters, we also probe the structure, formation and the evolution of external galaxies using their integrated light, where it is very hard to resolve the individual stars. Star clusters are identified as localized enhancement in the density of stars compared to the surrounding field. Characteristics of star clusters mainly depend on the host galaxy. Shapley first separated the star clusters in our Galaxy in two categories globular clusters and galactic clusters, later named as open clusters. These are discussed below.

1.1.1 Globular clusters

The globular clusters (GCs) are densely packed collection of stars and appear as spherical. They are distributed spherically around the Galactic center, and are found in the Galactic bulge and halo. The orbits of GCs are roughly isotropically distributed. In the MW, most of the GCs are presumed to be formed at the time of formation of the galaxy. Hence they are relics of the environment present during the early stage of formation and evolution of the MW.

Stars within these clusters are old and belong to the Population II class. There are two populations of GCs present in the MW. Type I GCs consist of metal-rich stars (example Terzan 7) as high as about solar metallicity and type II consist of very metal poor stars (example ESO 280-SC06) compared to the Sun. The similar kind of populations of GCs are also observed in other distant galaxies, especially massive elliptical galaxies. In the Milky Way, the type I GCs are associated with the halo and the type II GCs with the bulge. Multiple phases of star formation, mergers of gas-rich galaxies and accretion of dwarf galaxies are though to be the possible reasons behind the sub-populations of GCs. GCs contain 10 to 100 thousand stars within a diameter of 50-100 pc having the stellar density of the order of 1000 per cubic parsec at the densest core and 0.5 per cubic parsec in less dense regions. Ages of these objects are about 10-13 billion years and hence the mass of individual stars present in them is less than a solar mass.

1.1.2 Open Clusters

Open clusters are moderately denser than the surrounding field. They are situated in the disk of the Galaxy and are part of the recent activities in the Galactic disk. Stars within these clusters belong to the population I class. The open clusters

have a very wide range of age, ranging from almost as old as the disk (a few Gyr) to a few million years, the age of the newly born star cluster from the molecular cloud. As the present day star formation happens mainly in the spiral arms, the very young star clusters are found in these regions, which help us to reveal the features of spiral arms of our Galaxy and give us a better picture of the spiral structure of the MW. These clusters contain 50-1000 stars, with mass ranging from intermediate to low mass, located within a diameter of about 5 pc. The number density is about 0.1-10 per cubic parsec.

Open clusters (OCs) are classified by Trumpler (1930) and Ruprecht (1966) based upon their appearance. Trumpler (1930) classified OCs depending upon their degree of central concentration of stars, luminosity range of the cluster members and number of cluster members present in them. Each classification is further divided into sub-classes and assigned by a number or a letter. First the clusters were divided into four groups (I-IV) based on density of stars at the center and whether the clusters are distinguishable from field or not. The group I indicates that the clusters are well detached from the field and having strong star density at the center. The clusters that fall under group IV do not show any density enhancement at the center and are difficult to differentiate from surrounding field population. These clusters can be called as probable cluster candidates. Each group is subdivided and designated as 1, 2 & 3 depending upon brightness of the cluster stars. Clusters with stars having almost equal apparent brightness fall under subclass 1, clusters consisting of stars having medium brightness range fall under subclass 2 and subclass 3 suggests that clusters are composed of both bright (a few) and faint stars. The further distinction between clusters are made according to the number of stars present in a cluster.

Trumpler used letters to indicate richness classification of clusters : p indicates poor clusters with stars less than 50, m stands for moderately rich clusters having 50-100 stars and r for rich clusters having more than 100 stars. Trumpler (1930)

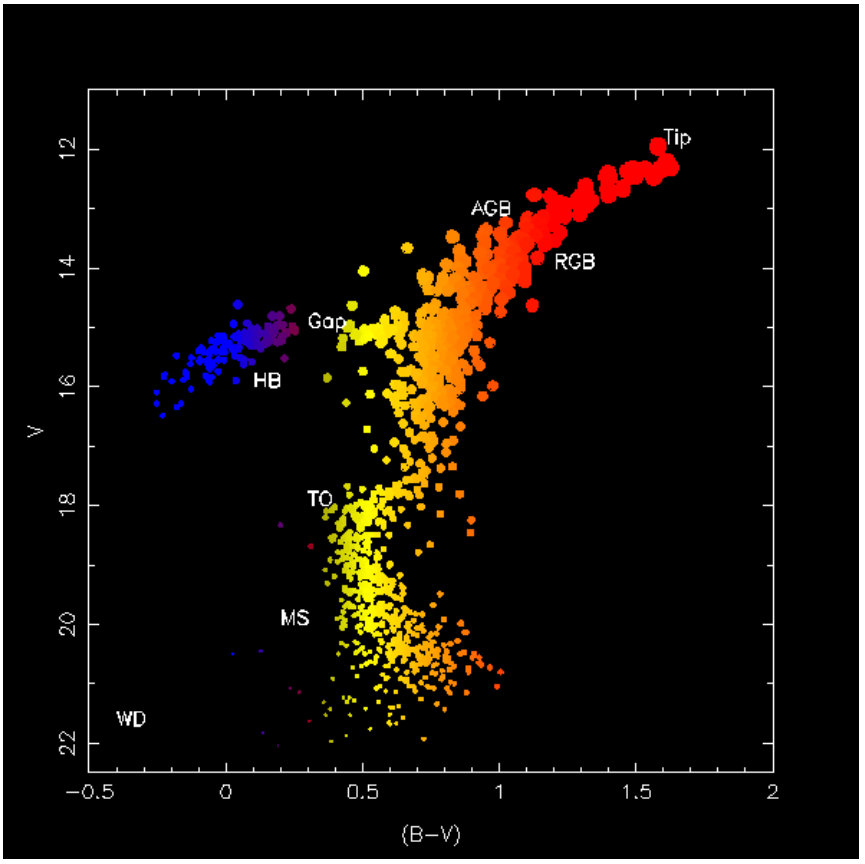

FIGURE 1.2: The plot shows the CMD of globular cluster M5. Different evolutionary sequence are also marked in the figure: main sequence (MS), turn-off (TO) in the MS, red giant branch (RGB), tip of the RGB, asymptotic giant branch (AGB), horizontal branch (HB), gap in the HB and white dwarf (WD). Image credit: http://community.dur.ac.uk

also found a considerable amount of differences in Hertzsprung-Russell (H-R) diagram of OCs. Some OCs do not show any signature of giant branch stars while some show equal extension of dwarf branch along the bluer or hotter side of color magnitude diagram. He divided the clusters into three groups and designated with number (1 to 3). 1 means giant branch stars are absent in the cluster color magnitude diagram (CMD) and only main sequence stars are present, 2 indicates that there are a small number of giant branch stars present in the cluster CMD, 3 signifies that most of the luminous stars of the cluster are in the giant branch. Such a detailed classification of OCs are done only for the MW. Thus it is very clear that the OCs in the MW have received a lot of attention over a long period. The online catalog of OCs along with other resources can be found in WEBDA.

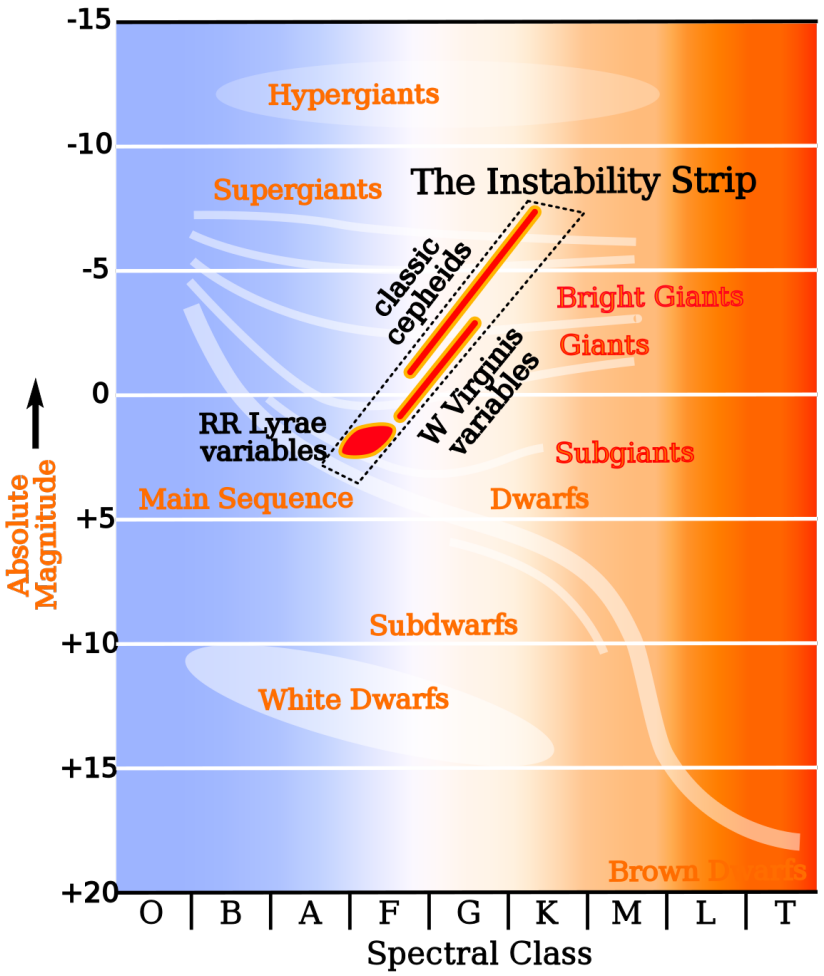

FIGURE 1.3: The plot shows locations of different types of variable stats in the HR diagram. Image credit: wikipedia

1.1.3 Star clusters in the MCs

If we look for a nearby galaxy, which can be used as a celestial laboratory to study the properties of star clusters as an extension to those in the MW, Magellanic Clouds (MCs) are the best option. The advantage of choosing the MCs is that we can resolve individual stars in a cluster even with ground based telescopes under good seeing conditions, which is not possible in the case of the other more distant neighbouring galaxies.

Study of rich and massive globular like star clusters in the MCs has been conducted

since early twentieth century. Shapley and Wilson (1925a,b) first cataloged position, angular diameter and integrated apparent magnitudes of star clusters in the MCs in the Bulletins of Harvard College observatory. The MCs are known to host mostly a class of populous star clusters, whose masses are typically an order of magnitude smaller than those of the average Galactic GCs ($10^{5.5}$ $M_{\odot}$), but an order of magnitude larger than those of most Galactic OCs (van den Bergh 1991). This class of clusters is not found in the Galaxy (Caldwell et al. 2009). Hence there is no clear cut distinction among the star clusters in the MCs like in our Galaxy. The massive clusters in the MCs are first characterized based on their (B-V) integrated color as blue ($0< (B-V) <0.3$) or red ($0.6< (B-V) <0.9$) clusters (Gascoigne and Kron 1952; Gascoigne 1965). The massive LMC clusters are almost equi-distributed in both red and blue types whereas the SMC clusters are mainly known to be red clusters (Gascoigne and Kron 1952; Gascoigne 1965; Bok 1966). The average color of Galactic GCs also falls in the red sequence.

There are only a few GCs present in the LMC (seven in the LMC and one in the SMC) which are older than 10 Gyr. The mean absolute magnitude of these clusters is found to be similar to that of GCs in M31 and our Galaxy. Recent studies suggest that MCs also host a lot of low mass clusters containing less number of cluster members, similar to Galactic OCs (Piatti 2012b, 2014; Palma *et al.* 2016; Choudhury *et al.* 2015). Therefore, the MCs contain three distinct types of clusters such as globular clusters, populous clusters and open clusters. The globular clusters are physically similar objects in the Galaxy and in the LMC. The populous and OCs can be put together such that the luminosity function (LF) of OCs extends to higher luminosities and masses to include the populous clusters.

Among the three types of clusters present in the MCs, the clusters that fall under the OC category are not well studied or unstudied due to lack of deep photometric data covering a large area of the sky. As low mass clusters are expected to be

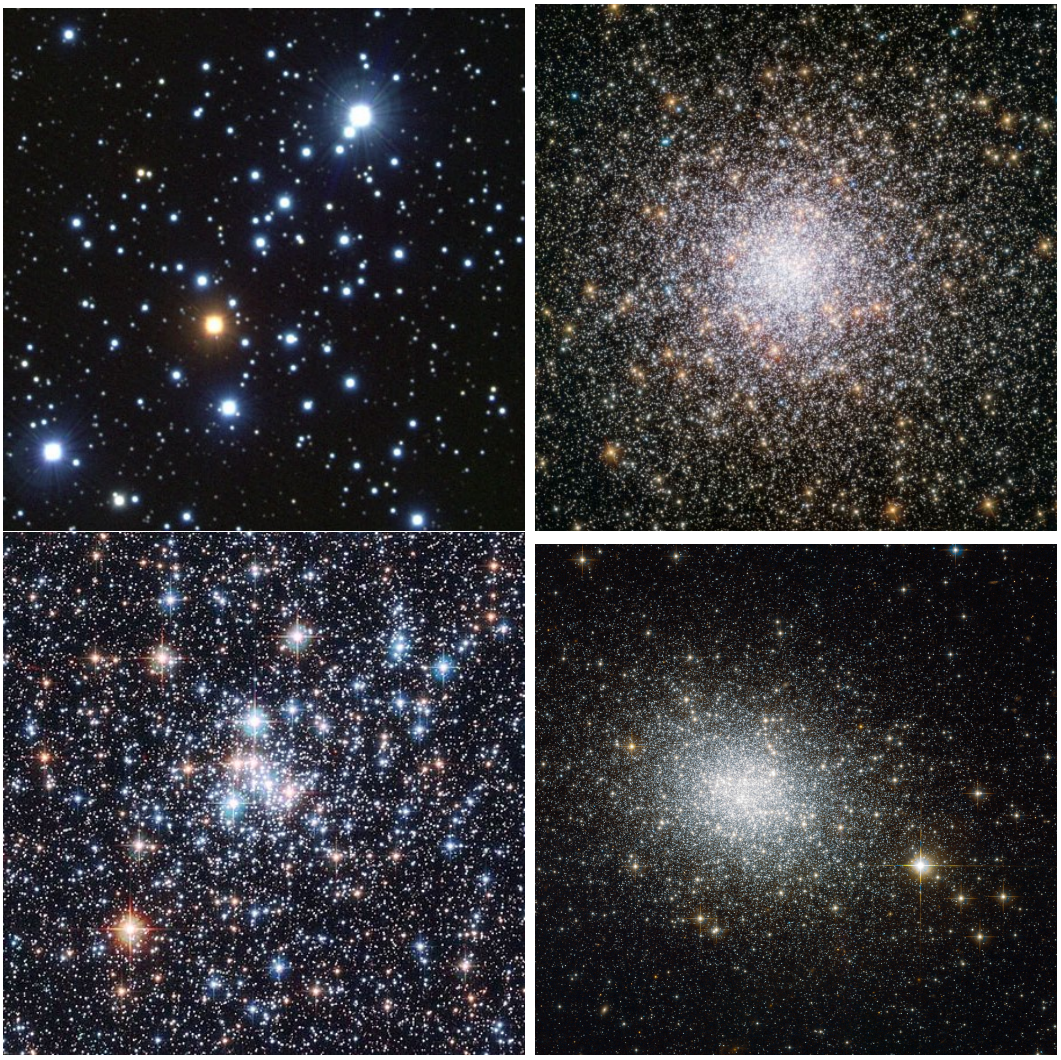

FIGURE 1.4: Figure represents color composite optical images of open and globular clusters in the MW (upper panels) and MCs (bottom panels), clearly shows the density variation of stars in different clusters.
Top left: Galactic OC M103 (NOAO/AURA), observed with KPNO ground based telescope, Top right: Galactic GC NGC362 (ESA/Hubble & NASA), bottom left: OC in the SMC, NGC290 (ESA/Hubble & NASA), bottom left: the only GC in the SMC, NGC121 (ESA/Hubble & NASA)

more than what is already catalogued (Bica *et al.* 2008), identifying and studying already catalogued clusters along with populous clusters is very important in order to understand formation and evolution of clusters in the MCs. The study of low mass clusters is also important to understand the stellar mass function, total mass of the clusters as well as to estimate the cluster mass function, which are all the byproducts of star formation. This will also help to understand the star and cluster formation history. The star clusters in the MCs are not yet classified in detail based on their richness. It is important to classify the clusters to address the details of cluster formation in the MCs and also to compare them with the OCs in the MW. As the star formation in the MCs are driven by the interactions, the age-dating of star clusters help to throw light on the details of recent interactions.

1.2 Recent interactions between MCs

It is a well established phenomenon that most of the massive galaxies have gone through multiple mergers with smaller galaxies at the early epochs. In the local universe, the MCs provide unique opportunity to study such an interaction between two dwarf galaxies among themselves and with our Galaxy. As the metallicities of the clouds are very low compared to Solar neighbourhood, the formation, evolution and interactions of these two galaxies resembles the scenario in the early epochs. The MCs appear well separated in the sky in optical images, whereas HI map shows that they are connected via a gaseous bridge (Kerr 1957; Hindman *et al.* 1963; Putman *et al.* 2003; Nidever *et al.* 2010), clearly indicating the interaction between them. Giant neutral hydrogen structures, known as the Magellanic Stream, the Magellanic Bridge and the Leading Arm, depict the Clouds interaction with each other and the Galaxy (Putman 2000).

HI Parkes All Sky Survey (HIPASS) provided a complete picture of MS and its

surroundings for the first time. Using HIPASS data, Putman *et al.* (2003) suggested that the MCs are bound systems and have completed orbital motion more than once. With the help of Green Bank Telescope (GBT), Nidever *et al.* (2010) reported that the MS is extended over $\sim 140^o$ in the sky and multiple bifurcation observed at the tip of the MS (Figure 1.5) could be due to the rotation of the LMC. The authors also estimated the age of the MS to be 2.5 Gyr and suggested that close interaction between the MCs could be the possible reason for the MS formation. In the Figure 1.5 we have shown a color composite image of the MCs, MS and the MW in radio and optical wavelength. The MW is represented as blue and white color in the middle of the image. The Galactic plane and the MCs (two bright patches below the MW plane) are labelled in the image. The dark shaded regions represent dust clouds in the MW. HI distribution in the MCs and MS is shown in red. The figure clearly shows that both the Clouds are connected via HI gas, which extends beyond the Clouds up to the MW galactic plane via close approach of southern pole. The extend of Leading Arm of the stream across the MW plane can be clearly seen in the HI distribution.

The VISTA survey of the Magellanic Clouds (VMC) has revealed many signatures of LMC-SMC interaction. A study based on the VMC data showed that the central region of the SMC has a bimodal distribution of red clump stars in the distance scale along the line of sight. The foreground population is located at a distance of $\sim 11.8 \pm 2.0$ kpc from the main body of the SMC (Subramanian *et al.* 2017). The authors explained the observed foreground population as due to the presence of tidally stripped stars from the SMC and/or the LMC. Nidever *et al.* (2013) reported that eastern region of the SMC has a larger line-of-sight depth ($\sim$23 kpc) compared to western side ($\sim$10 kpc). The authors also found that RC stars in the eastern part of the SMC showed a distance bimodality with a foreground component at 55 kpc. The authors suggested that the RC population at 55 kpc could be stripped from the SMC during recent interaction with the LMC and represented stellar counterpart of HI Bridge. A relatively large number of stars

with lower metallicity (lower than LMC) are found in the LMC, which resemble the giant population in the SMC (Olsen *et al.* 2011). RR Lyrae stars located in the eastern side of the SMC are found to be affected due to the interactions between the clouds, whereas they do not show any bimodal distribution in distance as noticed in the case of red clump stars (Muraveva *et al.* 2018). Muraveva *et al.* (2018) found an ellipsoidal distribution of RR Lyrae stars in the SMC. The authors reported that the SMC has a line-of-sight depth in the range 1-10 kpc, with an average depth of 4.3 $\pm$ 1.0 kpc. Ripepi *et al.* (2017) estimated age and metallicity of classical cepheids (CCs) in the SMC distributed over $\sim$40 square degree around the SMC center and found bimodal feature in the distribution of age. The age distribution shows peaks at 120 and 220 Myr. The metal-rich and young population of CCs are found to be more centrally located than the metal poor and old ones. Both old and young population exhibits off-centered structure, where the cause is attributed to the interaction between the clouds. The authors also observed that three-dimensional distribution of the CCs in the SMC is not planar but heavily elongated for more than 25-30 kpc approximately in the east/north-east towards south-west direction. The distribution of CCs also supports the existence of counter bridge (Ripepi *et al.* 2017). The distribution of red clump, RR Lyrae and classical cepheids in the SMC clearly suggest that the SMC has a large line-of-sight depth and the recent interactions between MCs probably the reason behind the observed depth.

Using 2MASS and WISE data, Bagheri *et al.* (2013) found a population of red giant branch (RGB) and asymptotic giant branch (AGB) stars in the MB with ages ranging from $\sim$400 Myr to 5 Gyr. This finding of old population clearly suggests that these stars are tidally stripped from the Clouds during the formation of the MB. The tidal effect which caused the formation of MB by stripping of gas and stars from the Clouds, also helped in-situ star formation in the Bridge (Harris 2007; Bica *et al.* 2015). Harris (2007) found that star formation of young population in Bridge near the SMC began $\sim$200-300 Myr ago and continued till 40 Myr ago.

Bica *et al.* (2015) studied 14 clusters in the Bridge region near the SMC and found that the age of the clusters ranges from a few Myr to 200 Myr.

There have been several advances in understanding the interaction between these three galaxies over the last decade. With the help of proper motion values of MCs, numerical models have been developed which are able to produce the observed features in the Magellanic system and predict the time scales of interactions between the Clouds. Diaz and Bekki (2012) suggested that MCs have undergone at least two pericentric passages about the MW during a $\sim$ 2 Gyr bound association. On the other hand, the recent high precision measurements of proper motion of the MCs using the Hubble Space Telescope (HST) data suggest that either the MCs are undergoing their first passage near to the MW (Kallivayalil *et al.* 2013) or they are orbiting with a long period ($>$ 6 Gyr) around the Galaxy (Besla *et al.* 2010). The new proper motion estimations suggest that the MCs have just passed their pericenter (45 kpc from the Galactic centre) with apocenter to pericenter ratio of 2.5:1 with an orbital period of 1.5 Gyr (Kallivayalil *et al.* 2006). Diaz and Bekki (2011, 2012) suggested that the SMC became a strongly interacting binary pair with the LMC only recently, suffering two strong tidal interactions $\sim$ 2 Gyr ago and $\sim$ 250 Myr ago. According to Besla *et al.* (2012), the SMC made close passages around the LMC at around 900 Myr and 100 Myr ago. These strong interactions between the MCs pulled out not only gas from the disc of the SMC, but also stars. The *Gaia* DR1 data revealed stellar tidal tails around both the Clouds and an almost continuous stellar bridge (Belokurov *et al.* 2017) connecting the two clouds. A significant number of Miras* were found in the east of the LMC by Deason *et al.* (2017) using *Gaia* DR1 data and they inferred that these are likely to be stripped from the SMC due to interaction with the LMC. As the simulations predict slightly different ages for the interaction between the Clouds and

*A class of pulsating variable stars characterized by very red colours with pulsation periods longer than 100 days and amplitudes greater than one magnitude in infrared and 2.5 magnitude at visual wavelengths. They are red giants in the very late stages of stellar evolution, on the asymptotic giant branch, that will expel their outer envelopes as planetary nebulae and become white dwarfs within a few million years.

FIGURE 1.5: Figure shows color composite image of Milky Way, Magellanic Clouds and Magellanic Stream in radio and optical. Blue and white patches in the middle of the image represent the Milky Way (MW) and two bright patches below the MW plane represent both the Clouds. Dust clouds in the MW are indicated as dark patches. The red color indicates the distribution of HI gas which connects both the Clouds is extended over a large region in the Magellanic Stream. The Leading Arm of the stream towards the MW is also clearly seen. Image credit : Nidever *et al.* (2010)

their signatures, it is important to obtain the above parameters from observations, such as star formation history.

1.3 Star formation history in the MCs

The close encounter between the MCs can trigger star formation in both the Clouds. Using Magellanic Clouds Photometric Survey (MCPS, Zaritsky *et al.* (2002, 2004)) data, Harris and Zaritsky (2004) showed that the burst of star formation happened at ages of 2.5, 0.4 and 0.06 Gyr in the SMC. The burst timescales more or less coincide with the two past encounters between the MCs. The peaks at 2.5 and 0.4 Gyr also coincide with the star formation peaks in the LMC (Harris and Zaritsky 2009). Any such triggered star formation can also lead to the formation of star clusters within a galaxy.

In the LMC, Glatt *et al.* (2010) (hereafter G10) found the cluster formation to peak at t= 125 and 800 Myr, whereas Pietrzynski and Udalski (2000) (hereafter PU00) found the cluster formation to peak at t= 7, 125 and 800 Myr. In the SMC, G10 found the age distribution of the clusters to have peaks at t= 160 Myr and 630 Myr, and they suggested that the interaction between the MCs resulted in the formation of these peaks. Pietrzynski and Udalski (1999) (hereafter PU99) studied mostly younger cluster (t <200 Myr) and found a peak of cluster formation at t= ∼20 Myr. Chiosi *et al.* (2006) found that the age distribution of clusters showed an enhancement between 15 and 90 Myr ago. The previous studies suggest that there is an increase in cluster formation happen in the last ∼100-150 Myr. This could be due to the recent interaction between the MCs aroound a few Myr ago as discussed in the above section. The difference in values of cluster formation peak proposed by previous authors could be due to various reasons. Pietrzynski and Udalski (1999, 2000); Chiosi *et al.* (2006) used OGLE II data for their studies, which cover only central bar region of both the Clouds. Glatt *et al.* (2010) used MCPS data, which cover the inner regions of both the clouds including the bar region. Though MCPS covered larger area than OGLE II, G10 did not take care of field star contamination within the cluster region in their study. Field star contamination can affect the result significantly in the case of clusters located in very crowded regions like in the bar region of the Clouds. Hence it is necessary to decontaminate the clusters from field stars for better estimation of their parameters and understand the cluster formation history in the MCs.

Though there are many attempt to estimate the age of clusters in order to investigate the cluster formation history, a large number of identified clusters located in the central region of MCs do not have age information. At the same time it is also required to cover larger region in both the Clouds and study the clusters to understand the cluster formation history and evolution of MCs.

The LMC has an off-centred bar that appears as an overdensity in young and

old stellar populations (Cioni *et al.* 2000; Nikolaev *et al.* 2004; Subramanian and Subramaniam 2013; van der Marel and Kallivayalil 2014; Zhao and Evans 2000; van der Marel 2001) as well as in the numerical simulations (Bekki 2009; Besla *et al.* 2012). Presently, there is no enhanced star formation in the bar, suggesting that it is not actively forming stars now. Using MACHO Cepheids data Alcock *et al.* (1999) found that there is a propagating star formation in the last 100 Myr, along the bar, from southeast to northwest. Recently, Jacyszyn-Dobrzeniecka *et al.* (2016) analyzed OGLE IV Classical Cepheids and found that the central part of the bar has the youngest Cepheids with relatively older Cepheids in the eastern and western parts. Piatti *et al.* (2015a) studied the VMC tiles in the central LMC and found that the outermost regions of the bar experienced star formation earlier and the central regions have younger clusters. The authors also found that the 30 Dor region is dominated by recent cluster formation. Therefore, a comprehensive age-dating of clusters in the bar as well as the inner LMC is necessary to map the demographics of cluster formation.

1.4 Multiple stellar populations in the MCs

Star clusters were known to be best examples of coeval systems and thought to follow simple stellar population models. Recent HST observations of Galactic GCs have changed our understanding of cluster formation. It is found that many GCs in the MW show extended main sequence or/and multiple evolutionary sequence in sub-giant and red giant branch (SGB & RGB), which can not be explained through photometric errors or binarity present in the clusters.

Using the B and I bands photometric data obtained from 2.2 m ESO-MPI telescope at La Silla (Chile), Pancino *et al.* (2000) showed the first ever photometric evidence of having multiple stellar population in the globular cluster w Centauri

(NGC5139). They noticed a metal rich ([Ca/H] > -0.3) anomalous branch (named as RGB-a) in the cluster CMD, well separated from the bulk of the RGB stars ($-0.4 >$ [Ca/H] > -1.0). Using HST/WFPC2 data D'Antona *et al.* (2005) discovered multiple stellar population in the globular cluster NGC 2808. They found that 20% main sequence stars appear bluer than expected. They suggested that these stars have enhanced helium compared to the majority of the main sequence stars. HST/ACS observations of NGC 2808 brought out the above evidence more clearly (Piotto *et al.* 2007). Three distinct main sequences are noticed, but single main sequence turn-off (MSTO) (Figure 1.6), explained by a spread in helium abundance for a single age (12.5 Gyr). Following this study, there are many studies which focus on massive GCs to understand multiple populations. Multiple sub-giant branches observed in NGC 1851, NGC 6388, NGC 6715, NGC 6656 and 47 Tuc indicates a likely age spread in these GCs (Milone *et al.* 2008; Anderson *et al.* 2009; Piotto 2009).

The studies of young (upto a few 100 Myr old) and intermediate age (a few Gyr old) Galactic open clusters using *Gaia*-DR2 data (Bastian *et al.* 2018; Cordoni *et al.* 2018; Marino *et al.* 2018; Lim *et al.* 2019; Sun *et al.* 2019; Li *et al.* 2019; Gossage *et al.* 2019) also show extended features in both MS and MSTO in the CMDs. Using spectroscopic studies of these extended MSTO stars, Bastian *et al.* (2018); Cordoni *et al.* (2018); Marino *et al.* (2018); Sun *et al.* (2019) suggest that the distribution of the projected rotational velocity of stars in the Galactic OCs play a major for getting extended MSTO in those OCs. The fast rotating stars appear in the redder side of the extended MSTO, whereas slow rotating stars appear in the bluer side due to limb darkening effect. Li *et al.* (2019) reported that variable stars, binary interactions are also the reasons along with stellar rotation for the extended MSTO morphology in the very young ($\sim$ 14 Myr) double clusters h and χ Persei (NGC 869 and NGC 884). Comparing the CMDs of 12 Galactic OCs with synthetic diagrams obtained from Geneva models, Cordoni *et al.* (2018) found that stars with coeval populations but difference in rotation rates are responsible for the

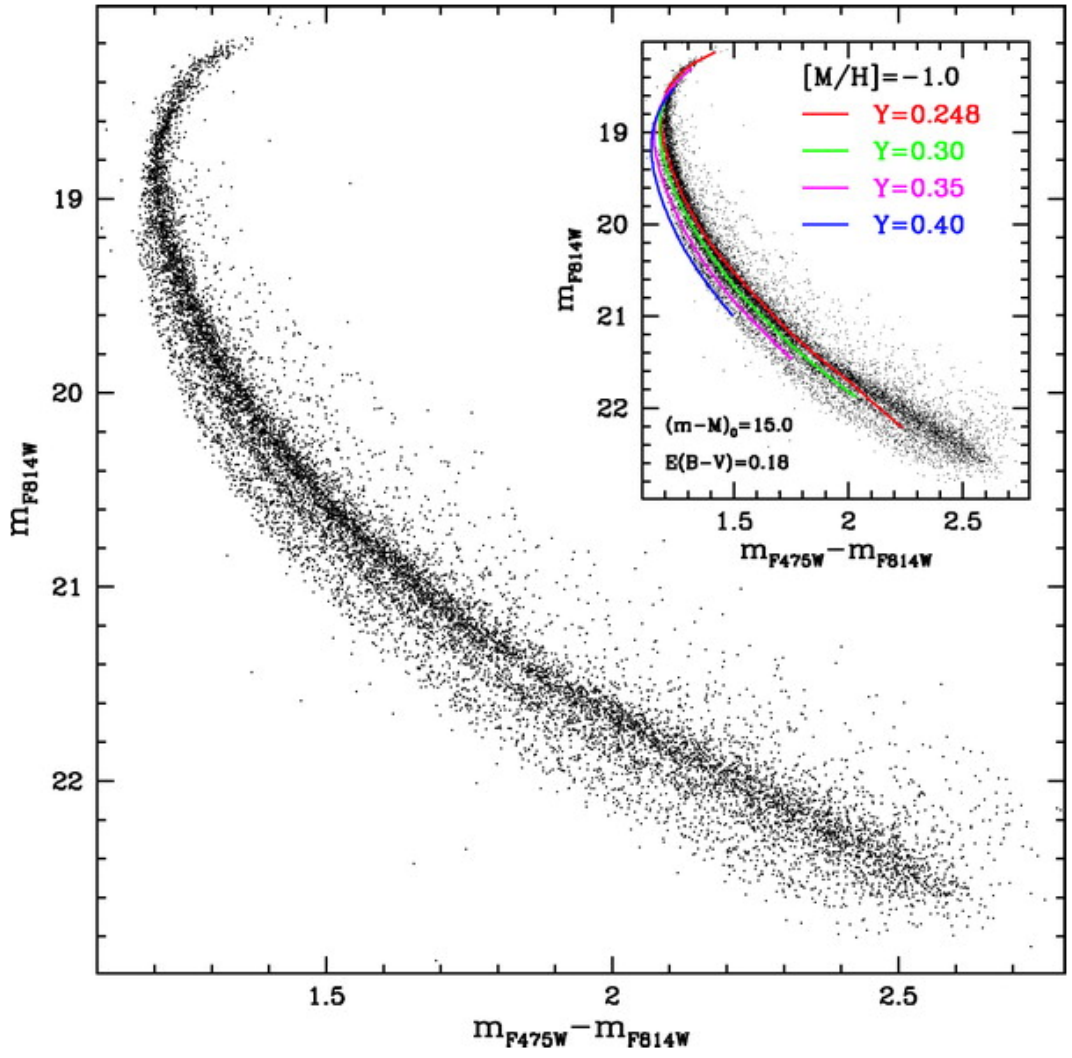

FIGURE 1.6: The figure shows the CMD of the MW globular cluster NGC 2808. All the stars are proper motion members of the cluster. The CMD clearly shows three distinct main sequences. Inset image shows that an isochrone of 12.5 Gyr age with different helium abundances (noted in the figure) fit the multiple main sequences, suggesting the presence of spread in helium abundance among stars within NGC 2808. Image is taken from Piotto *et al.* (2007)

extended MSTO and the broadened MS. Gossage *et al.* (2019) used MESA stellar models to simulate the observed extended MSTOs and found that distribution of stars' rotation rates alone can match the observed extended MSTO without incorporating the age spread.

Massive young to intermediate age clusters in the LMC have also been targeted to

study multiple populations in low metallicity environment. Mackey *et al.* (2008) studied three intermediate age LMC clusters which show split in the MSTO. They suggested that these clusters host at least two different population of same metallicity but with age difference ∼300 Myr. Milone *et al.* (2009) also found the existence of multiple stellar population in six intermediate age LMC clusters and proposed that those clusters have star formation time scale in between 150 to 250 Myr. Multiple stellar populations have also been observed in young LMC clusters (Milone *et al.* 2013, 2015, 2016, 2017). Recent study of thirteen young (∼40 to ∼1000 Myr) LMC clusters by Milone *et al.* (2008) confirmed the presence of extended MSTO in all the clusters. The clusters also exhibit two distinct main sequence populations (blue and red) for stars massive than ∼1.6 $M_{\odot}$. The blue MS represents the slowly rotating stars while red MS indicates stars are rotating with very high velocities, close to breakup velocity. Martocchia *et al.* (2018) observed a split in the SGB and RGB of an intermediate age (∼2 Gyr) LMC cluster NGC 1978.

NGC 121, the only globular cluster in the SMC also exhibits signatures of multiple populations. Using HST/WFC3 observation, Niederhofer *et al.* (2017b) found that the cluster hosts ∼32% (±3) chemically enriched stars (N rich, C poor). Three intermediate age SMC clusters with age between 6.0 to 7.5 Gyr are also found to host chemically enriched stars: Lindsay 1 (∼36%), NGC 416 (∼45%), NGC 339 (∼25%) (Niederhofer *et al.* 2017a). Previous studies suggest that the SMC clusters did not get much attention with respect to multiple population study. It is required to study more such star clusters in the SMC as SMC hosts a relatively large number of rich clusters in the age range 4-9 Gyr. It is well known that there is a paucity of clusters in the above age range in the LMC (van den Bergh 1991) and there are only a few poor clusters older than 4Gyr in our Galaxy.

1.5 Initial Mass Function

Stars are assumed to be born in groups from molecular clouds. Distribution of stars in mass at the time of their birth is assumed to follow a power law, called the initial mass function (IMF). The IMF can be defined as

$$dN/dM = AM^x \tag{1.1}$$

where dN represents the number of stars between the mass interval M to M+dM, A is constant, and x is defined as mass function slope. At the time of birth all the stars lie on the main sequence. The life time of a star mainly consists of the time it spends on the main sequence, as the time spent on the post-main sequence phases is very short. The life time of a star depends mainly on its mass. Estimation of star counts provides us the present day mass function (PDMF). To determine the mass function, one has to first construct an observed luminosity function from the star counts by calculating the frequency distribution of stars in different luminosity range. Then luminosity is converted to mass using standard mass-luminosity relation. There have been many attempts to estimate the stellar mass function (MF). The seminal study by Salpeter (1955) used field stars in the solar neighbourhood and estimated the MF slope value $x = -2.35$. The stars in the field are of different age and metallicities, and also suffer from large spatial variation, whereas, the study of IMF using star clusters has a great advantage. The stars in a cluster are of same age, metallicity and located at same distance. The IMF study in different types of star clusters helps us to investigate the IMF dependency on age, metallicity and surrounding environments. It also helps to identify variation in the IMF between clusters and field population and whether universal IMF does exist or not. For young star clusters where the formation time scale is less than the age of the clusters and dynamical relaxation time scale is more than the age of the clusters, mass function estimation using stars fainter than main sequence turn-off can be considered as the IMF. In the case of dynamically relaxed

clusters, with evidence of mass segregation, a large fraction of low mass mass stars could have escaped from the cluster. Another advantage of IMF study using stars clusters is that time dependent IMF assumption is not required unlike for the field stars. On the other hand one can use star clusters of different age to study the time dependency of PDMF.

To construct a MF from the LF of a cluster, the clusters has to be rich enough to populate the MS in a relatively large mass range. The young Galactic OCs contain less number of cluster members. The solution to this problem comes by combining the CMDs of multiple clusters and then construct the LF (Taff 1974; Piskunov 1977). Taff (1974) combined data from 62 clusters and found that slope value as $x = -2.8$ for the mass range 1-10 $M_{\odot}$. He also found similar IMF slope value for field stars within the above mentioned mass range. Piskunov (1977) combined 61 clusters to construct LF and determine the IMF. He found the IMF slope value as -2.3 for a larger mass range (1-25$M_{\odot}$). Burki (1977) combined the data of 27 clusters and estimated a range of IMF slope from -2.2 to -2.7. Kjeldsen and Frandsen (1991) estimated the IMF slope value as -2.3 by combining 8 clusters. Piskunov (1977); Kjeldsen and Frandsen (1991) obtained the IMF value very similar to the value provided by Salpeter (1955). The estimation of IMF has also been done using the LF of individual clusters (Sagar *et al.* 1986; Scalo 1986; Kumar *et al.* 2008). Sagar *et al.* (1986) studied 11 young open clusters and reported an average IMF slope value of -2.4 ± 0.3 for the mass range 1.25-60 $M_{\odot}$. Sagar *et al.* (1986) also did not find any significant variation in the slope value from cluster to cluster. Hence, the previous study suggest that the Galactic OCs mostly follow the IMF of field stars in the solar neighborhood proposed by Salpeter (1955). It will be interesting to check whether clusters in the MCs also follow the similar IMF or not.

The MCs are well known to host rich young star clusters which are more massive than galactic open clusters. Hence study of mass function using individual star

clusters in the MCs will put more constraint on IMF in low metallicity environments. The stars clusters in MCs also do not suffer from the galactic extinction due to their location at high galactic latitude. Both the Clouds also host intermediate age massive star clusters, which are yet to be dynamically relaxed. These clusters will help us to study cluster to cluster variation of IMF value and age dependency of IMF. The effect of LMC-SMC interaction on the IMF values can also be studied. The IMF study using star clusters in the MCs is not yet explored much. Kumar *et al.* (2008) investigated mass function of nine young clusters (age $<$ 100 Myr). One cluster out of nine shows flatter IMF slope value as $x = -1.23\pm0.27$, whereas other eight clusters showed almost similar slope values ranging from $x = -1.90\pm0.16$ to -2.28 ± 0.21 for the range in mass $\sim$2-12 $M_{\odot}$. The authors have also reported an average mass function slope value of $x = -2.22\pm0.16$ for 25 stellar systems in the LMC younger than 100 Myr for the stellar mass range $\sim$2-10 $M_{\odot}$. This study suggests that mainly star clusters younger than 100 Myr are focused for the study of MF and the MF values of these clusters are similar to Salpeter's IMF. Recently Schneider *et al.* (2018b,a) investigated star formation history of massive stars (>15 $M_{\odot}$) in the 30 Dor region and inferred that the IMF of those massive stars is shallower ($x = -1.9$) than a Salpeter's IMF. Study of mass function of populous star clusters for a large number of sample in both the Clouds with a wide range in ages and comparison with mass function of Galactic OCs will help us to understand the metallicity and age dependency of IMF and to put better constraints on theoretical prediction that IMF depends of environmental conditions (pressure and temperature) of star forming clouds (Larson 1998; Elmegreen 2000a).

1.6 Motivation and Aim of the study

The most recent and extensive catalogue of known clusters in the MCs is by Bica *et al.* (2008)(hereafter B08). However, the cluster sample, as mentioned by the authors, is still incomplete and a large number of poor clusters are yet to be identified. At the same time many clusters in the catalog are found to be asterisms (Choudhury *et al.* 2015). Most of the previous studies of star clusters in the MCs have targeted rich clusters which stand out from the field due to their high stellar density. Using CMDs Pietrzynski and Udalski (2000, 1999)(hereafter PU) studied about 693 clusters utilizing the OGLE II data, whereas Glatt *et al.* (2010)(hereafter G10) identified 1516 star clusters and estimated their ages utilizing the MCPS (Zaritsky *et al.* 2004) data. The studies suggest that only $\sim 50\%$ of the cataloged clusters by B08 have estimations of age and reddening. Recently many poor clusters are studied by Piatti (2011b, 2012b, 2014).

The proper motion study of MCs suggested that the SMC became a strongly interacting binary pair with the LMC only recently, suffering strong tidal interactions, a few 100 Myr ago (Diaz and Bekki 2011, 2012; Besla *et al.* 2012). These strong interactions between the MCs could have triggered star formation in both the galaxies, which can be confirmed by studying formation and evolution history of star clusters in the MCs. Therefore, it is necessary to identify the maximum number of star clusters, including the less massive clusters, to complete the catalog and age-date them, to map the demographics of cluster formation and their correlation in the L&SMC.

The ages and reddening of star clusters are generally estimated by a visual fitting of isochrones to the MSTO of cluster CMD. However, a visual fitting of isochrones to more than 100 clusters is not only a laborious task, but also produces inconsistently estimated parameters across the sample. Therefore, it is necessary to develop an automated method to estimate cluster parameters, so that we can not only

estimate the parameters accurately and consistently, but also quantify errors in them. There are many studies to understand the cluster mass function of star clusters (Kontizas *et al.* 1982, 1990; Searle *et al.* 1980; Hunter *et al.* 2003; Mackey and Gilmore 2003) in the MCs, but there has been no attempt to classify each star cluster and group them according to their mass/strength, so far, whereas the MW clusters are classified based on their richness. Classification is important and helps to compare the cluster properties across the three galaxies.

Aim of the study: The aim of this study can be divided into two parts,
1. A comprehensive and consistent estimation of parameters (age and reddening) of a large number of star clusters in the MCs to compare (a) the cluster formation, (b) cluster properties and (c) signatures of interaction.
2. Study of UV bright stellar population in a rich star cluster in the SMC using the UVIT-HST-*Gaia*-VISTA multi-wavelength data. This study helps to address the phenomenon of multiple populations observed in rich intermediate age star clusters in the MCs.

In order to meet the first aim of this study, we have to (1) increase the sample of well studied clusters and consistently estimate the parameters such as age and reddening of already identified star clusters of the MCs utilizing available photometric survey data, covering a large area of both Clouds, (2) develop a quantitative method to estimate cluster parameters and (3) classify clusters based on their richness/mass. We have done this analysis using the OGLE III data, where we study 1072 star clusters in the LMC and 169 star clusters in the SMC. We also estimated the stellar IMF of 66 moderately rich clusters in the LMC and compared with the estimated values for star clusters in the MW.

To address the second aim, we studied the star cluster Kron 3, in the southern SMC. Kron 3 is a well studied cluster in the optical wavelengths and we find

that the cluster is reported to have a large spread in age (Gascoigne and Kron 1952; Rich *et al.* 1984; Alcaino *et al.* 1996; Glatt *et al.* 2010) and reddening (Dias *et al.* 2010; Glatt *et al.* 2010). We aim to study, identify and characterize the stellar population in Kron 3 using UVIT-HST-*Gaia*-VISTA data. We focus on the following aspect of the cluster : (a) estimate the radius of the cluster (b) study the age and metallicity spread in the cluster using multi-wavelength data. In order to achieve the above aims, we combine our UV observations of this cluster using UVIT with HST observations (for the central regions of the cluster) and *Gaia* and VISTA observations (for the outer regions of the cluster). We obtained UVIT images of this rich intermediate age star cluster in the near and far-UV. We have taken advantage of the large field of view of the UVIT to study the outer regions of the cluster as well as to remove field star contamination, by combining it with the *Gaia* DR2 data.

1.7 Overview of the Thesis

- **Chapter 1:** We have introduced the Magellanic System, star clusters and their properties and characteristics relevant to the thesis. We have presented the motivation and aim the thesis.

- **Chapter 2:** The observations and multi-wavelength data used in this study are presented in this chapter.

- **Chapter 3:** In this chapter, we describe the methods used to estimate parameters (age, reddening and mass) of clusters in the MCs. We also present the classification scheme of the clusters in the MCs based on their masses.

- **Chapter 4:** We present the results obtained for the LMC clusters. We have compared estimated clusters parameters with previous estimation. We have studied the distribution of clusters as a function of age, reddening and

richness. We discuss propagation of cluster formation as a function of age and mass in the LMC.

- **Chapter 5:** We present the analysis of stellar mass function of 66 star clusters in the LMC along with their total mass. We also estimate the cluster mass function of the LMC.

- **Chapter 6:** We present the results obtained for the SMC clusters. We have compared estimated clusters parameters with previous estimation. We have studied the distribution of clusters as a function of age, reddening and richness. We have also studied cluster formation history and propagation of cluster formation in the SMC.

- **Chapter 7:** We present the analysis of UVIT-HST-*Gaia*-VISTA data for the intermediate age cluster Kron 3 in the SMC. We have estimated the age and metallicity spread present among the red clump stars in Kron 3.

- **Chapter 8:** We summarize the results of this study and conclude in this chapter. A few potential future projects are also presented here.

Chapter 2

Observations and data

2.1 Introduction

The MCs cover a large area in the sky, and hence it requires a large amount of observing time to obtain data covering the two galaxies. As we plan to study a large number of star clusters present in the LMC and SMC, it is important that the data and the analysis are homogeneous. It is therefore beneficial to use large area survey data with sufficient spatial resolution which covers the main body of the MCs. We thus use the ground based survey data for the first half of the study. On the other hand, the space observations have unbeatable resolution. Therefore, to study the evolved stellar population in a rich cluster in detail, we combine the ground and space observations to obtain multi-wavelength coverage as well as spatial coverage. Therefore, ground based as well as space based observations are used in this study. In this chapter, we briefly describe the data, observations and the facilities relevant to this study.

2.2 Optical Gravitational Lensing Experiment

The Optical Gravitational Lensing Experiment (OGLE) project started in 1992 with primary goals of searching for dark matter in our Galaxy using gravitational microlensing phenomena and study the Galactic structure. The first phase observation of the OGLE was carried out with 1-m Swope telescope at the Las Campanas Observatory, Chile, operated by Carnegie Institution of Washington, equipped with 2048×2048 Ford/Loral CCD camera and provided about 20 microlensing events in the Galaxy (Udalski *et al.* 1994; Wozniak and Szymanski 1998). Before starting the second phase of observation, a substantial amount of upgradation was made in the project by introducing new generation instruments and installing a dedicated 1.3-m Warsaw telescope at the Las Campanas Observatory to achieve the scientific goals of the OGLE project.

The second phase observation of OGLE II started in 1997 and the focus was not only the Galactic bulge but also the MCs. The OGLE II covered mainly the central bar region of the MCs (∼2.4 square degrees in the SMC and ∼5.7 square degrees in the LMC) and provided photometric and astrometric information of ∼ 2.2 million sources in the SMC (Udalski *et al.* 1998a) and ∼ 7 million sources in the LMC (Udalski *et al.* 2000) in B, V and I pass bands. The telescope was equipped with a first generation camera consisting of a SITe 2048×2048 CCD detector. The pixel size of the detector was 24 μm, which corresponds to 0.″417/pixel scale at the focal plane of the telescope. The red boxes in the Figure 2.1 and 2.2 represent the OGLE II observed field regions in the LMC and SMC respectively. Each field region (red box) covers around 14.′2×57.′0 in the sky plane, which represents the field of view of the mosaic CCD camera. The median seeing throughout the observation was 1.″25 for the SMC and 1.″3 for the LMC in I band.

In the third phase of the OGLE survey (OGLE III : 2001-2009) second generation mosaic camera (Udalski 2003) was used, consisting of eight SITe 2048 × 4096

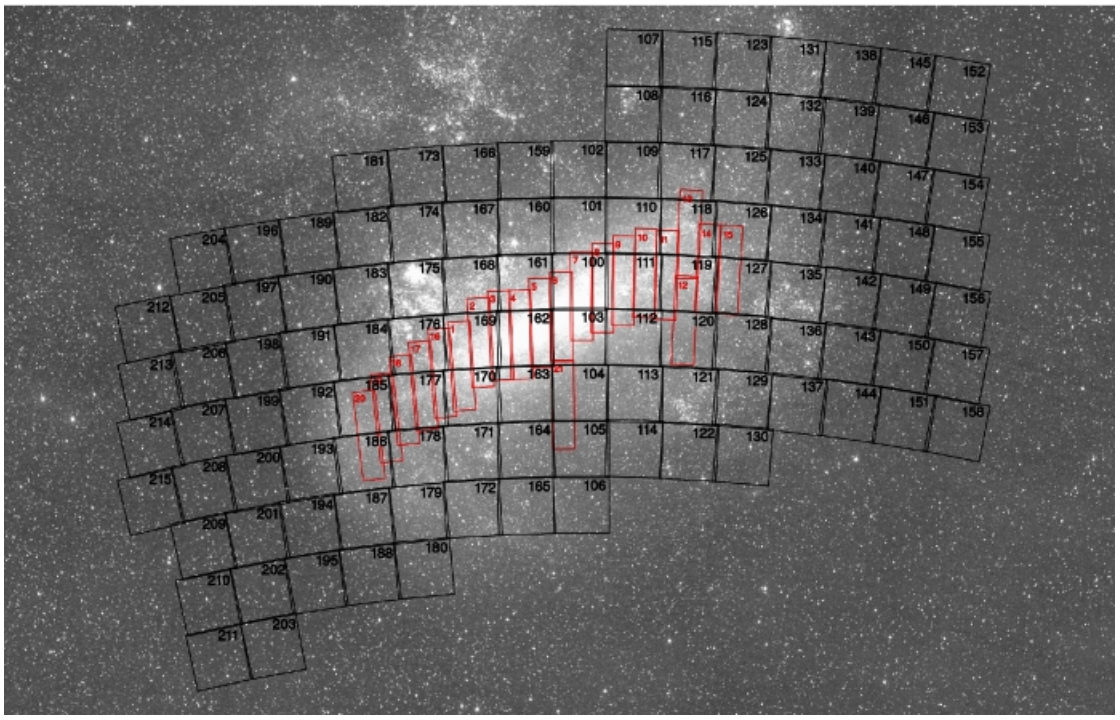

FIGURE 2.1: The figure shows the coverage of OGLE III (black boxes) in the LMC. The red boxes denote the regions covered by OGLE II, which suggests that OGLE II covered only the dense bar region.

CCD detectors with pixel size of 15 μm. Each pixel corresponds to 0.″26 at the focal plane of the telescope. The field of view of full mosaic was larger ($35' \times 35'$) than OGLE II survey. OGLE III covered a larger fraction of LMC, SMC and the Galactic bulge compared to OGLE II with better resolution. The OGLE III survey observed an area of about 40 square degrees around the LMC centre, and presented the V and I magnitudes of about 35 million stars in the LMC fields (Udalski *et al.* 2008a). For the SMC, the observations covered a total area of about 14 square degrees in the sky around the SMC center and produced a catalogue of V and I magnitudes of about 6.2 million stars (Udalski *et al.* 2008b).

The OGLE III data covers the central region of the LMC and the SMC (including the bar regions) but does not cover the northern star forming regions of the LMC. This data is therefore ideal to study the cluster formation in the central regions of both the MCs, particularly in the bars. This study is complementary to that of Glatt *et al.* (2010) (hereafter G10), where most of the clusters studied are located

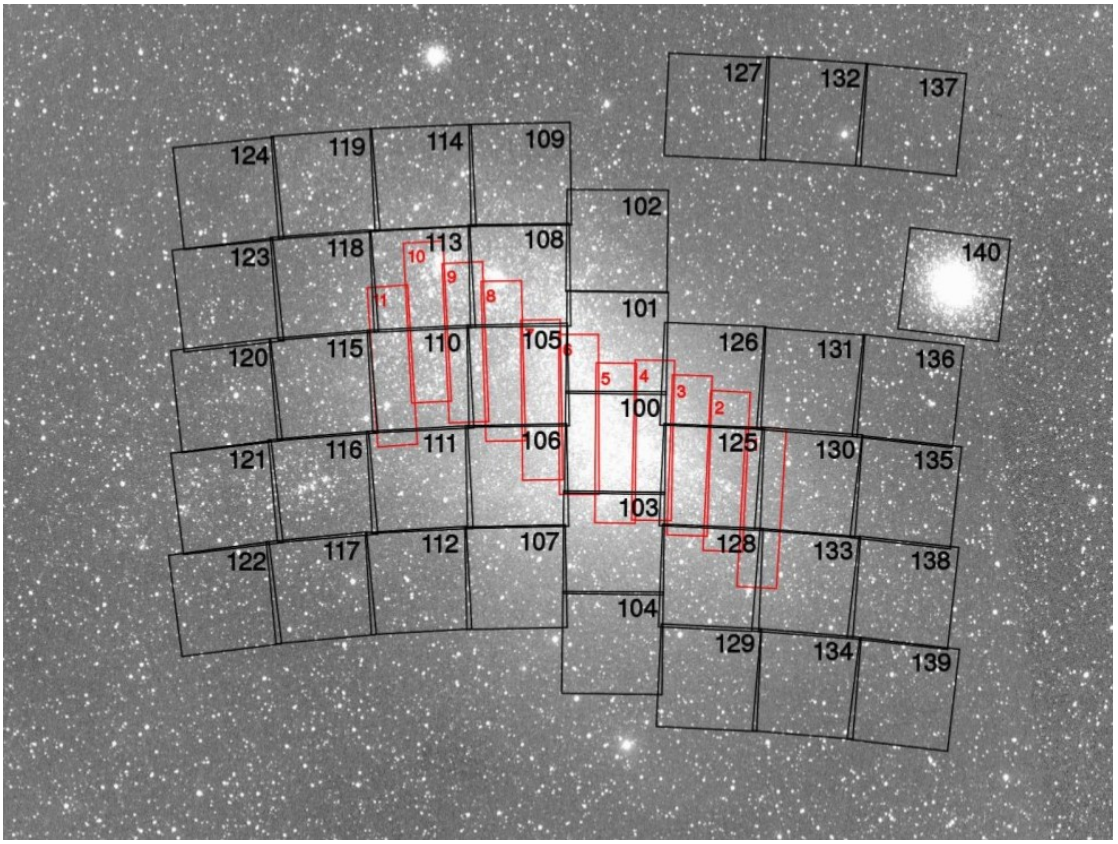

FIGURE 2.2: OGLE III coverage of the SMC is denoted by black boxes. The red boxes indicate the central region covered by OGLE II survey.

outside the bar regions. Pietrzynski and Udalski (2000) (hereafter PU00) used the OGLE II survey data and studied clusters located in the bar region of the LMC. Using OGLE II data, Pietrzynski and Udalski (1999) (hereafter PU99) and Chiosi *et al.* (2006) (hereafter C06) studied star clusters in the central bar region of the SMC. As the resolution of OGLE III data is better than the OGLE II data, a study based on OGLE III will be able to improve the estimates of PU00, particularly in the bar region which has maximum crowding. The OGLE III data is also useful to characterize young star clusters, with ages < 1 Gyr. This data will therefore be useful to detect the bursts of cluster formation, which are linked to the interaction between the LMC and the SMC.

In this study, we have estimated the parameters (age, reddening, mass and richness) of star clusters that can be affected by photometric incompleteness of the

data. Photometric incompleteness will lead us to a wrong determination of cluster richness. The LF of a cluster will also be biased due to photometric incompleteness and it will lead to a wrong estimation of mass function as well as total mass of the clusters. The method used here to estimate age and reddening of clusters will also be affected by photometric incompleteness as well as photometric error. Therefore, we have considered stars having photometric errors ≤ 0.15 mag in both V and I bands with photometric completeness more than 90% to construct LF. We used the entire data when it comes to plotting CMDs.

2.3 Ultra-Violet Imaging Telescope (UVIT)

India's first space based multi-wavelength observatory named *AstroSat* was launched successfully on 28 September 2015 by the Indian Space Research Organization (ISRO). There are five payloads on-board *AstroSat* including the Ultra Violet Imaging Telescope (UVIT). The other payloads are three Large Area X-ray Proportional Counters (LAXPCs), Cadmium-Zinc Telluride Imager (CZTI), Soft X-ray imaging Telescope (SXT) and Scanning Sky Monitor (SSM). The three X-ray payloads (CZTI, LAXPC and SXT) and UVIT are co-aligned to observe the flux and time variation of celestial sources simultaneously in the wavelength ranging from hard X-ray to near UV. The SSM is dedicated to search for X-ray transient events by scanning the sky.

The primary science goals of UVIT include the study of hot stars in stellar clusters, star formation in nearby galaxies, the history of star formation at higher redshift. UVIT is composed of two 38-cm telescopes with a field of view of $28'$ in diameter. One telescope is dedicated for observations in the FUV region (130-180 nm), while the other one is for NUV (200-300 nm) and visible regions (320-550 nm). Observations in both the telescopes take place simultaneously with a spatial

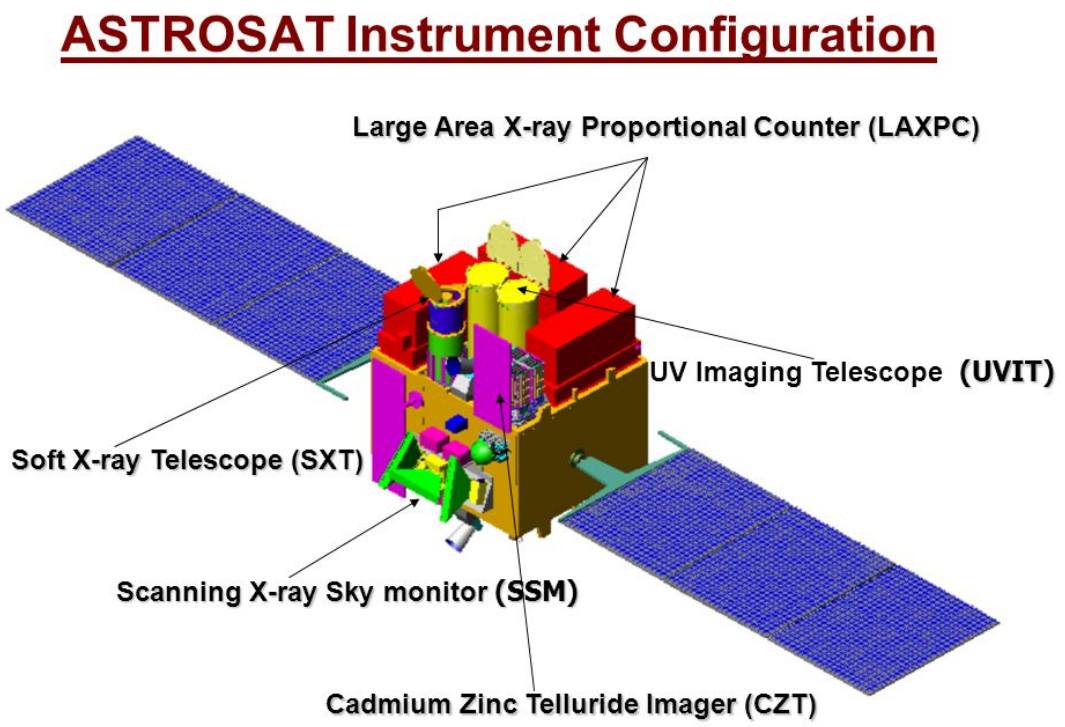

FIGURE 2.3: A schematic diagram of *AstroSat* satellite. Different payloads are marked in the figure.

resolution <1.″8, better than the resolution of GALEX ($\sim 5''$). Another advantage of the UVIT is that it has multiple filters for narrow ($\delta\lambda \sim 9$ nm) and medium ($\delta\lambda \sim 28$ nm) band imaging. Figure 2.4 shows the structure of the UVIT payload. The two tubes separated from each other hold the optical components and focal plane instruments. The cross-section of one of the tubes is presented to show the location of different components such as primary mirror, secondary mirror and detector. The doors work as a shield to protect mirrors from the sunlight. The cone integrates the two telescope and connects to the spacecraft. UVIT also has a facility for slit-less spectroscopy at low resolution (∼100) in both NUV and FUV bands. A 200 seconds exposure in FUV corresponds to a sensitivity of ∼20 magnitude (AB magnitude system).

The observations of Kron 3 were carried out with UVIT telescope in FUV and NUV

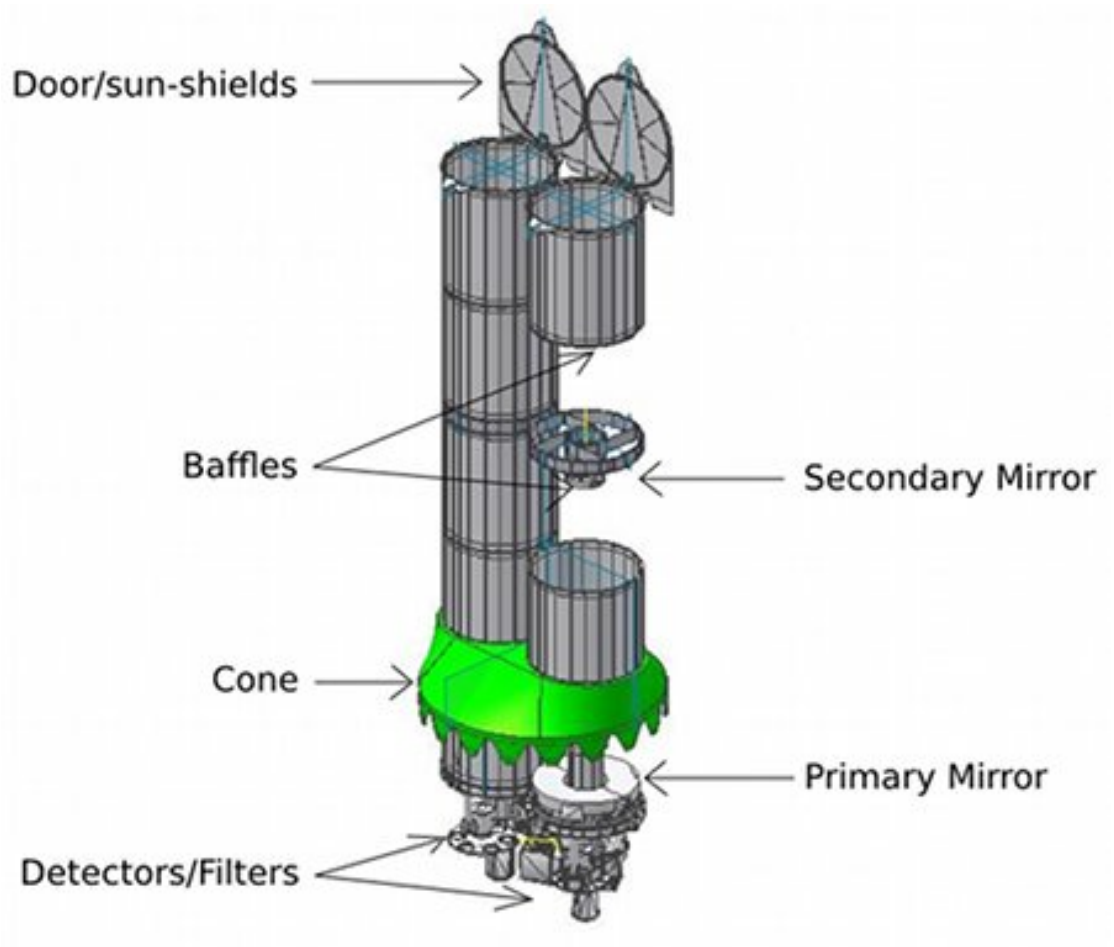

FIGURE 2.4: A schematic diagram of UVIT telescope.

bands as a part of GT proposal (G08) on 25th March 2018. Kron 3 was observed in one FUV (F148W : 125-175 nm) and one NUV (N242W : 203-281 nm) filters. The total exposure time was 7194 seconds. The observation was completed in multiple orbits. We applied corrections for spacecraft drift, flat-field and distortion, using the software CCDLAB (Postma and Leahy 2017) and created images for each orbit. Then the orbit-wise images are co-aligned and combined to generate science ready images. The science ready images were created for 4K×4K size with a scale of 0.4125″/pixel. The calibration of the instrument can be found in Tandon *et al.* (2017b). The details of the telescope and instrument are available in Tandon *et al.* (2017a); Subramaniam *et al.* (2016). Fig 2.5 shows a color composite image of the cluster Kron 3. Stars detected in NUV are color coded with yellow, while the FUV detected stars are color coded as blue.

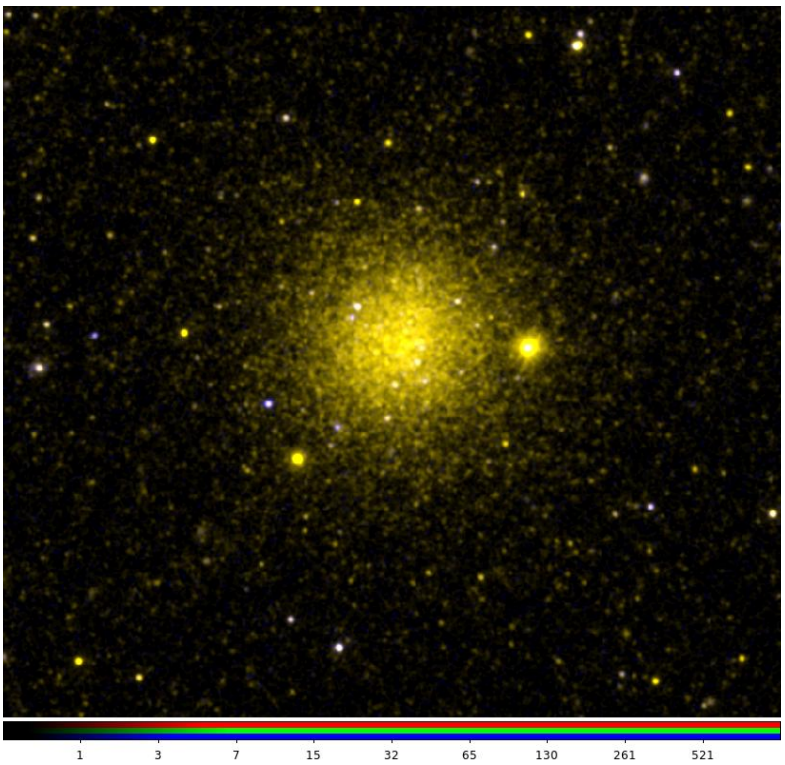

FIGURE 2.5: The colour composite image of the Kron 3 cluster. Yellow and blue colours correspond to stars detected in NUV and FUV bands.

2.3.1 UV photometry of Kron 3

Kron 3 was observed in one FUV (F148W) and NUV (F242W) band each, using UVIT. We need to convert the stars registered in the image to their equivalent magnitudes for further study. There are two stellar photometric methods to measure brightness of stars from an image. One is aperture photometry and other method is point spread function (PSF) fitting. The basic idea of aperture photometry is to first estimate the total brightness enclosed within a circular aperture around the star and then subtract the amount of brightness accumulated by sky background. The subtracted brightness will be the actual brightness of that star. The aperture photometry is later converted to magnitude in any standard system. The problem arises when stars are located in close proximity to each other and light of one star overlaps with the light of another. Even the brightness of faint

stars get affected by a neighboring bright star. Hence aperture photometry becomes inaccurate in images with a large number of stars located very close to one another, known as crowded fields.

Stars can be considered to be point source like objects due to their smaller angular dimension (< milli-arcsec) on the sky. The light of a point source gets spread out and becomes a circular patch in the focal plane, after convolving with optics of the telescope and the turbulence of Earth's atmosphere (for ground based telescopes). The basic idea of a PSF is that, as all stars in a image have similar intrinsic profile though they are different in brightness or amplitude, one can generate a standard profile for stars of an image and convolve with any star to get the brightness of that star after scaling with its amplitude. PSF fitting is useful for crowded regions as the best fit to star's profile can be achieved for central core pixels of the star's profile, which contains most of the flux of the star and then the function can be extrapolated to get the flux from star's wings. Therefore in the crowded region where the stellar profiles overlap with each other, we can still extract the flux of individual stars accurately.

The NUV image of Kron 3 suffers from crowding in the central region, whereas FUV image has only a few stars detected even in the central region and is not affected by crowding. Though crowding affects only NUV image, PSF photometry was performed on both the images of Kron 3 to estimate the magnitudes of stars. We first inspect the images and measured the FWHM of a typical star, mean sky intensity and the standard deviation of the sky. A mean value of the sky noise (σ) is calculated by taking the average of standard deviations. The values of FWHM and σ are used to find the candidate stars in the images. We putted a threshold for sky noise as 4σ to avoid the selection of random clumps which are brighter than average level of sky noise. Then we performed the aperture photometry with an aperture radius of four times the FWHM to get magnitudes of the detected candidate stars. We used the inner radius for the sky annulus as five times the

FWHM and width of the annulus as 3 times the FWHM.

Now to perform PSF photometry, first thing is to build a model PSF by averaging together several bright, isolated stars in the image. This task can be done in both interactive and non-interactive way. We used the non-interactive path and chose a set of isolated bright candidate stars based on their profile. The candidate stars are then combined and a Gaussian function is fitted to the core and bright part of the empirical bright stars to construct the model PSF. We considered the PSF radius as four times the FWHM to see the shape of the wings of the stars. We chose PSF fit radius equal to the FWHM. This is an optimum choice of radius in order to avoid from including much sky noise and enclose most of the signal from the star. For a very crowded region one can use fit radius less than the FWHM. It is a time consuming process with respect to interactive mode in order to find the candidate stars to generate the model PSF but more effective. In the interactive mode, the software will look for all the best possible stars that it can find and then we have to select candidate stars by looking into the profiles of these stars. In this mode, there is a possibility to miss some stars with good profile.

The next task is to apply the model PSF to all the stars detected in the aperture photometry. After estimating the psf magnitude (m_{psf}), we calculated the difference between the aperture and psf magnitude ($m_{app} - m_{psf}$) for the bright isolated stars and added the average of the differences to all the stars selected in the psf photometry in order to converted them to the aperture-photometry scale. Then we again performed aperture photometry on the isolated bright stars (used to calculate the model PSF) for multiple apertures up to six times the FWHM and analyse curve-of-growth to determine the fiducial aperture that contains all of the light of a star. We calculate the difference in magnitudes for the fiducial aperture and previously considered aperture for the isolated candidate stars and averaged up to get the aperture correction. We added the aperture correction value to the all the stars to determine the final magnitudes in the corresponding bands.

Photometric calibrations to calculate the zero-points magnitudes and unit conversion factors for all the FUV and NUV filters are done using a standard star HZ4, a moderately bright WD. The details about the calibration will be found in Tandon *et al.* (2017b). The adopted magnitude system for te UVIT filters is in AB system (Oke 1974) and therefore the derived magnitudes are in this system. The equations used to derive flux and magnitude of observed objects are:

$$Flux(ergs\ cm^{-2}\ s^{-1}\ \mathring{A}^{-1}) = CPS \times Unit\ Conversion \tag{2.1}$$

$$Magnitude(ABsystem) = -2.5\ log(CPS) + Zero\ Point \tag{2.2}$$

where CPS corresponds to observed, background-subtracted counts per sec with a filter, and unit conversion factor and zero-point magnitude are for the filter.

The zero-point of FUV (F148W) and NUV (N242W) bands are 18.003 and 19.81 mag, respectively. During both aperture and PSF photometry, we used zero point magnitudes for the corresponding bands to convert instrumental magnitude to standard magnitude system. We used DAOPhot/IRAF tasks and packages (Stetson 1987) to carry out all of the above tasks. The FWHM of the model PSF for FUV and NUV filters are 1.″65 and 1.″24 respectively.

2.4 Hubble Space Telescope (HST)

The history of the Hubble Space Telescope dates back to 1946, when the astronomer Lyman Spitzer published the famous paper "Astronomical advantages

of an extraterrestrial observatory". There are mainly two advantages of a space-based observatory over a ground-based one. Firstly, the primary factor affecting angular resolution (minimum separation at which the objects are clearly differentiable) would be diffraction instead of atmospheric turbulence, which causes the twinkling of stars also known as seeing in astronomy. The ground based telescopes are limited to resolutions $\sim 0.''5$ to $1.''0$, whereas the theoretical limit is $\sim 0.''05$ for a 2.5 m class telescope. The second advantage is that ultraviolet and infrared observations get hindered due to strong absorption by the Earth's atmosphere, which can be avoided in the space-based observations.

The Hubble Space Telescope (HST), named after the astronomer Edwin P. Hubble, was launched in April 24, 1990 from space shuttle Discovery (STS-31) and is still performing well. HST opened a new era in astrophysical studies. Unprecedented number of discoveries are made using HST observations. The telescope has a primary mirror with a diameter of 2.4m, with an angular resolution of $0.''05$/pixel in the visible wavelength. Hubble's four main instruments observe in the near ultraviolet, visible, and near infrared spectral regions. HST was designed in such a way that astronauts can visit the telescope in space to repair and replace old instruments with new generation instruments. The first Hubble Servicing Mission (HSM) was conducted in December 1993 for maintaining the telescope. The primary instrument Wide field Planetary Camera 1 (WFPC1) was replaced by WFPC2 in order to improve the telescope performance in the UV region. In addition to that the fault in the optics of HST's primary mirror was corrected and new generation advanced detectors were installed. In the second HSM (February 1997), two new instruments, the Space Telescope Imaging Spectrograph (STIS) and the Near Infrared Camera and Multi-Object Spectrometer (NICMOS) were installed. The main science goal of STIS was to study the dynamics of gas and stars around the centers of galaxies to confirm the presence of massive black holes. The NICMOS has both the facility of imaging and spectroscopic observations in the wavelength range 0.8 to 2.5 μm.

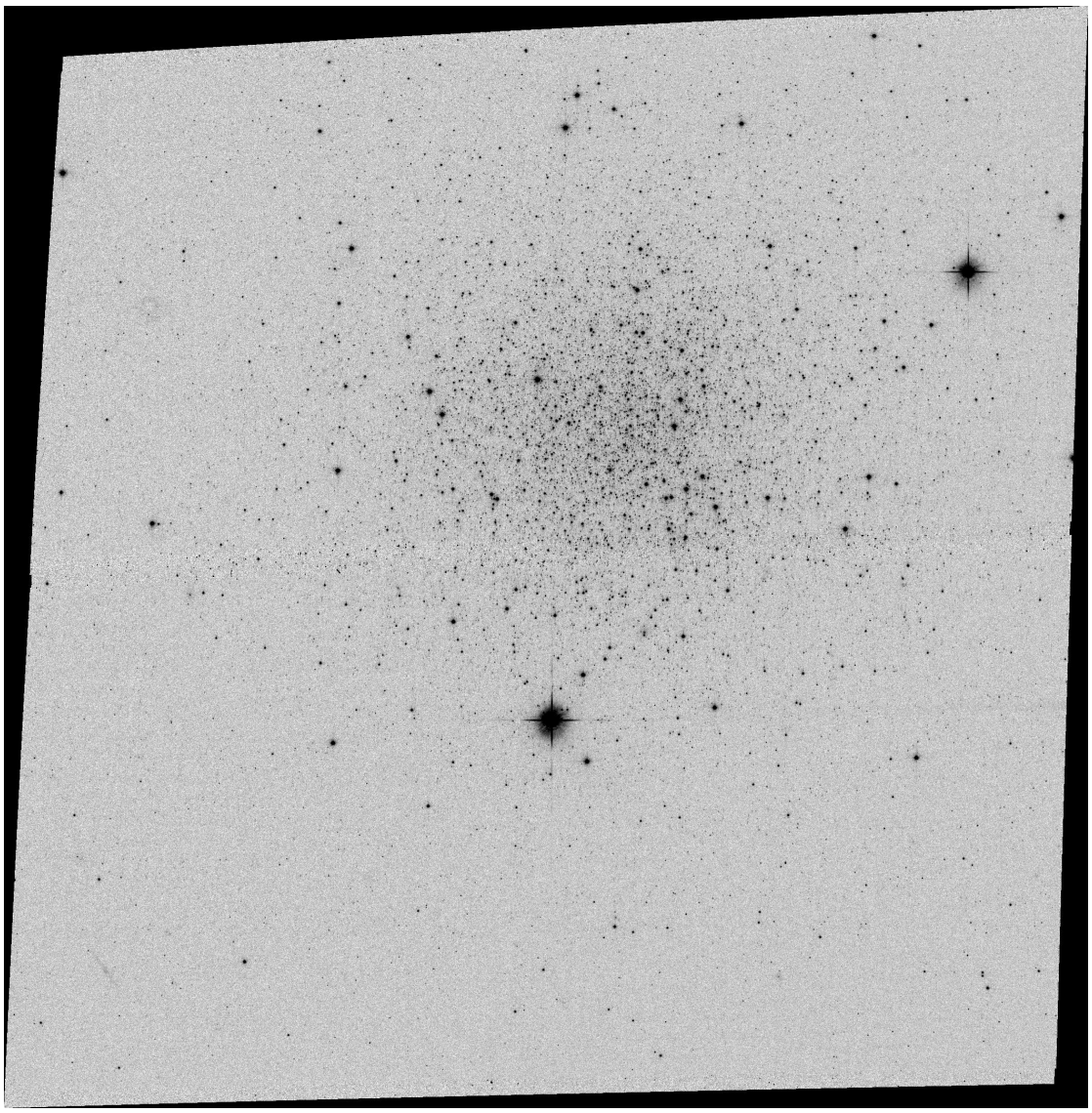

FIGURE 2.6: Figure shows the HST image of Kron 3 observed in F555W filter.

In 2002, astronauts installed the Advanced Camera for Surveys (ACS) which has a wide field of view and capability to generate better image quality than the replaced one. There were three independent channels present in the ACS: Wide Field Channel (WFC), High-Resolution Channel (HRC) and Solar Blind Channel (SBC). Each channel is designed for specific science goals, optimized in different wavelength range. The most exploited channel is ACS/WFC, equipped with two 2048×4096 CCD detector with a pixel size of 15μm. Each pixel corresponds to 0.″05 on the sky plane. The field of view (FoV) of the ACS/WFC detector is $\sim 200'' \times 200''$. The WFC detector is optimized in the visible range (350-1100

nm). The ACS/HRC provided a smaller FoV ($26'' \times 29''$) compared to ACS/WFC but better spatial resolution ($0.''025$/pixel). The ACS/HRC observed in the spectral range of 190-1100 nm. With the ACS/HRC, the inner regions of galaxies are imaged and studied in extreme details. The last and final HSM took place during 2009 and gave a new life to the HST. The STIS and ACS stopped working and got their new life during last visit to the HST, though ACS/HRC remains inactive due to electrical fault. Also, WFPC2 was replaced with the new generation powerful imaging instrument Wide Field Camera 3 (WFC3), setting a new limit to the observing capabilities of the HST into deeper universe. WFC3 acts as a complementary instrument to the ACS/WFC, puts new constraints to the wavelength range from ultraviolet to infrared, whereas the ACS/WFC is mostly active in visible range (blue to red).

In this study we have used archival DAOPhot photometric catalogue (version V10.0 *) of Kron 3, obtained from Hubble Legacy Archive (HLA). The observations were made on 17th January, 2006 with the NASA/ESA Hubble Space Telescope in the F555W and F814W filters using ACS/WFC detector. Total exposure time was 2024 seconds. The images covered an area of $200'' \times 200''$ in the sky plane with a pixel resolution of $\sim 0.''05$. The photometric reductions were performed on DRIZZLed images using DAOPhot package in the IRAF software for two apertures ($0.''05$ and $0.''15$). All the stars detected in the above task are designated as whether its a stellar/extended source or a hot pixel based on concentration index (defined as difference in magnitudes for two apertures). The stars are also assigned with different flag values based upon stellar/extended source, poor photometry (multi-pixel saturation), false detection, bleeding sources, cosmic rays etc. In our study, we considered only stellar sources, flagged as 0 with magnitude estimation done with $0.''15$ aperture. As we excluded extended sources in our analysis, we missed some RGB and AGB stars.

*Based on observations made with the NASA/ESA Hubble Space Telescope, and obtained from the Hubble Legacy Archive, which is a collaboration between the Space Telescope Science Institute (STScI/NASA), the Space Telescope European Coordinating Facility (ST-ECF/ESA) and the Canadian Astronomy Data Centre (CADC/NRC/CSA).

2.5 Global Astrometric Interferometer for Astrophysics (*Gaia*)

Gaia is a space observatory, launched in December 2013 by European Space Agency, operates in the Sun-Earth L2 Lagrangian point. The telescope is mainly designed to measure the position, distances and space motions of more than one billion stars in our Galaxy and throughout the Local Group, and create a 3D map of our Galaxy. The aim of the *Gaia* mission is to untangle the dynamical evolution of our Galaxy. *Gaia* has a resolution of 0.″1 on the sky plane. *Gaia* consists of two identical telescopes separated by 106° viewing angle. Field of view of both the telescopes is 0.32 deg^2. Primary mirrors have an area of 1.7×0.7 m^2. *Gaia* has three optical photometric pass bands : G (330-1050 nm), G_{bp} (330-680 nm) and G_{rp} (640-1050 nm). Second Phase of *Gaia* data was released on 25th April, 2018. It provides astrometry of stars brighter than 20 magnitude in G with an accuracy of 26 μarcsec at G=15 magnitude and 600 μarcsec at G=20. The accuracy in radial velocity is 15 km/s at G_{RVS} <16 magnitude. *Gaia* is designed for continuous scanning of the sky in two simultaneous fields of view along great circles.

The Gaia DR2 catalogue is essentially complete between G magnitude 12 and 17. The sources brighter than 7 mag in G band are still incomplete and the incompleteness in the fainter limit (G>19 mag) depends on celestial position of the sources. In dense areas on the sky (above some 400,000 stars per square degree) the magnitude limit of Gaia DR2 is as bright as G=18. Near very bright sources, in crowded regions, and at the faint end (G>19) of the survey, the photometric measurements in G_{bp} and G_{rp} bands suffer from an insufficiently accurate background estimation and from the lack of specific treatment of blending and decontamination from nearby sources. Parallax uncertainties are in the range of up to 0.04 milli-arcsecond (mas) for sources at G < 15, around 0.1 mas for sources with G=17 and at the faint end, the uncertainty is of the order of 0.7 mas at G =

20. The corresponding uncertainties in the respective proper motion components are up to 0.06 mas yr^{-1} (for G ¡ 15 mag), 0.2 mas yr^{-1} (for G = 17 mag) and 1.2 mas yr^{-1} (for G = 20 mag). The effective angular resolution of the survey has improved with respect to DR1 and is about 0.4 arcsec.

Gaia data release 2 (DR2) data was used for a detailed study of the star cluster Kron 3 in the SMC. We used stars detected within a radius of 15 arcmin from the cluster center, in order to isolate the cluster members from the field stars present in the cluster region.

2.6 Visible and Infrared Survey Telescope for Astronomy (VISTA)

Visible and Infrared Survey Telescope for Astronomy (VISTA) is a 4.1-m telescope, dedicated for observing the sky in the near infrared domain, located at Paranal Observatory, Chile. VISTA Magellanic Clouds (VMC) Survey, one of the six surveys started in November 2009 with the primary aim of studying star clusters and star formation history of the Magellanic System (MS), explore the 3-D structure using variable stars i.e. RR Lyrae and classical Cepheids. The survey also aimed to study the proper motion of the MS to disentangle the interaction history among the MCs by combining the data with 2MASS, which will provide ∼15 years of time baseline data to improve proper motion estimation. The survey has already achieved most of the science goals. The total area covered by the VMC survey is 170 sq. deg, which includes the LMC (105 sq. deg.), SMC (42 sq. deg.), Magellanic Bridge (21 sq. deg.) and a small part of the Magellanic Stream (3 sq. deg.). The full coverage of the survey is shown in the Figure 2.7 with blue rectangles. The LMC region is covered with 68 tiles, whereas 27 tiles are required to cover SMC region and 13 for the Bridge. Only three tiles have been

used to observe a small region in the Stream. Each tile of the VMC corresponds to 1.5×1.18 sq deg in the sky plane. The tiles overlap with each other in both horizontal and vertical direction by 0.016 and 0.1 deg respectively. The VISTA infrared camera VIRCAM (Emerson *et al.* 2006; Dalton *et al.* 2006) is equipped with 16 detectors, placed in 4 × 4 array. Each detector consists of 2048 × 2048 pixels with a pixel size of 0.″34. The photometric calibration of data taken with the VIRCAM instrument in the broad-band YJKs are directly calibrated from Two Micron all Sky Survey (2MASS) point sources visible in every VISTA image. For more details about the empirical transformations between the 2MASS and VISTA, and Wide-Field Camera and VISTA are available in González-Fernández *et al.* (2018).

In the Figure 2.7 small black points indicates carbon star distribution, whereas blue and red points indicate the stellar clusters and associations. The thick cyan and pink points represent the locations studied with VLT Survey Telescope in the optical wavelength range. The VMC survey provides deeper data by observing ∼6 magnitude fainter sources compared to 2MASS and DENIS survey. The detection limit of 2MASS and DENIS restricts observation down to the RGB of the old population, whereas VMC survey reaches MSTO of oldest populations in the MCs. The data of the VMC survey are obtained in Y, J and Ks bands. The central wavelength of Y, J and Ks bands are 1.02 μm, 1.25 μm and 2.15 μm respectively. The observation was carried out at an average seeing value of 0.″8. The data was obtained under good signal to noise ratio (S/N=10) up to a fainter limit of 21.9, 21.4 and 20.3 magnitudes (vega system) in Y, J and Ks bands respectively.

In this study we have used the VMC data of stars in the region of Kron 3 star cluster. The VMC observation of Kron 3 falls in the tile of SMC 4_2. The central co-ordinate of the tile is $\alpha_{2000} = 00^h25^m14.^s088$ and $\delta_{2000} = -73^o01'47.''640$. The observation in this tile is completed, which corresponds to three epochs of observations in the Y and J bands, and at least 12 epochs (∼9000 s integration time) in

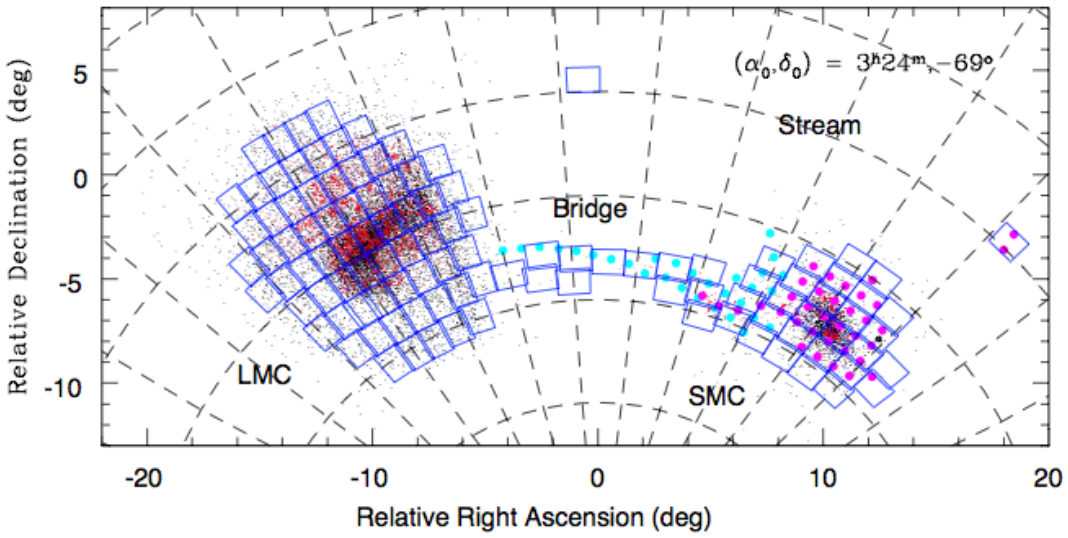

FIGURE 2.7: The blue rectangles represent the coverage of the VISTA Magellanic Survey. The black points indicate carbon star distribution, whereas blue and red points indicate the stellar clusters and associations. The thick cyan and pink points represent the locations studied with VLT Survey Telescope in the optical wavelength range. Image credit: ESO/VISTA

the Ks band. The PSF photometry of the tile has been performed by Rubele *et al.* (2018). We have used the photometric catalog of Rubele *et al.* (2018) for Kron 3 cluster. We refer the readers to Rubele *et al.* (2015) for more details about the SMC data and to Cioni *et al.* (2011) to know more information about the VMC survey.

2.7 Summary

The data and observations used in this study are summarised below:

- We used the OGLE III data to study the star clusters located in the LMC and the SMC. The analysis of the OGLE III data and results from it are described in the Chapters 3, 4, 5, 6.

- The cluster Kron 3 is observed using the UVIT and we list out the details of UVIT and observations in this Chapter. A details analysis of UVIT data, the usefulness of this data in order to study Kron 3 and interesting results are discussed in the Chapter 7.

- We describe the PSF photometry performed on the FUV and NUV images.

- The HST and *Gaia* are also discussed briefly in this Chapter. We have have use this data to study the presence of age and metallicity spread in Kron 3 in the Chapter 7.

- We briefly describe the VISTA-VMC survey, which obtains data in Y, J and Ks bands. This data is also used to study the metallicity spread in Kron 3. The details will be found in the Chapter 7.

Chapter 3

Estimation of cluster parameters in MCs: Semi-automated Quantitative Method[†]

3.1 Introduction

A number of previous studies have been carried out to identify star clusters within the MCs. The most recent and extensive catalogue of star clusters in the MCs is given by Bica *et al.* (2008) (hereafter B08). It provides central coordinates, radii and position angles for $\sim$ 3700 star clusters. However, the ages, reddening and mass of the clusters are not available in their catalogue. The parameters of some of these clusters have been estimated by a number of investigators. Glatt *et al.* (2010) (hereafter G10), using the MCPS (Zaritsky *et al.* 2002, 2004) data, presented ages, reddening and luminosities of 1194 star clusters and associations

[†]Results of this chapter are published in Nayak *et al.* (2016, 2018)

in the LMC and 324 in the SMC. Pietrzynski and Udalski (1999) (hereafter PU99) provided the age information of 93 well-populated SMC clusters. Pietrzynski and Udalski (2000) (hereafter PU00) estimated ages and reddening of 600 star clusters in the central LMC. PU99 and PU00 both have used OGLE II survey data (Udalski *et al.* 1998b) to determine the cluster parameters. Using Washington photometric data, parameters of 277 LMC star clusters were estimated by Palma *et al.* (2016), Choudhury *et al.* (2015), Piatti *et al.* (2002, 2003a,b, 2009), Piatti (2011b, 2012b, 2014). Recently Piatti *et al.* (2014, 2015a) estimated parameters of 378 star clusters using near-IR data from the VMC survey. Chiosi *et al.* (2006) presented the ages of 311 clusters younger than 1 Gyr. The authors used two sets of data for their analysis: OGLE II for the SMC disc and the data obtained from the ESO 2.2 m telescope for the region around NGC 269, located in the south-east end of the disc. Most of the well studied clusters in the MCs are rich star clusters, which stand out from the field region due their high stellar density. A large fraction of star clusters are either not well-studied or are unstudied due to the poor nature of the cluster (Choudhury *et al.* 2015). A more precise determination of cluster parameters of a larger sample is required to understand the star cluster formation history of the MCs. In our study we tried to estimate parameters of already identified star clusters, catalogued by B08.

The parameters of a star cluster are estimated from its CMD. Generally, a visual fitting of the isochrone is performed to the cluster CMD to estimate the reddening and age of the cluster. The visual fitting of the cluster CMD can be performed effectively for a sample of a small number of clusters. When the cluster sample exceeds a few hundred, this method is not very efficient. Also, to estimate the parameters in a self-consistent way, it is ideal to use a quantitative method in order to eliminate systematic errors.

Both the Magellanic Clouds (MCs) are well known for the presence of rich star clusters, which are a few 100 Myr old. Nevertheless, recent studies have shown

that the MCs also contain a relatively large number of poor star clusters, which are similar to the open star clusters of our Galaxy (Piatti 2012b; Choudhury *et al.* 2015). Recent studies also suggest that the MCs host star clusters with a wide range of masses (Hunter *et al.* 2003; Baumgardt *et al.* 2013). Using integrated color in UBVR passbands and evolutionary models, Hunter *et al.* (2003) estimated masses of 748 clusters in the LMC and 191 in the SMC having a range between $\sim 10^2$ to 10^6 $M_\odot$. Baumgardt *et al.* (2013) studied the mass function of the LMC clusters more massive than 5000 $M_\odot$, though the cluster mass range extended down to a few 100 $M_\odot$ in the low mass limit. The cluster mass function of LMC clusters were studied by de Grijs *et al.* (2013), where they do not find any evidence of early disruption of young clusters more massive than 10^3 $M_\odot$. Kontizas *et al.* (1982) calculated masses of 20 clusters in the SMC using King (1962) model and found that derived masses are about ten times smaller than those in our Galaxy. Using archival HST snapshot data, Mackey and Gilmore (2003) determined masses of ten rich clusters from their surface brightness profiles. The estimated mass of those clusters range from $10^{3.6}$ to $10^{5.5}$ $M_\odot$. Recent study by Maia *et al.* (2014) has provided masses of 29 young and intermediate clusters within a range of 300 to 3000 $M_\odot$. Thus, the star clusters in the MCs have a wide range in mass and it is essential to classify star clusters into groups corresponding to their mass.

Kontizas *et al.* (1990) had classified clusters in the LMC as Compact (C) or Loose (L) based on their appearance in the photographic plates, which is not related to any physical parameters of the clusters. Searle *et al.* (1980) classified 61 star clusters in the MCs as type I to VII based on four color photometry of integrated light. Even though there are many studies to understand the cluster mass function of star clusters in the MCs (Hunter *et al.* 2003; Popescu *et al.* 2012), there has been no attempt to classify each star cluster and group them according to their mass/strength, so far. On the other hand, there are well known classification schemes for Galactic Open Clusters (Trumpler 1930) based on the degree of central concentration of stars, the range in luminosity of the members, the number of stars

contained in the cluster and necessary conspicuous properties (Ruprecht 1966). This system known as Trumpler′s system of classification is used to homogeneously classify most of the open clusters.

In this chapter, we present a semi-automated quantitative method to estimate the parameters of a large number of clusters in the MCs. We also estimate the mass range of the star clusters in MCs and classify them based on their mass as well as richness. Systematic estimation of the mass and age of cluster sample will help in understanding cluster formation, evaporation, and dynamical evolution of the cluster system in the interacting environment of the MCs.

3.2 Analysis

3.2.1 Cluster sample

We adopted the most extensive catalogue of star clusters in the MCs by B08 as a reference and tried to identify the clusters in OGLE III observed regions of the MCs. We found 1765 star clusters in the LMC and 492 in the SMC, located well within the OGLE III observed field. We have used the major and minor axes of each cluster listed in the catalog by B08 to calculate their radius, which is defined as 1/4(major + minor axis). The estimated cluster radii of the LMC clusters are found to range from 0.′20 to 1.′75 on the sky, with physical sizes corresponding to ∼2.9 to 25.4 pc respectively. The SMC clusters appear smaller than the LMC clusters in the sky plane, ranging from 0.′07 to 1.′70, but their physical sizes have a larger range (∼ 1.22 to 29.6 pc) than the LMC clusters. We extracted data of the cluster regions (stars within the cluster radius) from the OGLE III observed regions along with a few arcmin field region around them, depending upon their radii.

A cluster region is identified as a density enhanced region with respect to the surrounding field, and consists of cluster members as well as field stars. The MCs are known to host very rich as well as poor clusters, located in a range of environments with varying stellar density. The fundamental feature of a cluster which is used to estimate the reddening, age and distance is the MS and the location of turn-off in the CMD. The field star removal is necessary to define the above two, which depends on the field star density and its variation in the vicinity of the cluster. Therefore, we restricted our analysis to star clusters where one can reliably remove field stars and identify the desired cluster features. As a first step, we identified clusters which are located in regions with large variation in the field star density. We describe the adopted method below. In order to measure the variation in field star distribution surrounding the cluster field, we chose four annular field regions (each of equal area as the cluster region) around each cluster. The inner radii of the four annular field regions are chosen as $0.'5$, $1.'0$, $1.'5$ and $2.'0$ larger than the cluster radius. Number of stars in each field region is counted. The estimated number of stars within the cluster radius is denoted as (n_c). The number of field stars contaminating the corresponding cluster is estimated as the average number of stars of four field regions (n_f). Standard deviation (σ_f) about the average indicates the variation in the stellar field counts. The number of cluster stars (n_m) or the strength of the cluster is then defined as $n_m = n_c - n_f$.

We have then separated star clusters on the basis of variation in the field star distribution. We have excluded clusters which are embedded in fields suffering from large dispersion in the field star count with respect to the average. We have also excluded clusters, where the value of dispersion in the field star count is equal to or greater than the number of stars in the cluster. In order to achieve this, we have used the following criterion :

(i) We estimated the fractional standard deviation (σ_f/n_f) to quantify the variation in field star count. We excluded clusters where variation in the field stars count is greater than or equal to 50% of the average count, i.e. $\sigma_f/n_f \geq 0.5$. With

this criteria, we excluded 48 LMC clusters and 29 SMC clusters.
(ii) The variation in the field star counts will propagate as an error when we estimate the strength of the cluster. The error associated with the estimation of n_m can be defined as :

$$e = |(n_c - (n_f + \sigma_f)) - (n_c - (n_f - \sigma_f))|, \tag{3.1}$$

which is basically the difference between the maximum and minimum value of n_m, for σ_f deviation in the field star distribution. For crowded field regions, there is a possibility that σ_f is high, so will be the value of e. In order to remove clusters, where the error itself is greater than the number of stars in the cluster, we calculated the fractional error as e/n_m and excluded cases with $e/n_m \geq 1$. Based on this criterion, we excluded 310 LMC clusters and 126 SMC clusters from our sample. Figure 3.1 shows a plot between e and n_m. Clusters with $e/n_m \geq 1$ are shown in red, whereas those with e/n_m <1 are shown as blue points. It is seen that clusters which are relatively poor, with $n_m \leq 30$, have $e/n_m \geq 1$.

The number of clusters remaining in the sample, after implementing the above two cut-off criteria is 1407 in the LMC and 337 in the SMC. Out of these clusters, 46 LMC clusters and five SMC clusters are found to be relatively rich having $n_m > 400$. We have excluded these rich clusters from our analysis as they are already well studied using better data. Thus we proceeded with the sample of 1361 LMC clusters and 332 SMC clusters to decontaminate their cluster CMDs. This exercise also points out that 20% LMC clusters and 30% SMC clusters are located in regions with significant variation in field star density.

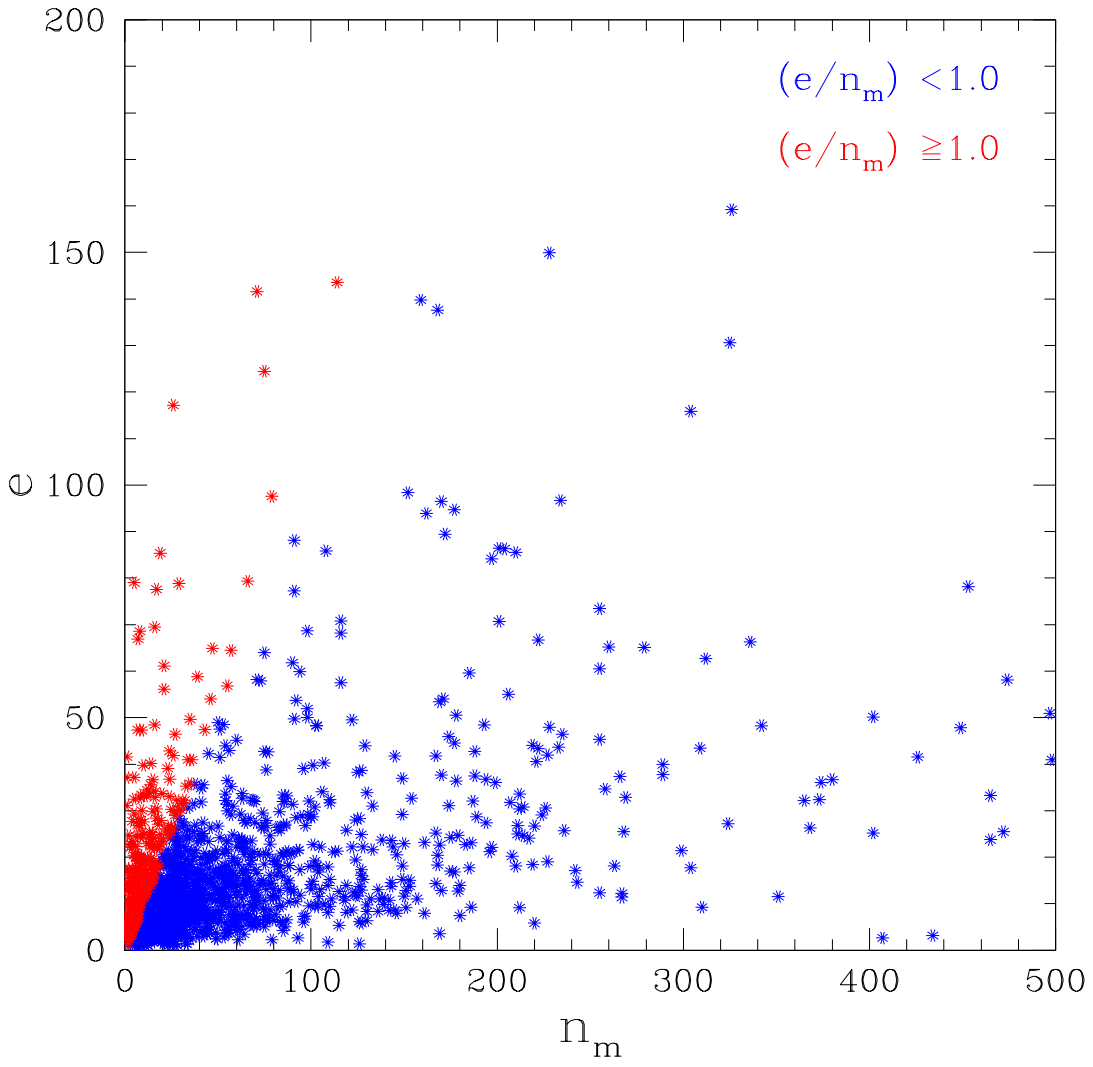

FIGURE 3.1: The distribution of error (e) with respect to cluster member strength (n_m). The clusters with $e/n_m > 1$ are denoted as red points, whereas, the blue points denote the clusters with $e/n_m \leq 1$.

3.2.2 Removal of field star contamination from cluster CMDs

We constructed (V, V − I) CMDs for cluster and field regions to compare and remove field star contamination from the cluster region, using a statistical process. The annular field chosen to carry out this process is the one with inner radius 0.5′ larger than cluster radius. The field stars within the cluster region are then removed by considering each star in the field CMD and finding its nearest

counterpart in the cluster CMD. We considered a grid of [magnitude, color] bins with different sizes, starting with $[\Delta V\ ,\ \Delta(V-I)] = [0.02, 0.01]$ up to a maximum of [0.5, 0.25], where the units are in magnitude. This procedure is repeated for all the clusters. The cleaned cluster CMDs show prominent cluster features with minimum unavoidable field star contamination. The similar technique has been used earlier by Choudhury *et al.* (2015).

3.2.3 Semi-automated quantitative method

Now we have the CMDs of all the above star clusters with field stars removed and ready for the estimation of cluster parameters. The age and reddening of star clusters are generally estimated by the visual fitting of isochrones to the MSTO of cluster CMDs. However, visual fitting of isochrones to more than a thousand of clusters sample is not only a laborious task, but also produces inconsistently estimated parameters across the sample. For the first time, we have developed a semi-automated quantitative method to estimate cluster parameters, age and reddening. This method helps us not only to estimate these two parameters accurately and consistently, but also to quantify errors. We adopted a two step process for the estimation of cluster parameters. In the first step, we developed a quantitative automated method to estimate the age and reddening (as described below). This method is applied to all clusters to estimate the reddening and age. In the second step, we plotted the isochrones on each of the cluster CMDs sampled in this study, for the estimated age and corrected for the estimated reddening. All the CMDs were visually checked and corrected for any error in the fit. The second step is used to check and correct for improper estimation of parameters by the automated method. Thus, the method we developed in this study could be termed as a semi-automated quantitative method. We describe the development of the automated part below.

The processes involved in this method are :
(a) Identifying the MS in the cleaned cluster CMD and constructing the MS luminosity function (MSLF).
(b) Identifying the MSTO and estimating the corresponding apparent magnitude and color.
(c) Estimating the reddening from the (V−I) color of the MSTO.
(d) Estimating the absolute magnitude of the MSTO after correcting for reddening and distance.
(e) Estimating the age using age-magnitude relation derived using Marigo *et al.* (2008) (hereafter M08) isochrones.

The above steps are described in detail below.

(a) We consider stars brighter than 21 mag in V and bluer than 0.5 mag in (V − I) color as the MS stars. To construct the MSLF, the magnitude axis is binned with a bin size of 0.2 mag. The brightest bin with a minimum number of stars (η) is identified as the bin corresponding to the MSTO. The mean V magnitude of the brightest bin is considered as turn-off V (V_{TO}) magnitude. The MSTO bin (which is likely to be the brightest bin of the MSLF) needs to be identified from the MSLF using statistically significant value of η so that it excludes blue super-giants. The value of η in a cluster will depend mainly on richness as well as age of the cluster. Two clusters which are similar in richness, but with different age will have different MSTO bin with different η. The MSTO bin will be less populated for a younger cluster than the older one with similar richness. Two clusters with same age but different number of cluster stars will also have different values of η for their MSTO bin. A very similar idea was used by Indu and Subramaniam (2011) to identify the MSTO of field regions in the Magellanic Clouds. As mentioned by these authors, the identified bin and the number of stars in the bin are dependent on the richness/area of the field. Here, the known parameter is the richness (total number

of cluster stars) of the cluster, as we are yet to estimate their age. Therefore, we have grouped the clusters according to their strength and fixed η value for each group. We have discussed the groups and the selection of η for each group in section 3.2.4.

(b) The mean V magnitude of the MSTO bin is considered as turn-off V magnitude of cluster (V_{TO}). Once we have identified the V_{TO} the next task is to estimate the color of the MSTO. The color of the MSTO can be identified as the peak in color distribution near the MSTO. To estimate the peak color of the MSTO, a strip parallel to color axis with a width of 0.6 mag about V_{TO} is considered (V_{TO} + 0.4 mag to V_{TO} - 0.2 mag). This is to ensure that we have a statistically significant number of stars near the MSTO. For the clusters with $n_m \leq 100$, a width of 0.8 mag is considered (given by V_{TO} + 0.6 mag to V_{TO} − 0.2 mag). The choice for width of the strip does not affect the position of the peak color, as the isochrones for younger ages are almost vertical to the color axis near the MSTO. This strip is binned in color with a bin size of 0.1 mag to estimate the distribution of stars along the color axis. The distribution is found to have a unique peak (in most of the cases) with asymmetric wings. The mean color of the bin corresponding to this unique peak is chosen as the apparent color, $(V - I)_{app}$, of the MSTO.

(c) The reddening of the cluster is defined as the difference between the apparent and absolute color of the MSTO. To begin with, we adopted initial values of extinction (A_V) = 0.55 (Zaritsky *et al.* 2004) for the LMC and 0.46 mag (Zaritsky *et al.* 2002) for the SMC, and considered distance modulus (DM) as 18.50 (Saha *et al.* 2010) and 18.90 mag (Storm *et al.* 2004) for the LMC and SMC respectively. If M_V is the absolute magnitude of the MSTO, then assuming a distance modulus and an average value of A_V for the cluster, the apparent magnitude (V_{TO}) is related to M_V as:

$$M_V = V_{TO} - DM - A_V, \tag{3.2}$$

The estimated value of M_V is cross-matched with the absolute V magnitude of MSTOs from the isochrones tables of M08, with Z = 0.008 (Piatti and Geisler 2013) for the LMC and Z = 0.004 for the SMC. The (V − I) color corresponding to the closest match of absolute MSTO V magnitude gives the absolute color for the MSTO, $(V - I)_0$. The reddening (E(V − I)) for the the cluster is then given as:

$$E(V - I) = (V - I)_{app} - (V - I)_0. \tag{3.3}$$

The extinction for the cluster region is estimated as $A_V = 2.48 \times E(V - I)$ (Nikolaev *et al.* 2004). The extinction corrected value of M_V of the MSTO is then calculated again by using this value of A_V in Equation 3.2. This process was iterated a couple of times and it was found that the values estimated do not change with respect to the values obtained in the first iteration. The method used here is similar to that adopted by Indu and Subramaniam (2011), for estimating the reddening of field regions.

(d) Figure 3.2 shows the relation between the absolute magnitude M_V of the MSTO and their corresponding ages (log(t)) for M08 isochrones of LMC metallicity (Z = 0.008). The relation is found to be linear, and is given as:

$$log(t) = 0.357(\pm 0.002)M_V + 8.350(\pm 0.006). \tag{3.4}$$

A similar M_V vs log(t) relation has also been obtained from M08 isochrones for SMC metallicity (Z = 0.004) as shown in Figure 3.3. The relation is given as :

$$log(t) = 0.372(\pm 0.002)M_V + 8.348(\pm 0.006). \tag{3.5}$$

The extinction corrected M_V derived in step (c), is used in the above relations to estimate the ages of the sampled clusters located within the LMC and the SMC.

Thus, we have described a quantitative method to estimate the reddening and age

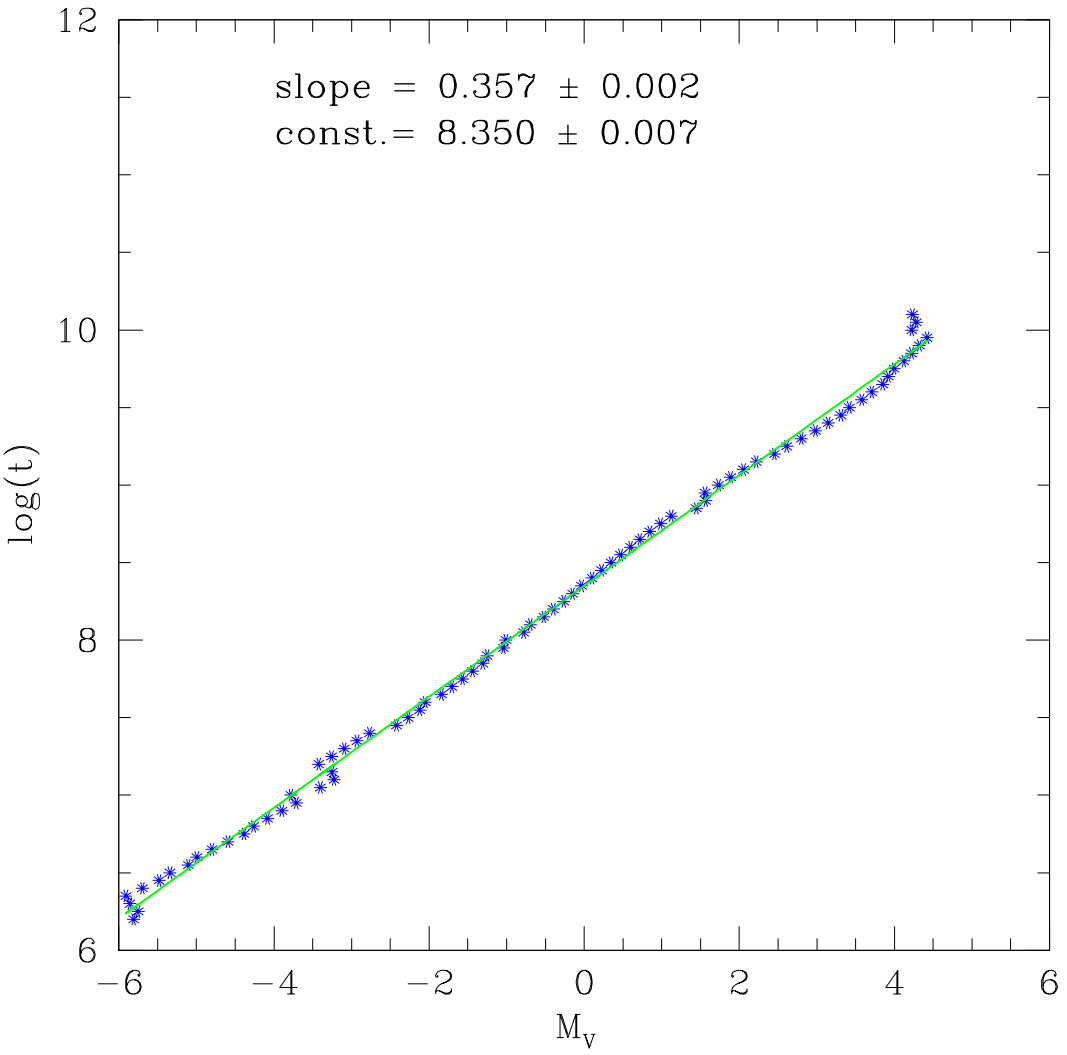

FIGURE 3.2: The relation between the absolute turn-off V magnitude (M_V) and age, within the range log(t) = 6.2 to 10.2 for M08 isochrones of LMC metallicity (Z = 0.008). A straight line (green) fitted through the points is also shown.

of star clusters. This method primarily depends on the unique identification of the MSTO. As mentioned earlier, it is a function of age and richness of the cluster.

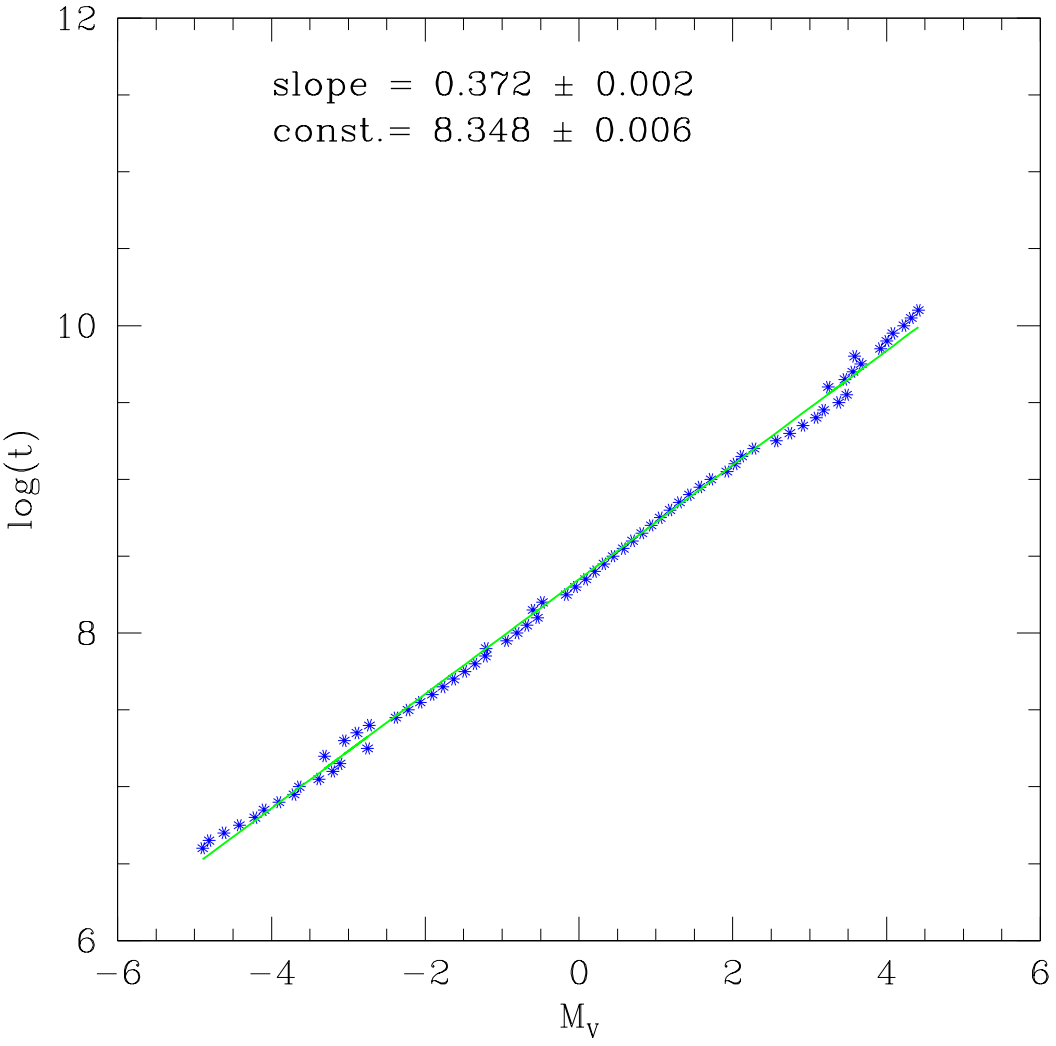

FIGURE 3.3: Relation between the absolute turn-off V magnitude (M_V) and age, within the range log(t) = 6.2 to 10.2 for M08 isochrones of SMC metallicity (Z = 0.008). The data points are fitted with a straight line (green).

3.2.4 Identification of MSTO and estimation of cluster parameters

In this section, we describe the method to identify the MSTO in the MSLF. The brightest bin with a minimum number of stars (η) is identified as the bin corresponding to the MSTO. The bin corresponding to the MSTO will depend upon the selection of the minimum number criteria (η) for the brightest magnitude

bin. As mentioned earlier, the value of η will depend on the richness of the cluster. In subsection 3.2.1, we estimated the number of member stars in the cluster n_m, after subtracting the average field population. We have grouped clusters based on n_m, which is a measure of the richness of clusters and are shown in Table 3.1. We have performed this classification based on the number of cluster member stars which are brighter than V=21 mag, though it is directly linked to the mass of the clusters.

The aim is to fix the value of η for each group of clusters, classified according to their richness/mass so that a realistic MSTO and corresponding age of the cluster can be identified. If we fix the value low, then we would identify a brighter MSTO and estimate a younger age. And if we fix a higher value, we would then identify a fainter MSTO and estimate an older age for the same cluster. Thus, it is important to fix an appropriate value for this parameter for each group.

In order to calibrate the value of η, we identified the LMC clusters whose parameters (age and reddening) are already determined by G10, in each group. As we already have the field star corrected MSLF for these clusters, we estimated their age and reddening using our method, for a range of η values. The estimated ages and reddening (E(V $-$ I)) were compared with those estimated by G10 for the considered η values. The maximum error in the age estimation of G10 is 0.5 (in the log scale) and we choose this as the limit for comparing the age differences between the two estimates (δlog(t)). The maximum error in the reddening (δE(V $-$ I)) is 0.1 mag, corresponding to the error related to estimating the color peak in the MSTO magnitude bin. The value of η, for each group of clusters is chosen such that there is least scatter in δlog(t) and δE(V $-$ I) and the deviation is centered around the zero value. The values of η determined for each group of clusters are listed in Table 3.1. In the table, we have also listed the number of clusters in each group whose ages and reddening have been compared with G10 (N_{G10}). In order to demonstrate the process, we discuss the analysis performed

TABLE 3.1: Grouping and classification of clusters based on their richness (n_m)/mass range (M_c) :

Group No.	Range of n_m	η	$\eta_{simulated}$	N_{LMC}	N_{G10}	N_{SMC}	Mass range ($M_\odot$)	Classification
I	6< n_m ≤30	2	1.23	438	149	94	< 800	very poor
II	30< n_m ≤100	3	2.88	460	181	69	800 - 1700	poor
III	100< n_m ≤200	5	6.16	122	47	13	1700 - 3500	moderate
IV	200< n_m ≤300	10	10.27	43	15	2	3500 - 5000	moderate
V	300< n_m ≤400	14	14.38	9	4	1	> 5000	rich

for one group of clusters (Group IV) with 200< n_m ≤300. Figure 3.4 and Figure 3.5 show plots of δlog(t) and δE(V − I) against age and reddening respectively, estimated by the above mentioned method. Four values of η were used to estimate age and reddening. An inspection of Figure 3.4 shows that the age estimation is better for $\eta \geq 10$, as the deviation of δlog(t) is almost symmetric about zero and has a spread over large age range with minimum error. For $\eta \geq 12$, we observe clumping of data points, and for rest of the two η values we estimated older age than G10 with relatively large error. In the Figure 3.4 the points with red circle indicate that the clusters have δE(V − I) > 0.1 for the corresponding η value. In the Figure 3.5 the clusters with δlog(t) > 0.5 for the corresponding η value are marked as red circle. The comparison plots with η value 10 show that the error in reddening value is not affecting the age estimation but for other η values, it is found to affect the age estimation.

We should point out that, initially we created 6 groups based on the value n_m and estimated η values for all the groups. It was found that the η value was the same for two groups, which we merged together to create the above five groups. These groups have different values of η. The comparison of estimated ages with those estimated by G10 reveals that the dependency of age on the value of η is not very large. This may be due to the fact that the age range considered in this study is not very large and most of the clusters are younger than 300 Myr.

We performed the above process for all the groups mentioned in the Table 3.1 and

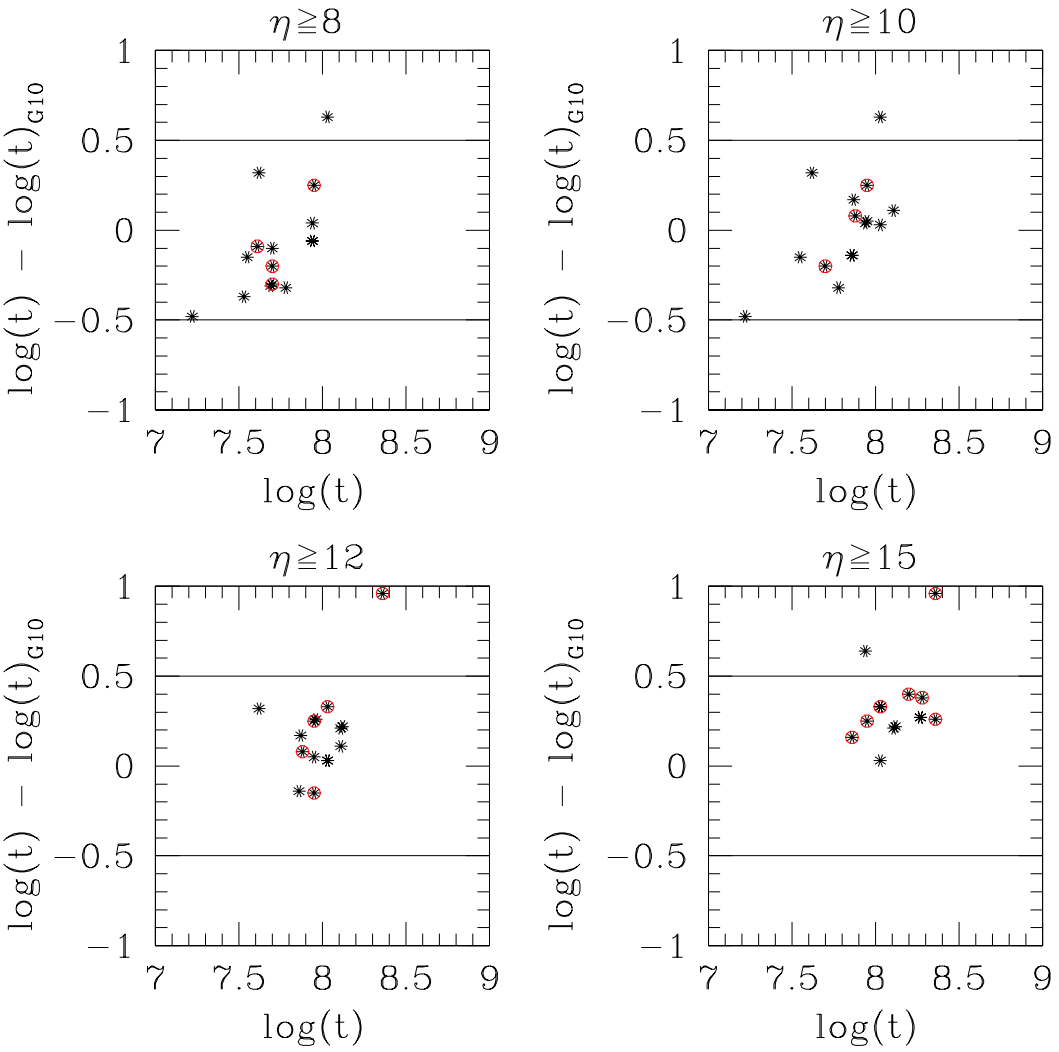

FIGURE 3.4: Estimated age distribution of clusters for $200< n_m \leq 300$ with respect to G10's estimation of age for different values of η. The clusters with $\delta E(V-I) > 0.1$ shown in Figure 3.5 are marked as a red circle for corresponding values of η.

estimated the appropriate value of η for each group of LMC clusters. Now, we are ready to apply our quantitative method to all the clusters in our study. We should specify that we used the similar η values, calibrated using LMC clusters to estimate the parameters of SMC clusters. Since the limiting V magnitude of the OGLE III survey is ∼21 mag, the age and reddening of the clusters having $V_{TO} \geq 19$ mag could not be determined reliably using our method. There are 386 such clusters in the LMC and 143 in the SMC, which we have considered later.

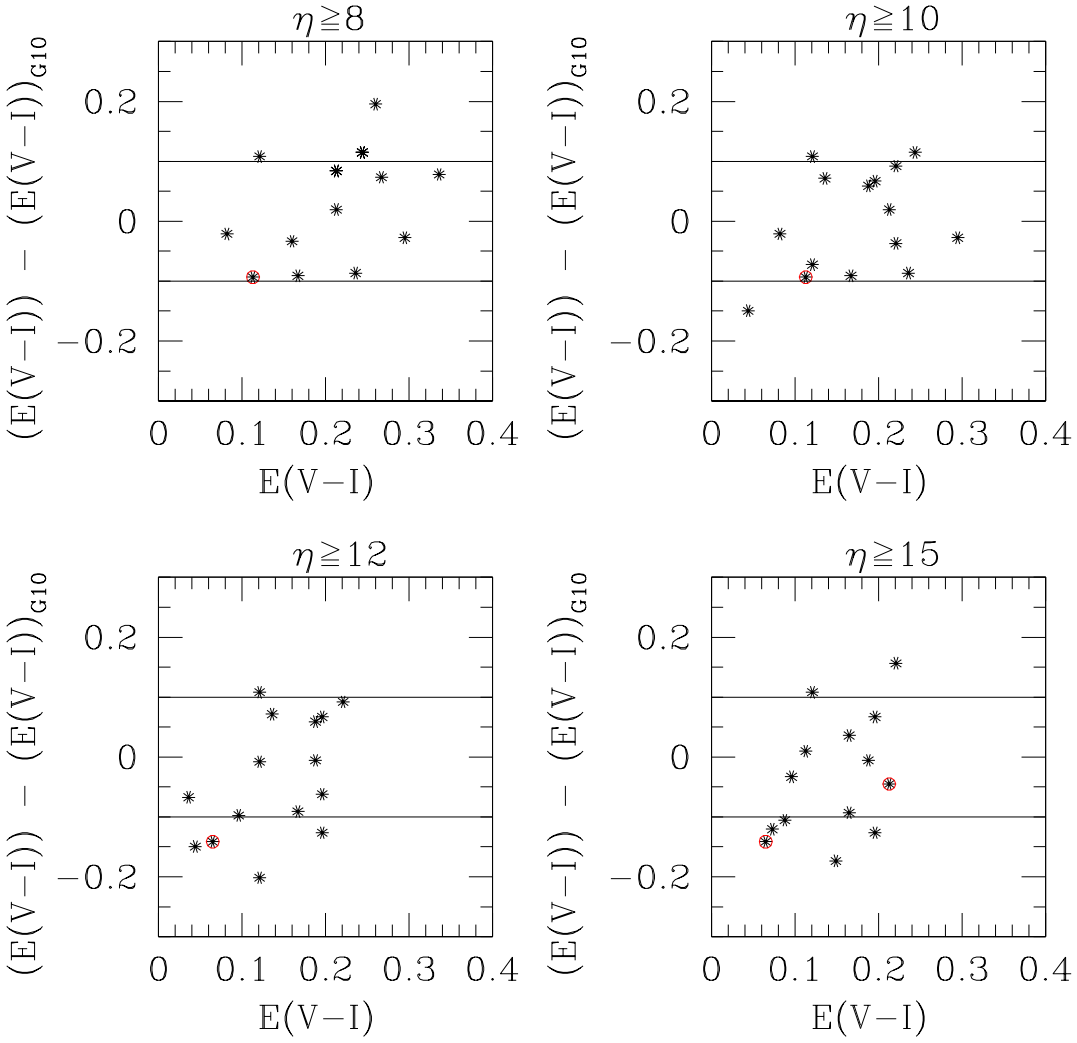

FIGURE 3.5: Estimated reddening distribution of clusters for $200 < n_m \leq 300$ with respect to G10's estimation of ages for different value of η. The clusters with $\delta\log(\text{age}) > 0.5$ shown in Figure 3.4 are marked as a red circle for corresponding values of η.

We applied our method to the remaining clusters (975 in the LMC and 189 in the SMC) and estimated their age and reddening. A sample cluster is shown in Figure 3.6, where the spatial location of the cluster along with the field region, CMD of all stars within the cluster radius, CMD of the field region and the CMD of the decontaminated cluster over-plotted with the isochrone for the estimated age and corrected using the estimated reddening and DM are shown in four panels.

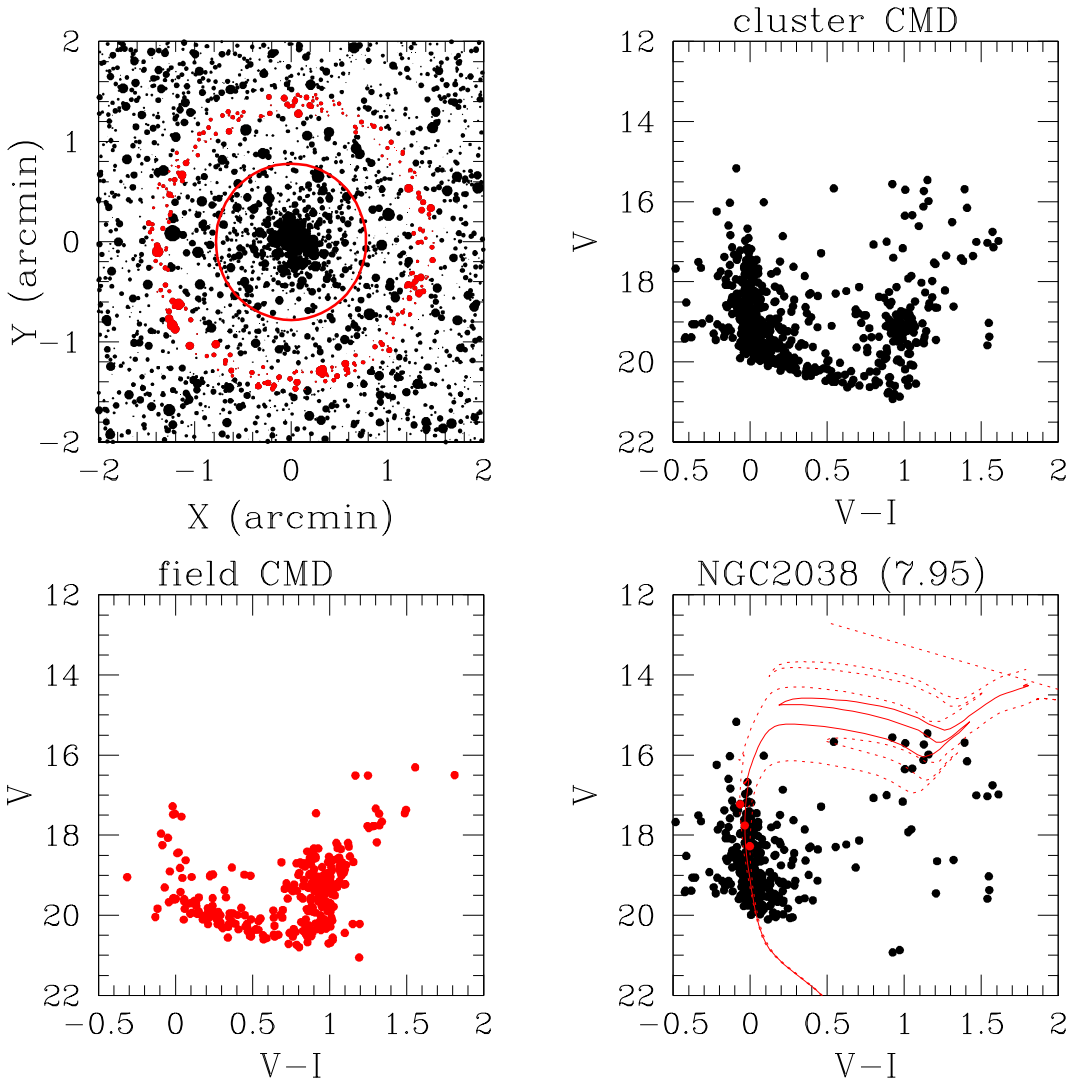

FIGURE 3.6: Top left panel shows an example of a spatial plot of a cluster (NGC2038) and its surrounding field region, where the point sizes are proportional to brightness of stars in V magnitude. Cluster region is shown within the red circle whereas considered field stars are denoted as red points. The CMDs of cluster region (top right), annular field region (bottom left) and field star decontaminated cluster region (bottom right) are also shown. In the bottom right panel, isochrone of estimated age (red solid line) with an error of ±0.2 (red dotted line) are over-plotted on the cleaned CMD, where red dots are turn-off points of corresponding isochrones.

Once we estimated the values of age and reddening for each of the clusters (having $V_{TO} \leq 19$ mag) using the automated quantitative method, we proceed to the second step of our two step process. The second step is the manual check performed visually and is aimed at correcting the improper estimations of the automated method. The M08 isochrone for the estimated age (along with isochrones corresponding to age, log(t) $\pm$ δlog(t)) were over-plotted on the cleaned cluster CMD after accounting for the reddening value. All the plots are visually inspected for any mismatch between the plotted isochrone with respect to the MS and MSTO in the cluster CMD.

3.2.4.1 Visual inspection of LMC cluster CMDs

After visual inspection we found that in the case of LMC, age and reddening of 752 (77.13%) clusters out of 975 are estimated reliably by the automated method, as the superimposed isochrones for the estimated age and reddening fit well to the cluster sequence. Whereas, a small correction in the reddening and age were found to be needed for 43 (4.41%) and 67 (6.87%) clusters respectively, to fit the isochrones in the cleaned CMD. Thus, we find that, the automated quantitative method is able to produce reliable fits for the majority of clusters in the sample. Including this small manual correction in the reddening and age, we are able to estimate cluster parameters of 862 clusters, which is 88.4% of the LMC clusters studied here. It is worth mentioning that we changed the fitted values only if the required shift is more than the error in the estimation. That is, if there is a shift in reddening, which is less than 0.1 mag, we have not corrected it. And the same applies to the age estimation as well. We also tried to understand the reason for incorrect estimation of the parameters. We found that clusters with a flat profile for color distribution, instead of a peak, had incorrect reddening estimation. Similarly, clusters with gaps in the MS or clumpy MS, resulted in

erroneous estimation of the MSTO. These are the cases which needed manual intervention to estimate reddening and age.

For the remaining 113 out of 975 clusters, visual inspection revealed that the cleaned cluster CMDs have either large spread in the MS along the color axis or clumpy distribution along the MS. In some cases, there are big gaps in the MS along the magnitude axis. These features can be genuine or due to differential reddening, being located in crowded fields or variation in the field star counts. The above problems may be due to the choice of a particular field region and hence we created three cleaned CMDs using three different field regions and plotted all the cleaned CMDs together. Stars which are not removed from the cluster CMD for at least two decontamination processes are considered as genuine cluster candidates. By this method, we were able to identify 22 clusters with prominent cluster features and corrected their parameters manually to get the best fit of isochrones.

We examined the CMDs of the 386 clusters with $V_{TO} > 19$ mag and found that there are a few clusters with prominent cluster features or prominent features that can be extracted by using decontaminated CMDs using multiple field regions. We applied similar automated process to estimate the age and reddening of these clusters. We over-plotted isochrones for estimated ages on cleaned CMDs of these clusters and manually corrected for ages and reddening wherever needed. With this analysis we added 188 more clusters to the above mentioned 884 clusters with precisely estimated parameter. Thus we were able to determine ages and reddening for 1072 clusters, from the sample of 1361 LMC clusters. The rest of the 289 clusters need more attention to estimate the cluster parameters. We plan to study these cluster in a separate future study.

3.2.4.2 Visual inspection of SMC cluster CMDs

In the case of SMC clusters we noticed that the success rate of the quantitative method is reduced. We found that the isochrones fitted very well for 62 clusters (32.8%) out of 189 and a small correction in age and/or reddening were required for 75 clusters (39.7%). The remaining 52 clusters (27.5%) have ambiguous cluster sequence. To identify the cluster sequence we decontaminated the cluster region for these 52 clusters with two more field regions and over-plotted all decontaminated CMDs, as we did in the case of 113 LMC clusters. The sources which have not been removed for at least two different decontamination processes were considered as a cluster member. Out of the 52 clusters, 12 were found to show prominent cluster features, and required minor modification in age or/and reddening to the automated estimation. Whereas, 40 clusters were found to have no clear feature in the CMD prohibiting any reliable estimation of parameters. Hence we have excluded these 40 clusters from our study. Among these 40 clusters, four are found to be in common with the cluster candidates identified by Piatti *et al.* (2015b). The reason for reduced success rate in the case of the SMC is probably due to a smaller number of cluster members ($n_m \leq 30$), resulting in sparsely populated CMDs and MS.

To increase the number of parameterized clusters in the SMC, we also inspected the 143 cases (out of 332) with $V_{TO} > 19$ mag. After the visual inspection of their CMDs, 30 clusters are found to have reliable estimation (including a minor correction in estimated age and/or reddening with respect to automated estimation for a few). Thus, we were able to estimate the parameters of a total 179 clusters within the SMC.

3.2.5 Calibration of η using synthetic CMDs

We also calibrated the η value by generating synthetic CMDs and comparing it with observed CMDs. In this study, we found that ages of the SMC clusters peak at ∼100 Myr and reddening peaks between 0.10-0.20 mag. We took age to be 100 Myr and reddening value as 0.15 mag to produce synthetic CMDs. In this analysis, we used Padova isochrone model (Marigo *et al.* 2008) and Salpeter's mass function (Salpeter 1955). We produced synthetic CMDs by populating stars in the main sequence (MS) for observed ranges of V and I mag. We have also taken care of photometric incompleteness while generating synthetic CMDs. We calculated the number of stars present in the turn-off bin, which is the value of η, for different groups (I−V) of clusters. We have run the simulation for multiple iteration with different initial normalizing star-counts. We have also run the simulation for another two age values (200 and 300 Myr). We found that the η values estimated from the above two methods match very closely and are tabulated in Table 3.1.

3.3 Classification of clusters and their mass range

In section 3.2.4 we grouped star clusters based on the number of stars present in the cluster. We created groups as I, II, III, IV & V, which are arranged in the increasing strength of richness. As mentioned earlier, the grouping is based on the number of stars present in the bin corresponding to the MSTO, which in turn is a function of the total number of stars. Also, the number of stars in each cluster is directly related to the mass of the cluster. Basically, the fundamental parameter which separates our sample into various groups is the mass of the cluster. Therefore, it will be interesting to estimate the mass range for the above mentioned groups. It is to be noted that the aim here is to give a physical sense to the above classification based primarily on the richness of the clusters.

As most of the clusters studied here are younger than 300 Myr, we can estimate the range of mass (M_c) occupied by these groups using the η parameters and assuming a typical age of 100 Myr. We constructed synthetic CMD for the clusters using M08 isochrones, for a mass range of 0.1-15.0$M_\odot$. We assumed Salpeter′s mass function and also incorporated observational errors. In order to suppress statistical fluctuation due to the low value of η, we simulated cluster CMD for a large value of the total cluster number ($\sim 10^6$). The synthesized LF is then scaled for the value of η (for the MSTO bin) and the total mass of the cluster is estimated using the scaling factor. We have allowed for statistical error, while matching the value of η. Thus, we estimated the masses for the groups and classify the above groups as follows:

(1) Group I: This group has a very low number of stars and has mass $M_c < 800$ $M_\odot$. Clusters in this group are classified as *very poor* clusters. This group has 438 LMC clusters and 94 SMC clusters.
(2) Group II: This group has relatively less number of stars and has mass in the range $M_c \sim 800$ - 1700 $M_\odot$. Clusters in this group are classified as *poor* clusters. This group has 460 LMC clusters and 69 SMC clusters.
(3) Groups III & IV: This group has relatively large number of stars and has the mass range $M_c \sim 1700$ - 5000 $M_\odot$. Clusters in these two groups are classified as *moderately rich* clusters. These groups have 122 clusters in the LMC and 15 in the SMC.
(4) Group V: These clusters have a large number of stars as members and are also massive, with mass > 5000 $M_\odot$. Clusters in this group are classified as *rich* clusters. This group has only 9 LMC clusters and one SMC cluster in our study.

Above mentioned mass range and classification are also presented in columns 8 and 9 of Table 3.1.

3.4 Error estimation

In this study, we have used a quantitative method to estimate age and reddening and hence we can clearly estimate the error in the estimation of these parameters using the method of propagation of errors. The error in estimating the reddening depends upon the photometric error and binning resolution along the color axis, and this error will propagate to age estimation. The error associated with the age estimation depends on the errors in estimating extinction and absolute magnitude, and binning resolution along the magnitude axis. The error in estimated age also depends on the uncertainty related to DM value, adopted in this study. The LMC has an average depth of 4 kpc (0.17 mag) in the bar region and 3.44 kpc (0.14 mag) in the disk (Subramanian and Subramaniam 2009). Whereas The SMC has a large range of line of sight depth from 670 pc to 9.53 kpc (0.025 to 0.34 mag; Subramanian and Subramaniam (2009)).

In our error analysis we considered the depth of the SMC as 9.53 kpc and for the LMC 4 kpc. As the reddening is estimated using the stars in the upper MS and the photometric error is very small (≤ 0.05) in the upper MS, the effect of photometric error in estimating reddening could be neglected. Thus, the error in the estimated reddening, E(V−I) is chosen to be same as the bin size, 0.1 magnitude. Errors in the estimation of extinction and age are given by the following relations

$$\sigma A_V = 2.48\sqrt{\sigma(V-I)^2 + (V-I)^2_{bin}} \tag{3.6}$$

$$\sigma M_V = \sqrt{\sigma V^2 + V^2_{bin} + \sigma A^2_V + \sigma(DM)^2} \tag{3.7}$$

$$\sigma(age) = constant \times \sigma M_V \tag{3.8}$$

where V_{bin} & $(V-I)_{bin}$ are half the bin sizes used for magnitude & color binning, σM_V is the error in absolute magnitude, σA_V is the error in the estimated extinction, $\sigma(DM)^2$ is the uncertainty in the distance modulus due to maximum line of sight depth in the SMC/LMC and σ(age) is the error in estimated age in (log(t)). The maximum errors in estimated ages are 0.21 for LMC clusters and 0.25 for SMC clusters.

The studies of intermediate and old SMC clusters by Parisi *et al.* (2009) suggested that metallicity of the SMC clusters ranges from -0.60 to -1.30 dex with a mean of -0.96 dex. Therefore, we have also examined the effect of metallicity on estimated age. We derived M_V vs log(age) relation for three different metallicities (Z = 0.001, 0.004, 0.008) and found that the variation in the slope and the y-intercept are in second and third decimal place respectively. The errors in the age estimation for different metallicities are calculated using equation 3.8 for corresponding slope values and the error varies from 0.24 to 0.26 in log scale for SMC clusters due above mentioned metallicity range. For LMC clusters the error values ranges from 0.2 to 0.21 in the log scale.

3.5 Summary

1. We have developed a semi-automated quantitative method and applied it on large optical survey data OGLE III to estimate the parameters (age and reddening) of more than 1000 star clusters in the MCs.

2. We have estimated the parameters of 1072 star clusters in the LMC and 179 in the SMC.

3. Visual inspection of all the cluster CMDs over-plotted with isochrones of corresponding estimated ages suggest that the quantitative method works very well in the case of LMC. The success rate becomes relatively low for SMC clusters. The reasons could be due to more poor clusters present in the SMC, sparse distribution of stars in the MS and large line of sight depth of the SMC.

4. The star clusters of both the MCs are divided into five groups (I to V) based on their strength (number of cluster members). We have estimated the mass range for each group of clusters. Based on the mass range, clusters are classified in four groups : very poor (<800 $M_{\odot}$), poor (800 - 1700 $M_{\odot}$), moderate (1700 - 5000 $M_{\odot}$) and rich (>5000 $M_{\odot}$).

5. We have also calculated errors associated with estimated reddening and age. The error in reddening is 0.1 mag for star clusters of both MCs. The errors in age estimation are 0.21 and 0.25 in logarithmic scale for star clusters in the LMC and the SMC, respectively. If we include the metallicity spread in the MCs from Z=0.001 to 0.008, the error values range from 0.2 to 0.21 and 0.24 to 0.26 in the log scale for LMC and SMC clusters, respectively.

6. We found that 20% LMC clusters and 30% SMC clusters are located in regions with significant variation in field star density.

Chapter 4

Demographics of cluster richness and distribution in the LMC[†]

4.1 Introduction

We classified and estimated the age and reddening of 1072 star clusters in the LMC, using the semi-automated quantitative method, as described in Chapter 3. Although there have been many studies of the LMC star clusters in the past, this is the first attempt to classify LMC star clusters into groups based on richness/mass and a quantitative method is introduced for their parameterisation.

The estimated age and the reddening, along with the group number based on the richness class is a rich source to understand the details of distribution of clusters as a function of age and richness, in the LMC. The above data for all the clusters are presented as a catalog of clusters and it is available as an on-line[*] catalog. A

[†]Results of this chapter are published in Nayak *et al.* (2016)

[*]http://vizier.cfa.harvard.edu/viz-bin/VizieR?-source=J/MNRAS/463/1446

sample of this catalog is shown in Table 4.1. This catalog contains the name of the cluster, central coordinates (RA and Dec) as in B08, size of the cluster taken from B08, estimated reddening and age, earlier estimations of ages by G10, PU00, Palma *et al.* (2016), Piatti *et al.* (2014, 2015a) and the designated group number (I-V) respectively. We also present the CMDs of all the 1072 clusters in the same order as in the Table 4.1, as online-only[†] figures. The cluster CMDs are field subtracted, over-plotted with the M08 isochrone, with an uncertainty of log(t) = $\pm$0.2 for the estimated age and reddening. The location of the turn-off as per the isochrone is shown as red dot, on the MS in the CMD. In some of the CMDs, data points are shown in different point types. These are the clusters for which we identified the cluster sequence after performing field star subtraction with three different annular field regions. Most probable cluster members are those which survive at least two separate field subtraction process and these can be identified as those with at least two point types appearing one on top of another. These are also available in the online version. As an example, we present one CMD each from the four groups of clusters in Figure 4.1. The top left panel shows the cluster SL 51, which belongs to the very poor cluster. The top right panel shows the CMD of SL 383, which is a poor cluster. The bottom left panel shows the CMD of the moderate cluster SL 690, whereas the bottom right panel shows the CMD of a rich cluster, NGC 2038.

We estimated parameters of 308 clusters for the first time. Among these new estimates, 156 are group I (very poor) clusters, 111 are Group II (poor) clusters, 39 belong to groups III & IV (moderate) clusters and 2 clusters belong to group V (rich). In the Table 4.1, these clusters can be identified as those with columns 7-10 as blank.

In this chapter, we first compare our results with the previous estimates to prove the consistency of our estimations. We use this sample of clusters to map the

[†]https://academic.oup.com/mnras/article/463/2/1446/2892427#78711612

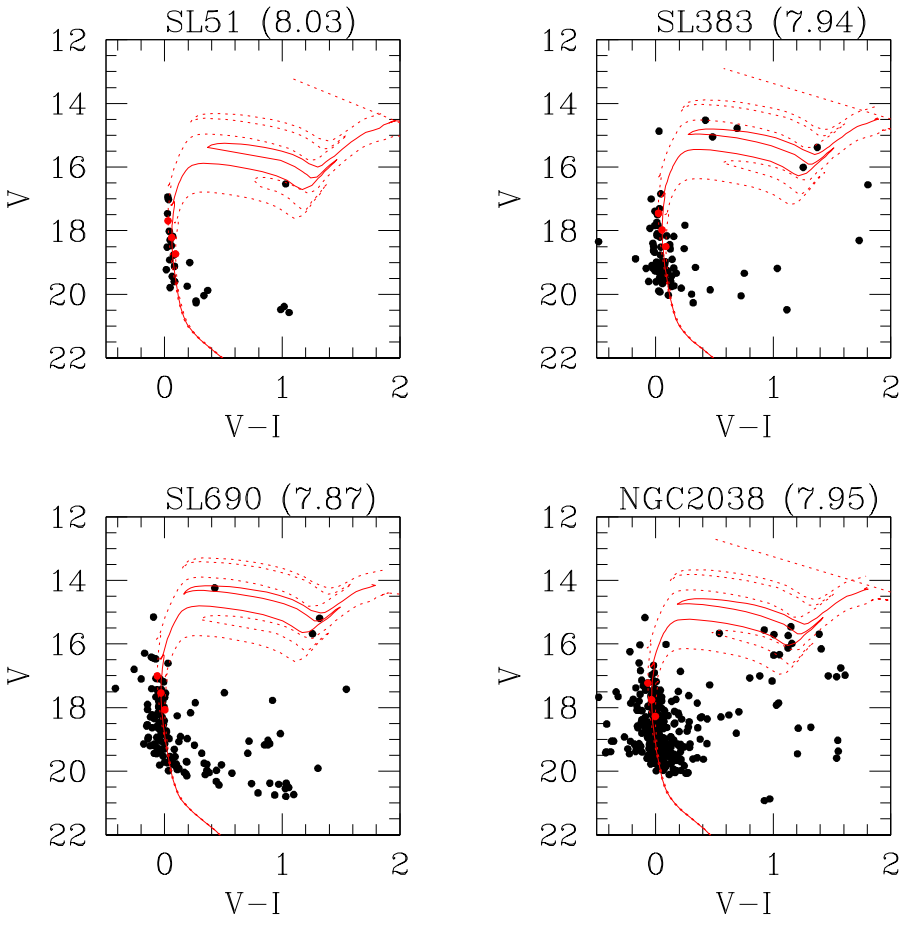

FIGURE 4.1: An example of cleaned cluster CMD from four groups with over-plotted isochrones of estimated ages (red solid line) along with error (red dotted line). The top left panel shows the CMD of SL 51 from very poor group, top right panel shows the CMD of SL 383 from poor group, bottom left panel shows the CMD of SL 690 from moderate group and bottom right panel shows the CMD of NGC 2038 from rich group. CMDs of all 1072 clusters are available online.

demographics of cluster population as a function of age, reddening and richness in the LMC.

4.2 Comparison of age and reddening with previous estimations

Among the clusters studied here, many clusters are common with various previous studies. There are 366 clusters in common with G10, 287 clusters with PU00, 208 clusters with Piatti *et al.* (2014, 2015a) and 131 clusters with Palma *et al.* (2016). We compared our estimations of reddening and age with these studies. Figure 4.2 shows the difference in reddening where the difference is estimated as (our study - previous study). Our estimates compare very well with the reddening estimates of previous estimations, except in the case of Piatti *et al.* (2014, 2015a); Palma *et al.* (2016). The difference in reddening with the estimation of G10 and PU00 is centered around zero, while difference with respect to Palma *et al.* (2016) is centered at 0.1 mag, which is within the error (1 σ) in our estimation. The difference in reddening with respect to the estimation of Piatti *et al.* (2014, 2015a) is centered around -0.1 mag, which is also 1 σ error in our estimation, suggesting that the reddening estimated by Piatti *et al.* (2014, 2015a) is slightly higher than our estimates. We also note that the study by Piatti *et al.* (2014, 2015a) is based on near-IR data, whereas the rest of the studies are based on optical data.

We compared our age estimations with the above mentioned four estimates. In Figure 4.3, we have shown our estimation in the x-axis and the previous study in the y-axis, such that comparison with the four studies are shown in four different panels. A straight line with slope equal to one, is also shown indicating the location of clusters with identical age estimation in both the studies. We have also shown clusters in different groups using different symbols as explained in the Figure 4.3 caption. It can be seen that our age estimations match very well with the estimation of G10, except in a few cases (top left panel (a)). The observed scatter is found to be relatively large for the very poor clusters which is found to decrease for the poor and moderate clusters. In the top right panel, we compared

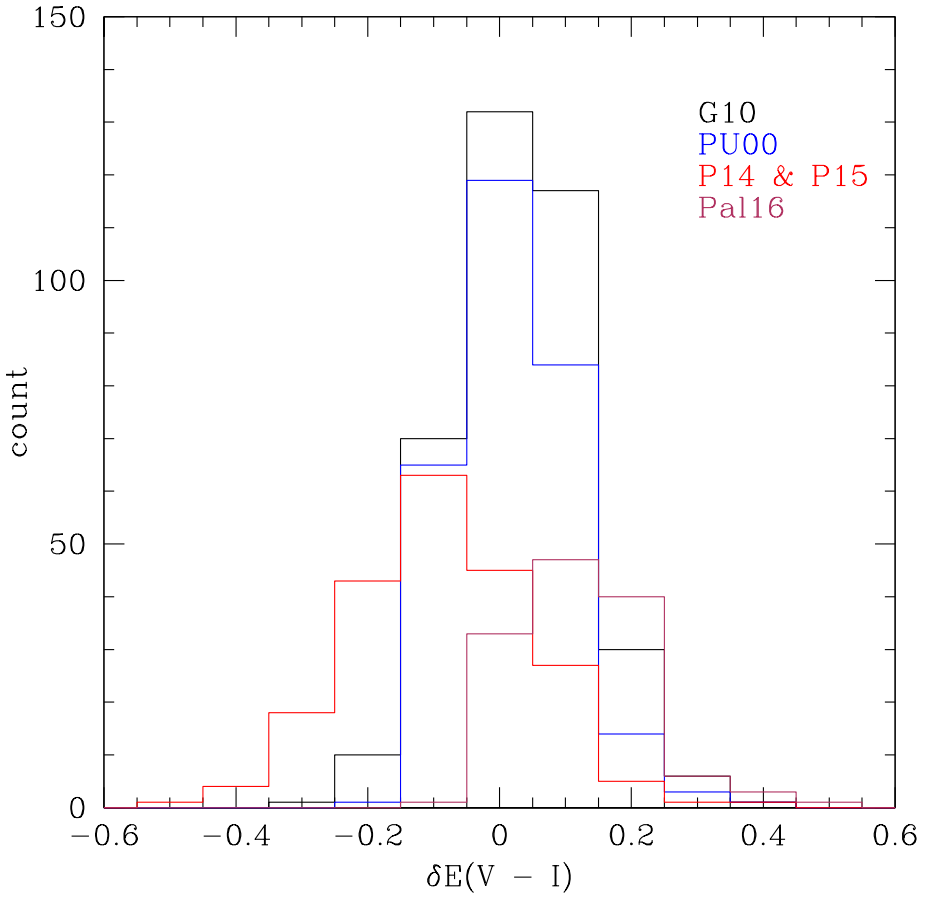

FIGURE 4.2: The distribution of difference in reddening (this study − previous estimation). The previous studies used for comparison are those of G10 (black), PU00 (blue), Piatti *et al.* (2014, 2015a) (red) (in the figure mention as P14 & P15) and Palma *et al.* (2016) (maroon) (in the figure mention as Pal16).

our estimations with those of PU00. In this plot, we can detect two patterns, one almost along the straight line and a horizontal one. The horizontal pattern consists mostly of very poor and poor clusters and two moderate clusters. This pattern suggests that we estimated a range of ages for these clusters, whereas PU00 estimated a constant age of ∼10Myr. We visually checked all the clusters in this pattern and re-confirmed our estimated parameters. We also notice that PU00 estimated relatively older ages for clusters older than 100 Myr, whereas the clusters younger than 100 Myr have ages within the error (as seen from the pattern close to the straight line). We would like to point out that PU00 used OGLE II data which has lower resolution than the OGLE III data. As all these clusters are

located in the bar region of the LMC, effect of crowding may be more severe in the OGLE II data. Also, these authors used isochrone model by Bertelli *et al.* (1994). We speculate that the difference in age estimation noticed here could be due to these reasons. In the panel (c), we compare our estimation with those of Piatti *et al.* (2014, 2015a). There is a large range in age and most of the common clusters are in the poor and moderate category. For clusters younger than 100 Myr, the ages compare very well. For older clusters, we estimated younger ages relative to the estimation of Piatti *et al.* (2014, 2015a). In the panel (d), we compare our estimation with Palma *et al.* (2016). These clusters are mostly older than 100 Myr and we do not detect any systematic trend, but a large scatter.

In summary, the comparison suggests that the age and reddening estimations compare well with the previous estimations, though we do detect discrepancies in the case of a few clusters. The average difference in the estimation of age with G10 is zero whereas age difference with other literature peaks at 0.2 dex. The differences could be due to various reasons, such as difference in the data used, difference in the isochrones and the assumed metallicity and the adopted field star removal process. For example, Palma *et al.* (2016) and Piatti *et al.* (2014, 2015a) used data from bigger telescopes and also different photometric system. Choudhury *et al.* (2015) found that the brighter stars were saturated in the data (which is similar to the data used by Palma *et al.* (2016)) and therefore estimated a relatively older age for young clusters. On the other hand, Piatti *et al.* (2014, 2015a) used near-IR data from the VMC survey and hence a direct comparison is difficult. Piatti *et al.* (2014, 2015a) used the metallicity Z=0.006 and isochrones from Bressan *et al.* (2012). They also mention that the ages are not sensitive to the adopted metallicity. There are also differences in the isochrones used. Palma *et al.* (2016) used theoretical isochrones computed for the Washington system by the Padova group (Girardi *et al.* 2002; Bressan *et al.* 2012) and Geneva group (Lejeune and Schaerer 2001). They have also shown in their Figure 5 that age estimation does not differ much between these two isochrone model. Glatt *et al.*

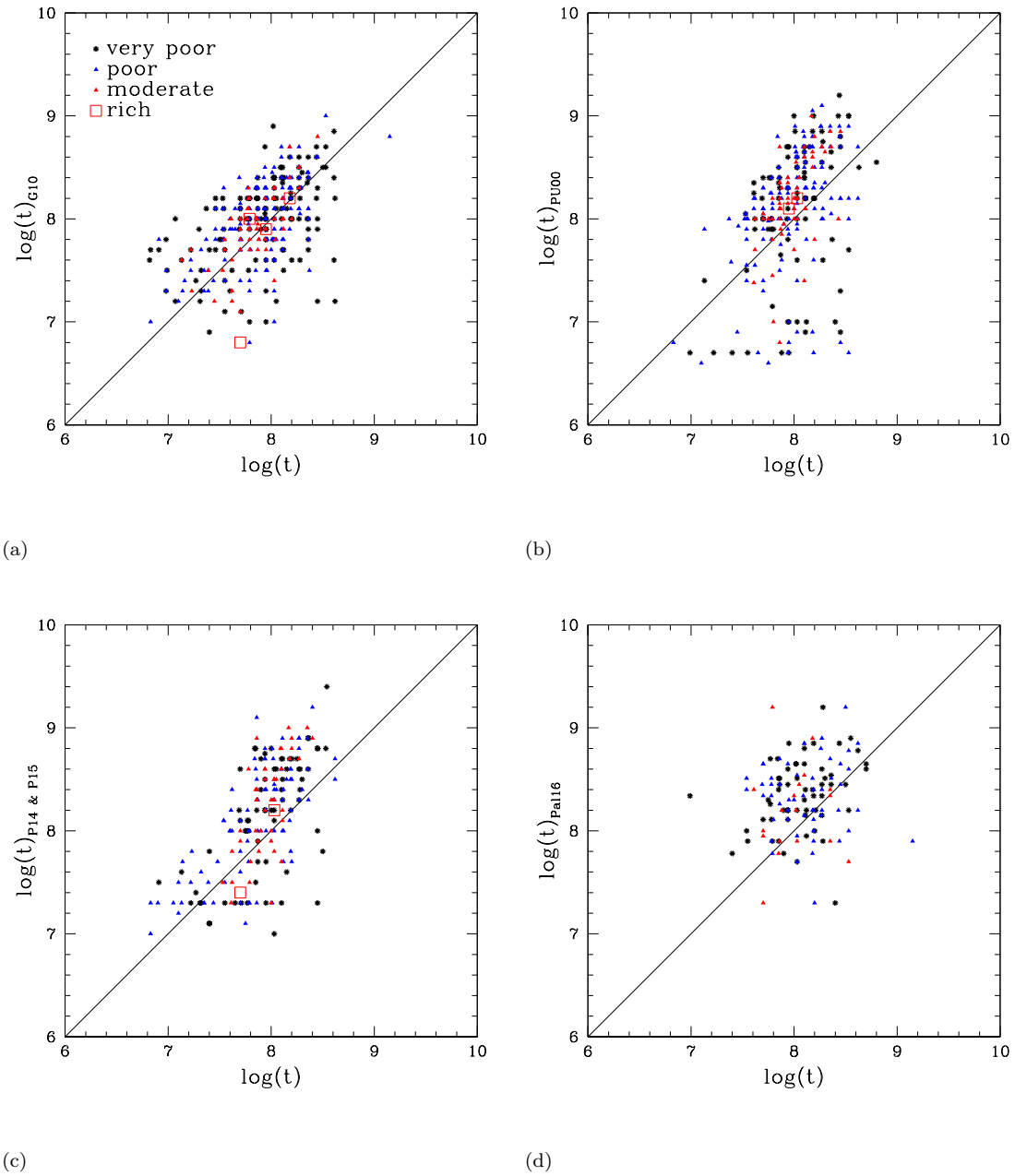

FIGURE 4.3: The previous studies used to compare our age estimation are those of G10 (Fig.a), PU00 (Fig.b), Piatti *et al.* (2014, 2015a) (Fig.c) and Palma *et al.* (2016) (Fig.d). Different point types are used for different group of clusters as mentioned in the top left panel.

(2010) had also used two different isochrone models : Padova isochrones (Girardi *et al.* 1995) and Geneva isochrones (Lejeune and Schaerer 2001).

4.3 Comparison of estimated mass range with previous studies

We found that star clusters in the LMC have a very large mass range (<800 to >5000 $M_{\odot}$), as shown in Table 3.1 in Chapter 3. It can be seen that the mass range we have chosen to group clusters, is similar to the mass range shown in Figure 3 of Baumgardt *et al.* (2013). They restricted their analysis to clusters more massive than 5000 $M_{\odot}$, which are basically *rich* clusters according to our classification criteria. de Grijs *et al.* (2013) analyzed different cluster mass range for estimating cluster mass functions in the LMC. In their Table 2, they used three cluster groups to estimate the cluster mass function, which are, clusters with $M_c > 1000$, 3000 and 10000 $M_{\odot}$ respectively. The clusters in the first group are similar to very poor clusters, those in the second group are a combination of poor and moderate clusters, and the last group consists of rich clusters. Thus, the classification introduced in this study is in tune with the grouping done by earlier studies.

There were previous attempts to group clusters into mass ranges, as mentioned in the above paragraph, primarily to study the slope of the cluster mass function. In these studies, the authors estimated the mass for individual clusters and then estimated the mass distribution. In this study, we classified each cluster according to the mass so that clusters can be pre-selected according to their mass to carry out studies of various properties of clusters which depend on their mass. The clusters of various mass may vary in the formation mechanisms and hence the episodes for cluster formation across the mass spectrum may or may not be similar.

Also, the survival of clusters is a function of mass and hence this classification will greatly help in understanding the dissolution of star clusters. Thus, this classification scheme will be very helpful to understand the formation, evolution as well as survival mechanism of these groups in the LMC. We also note that we have statistically significant number of clusters in these groups, such that we can study their properties as a function of group. We analyze the properties of these groups in the later sections and demonstrate the usefulness of classification.

Here, we compare the mass range of clusters with that of open clusters in the Galaxy. Piskunov *et al.* (2008), in their Figure 2, show the distribution of mass of 650 open clusters with mass range 50 $M_{\odot}$ to 10^5 $M_{\odot}$. Their Figure 5 shows the mass function of Galactic open clusters more massive than $\sim$ 300 $M_{\odot}$. Choudhury *et al.* (2015) found that the mass of the LMC clusters which were identified as probable asterisms were $\sim$ 300 $M_{\odot}$. Lamers *et al.* (2005), in their Figure 9 show the mass distribution of clusters in the solar neighbourhood, which is similar to the estimated mass range shown in Table 3.1. Thus, the LMC cluster mass range is very similar to the mass range of the Galactic open clusters, at least in the low mass end of the cluster mass distribution.

4.4 Reddening distribution across groups

In this section, we compare the reddening of clusters across various groups. The distribution of the estimated reddening is shown in Figure 4.4 for various cluster groups. The estimated reddening is found to be in the range 0.05 - 0.55 mag. The distributions have a peak between the values 0.1 - 0.3 mag in E(V−I) for all the four groups. The distribution is also found to be similar for all the 4 groups of clusters. We also notice that the tail of the distribution towards higher reddening is also similar for the very poor, poor and moderate clusters.

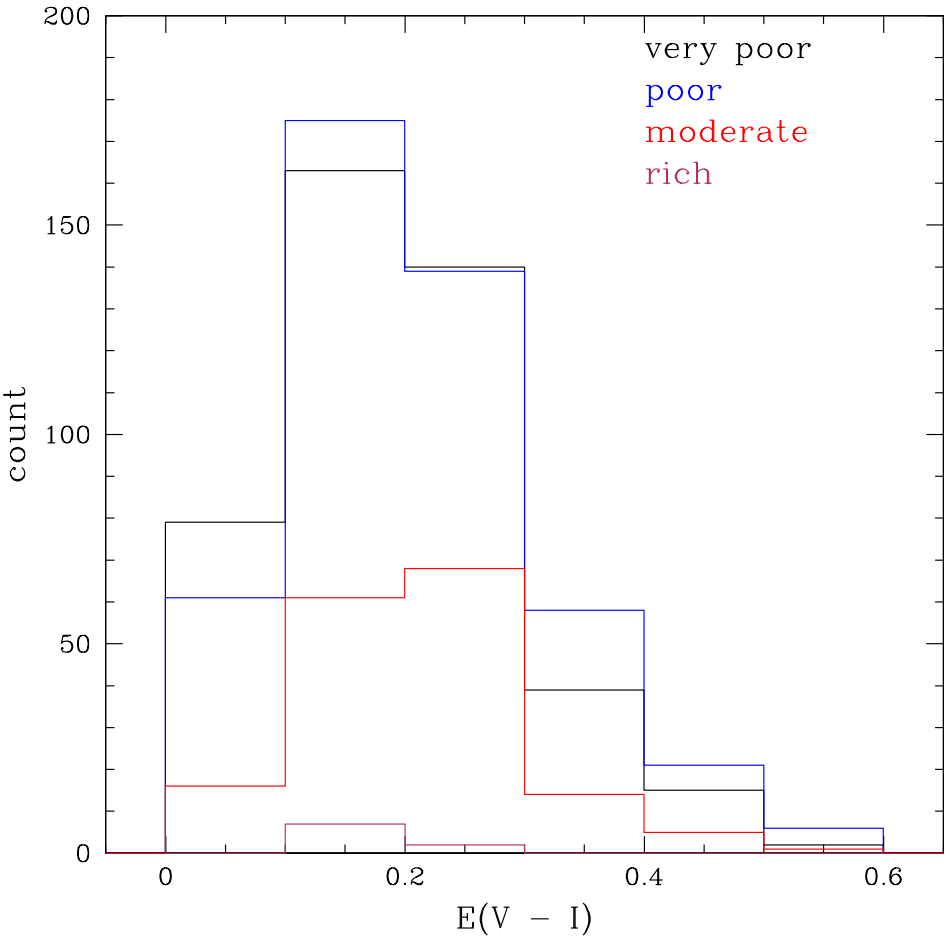

FIGURE 4.4: Histogram of estimated reddening for very poor (black), poor (blue), moderate (red) and rich (maroon) clusters. For all the four groups reddening peaks around 0.2 magnitude.

The distribution of reddening as a function of position is shown in Figure 4.5. Here we have shown all the groups together, as we did not find any difference in reddening among the groups. The Figure shows that the reddened clusters are, in general, located in the central regions. The bar region has a larger range in reddening. The clusters in the south have relatively less reddening, whereas a few clusters located in the south-east corner and east have relatively large reddening. Most of the clusters located near the center of the bar show relatively low reddening, when compared to those located near the ends of the bar. We compared the estimated reddening with those estimated for the field regions by Indu and Subramaniam (2011), which is a high resolution map covering the central LMC.

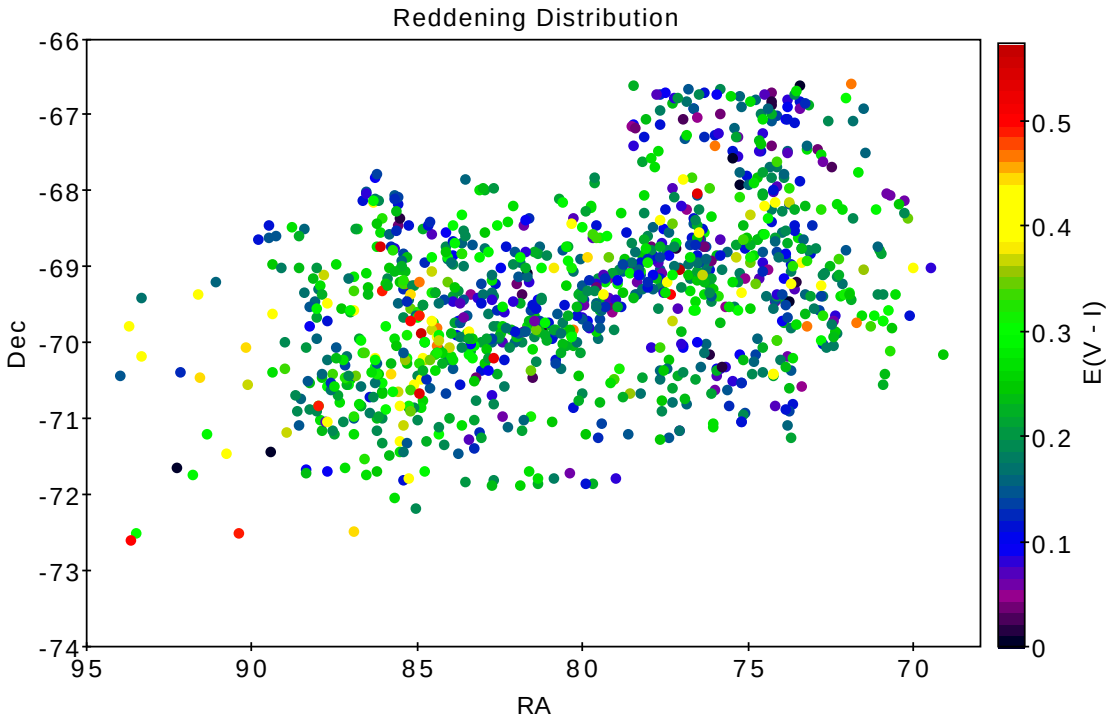

FIGURE 4.5: The spatial variation of estimated reddening for all the clusters.

We did not find any significant variation in reddening with respect to the field reddening.

4.5 Age distribution across groups

The spatial distribution of age of all clusters studied here, is shown in Figure 4.6. The plot indicates the recent sites of star formation in blue and the older clusters are shown as brown. The younger clusters are found to be located in the inner part of the LMC, whereas the older clusters show a more spread out distribution. We can clearly see the southern arm like pattern and also a western counter part with the presence of some young clusters. The LMC is known to be a barred spiral galaxy and the distribution of young clusters in the plot clearly depict the fact. As we have a large sample of clusters, we can study the age distribution of the clusters studied here, as a function of groups. The distribution of the estimated

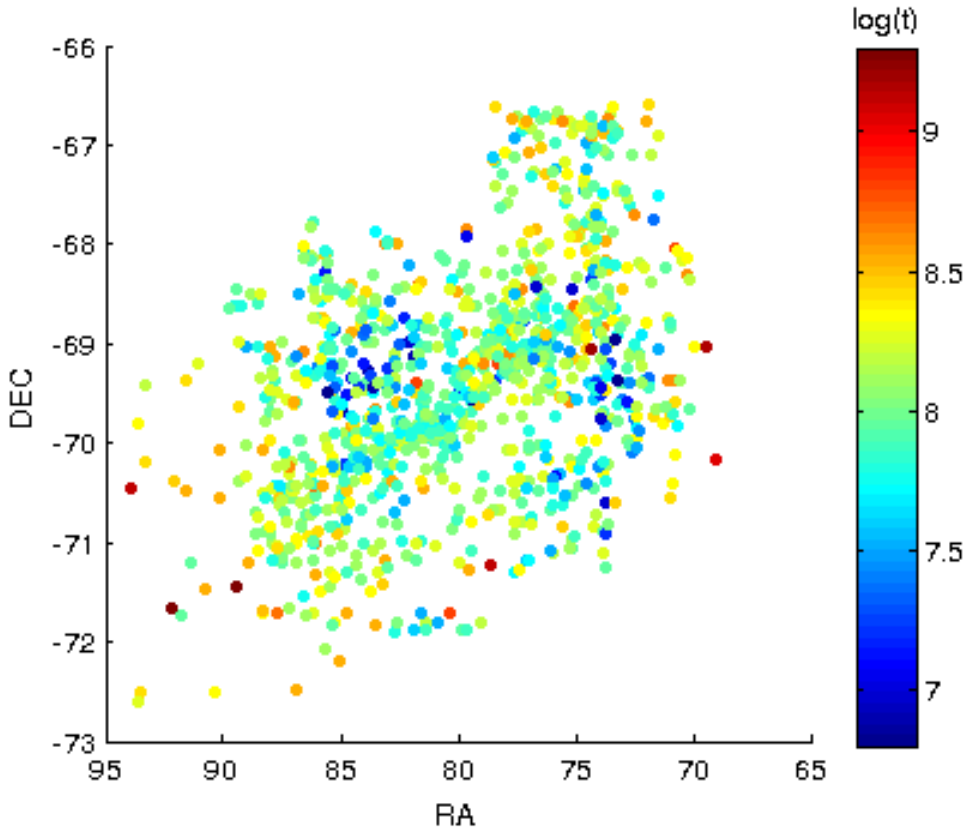

FIGURE 4.6: Plot shows spatial distribution of estimated ages of all the 1072 clusters.

age is shown in Figure 4.7. The age distribution of various groups are also shown separately in the figure. The figure shows that the peak of the cluster age for the poor and the very poor clusters lie in the bin log(t) = 8.0 - 8.2. This peak in the age distribution can be considered to be at 125 ± 25 Myr. We have binned the distribution with a bin size of 0.2 in log scale, as this is the same as that of the error in age estimation. This peak is similar to those found by G10 and PU00. The moderate clusters show a broad peak between log (t)= 7.8 - 8.2 with the mean at 100 Myr. The rich clusters also show a peak similar to the poor and very poor clusters, though their number is very small. This peak is attributed to the interaction between the LMC and the SMC, about 100 - 250 Myr ago (Besla *et al.* 2012; Diaz and Bekki 2011).

The point to be noted is that on the whole, the age distributions of poor and

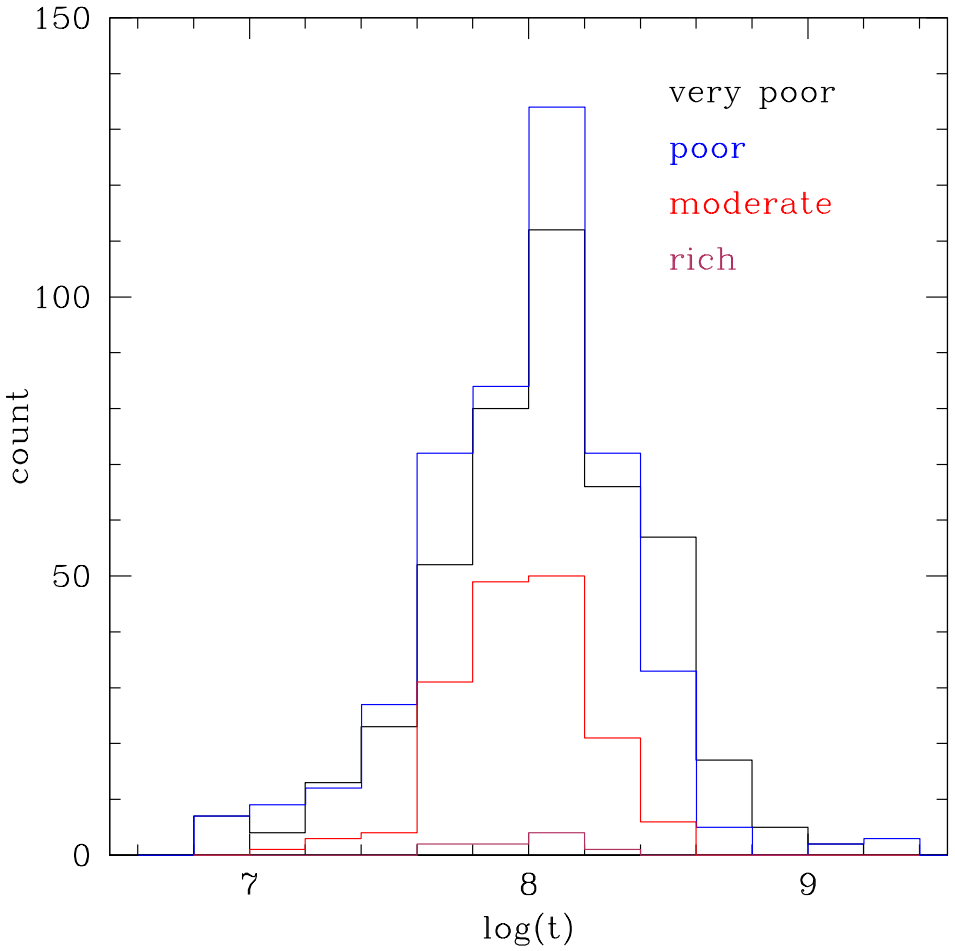

FIGURE 4.7: Distribution of cluster age. Age distribution of very poor, poor and clusters peak between log(t) = 8.0 - 8.2 where moderate clusters has a broader peak (log(t) = 7.8 - 8.2).

very poor clusters are very similar. A careful inspection reveals that the very poor cluster group has more older clusters (log(t) = 8.4 - 8.8), whereas the poor cluster group has more younger clusters (log(t) = 7.6 - 7.8). This trend is found to be more pronounced in the age distribution of moderate clusters, where the peak itself extends to younger ages. The above mentioned trend is observed only up to log(t) = 7.6. Relatively fewer moderately rich clusters are found in the bins older than log (t) = 8.0, up to log (t) = 8.6. If we consider a progressive formation of clusters from the age of log(t) = 8.6 to younger ages, the very poor clusters are formed first, followed by the formation of poor clusters and then the moderate clusters. Thus, in the inner LMC, our study suggests a hierarchical formation of

clusters from low to high, in terms of mass of the clusters. This suggestion needs to be tested in more detail to validate it.

In order to understand the spatial distribution of clusters as a function of age and richness, we have shown the spatial distribution of cluster ages separately for four richness groups in the Figure 4.8. The left top panel shows the spatial distribution of very poor clusters where the color coding is according to the age. It can be seen that the very poor clusters are formed all over the inner LMC. We cannot see the bar clearly, suggesting that the very poor clusters are not preferentially formed in the bar. The top right panel shows the distribution of poor clusters. Their distribution not only delineates the bar clearly, but they are also found located along the bar in the inner LMC. The bottom left panel shows the location of moderate clusters. They are preferentially located in the inner LMC and in the bar region. The rich clusters are shown in the bottom right panel. Thus, we see that the more massive clusters, are preferentially formed in the inner regions and along the bar, whereas the low mass clusters belonging to the very poor cluster group are found in a relatively scattered way. Thus we demonstrate that the formation of clusters in the inner LMC differs as a function of total mass of the cluster. We have been able to demonstrate it because of the classification scheme adopted in this study. It will be interesting to study the details of cluster formation as a function of mass in the regions outside the area of this study.

In order to elaborate this point, we have shown the spatial distribution of all clusters color coded according to number of members in the clusters in Figure 4.9. We can see that the clusters with members less than ~ 50 are spread across a larger area, whereas those with fewer stars are found in the bar and inner regions. In this figure, we also find that the bar region is delineated very well suggesting that, in the inner regions, the clusters are preferentially formed in the bar of the LMC. The clusters are also found to form at the western end of the bar, in a region extending from north to south, roughly perpendicular to the bar. In the eastern side end

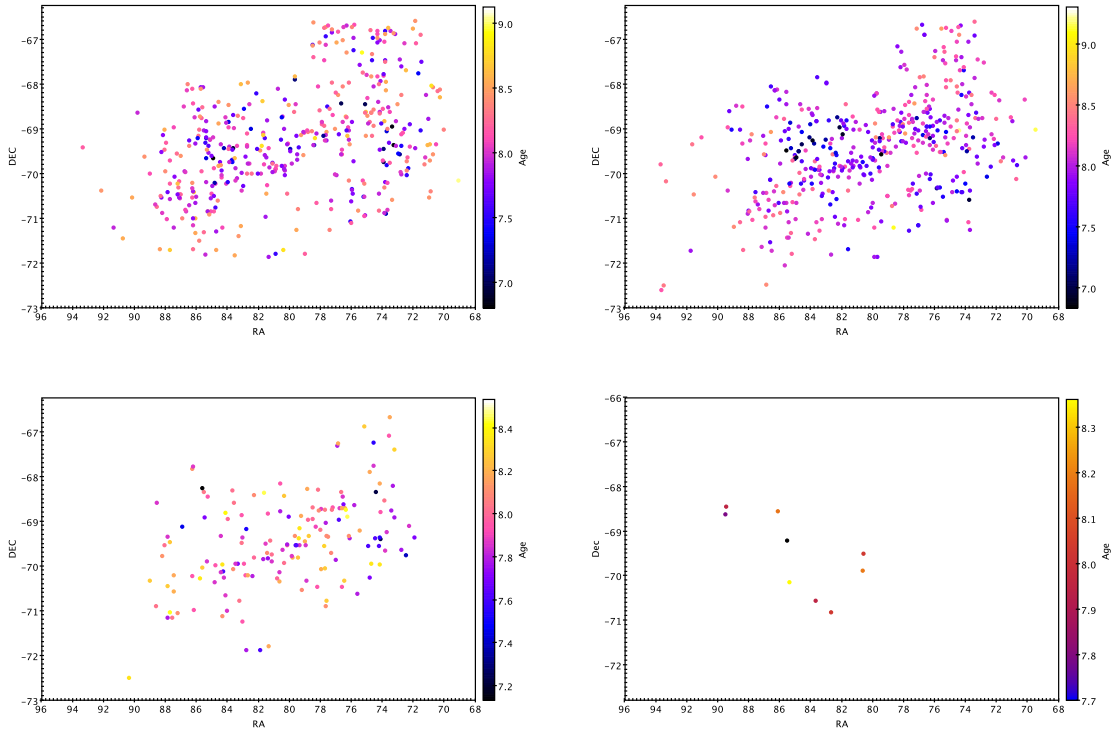

FIGURE 4.8: Spatial distribution of ages in the LMC field for (a) very poor, (b) poor, (c) moderate and (d) rich clusters.

of the bar, we identify two locations of cluster formation. Both the regions start from the bar and extend to the northern regions. The eastern most region has relatively fewer clusters, whereas the inner one has relatively many clusters. The inner one is coincident with the 30 Doradus star forming region and the nearby super giant shells. We also notice an arm like feature in the south, populated with relatively low mass clusters. We have demonstrated that the cluster formation in the inner LMC has taken place in specific locations, in particular, the bar region of the LMC. We also demonstrated that the relatively rich/massive clusters are preferentially formed in the inner LMC, including the bar. These give valuable clues to the formation mechanism of clusters in the inner LMC, as a function of cluster mass.

In the top panels of Figure 4.8, we find that the younger clusters are preferentially formed in the inner regions, whereas the outer regions have older clusters. This

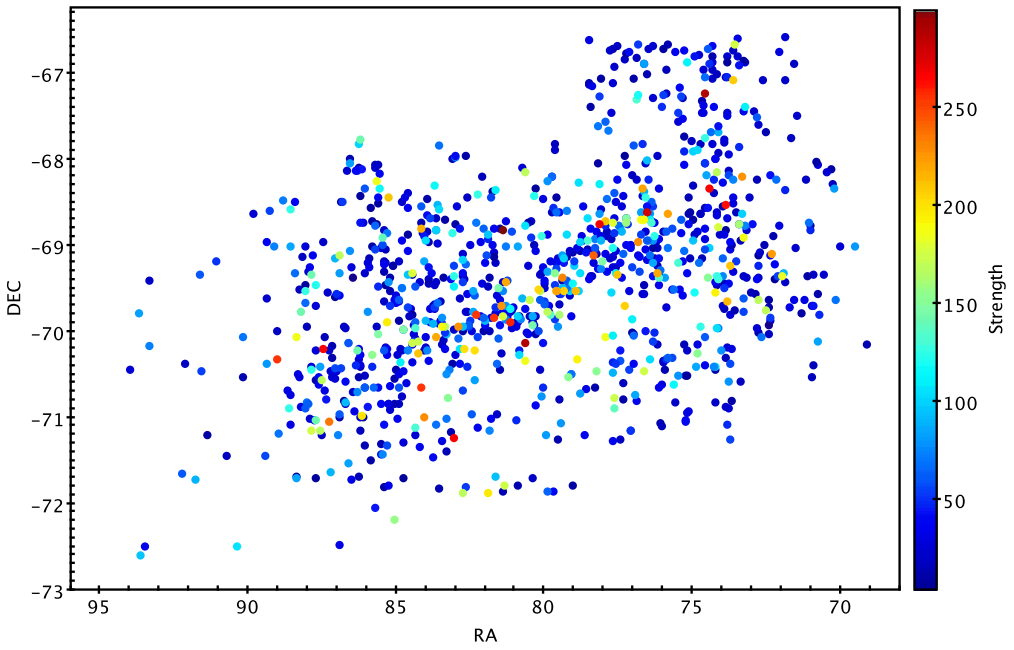

FIGURE 4.9: Distribution of all clusters as a function of strength in the LMC field.

trend is found in all the four richness groups of clusters. This means that, irrespective of the richness of a cluster, we identify a quenching of cluster formation form outside to inside. Combining the above two facts, we find a trend of cluster formation shifting to the central regions for younger ages and to massive clusters. In order to bring out this point clearly, we have created two videos (available online[‡] only), where the formation sequence of clusters are shown. In video-1, we show the sequence from younger to older ages, and in the video-2, we show the sequence from older to younger ages. The videos show clusters of the four groups in four different colors. These clearly suggest that the cluster formation has shrunk to the inner LMC. This is similar to that found for the field stars by Indu and Subramaniam (2011).

This section clearly brings out the advantage of classification of clusters based on groups. We have demonstrated that we are able to detect a significant difference in

[‡]https://academic.oup.com/mnras/article/463/2/1446/2892427#78711612

the spatial distribution of clusters as a function of mass. This study also suggests the importance of including the low mass clusters such as poor and very poor clusters in the cluster formation history of the LMC. The catalog as well as the classification can be used to understand the hierarchical formation of clusters in selected regions of the LMC.

4.6 Cluster formation in the LMC bar

In the last section, we demonstrated that the star clusters in the inner LMC are preferentially formed in the bar region. The video-1 and video-2 suggest that the bar region of the LMC is clearly visible in the age range 60 - 250 Myr. In Figure 4.10, we have plotted the distribution of clusters younger than 63 Myr, 63-251 Myr and >251 Myr, with all the groups put together. In the plots we have also shown the location of the Super giant shells (Kim *et al.* 1999). The younger clusters near the 30 Doradus region are found to be located close to the shells. As seen in the last sub-section, the bar region also has more of the poor and moderately rich clusters. The clusters older than 100 Myr, which is the peak of the cluster formation, is found to be located more towards the ends of the bar. On the other hand, around 100 Myr, we can detect the entire bar to be forming clusters. For younger ages, the clusters are formed preferentially in the central regions of the bar. Therefore, we clearly detect a propagation of cluster formation in the LMC bar, from the ends to the center of the bar. This is similar to that found by Jacyszyn-Dobrzeniecka *et al.* (2016) (OGLE IV Cepheid) and Piatti *et al.* (2015a). On the other hand, using MACHO Cepheids data Alcock *et al.* (1999) found that there is a propagating star formation in the last 100 Myr, along the bar, from southeast to northwest.

Based on our results, we suggest that the bar of the LMC witnessed a burst in the cluster formation during the period 60 - 250 Myr, where the cluster formation

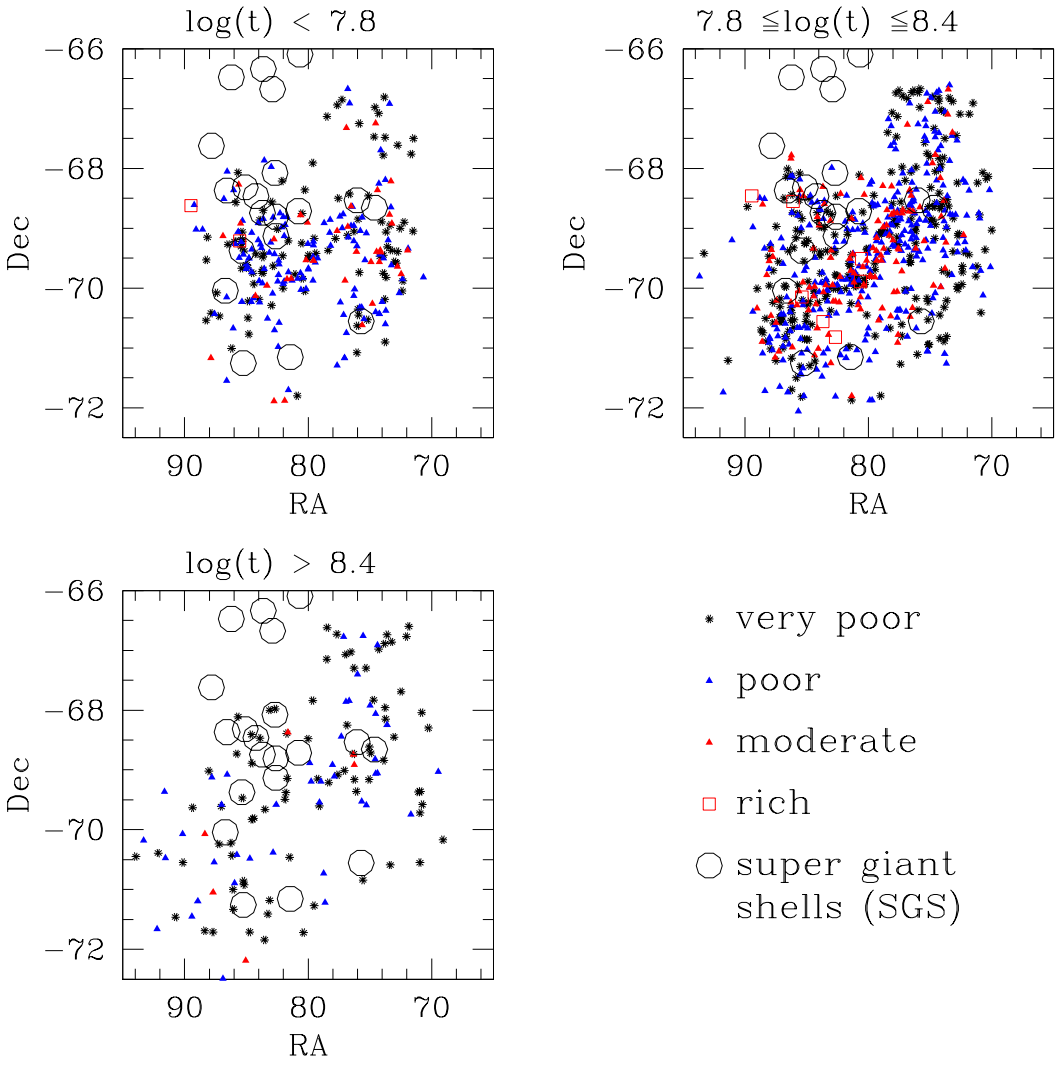

FIGURE 4.10: Distribution of different group of clusters younger than 63 Myr (top left panel), 63-251 Myr (top right) and >251 Myr (bottom left) along with super giant shells (black circle) in the LMC field.

started near the ends of the bar and then proceeded towards the centre of the bar. This could suggest that the bar of the LMC was active during this period and the direction of propagation of cluster formation could also support the idea that the bar was effective in driving the gas towards the central region of the LMC during this period. Thus the LMC bar was active at least up to 60 Myr. We also detected a shrinking of cluster formation in the eastern side of the bar. Between the ages 100 Myr to 60 Myr, the cluster formation is clearly seen to be shrunk to inner regions in the eastern side. We speculate that this may be due to the compression

of gas due to the movement of LMC in the Galactic halo. de Boer (1998) first suggested that the intense star formation currently occurring in the Eastern part of the LMC is due to ram pressure instantiated by the LMC's motion through the hot Galactic halo. Detailed inspection is needed to verify and validate this claim.

4.7 Mass-Radius relation

One of the fundamental relations concerning the structure of the clusters is the relation between the mass and radius of clusters. Since we have a large sample covering a range of strength, we tried to understand the correlation between the radius and strength of clusters. We estimated the number of cluster members in each cluster, which is taken as the proxy for the mass of the cluster. We plotted the radius (in pc) against the n_m and found that it is a non-linear relation. On the other hand, we find that the correlation is a power law, as shown in Figure 4.11. The four groups are shown in different colors and we see a continuous and similar variation across the groups. This shows that there is a fundamental relation between the strength of the cluster and its radius. The strength of the cluster used here is the star count, on the other hand, it is best to use the mass of the cluster instead. In order to obtain a first hand estimation of the slope, we took the average value of radius for the four groups of clusters and used the average of their mass range. The linear fit to the data gives a slope of 2.1 and a y-intercept of 1.4, as shown in Figure 4.12. A relation between the radius and mass of star clusters in the solar neighbourhood was derived by Pfalzner *et al.* (2016). They used the relation $\mathrm{M}_c = \mathrm{C}_m \times R^{\gamma}$, and estimated the value of gamma to be 1.71 for a large range of cluster mass. In our simplified method, we estimate the slope to be 2.1. As mentioned by Pfalzner *et al.* (2016), it is necessary to find if there is a universal mass-radius relation, and the effect of environment on this. In this study, we have attempted to estimate such a relation in the LMC, which has very

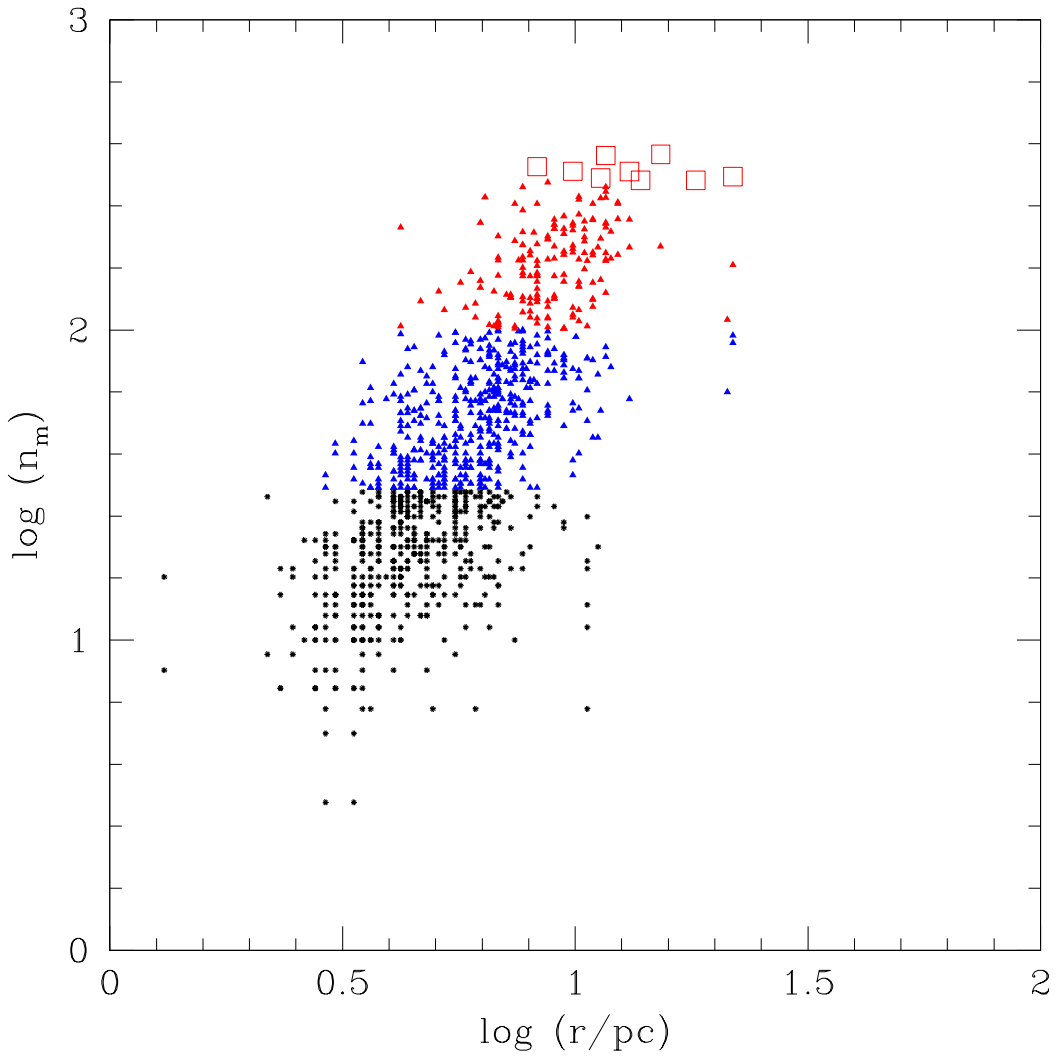

FIGURE 4.11: Correlation between the radius and strength for different group of cluster. The point types used here are similar to Figure 4.10.

different star forming properties, when compared to our Galaxy. We find that the LMC clusters have smaller radii than similarly massive Galactic open clusters. Hence LMC clusters are tightly packed compared to open clusters in the Galaxy.

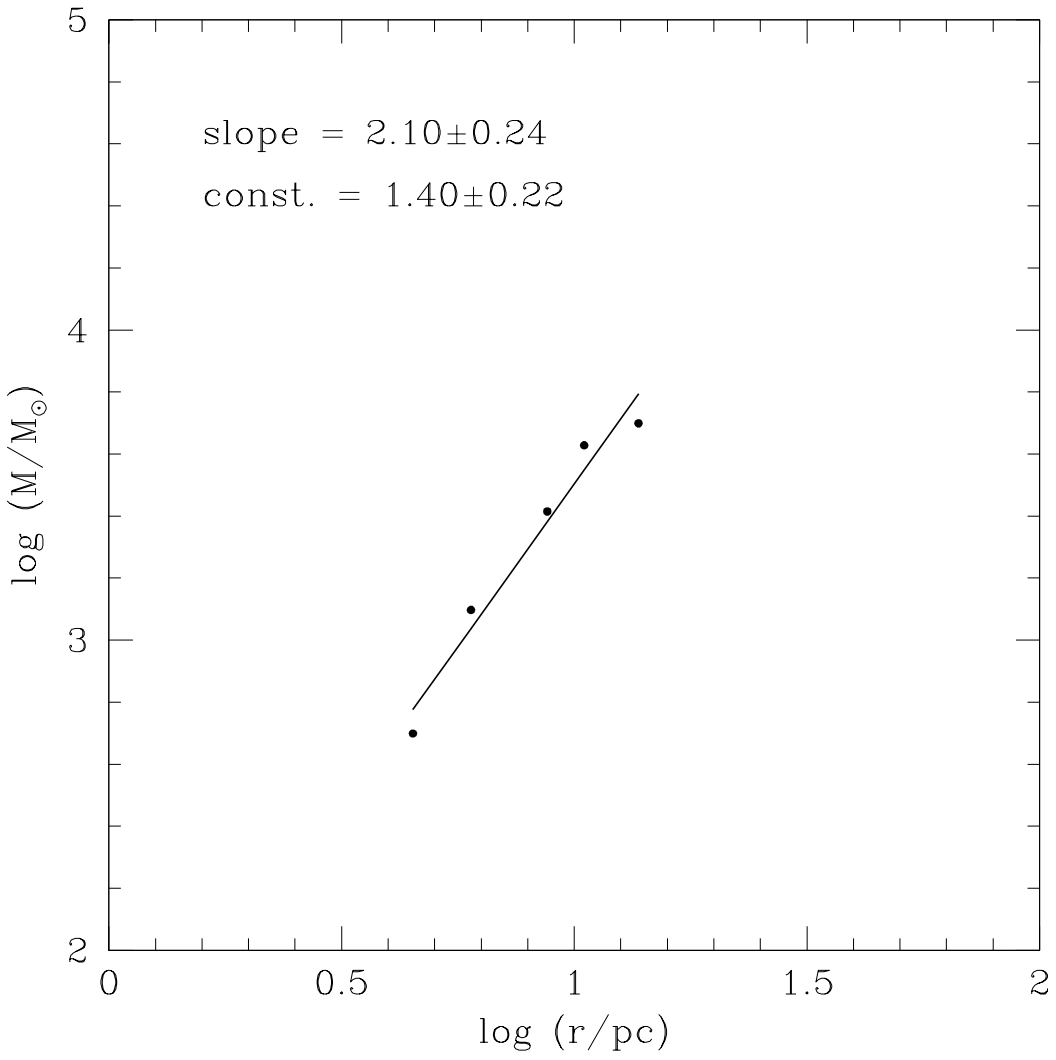

FIGURE 4.12: Correlation between average radius of clusters and average mass of clusters of different groups . Slope and y-intercept of linear fit are also shown.

4.8 Radius and age of clusters

As the MCs have different environment and kinematics when compared to our Galaxy, it will be interesting to study the rate of dissolution of star clusters. Such a study was presented by G10 and they did not find any significant difference in the size of the cluster with age covered in their study. The sample of G10 had clusters of different mass and as the dissolution is a function of the mass of the cluster, especially for the lower mass clusters, it is important to verify this for the

various groups identified in this study. As we have classified clusters as a function of strength, it will be interesting to find out whether there is any change in the radius of the cluster as a function of age, for different groups. We have shown the log - log plot of age against radius in Figure 4.13. The plots are fitted with straight line for different groups, and the coefficients a and b of the equation; log(r) = a×log(t)+b. The value of the coefficient, a, is found to be similar among all the groups, whereas the value of b, is found to be different. This suggests that there is no significant difference between various groups, as far as change is radius as function of age is concerned. Therefore, we have shown the fit to the entire sample in the figure. As demonstrated we do not see any significant change in slope for the various groups, which is similar to the result of G10. This might be due to the fact that the age range considered here is very narrow and hence we might not be able to see any dissolution effect within this age range for any of the groups. Nevertheless, it is interesting to notice that even the very poor group also did not show any indication of dissolution.

4.9 Cluster age and reddening

It is well known that young star clusters have more reddening due to the presence of left-over gas and dust from star formation around the cluster and also, young clusters are found near star forming regions. Over a time, the left-over material disappears and the reddening, in general, reduces with age of the cluster and also, the relatively older clusters are not found near star forming regions. Kawamura *et al.* (2009) studied the Giant Molecular Clouds (GMCs) massive than 5×10^4 $M_\odot$ in the LMC and found average life time of GMCs is $\sim$ 25 Myr. In the case solar neighbourhood GMCs, the value is $\sim$ 10 Myr (Elmegreen 2000b; Hartmann *et al.* 2001; Ballesteros-Paredes and Hartmann 2007). It will be interesting to find the variation of reddening as a function of cluster age.

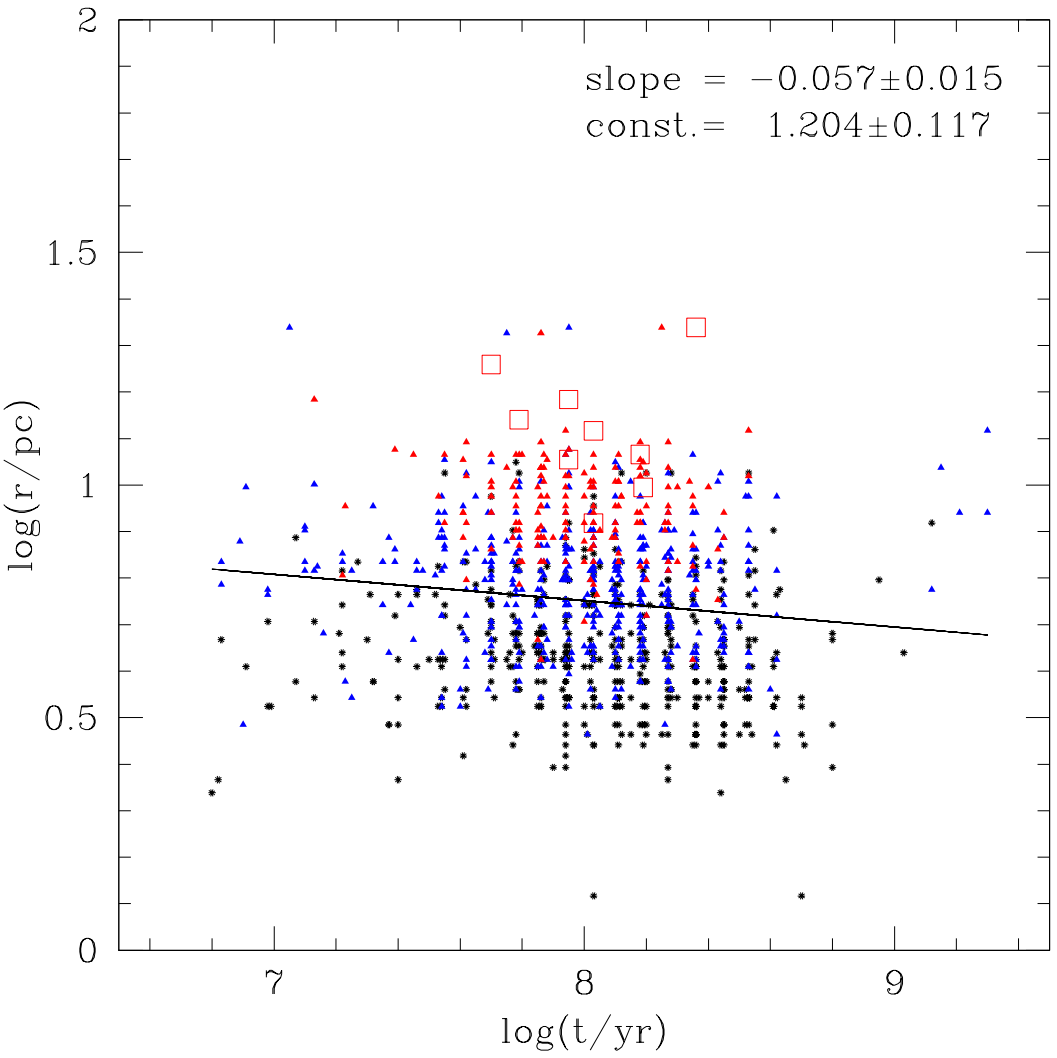

FIGURE 4.13: The distribution of cluster radius with respect to its age. The distribution shows a linear relation with a slope of −0.057. The symbols used here are similar to Figure 4.10.

Figure 4.14 shows the plot of age (log(t)) against reddening, E(V−I), for the four groups of clusters. As we can see, there is a range in reddening for a given value of age, which is due to the range of reddening estimated at various locations. We pay attention to the minimum reddening at a given age. The minimum reddening for a given age is found to decrease with age. The very poor and poor cluster have reddening $\sim$ 0.1 mag in E(V−I), whereas the moderate clusters have slightly higher reddening, for an age of log(t) = 7.0. This reddening is found to decrease with age and found to reach the minimum value of reddening, by the age log(t)

$\sim$ 7.6, for the very poor and poor clusters. In the case of moderate clusters, the reddening reaches a minimum by log(t) $\sim$ 7.8. Thus, we find that the minimum reddening found for three groups of clusters is found to decrease with age and this might suggest that there is dispersal of left-over material from the cluster with age. Our analysis suggests that it takes about 40 Myr for complete dispersal of material in very poor and poor clusters, which is comparable with the lifetime of GMCs in the LMC. Bonatto *et al.* (2012) reported that clusters with age $>$ 30 Myr old are not expected to have differential reddening, which matches with the time scale for the dispersing the remaining ISM for very poor and poor clusters, as suggested from our study. In the case of moderate clusters, we find that it takes slightly longer, about 60 Myr to disperse the material. We are unable to comment on the rich clusters as the sample is small. A similar study has been done by Sagar (1987) with 15 young open clusters but did not find any uniformity in the relationship.

4.10 Summary

We summarize the results of this study below:

1. We have classified and parameterized 1072 star clusters in the LMC using the OGLE III data and presented a catalog (full table available in the online[§] version). The parameters of 308 clusters are presented for the first time.

2. We introduced a classification scheme for the star clusters in the LMC, based on their mass and demonstrated its usefulness.

3. CMDs of 1072 clusters corrected for field star contamination and fitted with isochrones of estimated age and corrected for reddening are made available in the

[§]http://vizier.cfa.harvard.edu/viz-bin/VizieR?-source=J/MNRAS/463/1446

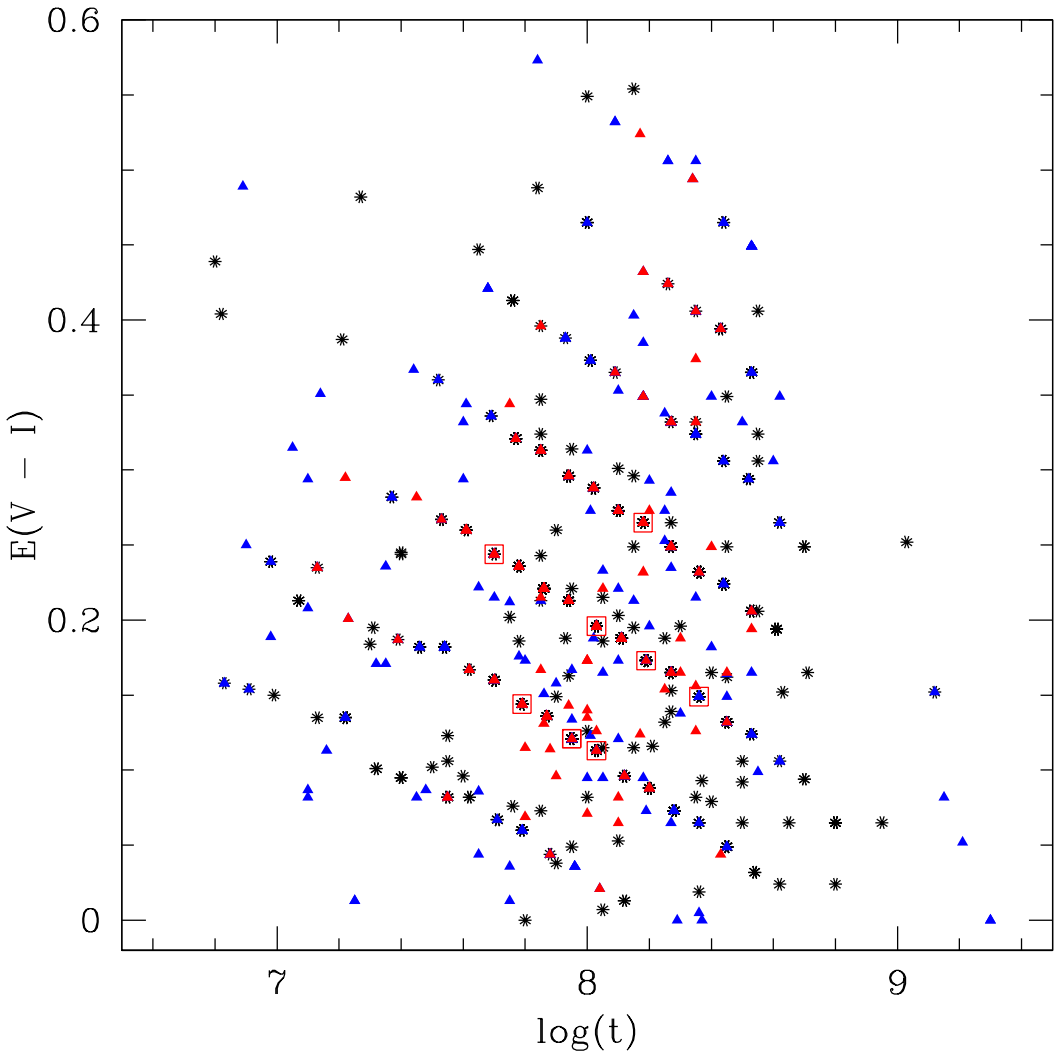

FIGURE 4.14: The distribution of cluster reddening with respect to its age. The symbols used here are similar to Figure 4.10.

online[¶] version.

4. Two videos which show the progression of cluster formation in the inner LMC as a function of age for various groups are available online[‖].

5. We demonstrate that there is a significant difference in the distribution of clusters as a function of mass, using a movie based on the propagation (in space

[¶]https://academic.oup.com/mnras/article/463/2/1446/2892427#supplementary-data
[‖]https://academic.oup.com/mnras/article/463/2/1446/2892427#supplementary-data

and time) of cluster formation in various groups. The importance of including the low-mass clusters in the cluster formation history is demonstrated. The catalogue with parameters, classification, and cleaned and isochrone fitted colour-magnitude diagrams of 1072 clusters, which are available as online material, can be further used to understand the hierarchical formation of clusters in selected regions of the LMC.

6. Our study detects the peak of the cluster formation to be 125 $\pm$ 25 Myr for the very poor and poor clusters, whereas the moderate clusters are found to have the peak at 100 Myr.

7. The bar region of the LMC is found to be active in cluster formation during the period 60 - 250 Myr. We also suggest a progression of cluster formation from the ends of the bar to the central region of the bar during the above period.

9. The low mass older clusters are found to have a scattered distribution whereas the more massive younger clusters are found in the inner LMC. We find evidence for outside to inside propagation of cluster formation.

8. We estimate a mass-radius relation for the LMC cluster. We find that the LMC clusters are tightly bound when compared to the open clusters in the Galaxy.

9. We demonstrate that the lower mass range of clusters found in the LMC is very similar to the open clusters in the Galaxy and that the LMC hosts a large number of such clusters.

TABLE 4.1: A sample of full catalog is presented here. The table contains the name of the cluster, central coordinates (RA and Dec) as in B08, size of the cluster taken from B08, estimated reddening and age in the columns 1-6 respectively. Columns 7-10 represent the earlier estimations of ages by G10 ($\log(t_{G10})$), PU00 ($\log(t_{PU00})$), Palma *et al.* (2016) ($\log(t_{Pal16})$) and Piatti *et al.* (2014, 2015a) ($\log(t_{P14,P15})$). The last column represents the designated group number (I-V) of cluster.

Star cluster	RA (h m s)	Dec (° ′ ″)	Radius (′)	E(V−I)	log(t)	$\log(t_{G10})$	$\log(t_{PU00})$	$\log(t_{Pal16})$	$\log(t_{P14,P15})$	Group
KMHK15	4 36 20	-70 10 22	0.30	0.25	9.03	-	-	-	-	I
SL8	4 37 51	-69 01 45	0.75	0.08	9.15	8.80	-	9.20	-	II
SL12	4 39 59	-69 01 44	0.40	0.41	8.35	-	-	-	-	I
SL14	4 40 28	-69 38 57	0.55	0.12	7.95	8.30	-	-	-	II
SL15	4 40 43	-68 21 21	0.65	0.35	8.18	8.70	-	-	-	II
KMHK32	4 41 00	-68 18 04	0.29	0.19	8.61	-	-	-	-	I
BSDL2	4 41 09	-68 07 53	0.24	0.07	8.36	8.40	-	-	-	I
LW25	4 41 46	-68 10 18	0.43	0.25	8.27	-	-	-	-	I
LW28	4 42 10	-69 21 50	0.38	0.27	8.10	8.40	-	-	-	I
NGC1673	4 42 39	-69 49 12	0.49	0.24	7.70	7.70	-	-	-	II

Chapter 5

Stellar mass function and cluster mass function of LMC clusters

5.1 Introduction

The stellar initial mass function (IMF) plays a vital role in astrophysics. The relative number of stars formed as a function of mass has implication on a wide variety of astrophysical topics starting from gravitational waves to formation of planets. In general the best estimate of this quantity comes from the studies of young star clusters in our Galaxy and nearby galaxies where one can resolve individual stars. The rich young clusters in the LMC have been the target of studies of IMF (Mateo 1988; Sagar and Richtler 1991; Sagar 1995; Kumar *et al.* 2008). Young clusters in the LMC are generally considered to be dynamically un-evolved and hence their mass function estimates approximately represent the IMF. As we have parameterized a large number of star clusters in the LMC in this study, it is natural to explore the nature of the mass function in these clusters.

In the previous chapter, we identified and discussed the mass range present among the LMC clusters. We also presented and discussed a classification scheme of the LMC clusters based on their mass range and strength. Initially we grouped the clusters based on cluster strength and then estimated mass range for each group by constructing synthetic CMD for Salpeter′s mass function using M08 isochrone (Marigo *et al.* 2008). We found that LMC shows a burst of cluster formation ∼100 Myr ago and most of the studied clusters are younger than 300 Myr. Therefore we used an age of 100 Myr to construct the synthetic CMDs. Now, as we have parameterized the sample in our study, it will be good to estimate the mass of individual clusters and the stellar mass function (MF) of the LMC clusters using their corresponding age and luminosity function. We can also examine the variation in stellar MF among the LMC clusters. The age and stellar MF of individual LMC clusters will help us in determining the actual mass of the cluster and to put better constraint on the mass range present in the LMC. We have also studied mass-radius relation for LMC clusters. The mass estimation of individual clusters will help us to improve the mass-radius relation.

Estimation of the mass function of star clusters of LMC, in a homogeneous way is a worthwhile exercise. There have been previous attempts to study the cluster mass function (CMF) in the LMC which is found to follow a power law relation : $(dn/dM_c) = M_c^{\alpha}$, where M_c is mass of cluster, dn is number of clusters present within a mass range M_c to $M_c + dM_c$ and α is slope of the mass function. Chandar *et al.* (2010) showed that LMC clusters more massive than 10^3 $M_{\odot}$ follow a CMF slope value of -1.8 ± 0.2 for ages up to one Gyr. de Grijs and Anders (2006) suggested the value of $\alpha = -2$ for clusters older than 100 Myr, whereas a shallower slope is proposed for younger clusters. Hunter *et al.* (2003) studied ∼900 clusters in the LMC and SMC using ground based integrated photometric data obtained in UBVR pass bands and found that clusters in both the Clouds follow a range of α $= -2$ to -2.4, nearly independent of their ages. Popescu *et al.* (2012) reanalyzed the data published by Hunter *et al.* (2003) and determined a smaller value of $\alpha =$

-1.5 to -1.6 for clusters younger than a few Gyr and more massive than 10^3 $M_\odot$.

In this chapter we present the mass function estimates of 66 star clusters in the LMC. We also examine the range in mass function, total cluster mass among the clusters and estimate the CMF.

5.2 Luminosity function (LF)

Luminosity function (LF) is defined as the frequency distribution of stellar luminosities among MS stars within a cluster. In order to generate a LF of a cluster, there has to be a sufficient number of stars spread over a large range in luminosity to get a statistically significant number of stars per unit luminosity. Table 3.1 of Chapter 3 suggests that ∼84% cataloged clusters (898 out of 1072) are classified as very poor or poor clusters with number (n_m) of cluster member less than 100. It is difficult to create a statistically significant LF for these clusters. Therefore, we restricted our analysis to 165 moderately rich ($100< n_m <300$) young clusters and generated the LF of the main sequence stars present in them. We binned main sequence of the clusters along the magnitude axis in different bin sizes based on magnitude. We have used three bin sizes: 0.4 mag for stars brighter than 17 magnitude, 0.3 mag for stars having brightness between 17.0 and 18.2 magnitudes and 0.2 mag for stars fainter than 18.2 magnitude. We considered different bin sizes in order to get statistically significant count in each bin. We reduced the bin size from 0.4 to 0.2 with the increase in magnitude value, as the number of stars increase rapidly in the lower mass limit in accordance with the initial mass function of a star cluster. Considering different bin sizes also helped to get more data points within a fixed range of luminosity. To get real LF of a cluster, we have included the correction due to incompleteness factor of the observed data. As discussed in Chapter 2, in our study we considered stars having photometric completeness

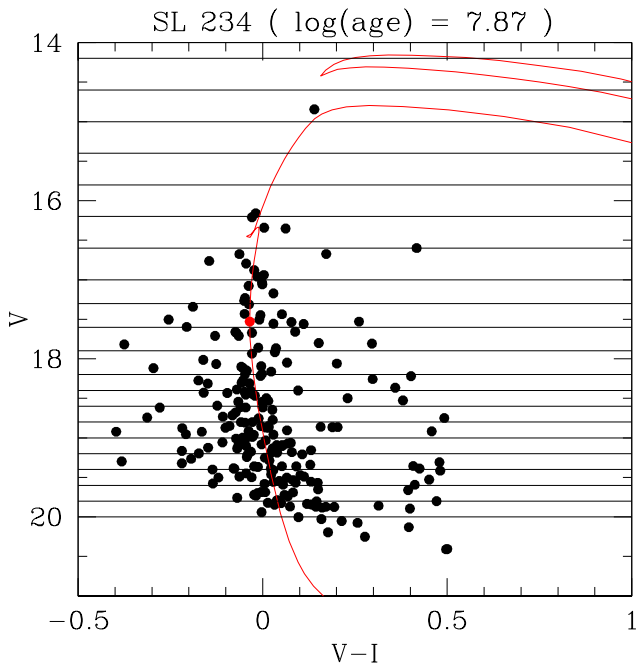

FIGURE 5.1: The plot shows the CMD of SL 234. An isochrone (red line) for corresponding age of the cluster is over-plotted after correcting for reddening and distance modulus. Turn-off point of the isochrone is marked with red dot. The black lines parallel to the color axis indicate the bin sizes considered to generate LF of the cluster.

value more than 90% and photometric error less than 0.15 magnitude in both V and I bands. We did not consider the bins whose average magnitudes are brighter than the turn-off magnitude of the corresponding cluster to avoid including giant stars. In Figure 5.1, we have shown the CMD of the cluster SL 234. The plot also shows the different bin sizes considered to construct the LF of the cluster. The red line represents the isochrone of corresponding age (7.87 in log scale, mentioned at top of the plot) and the red dot denotes the turn-off point of the cluster. We did not consider luminosity bin for magnitudes fainter than 20 as the completeness of the data is less than 90%.

To construct stellar mass function of a star cluster from its LF, one has to know the basic parameters of the cluster such as distance modulus, metallicity, age and reddening. The parameters will help to identify appropriate stellar evolutionary models and convert the luminosities of stars into masses. In Chapter 4, we have

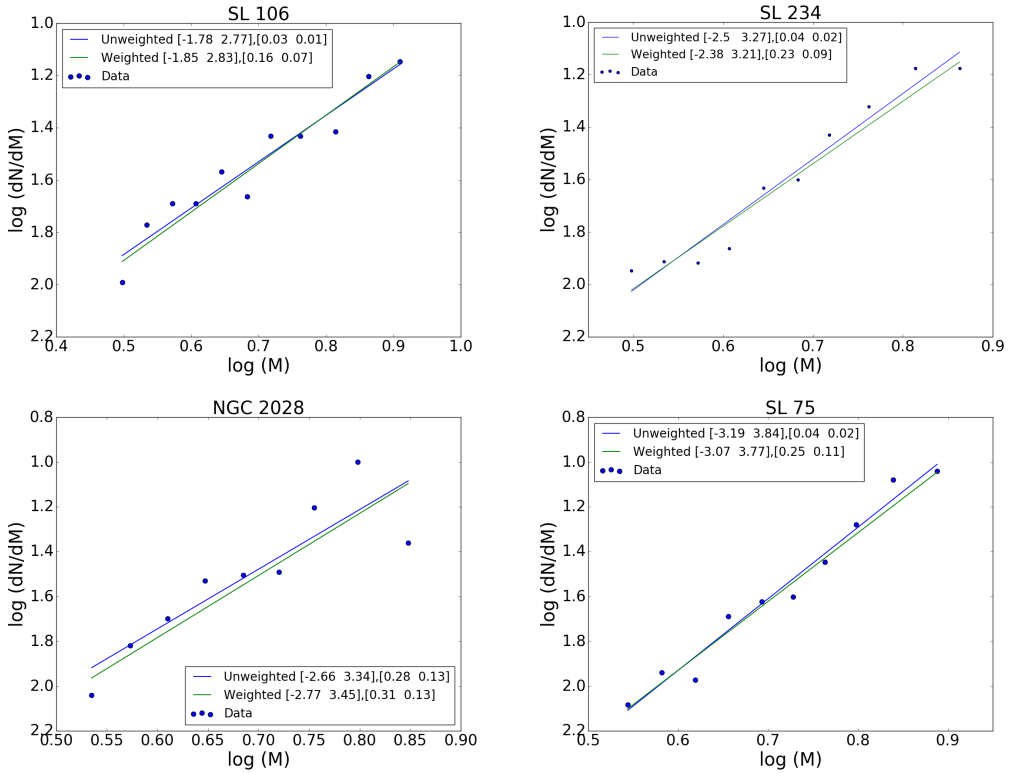

FIGURE 5.2: The figure shows the frequency distribution of stellar masses (dN/dM) against stellar mass (M) in the logarithmic scale of four clusters. Clusters' names are noted on top on each plot. The blue and green lines indicate the ordinary and weighted least square fit to the data points. Slope, constant and their respective errors are also noted in the figure.

already estimated the age and reddening of the LMC star clusters. For all the clusters, we considered average metallicity (Z) and distance modulus (DM) of the LMC as 0.008 and 18.5 magnitude respectively. Magnitude values of each bin of the LF are converted to mass range using mass-luminosity relation obtained from M08 isochrone model for LMC metallicity and OGLE-III filter systems, after correcting for DM and extinction of the corresponding cluster. The average mass value of each bin is considered as the mass of the stars within the bin. Then we divided the number of stars present (dN) in each bin by its corresponding mass range (dM), which gives the frequency distribution of stellar masses (dN/dM) of the cluster. We plotted (dN/dM) against the average mass value of corresponding bins in log scale (Figure 5.2) and fitted with a least square straight line (blue line) to get the slope of the mass function of the cluster. We have also performed

weighted fit (green line) to the data points (blue dots) in order to improve the fit and to obtain better estimation of the mass function slope (MFS). In the weighted fit, weightage is given to the data points based on their variance, the points largely deviated from the expected value are given lower weights. The uncertainties in M is obtained from difference of mass range correspond to the two ends of a bin times $(dN)/2$. The square-root value of (dN/dM) defines its uncertainty. In Chapter 4, we noticed that some of the LMC clusters show gaps in the MS, leading to fewer stars in the mass function bin than expected. This can lead us to a wrong estimation of MFS value by using equal weightage to each data point. In the case of weighted fit, less weight gets assigned to the deviating bins corresponding to gaps.

5.3 Stellar mass function (MF) of LMC clusters

Out of 165 moderately rich young clusters, we estimated the stellar MF of 91, as the remaining clusters suffer from multiple gaps in the MS, or large spread in the CMD along the color axis, making them not suitable for reliable MF estimates. We found that the MFS values of the 91 clusters have a large range as shown in Figure 5.3, mainly ranging from -1.2 to -3.8. We found one cluster (H9) with very high MFS value (-5.69), which is not shown in the figure. The figure also shows the MFS error as a function of the value of MFS. The steeper MFS values are in general found to have relatively large errors. In order to understand the pattern of distribution of MFS, we presented the distribution of MFS values in the upper panel of Figure 5.4. The figure shows that most of the LMC clusters have MFS values between -1.50 to -3.25. The peak of the distribution lies between -2.0 to -2.5. In the lower panel we plotted the distribution of errors associated with derived MFS values, which we use to eliminate MFS estimations with relatively large errors. The distribution clearly suggests that most of the clusters have error

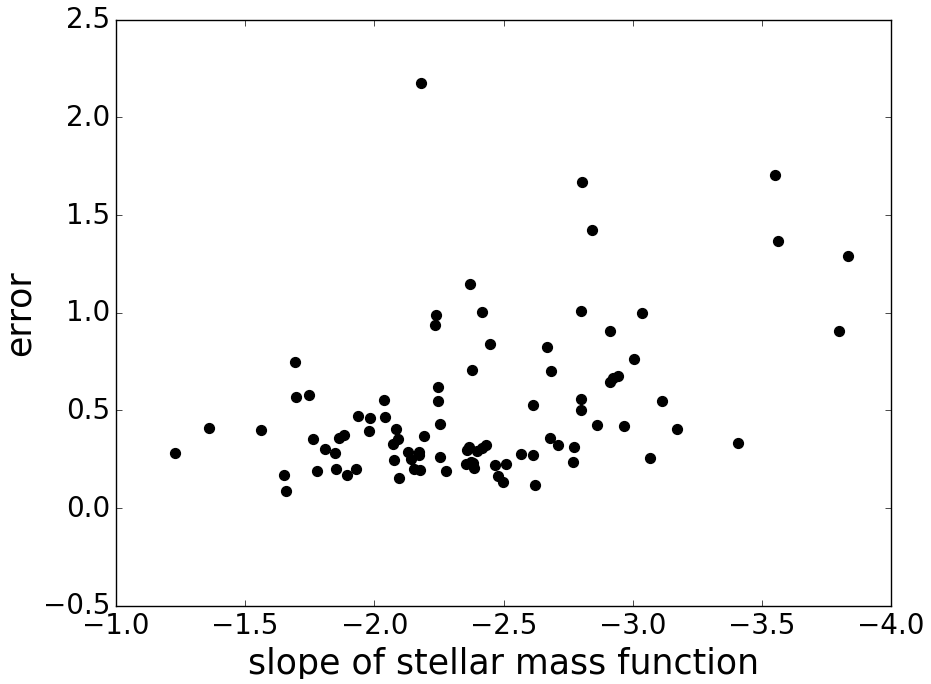

FIGURE 5.3: The figure represents the distribution of estimated stellar MFS against error associated with it. The figure suggests that the clusters with slope values steeper than −2.5 tend to have larger error.

in MFS less than 0.6. Therefore, we excluded the clusters having error in MFS larger than or equal to 0.6 from further analysis. So, we are left with 66 clusters now. The median value of error in the MFS is 0.369.

In the Figure 5.5 we have shown the distribution of MFS for those 66 clusters. The distribution ranges from −1.23 to −3.41, with most of the MFS values between −1.5 and −3.0. Figures 5.4 & 5.5 suggest that the clusters with MFS value steeper than −2.5 exhibit relatively large error in MFS. The second peak in MFS distribution found in Figure 5.4 between −2.75 and −3.0 disappeared in Figure 5.5, as only estimates with smaller errors are considered. We also fitted a Gaussian function to the distribution and found the peak to be at −2.26 with a standard deviation of 0.44. The 1-σ width of the slope of stellar MF ranges from −1.82 to −2.7. The mean of this distribution is found to be very similar to the IMF value given by Salpeter (1955) for the field stars in the solar neighbourhood.

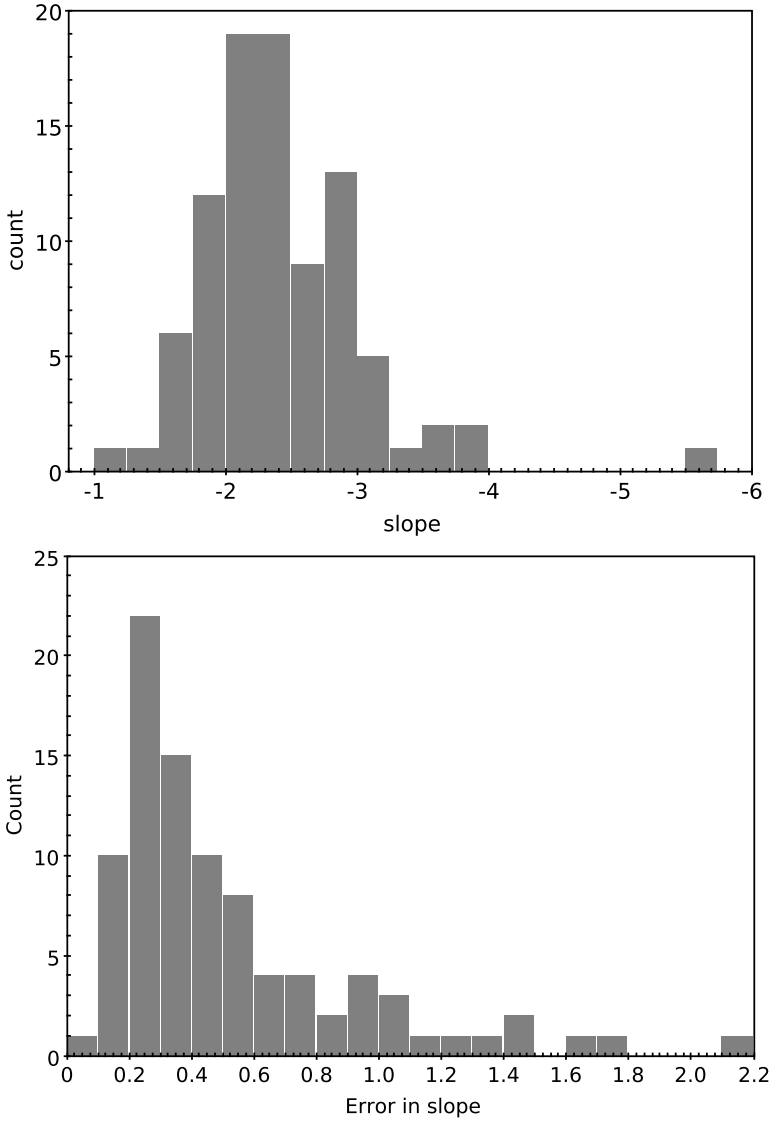

FIGURE 5.4: Top panel of the figure shows the distribution of stellar MFS. The distribution peaks between −2.2 to −2.4, similar to the initial mass function given by Salpeter (1955). The bottom panel shows the histogram of errors associated with the slope values.

The cluster sample has only clusters younger than 200 Myr, as shown in Figure 5.6. The stellar mass range considered for the slope is mainly in the range of 8 - 3.5 $M_{\odot}$. In some cases the upper mass limit goes beyond 10 $M_{\odot}$, with the highest mass considered being 13.9 $M_{\odot}$, in the case of the cluster SL 134 (which has a MFS of −2.5, for a lower mass range of 3.6 $M_{\odot}$). The lower mass limits are more or less the same for most of the clusters, and the lowest mass considered is 2.8 $M_{\odot}$ for a few clusters. The number of data points used for the fit range between 13 -

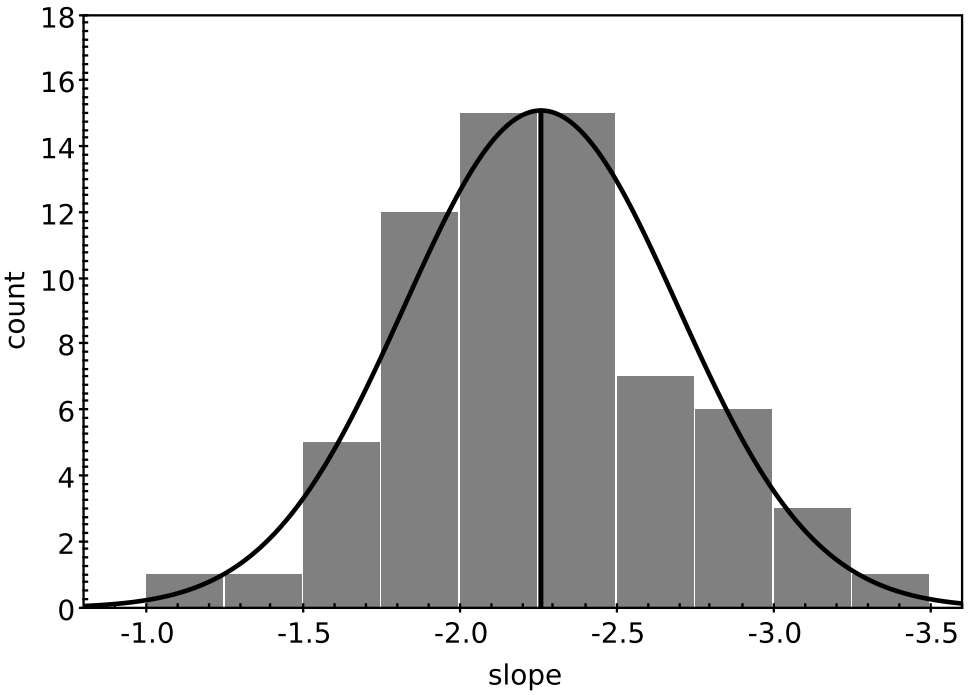

FIGURE 5.5: Distribution of stellar mass function with error less than 0.6 is shown in this figure. The distribution shows a peak between -2.0 to -2.5. A Gaussian function is fitted to the distribution, which provides a peak value of -2.26 and a standard deviation of 0.44.

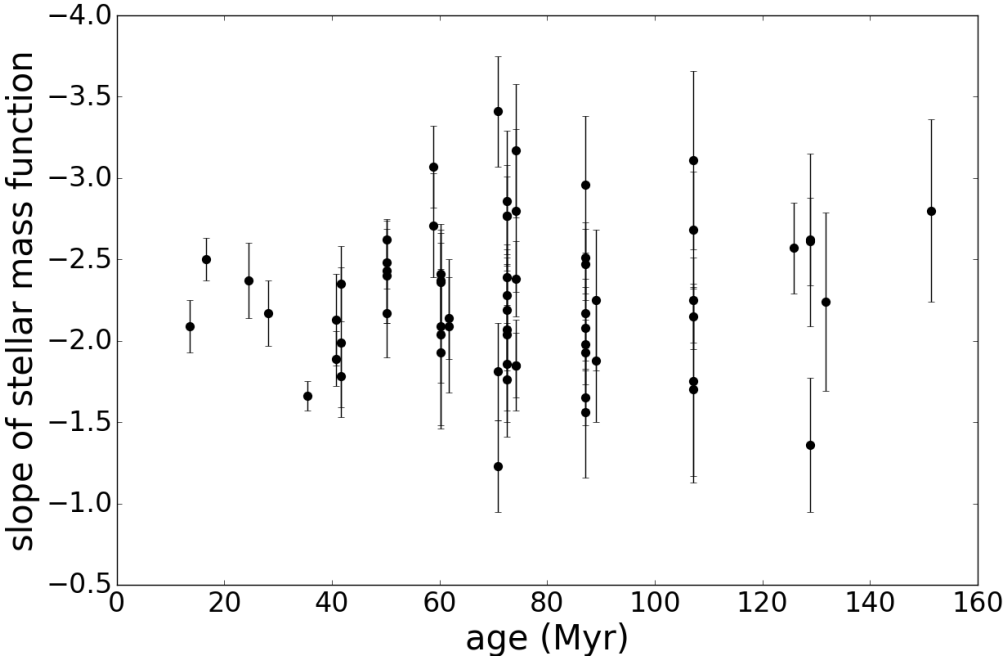

FIGURE 5.6: Stellar MFSs of the LMC clusters are plotted against age (for error in slope less than 0.6). Most of the clusters lie between 10 to 140 Myr age range.

7. We also note that the estimated value of the MFS does not depend on (1) the considered mass range, (2) the age of the cluster or (3) the number of data points.

In Table 5.1 we have listed all 66 clusters along with the estimated parameters. Columns 1, 2 & 3 represent the name, age (in log scale) and radius (in pc) of the clusters, columns 4 & 5 represent the upper and the lower mass limit of stars within the clusters which are used to calculate the mass function respectively and in column 6 we have noted the number of bins used to estimate the MFS. The slope and constant of the mass function are noted in the columns 7 & 9 respectively. The errors associated with the slope and constant are presented in the columns 8 & 10 respectively.

5.4 Total mass of individual clusters

We estimated the mass of individual clusters using their MFS. We have extrapolated the mass function from turn-off mass of corresponding cluster down to 0.15 $M_\odot$ and integrated the MF to get the total mass of the cluster. We have binned the mass range (from turn-off mass to 0.15 $M_\odot$) and calculated the number of stars present in that bin using the estimated mass function. The number is then multiplied with average mass of corresponding mass bin to get the stellar mass present in that bin. The cumulative mass of all the bins provides the total mass of the cluster (M_c). We have considered different bin sizes depending on the stellar mass. We chose a larger bin size (1 $M_\odot$) for higher mass ($\geq$8 $M_\odot$) and reduced to 0.05 $M_\odot$ near the lowest mass limit (0.15$M_\odot$). We have reduced the bin sizes with decreasing mass as the number of star increases rapidly with decrease in mass. We have also tried with different sets of bin sizes and noticed that a change in bin size does not produce large variation in estimated mass. We found that masses of moderately rich LMC clusters range from $\sim$1400 to 72400 $M_\odot$. We have also

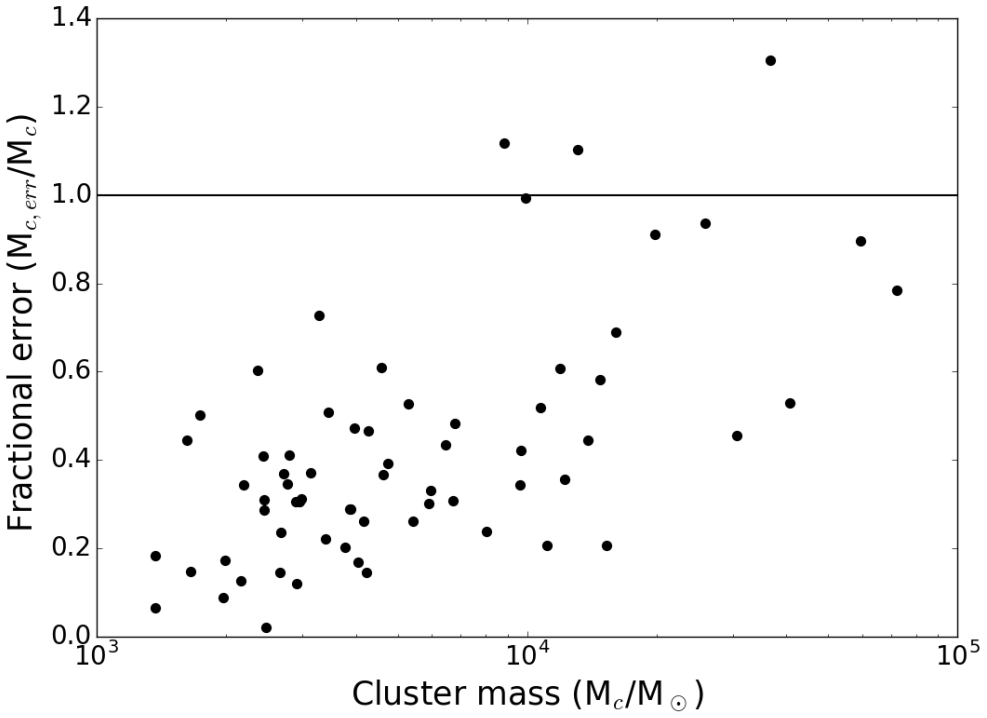

FIGURE 5.7: The figure shows the relation between estimated mass (M_c) of the LMC clusters and error ($M_{c,err}$) associated with it. The horizontal line indicates that the error is equivalent to the value.

estimated error ($M_{c,err}$) associated with the estimated cluster mass. The mass of individual cluster and corresponding error have been listed in the columns 11 & 12 of Table 5.1.

In Figure 5.7, we have plotted fractional error ($M_{c,err}/M_c$) against the cluster mass (M_c). We noticed that 48 clusters out of 66 have error less than 50%. We also noticed that clusters having mass more than $\sim 10^4$ $M_\odot$ have relatively larger error in mass. The reason could be due to the fact that steeper values of MFS result in massive clusters and a small error associated with steeper MFS leads to larger deviation in the estimated mass, which is clearly seen in the Figure 5.8. The Figure shows a linear relation between the mass function slope and cluster mass. The figure also shows that the error associated with the estimated mass increases for steeper slope values. The mass estimation of clusters with larger error ($M_{c,err}/M_c \geq 0.8$) may not be reliable.

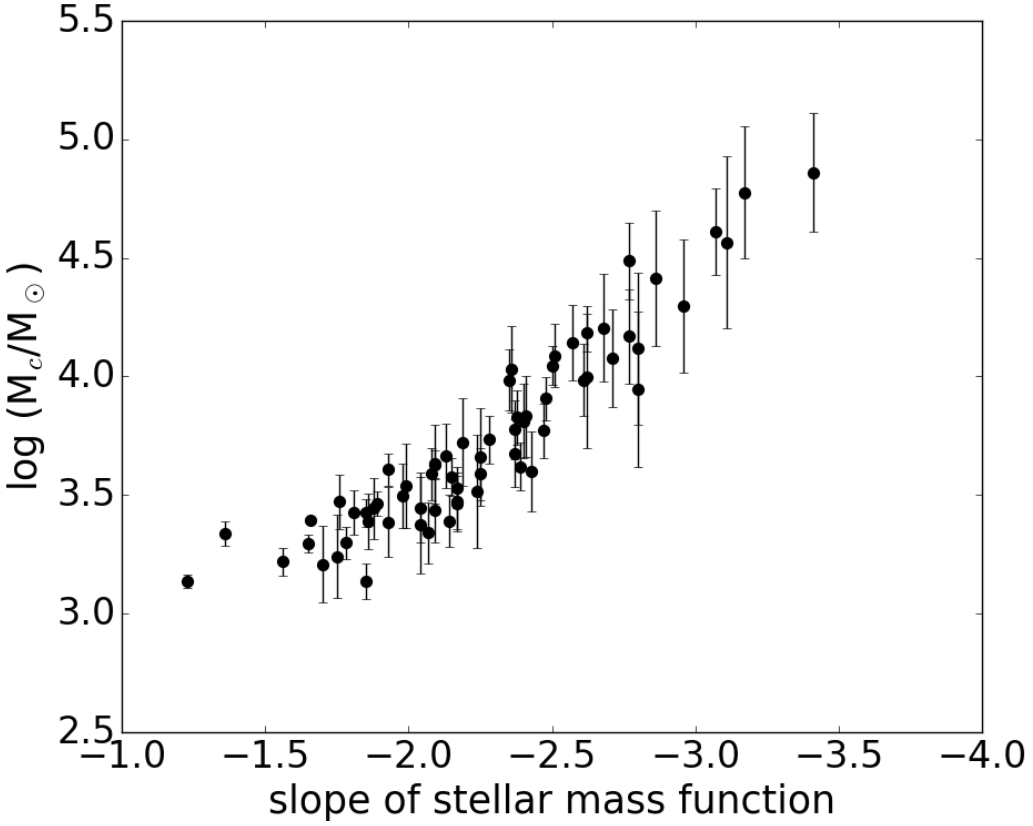

FIGURE 5.8: The figure shows a linear relation between slope of stellar mass function and cluster mass.

In the top panel of Figure 5.9 we have shown the distribution of estimated mass of moderately rich LMC clusters. The figure shows that there are few clusters more massive than 16000 $M_\odot$. In the bottom panel, we have shown the above distribution up to 16000 $M_\odot$. The figure suggests that most of clusters have mass range from 1500 to 5000 $M_\odot$, which matches well with our previous estimation (in Chapter 3) of mass range of clusters in the MCs belonging to the moderately rich group. Masses of open clusters in the MW lie between few hundred to few thousand solar mass, which clearly suggest that the LMC also has open clusters like systems. We also found that the distribution peaks between 2500 to 3000 $M_\odot$.

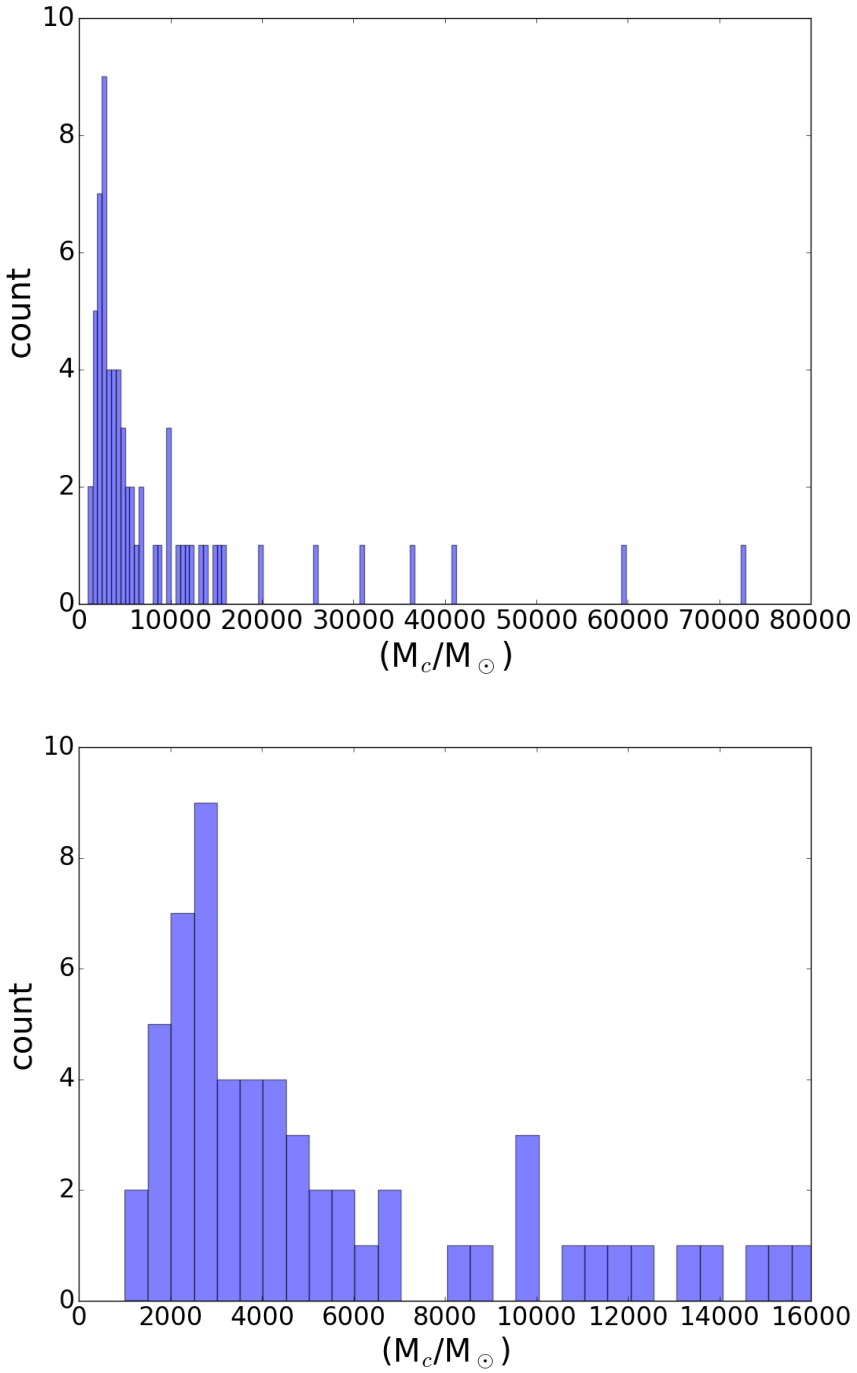

FIGURE 5.9: Top panel shows the distribution of estimated cluster mass. The distribution suggests that there are only a few clusters more massive than 16000 $M_\odot$. Hence in the bottom panel we have shown the distribution up to 16000 $M_\odot$, which indicates that most of the clusters lie between 1500 to 5000 $M_\odot$ with peak value between 2500 to 3000 $M_\odot$.

5.5 Cluster mass function (CMF) of LMC clusters

We estimated the CMF of the LMC using moderately rich young clusters. We calculated the number of clusters present per unit mass bin (dn/dM_c) and plotted against cluster mass (M_c) in logarithmic scale. We considered different bin sizes depending on mass range of clusters. We took smaller bin sizes (500 $M_\odot$) for low mass clusters and gradually increased up to 4000 $M_\odot$ for higher mass range ($M_c > 10000$ $M_\odot$). To determine the CMF, we excluded the clusters with masses less than 2500 $M_\odot$ due to incompleteness of cluster number. We also did not consider clusters having masses more than 14000 $M_\odot$ as there are only a few clusters present. We estimated the slope of the CMF as -1.66 ± 0.08. The value is very similar to the previous finding (between -1.5 to -1.6) by Popescu *et al.* (2012) for clusters younger than a Gyr and more massive than 1000 $M_\odot$. We suggest that a larger cluster sample is required mainly in the lower mass limit for a more precise estimation of the CMF.

5.6 Relation between mass and radius of clusters

In Figure 5.11, we have plotted masses of the clusters against their radii to established a relation between them. In the Chapter 4 we derived a relation and were expecting to refine that in this chapter with the estimation of individual masses. As shown in the figure, the data at hand is clearly insufficient to derive any sensible relation. All that the figure shows is that the clusters have a very limited radii. This basically demonstrates that deriving such a relation is not very easy, as it requires a large sample with reliable estimates of mass range as well as radii.

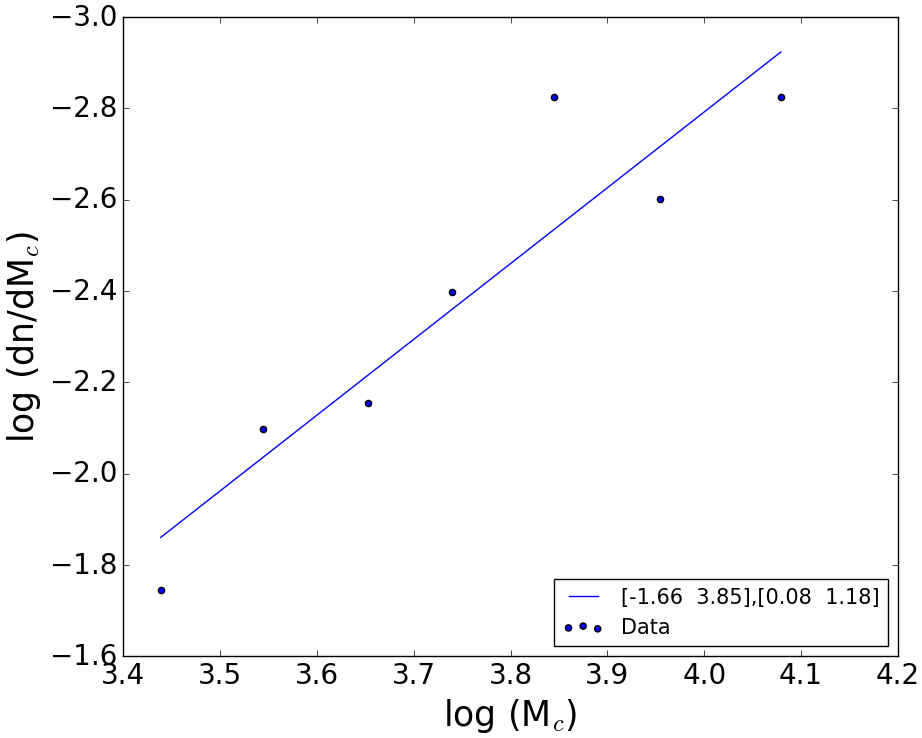

FIGURE 5.10: The figure shows (dn/dM$_c$) with respect to their masses (M$_c$). The blue line indicates the least square fit to the data points. The slope (-1.66) and constant (3.85) value are noted in the figure along with the errors associated with them.

5.7 Discussion

LMC star clusters fill a unique mass range in the study of stellar mass function in clusters. The rich and young star clusters in the LMC helps in a relatively more reliable estimation of the MF slopes (MFSs), where the Milky Way star clusters are plagued by stochasticity in the number of stars (Sagar and Qian (1993); Sagar and Cannon (1995) and references therein). The mass function estimates using the ground based observations as well as HST observations have been used to estimate the MFSs of mainly the rich star clusters in the LMC (for example, Sagar and Richtler (1991); Brocato *et al.* (2001); Liu et al. 2009 etc). In this study, we estimated the MFSs of 66 moderately rich star clusters in the LMC. This is quite a large number of clusters considered for the study in comparison

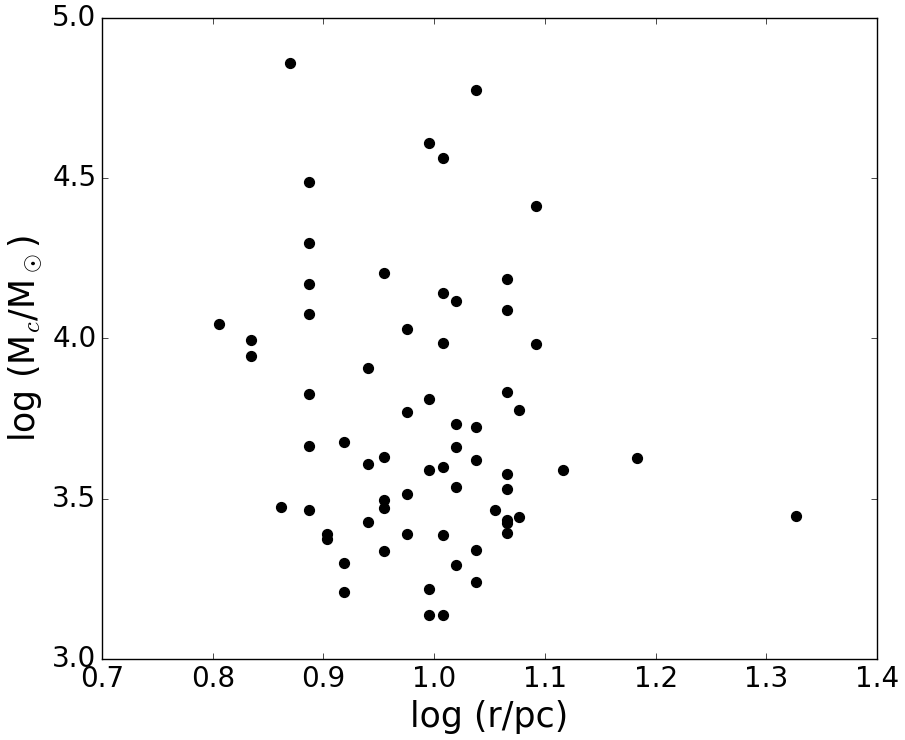

FIGURE 5.11: Masses of the LMC clusters are plotted against their radii in logarithmic scale.

to Kumar *et al.* (2008), where MFSs of 9 clusters were estimated using BVRI photometric data obtained from the 3.5-mNTT/EFOSC2 and a similar technique as ours.

5.7.1 Comparison with previous estimates:

As mentioned before, the MFSs are not estimated for most of the not-so-rich clusters. We have only one cluster in common with Kumar *et al.* (2008). They estimated the MFS of NGC 2098 as -2.19 ± 0.19, which is in very good agreement with our estimate (-2.09 ± 0.16). The mass ranges considered in both the studies are very similar and hence a direct comparison is possible. They estimated a very shallow slope for the cluster NGC 1767 (-1.23 ± 0.27), which is within the range

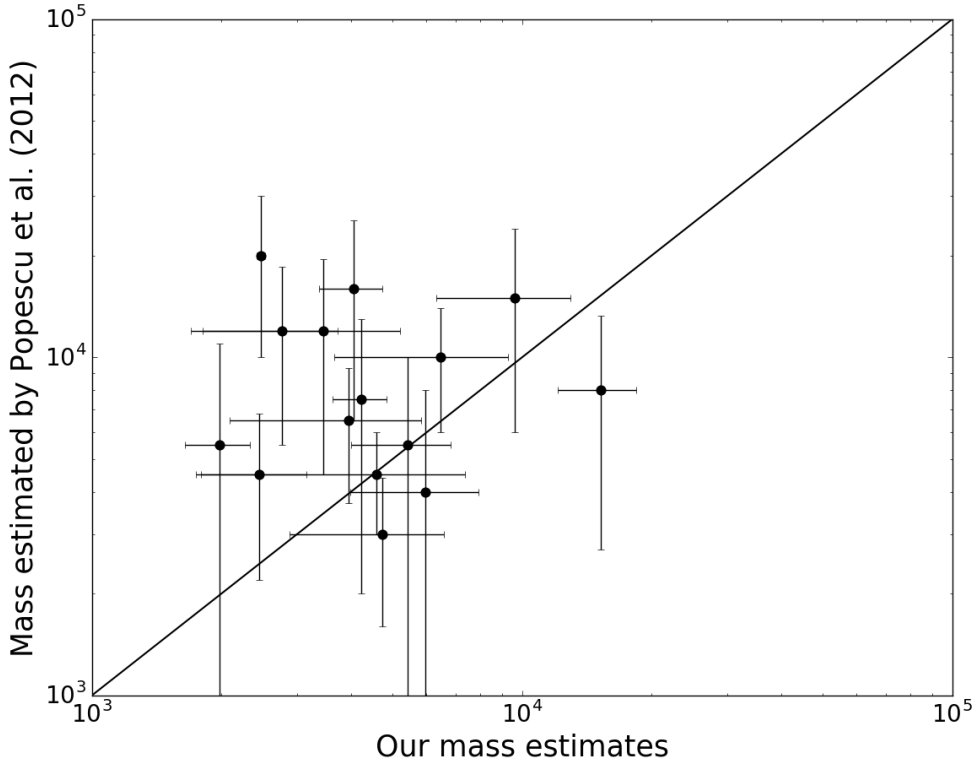

FIGURE 5.12: The figure shows comparison between our estimation of mass and previous estimation by Popescu *et al.* (2012). The errors associated with both the estimations are also shown. A straight line of slope one is plotted to indicate the clusters having similar mass estimation in both the studies.

of slope estimated in this study. Kumar *et al.* (2008) also reported a mean slope of -2.22 ± 0.16 for 25 dynamically un-evolved stellar systems younger than 100 Myr in the LMC. This value is in very close agreement with the peak of our slope distribution (-2.26 ± 0.44). The large value of standard deviation estimated here indicates a larger range in the estimated slope values.

Popescu *et al.* (2012) estimated ages and total mass of 920 LMC clusters using integrated photometry, whereas 288 cluster masses were estimated using CMDs. We have 15 clusters in common with this sample and we compare the total mass estimation for these clusters. A plot comparing the two estimations (Figure 5.12) shows that though there is a general agreement, a few clusters were found to have relatively large mass estimates by Popescu *et al.* (2012). This could be due to the

slight differences in age estimates as well as the method used for mass estimation. We also note that the CMF estimated by us is in very good agreement with that estimated by Popescu *et al.* (2012).

5.7.2 Implications of the MF slope estimates

Our estimation of the MF slopes for moderately rich young clusters show that there is a large range in the values, though the peak of the distribution is consistent with the generally accepted values. Here we explore the possible reasons for the large range in the estimated slope values.

Kumar *et al.* (2008) found that there is a significant variation in the slope estimation as a function of radius. They estimated MFS for two rings around the cluster and found that the values showed variation for a few clusters. They attributed this to the presence of mass segregation in the clusters. The dynamical time for relaxation for the massive clusters are a few 100 Myr, whereas this timescale could be much shorter for less massive clusters. Therefore, we need to explore the presence of any variation in the MFS as a function of radius of the clusters studied here. The very shallow MF slopes could be due to a combination of the presence of mass segregation and adoption of a smaller cluster radius. A more detailed analysis needs to be performed to address this point.

The peak of our MFS distribution matches well within the error with the estimation by Sagar (1995), where the author studied five young (<100 Myr) star clusters in the LMC and found that the MF slopes are in the range -1.8 to -2.3. Mateo (1988) investigated six massive star clusters of different ages (range from 10 Myr to 2.5 Gyr) in the MCs and found that a steeper slope of the MF (-3.52 ± 0.16). Though the value falls in our estimated MFS range.

We also find that a large fraction of clusters (∼30%) have relatively steeper MF slope values. We have to check whether this is due to incompleteness of the brighter stars in the data due to saturation effects or any missing bright stars in the catalog. We should point out that the clusters with the largest upper limit in magnitude bin did not show steeper slope values. We also find that the younger clusters, which are likely to have brighter stars do not have slopes steeper than −2.5 (Figure 5.6). This suggests that the bright stars are unlikely to be missing from our data.

We could also check whether the field star decontamination is introducing any stochasticity in the estimation of the MF slopes. We did perform this check by doing a field star decontamination using different field regions and estimating the MF values in each case. We did not detect any significant change between the various slope estimations, which were found to be within the errors.

We therefore conclude that though the large range seen in the MF slope among the LMC clusters could arise due to some artifacts, it is clear that some amount of deviation from the peak could be a real feature. We plan to do a thorough check of effects due to mass segregation, saturation effects and random noise due to field contamination, in the future. We point out that this work has quite a large sample of clusters and covers a large range in mass among the LMC clusters and thus, can significantly contribute to the understanding of MF slope in the LMC clusters.

5.8 Summary

1. We estimate the MF slope and total mass of 66 star clusters in the LMC and most of the estimates are done for the first time.

2. LMC clusters have a large range in slope of stellar mass function ranging from -1.5 to -3.0. Stellar mass function slope of LMC clusters peaks at -2.26, which is very similar to the IMF value obtained by Salpeter (1955) and the mean by Kumar *et al.* (2008) for the LMC clusters. The estimated slope values distributed within two sigma around the peak value with a average uncertainty in slope similar to sigma value (0.44).

3. We found that most of the moderately rich clusters in the LMC are distributed within the mass range of 1500 to 5000 $M_{\odot}$, which supports our previous estimation of mass range in Chapter 3 for moderately rich clusters in the MCs. Mass distribution of moderately rich star clusters in the LMC peaks between 2500-3000 $M_{\odot}$.

4. The slope of cluster mass function in the LMC is found to be -1.66 ± 0.08, matching the previous estimation (between -1.5 to -1.6) by Popescu *et al.* (2012).

TABLE 5.1: A catalog of moderately rich LMC clusters with their stellar mass function slope and total mass is presented here. The table contains cluster name, age (in log scale), radius, upper (U_{mass}) and lower(L_{mass}) mass limit of cluster stars used to determine the mass function, and the number of data points with the mass limit in the columns 1 to 6 respectively. The slope and constant of the stellar mass function are noted in columns 7 & 9 respectively. The errors associated with them are also given in the columns 8 & 10 respectively. Columns 11 & 12 represent estimated total mass (M_c) of each cluster and its corresponding error ($M_{c,err}$) respectively.

Cluster name	log(t/yr)	radius (pc)	U_{mass} ($M_\odot$)	L_{mass} ($M_\odot$)	number	slope	error	constant	error	M_c ($M_\odot$)	$M_{c,err}$ ($M_\odot$)
NGC1695	7.70	9.89	8.48	3.38	10	-2.40	0.29	3.18	0.12	6474	2807
NGC1704	7.39	11.92	11.60	3.46	12	-2.37	0.23	3.14	0.11	5970	1972
SL58	7.77	7.70	8.16	3.36	10	-2.71	0.32	3.37	0.14	11939	7244
SL75	7.77	9.89	8.16	3.36	10	-3.07	0.25	3.77	0.11	40747	21552
NGC1734	7.78	8.29	6.00	2.84	9	-2.37	0.31	3.06	0.10	4736	1860
SL116	7.94	9.89	5.48	2.80	8	-1.56	0.40	2.62	0.13	1651	245
NGC1772	7.62	10.47	7.92	3.69	9	-1.99	0.46	2.92	0.22	3448	1750
NGC1782	7.62	8.29	10.09	2.87	13	-1.78	0.19	2.62	0.08	1985	341
NGC1815	7.79	8.00	9.90	3.04	12	-2.14	0.25	2.80	0.10	2452	704
SL232	7.94	9.45	6.61	2.77	10	-2.47	0.22	3.14	0.07	5904	1777
SL234	7.87	7.70	7.70	3.01	10	-2.38	0.23	3.21	0.09	6707	2062
NGC1844	7.79	11.63	5.48	2.81	8	-2.09	0.41	2.85	0.13	2721	1004

Table 5.1: continued

Cluster name	log(t/yr)	radius (pc)	U_{mass} ($M_\odot$)	L_{mass} ($M_\odot$)	number	slope	error	constant	error	M_c ($M_\odot$)	$M_{c,err}$ ($M_\odot$)
SL397	7.70	7.27	8.74	3.09	11	-2.17	0.27	2.88	0.11	2987	929
NGC2000	7.61	11.34	9.53	3.16	12	-1.89	0.17	2.84	0.07	2909	352
SL543	7.78	10.18	6.00	3.08	8	-1.93	0.47	2.80	0.17	2431	996
NGC2093	7.70	10.18	8.74	3.09	11	-2.43	0.32	2.96	0.13	3963	1870
NGC2098	7.13	15.26	12.00	3.39	13	-2.09	0.16	2.99	0.07	4239	615
NGC2118	7.45	11.63	11.05	3.23	13	-2.17	0.20	2.91	0.09	3392	751
NGC2127	7.86	10.90	8.31	2.80	12	-2.39	0.20	3.00	0.07	4160	1084
NGC2133	7.78	11.63	8.42	3.35	10	-2.41	0.31	3.21	0.13	6786	3280
SL763	8.12	9.45	5.89	2.90	8	-2.24	0.55	2.93	0.18	3280	2387
NGC2140	7.86	10.90	8.31	3.03	11	-2.07	0.33	2.76	0.13	2190	751
NGC2145	8.03	10.90	6.51	3.21	8	-1.75	0.58	2.66	0.23	1738	871
NGC1698	7.86	10.47	10.54	3.30	12	-2.28	0.19	3.13	0.09	5418	1418
SL76	7.78	9.01	8.42	3.64	9	-2.09	0.35	3.05	0.17	4275	1989
NGC1735	7.95	11.92	6.80	3.23	8	-1.88	0.38	2.88	0.15	2774	960
SL106	7.87	11.63	7.70	3.01	10	-1.85	0.20	2.83	0.08	2658	389

Table 5.1: continued

Cluster name	log(t/yr)	radius (pc)	U_{mass} ($M_\odot$)	L_{mass} ($M_\odot$)	number	slope	error	constant	error	M_c ($M_\odot$)	$M_{c,err}$ ($M_\odot$)
SL105	8.03	10.18	5.77	3.21	7	-3.11	0.55	3.71	0.20	36643	47824
SL134	7.22	6.40	13.89	3.56	14	-2.50	0.13	3.38	0.06	11094	2291
NGC1774	7.55	11.63	10.73	2.63	14	-1.66	0.09	2.72	0.03	2471	54
NGC1839	7.70	11.63	12.08	3.38	13	-2.62	0.12	3.51	0.05	15276	3150
SL230	8.03	9.89	5.99	2.72	9	-2.25	0.26	3.00	0.08	3874	1115
NGC1847	7.62	12.36	10.09	3.69	10	-2.35	0.23	3.36	0.11	9635	3307
NGC1953	7.94	8.72	6.61	3.00	9	-1.93	0.20	3.04	0.07	4054	684
NGC2051	7.86	10.90	8.31	3.58	9	-2.19	0.37	3.13	0.17	5287	2781
NGC2088	7.95	10.47	5.36	2.74	8	-2.25	0.43	3.07	0.17	4582	2790
SL734	8.11	10.18	6.46	2.93	9	-2.61	0.27	3.32	0.09	9647	4063
NGC1756	7.85	9.89	7.83	3.34	10	-1.23	0.28	2.39	0.13	1368	90
NGC1830	8.11	9.01	5.73	3.19	7	-1.36	0.41	2.69	0.16	2166	276
NGC1865	8.10	10.18	6.23	3.20	8	-2.57	0.28	3.49	0.10	13847	6154
NGC1926	7.78	9.45	9.33	3.96	9	-2.36	0.30	3.42	0.16	10716	5548
NGC1943	7.86	7.70	8.31	3.58	9	-2.77	0.24	3.77	0.11	30671	13973

TABLE 5.1: continued

Cluster name	log(t/yr)	radius (pc)	U_{mass} ($M_\odot$)	L_{mass} ($M_\odot$)	number	slope	error	constant	error	M_c ($M_\odot$)	$M_{c,err}$ ($M_\odot$)
NGC1950	7.86	12.36	7.46	3.58	8	-2.86	0.43	3.66	0.19	25910	24265
SL453	8.03	9.01	7.29	3.49	8	-2.68	0.36	3.52	0.15	16028	11055
NGC2016	7.94	13.08	8.25	3.27	10	-2.08	0.25	3.02	0.10	3884	1120
SL562	7.94	11.63	7.40	3.27	9	-2.51	0.22	3.45	0.09	12219	4361
NGC2056	7.87	10.90	6.13	3.28	7	-3.17	0.41	3.89	0.15	59528	53401
NGC2057	7.86	9.01	8.31	3.58	9	-1.76	0.35	2.87	0.17	2956	905
NGC1733	8.18	10.47	5.27	2.92	7	-2.80	0.56	3.39	0.18	13083	14416
SL251	7.78	8.00	6.00	3.08	8	-2.04	0.56	2.79	0.21	2360	1421
SL260	7.94	7.70	7.98	3.28	10	-2.96	0.42	3.50	0.17	19815	18061
NGC1878	7.94	7.70	6.61	2.77	10	-2.17	0.29	2.89	0.10	2904	890
SL342	7.85	7.41	8.10	3.34	10	-3.41	0.34	3.86	0.14	72402	56826
HS218	8.11	6.83	5.73	3.19	7	-2.62	0.53	3.33	0.19	9915	9843
NGC1921e	7.87	6.83	7.70	3.28	9	-2.80	0.50	3.21	0.21	8823	9863
SL424	7.94	9.01	5.88	3.01	8	-1.98	0.40	2.93	0.14	3139	1167
SL566	8.03	8.29	6.51	3.21	8	-1.70	0.57	2.63	0.23	1615	719

Table 5.1: continued

Cluster name	log(t/yr)	radius (pc)	U_{mass} ($M_\odot$)	L_{mass} ($M_\odot$)	number	slope	error	constant	error	M_c ($M_\odot$)	$M_{c,err}$ ($M_\odot$)
SL574	7.70	8.72	10.73	3.10	13	-2.48	0.16	3.26	0.07	8058	1912
NGC2028	7.86	7.70	7.46	3.30	9	-2.77	0.31	3.45	0.12	14771	8601
NGC2059	7.61	7.70	9.53	3.74	10	-2.13	0.28	3.06	0.14	4623	1698
HS371	7.86	9.45	7.46	3.30	9	-1.86	0.36	2.80	0.15	2452	762
GKK-O116	7.86	21.22	5.46	2.80	8	-2.04	0.47	2.86	0.15	2798	1149
SL654	7.85	8.72	7.26	3.34	9	-1.81	0.30	2.83	0.13	2672	633
NGC2111	7.94	10.47	7.40	2.77	11	-1.65	0.17	2.71	0.06	1969	173
SL690	7.87	10.18	7.70	2.79	11	-1.85	0.28	2.54	0.10	1368	252
SL747	8.03	11.63	6.51	2.73	8	-2.15	0.20	3.00	0.07	3776	760

Chapter 6

Propagation of cluster formation in the SMC[†]

6.1 Introduction

We have estimated ages and reddening of 179 star clusters in the SMC using a semi-automated quantitative method. Out of these, 16 clusters are parameterized for the first time, which belong either to very poor or poor groups. We have also classified all the clusters based on their mass as well as strength for the first time. We have listed the results in a catalogue (available online[*]). A sample of this catalogue is presented in Table 6.1. The catalogue contains the name of the clusters, position (RA and Dec as given in B08), radius, estimated ages and reddening by our method, previous estimation of ages by G10, PU99, C06, and group number based on our classification. In the catalogue, the clusters' name designated by an asterisk and blank spaces in Columns 7 to 9 respectively imply

[†]Results of this chapter are published in Nayak *et al.* (2018)

[*]http://vizier.cfa.harvard.edu/viz-bin/VizieR?-source=J/A+A/616/A187

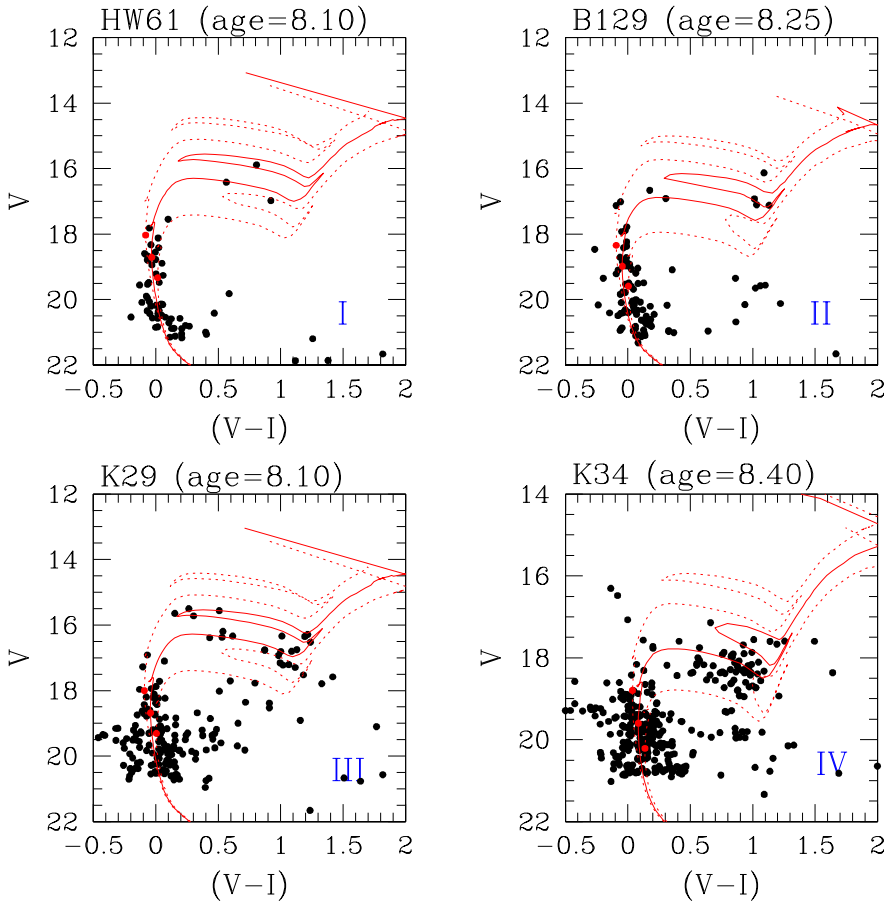

FIGURE 6.1: CMDs of clusters from each group (I - IV). The cluster's name and age (log(t)) are also marked.

newly parameterized clusters. We note that though there are 20 blank spaces in Columns 7 to 9, only 16 are new estimations, as parameters of NGC458 is estimated by Da Costa and Hatzidimitriou (1998) and other three clusters (SK157, HW77 and HW82) are estimated by Piatti *et al.* (2015b) and .

We have presented the field star decontaminated CMDs of all the 179 clusters, with over plotted M08 isochrones for the estimated age. Isochrones showing the typical uncertainty in the age estimation (0.25) are also over-plotted. All the CMDs are made available online[†]. As an example, we have presented four CMDs from four groups (I - IV) in Figure 6.1. In the figure, cluster stars are denoted as black

[†]available in the appendix of the paper Nayak *et al.* (2018)

points, red solid line denotes the isochrone corresponding to estimated age and red dashed lines denote the isochrones corresponding to the age uncertainty. The turn-off of each isochrone is indicated with a red point. The name of the cluster and their corresponding age are mentioned on top of each subplot, along with their group number labelled in blue. In this chapter, we first compare our results with the previous estimates to prove the consistency of our estimations. We use this sample of clusters to understand the demographics of cluster formation and its propagation in the SMC.

6.1.1 Comparison of age and reddening with previous studies

We found 119 clusters to be in common with G10, 56 clusters are in common with PU99 and 90 with C06. In Figure 6.2 we have compared our age estimation (X-axis) with previous estimations (Y-axis). We have drawn a straight line with slope = 1 in the plots to check the difference in age estimation. Clusters with different classification are denoted in different colors in the figure. The top left plot shows that our results match very well with G10 with an uncertainty of 0.25 in log scale except for a few very poor clusters. The top right plot also shows good matching of our results with PU99, although there are a few clusters for which we estimated older ages. Our results also match well within the error of log(t) = 0.25 with the estimation by C06 for most of the clusters older than $\sim$ 60 Myr (log(t) = 7.8) (bottom panel). In the case of clusters younger than 60 Myr, we have estimated relatively older ages. We checked our CMDs of those clusters where we find a discrepancy in estimated ages with previous results and confirmed our estimated values.

In general, the comparison indicates that our estimations compare well with the previous studies. We also note a few cases of discrepancy, which could be due

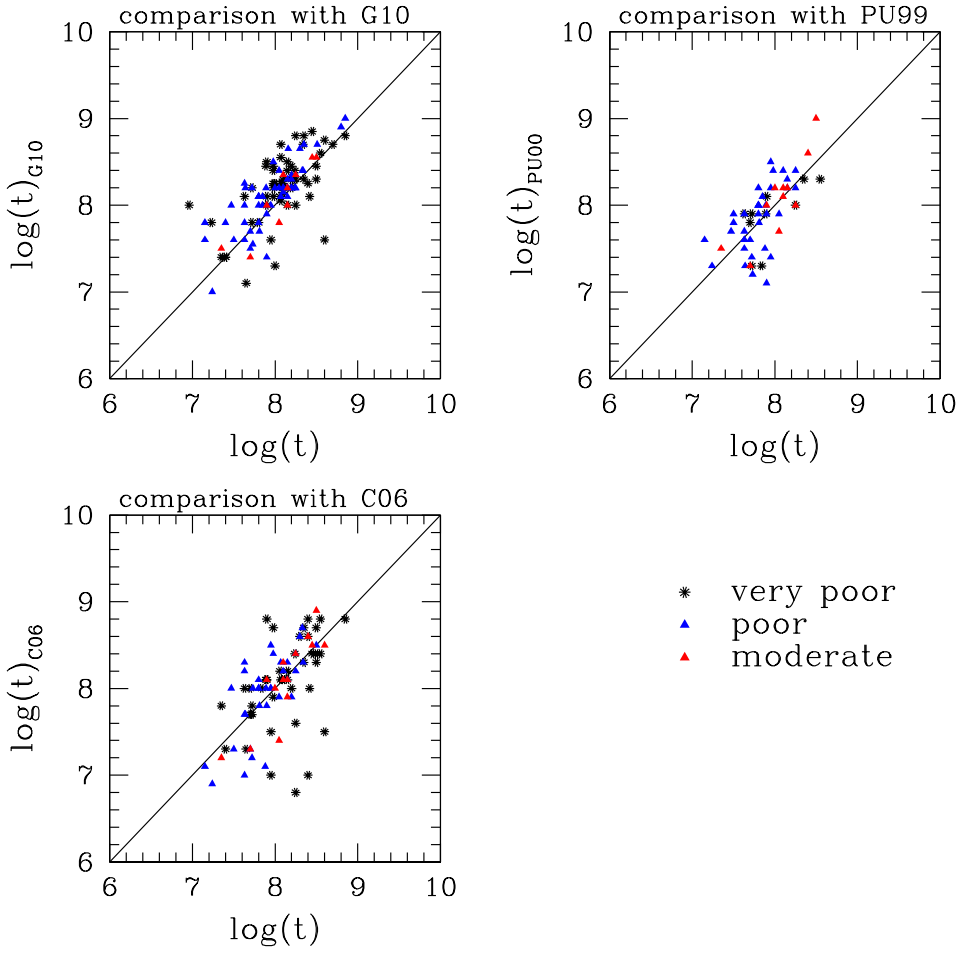

FIGURE 6.2: Comparison between our estimated age (X-axis) and age estimated by previous studies (Y-axis). We have compared our age estimation with that of G10 (top left), PU99 (top right) and C06 (bottom one). Different point types indicate clusters from different group of classification. A straight line with slope = 1 is shown in each plot to indicate the deviation in the estimated age.

to reasons such as different data used by different authors, the difference in the isochrone models used, and the difference in adopted methods. PU99 and C06 used OGLE II data, which have lower resolution than OGLE III data. Also, OGLE II covers the central region of the SMC, where the clusters may suffer more crowding. PU99 used isochrone model by Bertelli *et al.* (1994) and C06 used the isochrone model by Girardi *et al.* (2002), whereas G10 used MCPS data and two isochrone models for their analysis: Padova isochrones (Girardi *et al.* 1995) and Geneva isochrones (Lejeune and Schaerer 2001) for their age estimations.

6.1.2 Comparison of mass range with previous estimations

We found that star clusters in the SMC have a very large mass range (<800 to >5000 $M_{\odot}$), as shown in Table 3.1 in Chapter 3. The estimated mass ranges for different groups indicate that the SMC consists of clusters with a large mass range, similar to the LMC star clusters. The classification of clusters based on mass will help us to understand various properties, like formation and evolution of clusters, which depend on their mass. It will also help us in understanding the dissolution of star clusters in various groups in the SMC. Our estimated mass ranges match well with those of Maia *et al.* (2014) and Hunter *et al.* (2003). We have also compared the mass range of the SMC clusters with that of the open clusters in the Galaxy. We find that the clusters near solar neighbourhood have mass range (Lamers *et al.* 2005) similar to that in the SMC. Piskunov *et al.* (2008) studied 650 Galactic open clusters with mass range 50 $M_{\odot}$ to 10^5 $M_{\odot}$. Thus, SMC consists of clusters with a large mass range which is similar to Galactic open clusters. In our sample, about 50% of the SMC clusters belong to the very poor group, suggesting the presence of a large fraction of very low mass clusters in the SMC. On the other hand, we find that the LMC has $\sim$ 40% of very poor clusters. We also note that 90 % of the clusters are either in the poor or very poor class in the SMC. All these clusters have mass $<$ 1700 $M_{\odot}$. This suggests that the cluster population in the SMC is dominated by low mass clusters. This finding has implications for the cluster formation mechanism in the SMC.

6.1.3 Reddening distribution

We have constructed distribution of the estimated reddening E(V $-$ I) for different groups of clusters (shown in different color) in Figure 6.3. The distribution ranges from 0 to 0.4 mag for very poor and poor clusters, and from 0 to 0.3 mag for

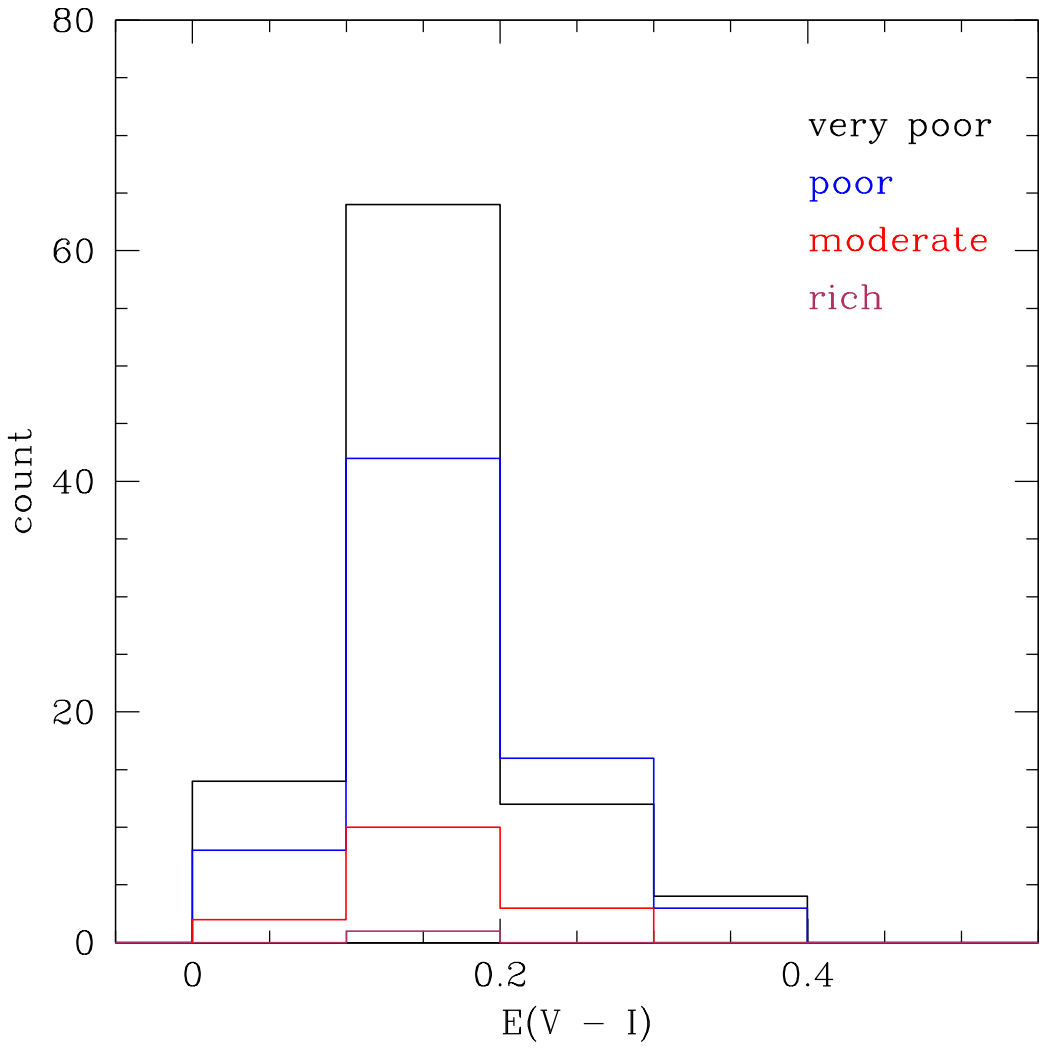

FIGURE 6.3: Reddening distribution of very poor (black), poor (blue), moderate (red) and rich (maroon) clusters. Reddening value peaks between 0.1 and 0.2 mag for all the groups.

moderately rich clusters. The distribution peaks between 0.1 to 0.2 mag for all the four groups. We have compared the estimated reddening with the high resolution map of field reddening in the central SMC by Indu and Subramaniam (2011) and found that they match well. We do not find any significant difference in reddening with that estimated using red clump stars by Subramanian and Subramaniam (2012). We have also compared our estimated reddening with previous studies by G10, PU99 and C06. The distribution of difference is found to be peaked at 0.1 mag, which is within the error (1σ) of our estimation.

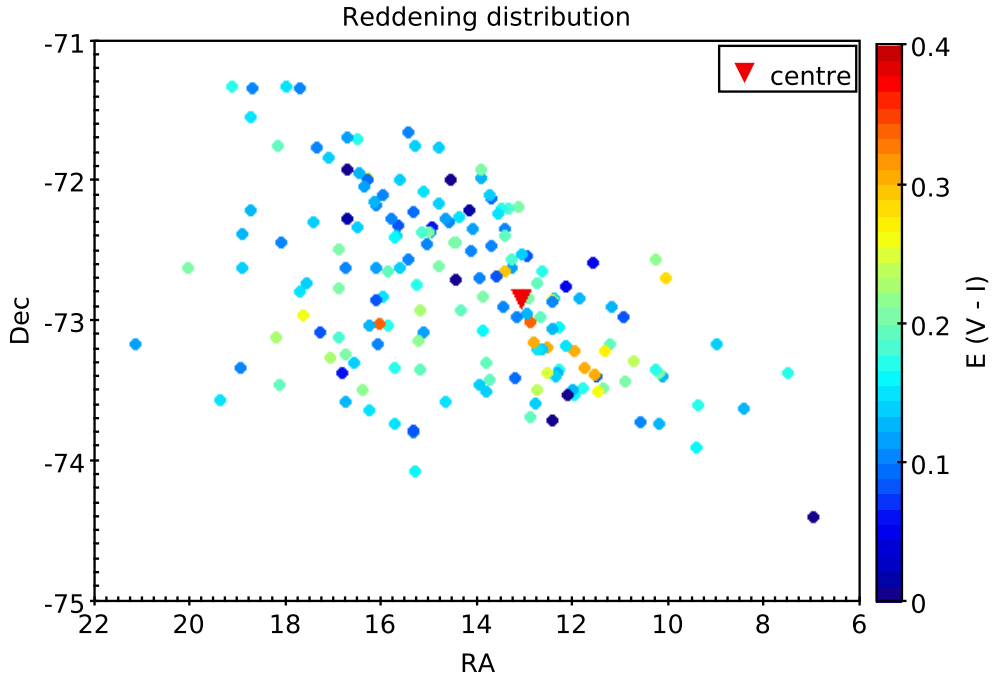

FIGURE 6.4: Spatial variation of estimated reddening across the SMC.

The spatial distribution of reddening across the SMC is plotted in Figure 6.4. The red triangle indicates the centre of the SMC, located at (0 h 52 m 45 s, -72^o 49′ 43″) (Crowl *et al.* 2001). Most of the regions have reddening within 0.1 - 0.2 mag with larger variation in reddening near the centre. The Southern part of the SMC consists of clusters with relatively large reddening value compared to the North-Eastern (NE) part.

6.1.4 Strength distribution

Spatial distribution of clusters as a function of their strength (n_m) is shown in Figure 6.5. The red triangle indicates the centre of the SMC. The figure shows that clusters with $n_m < 100$ are distributed all over the SMC observed region. The clusters with $n_m > 100$ are preferentially located in the inner SMC, mainly

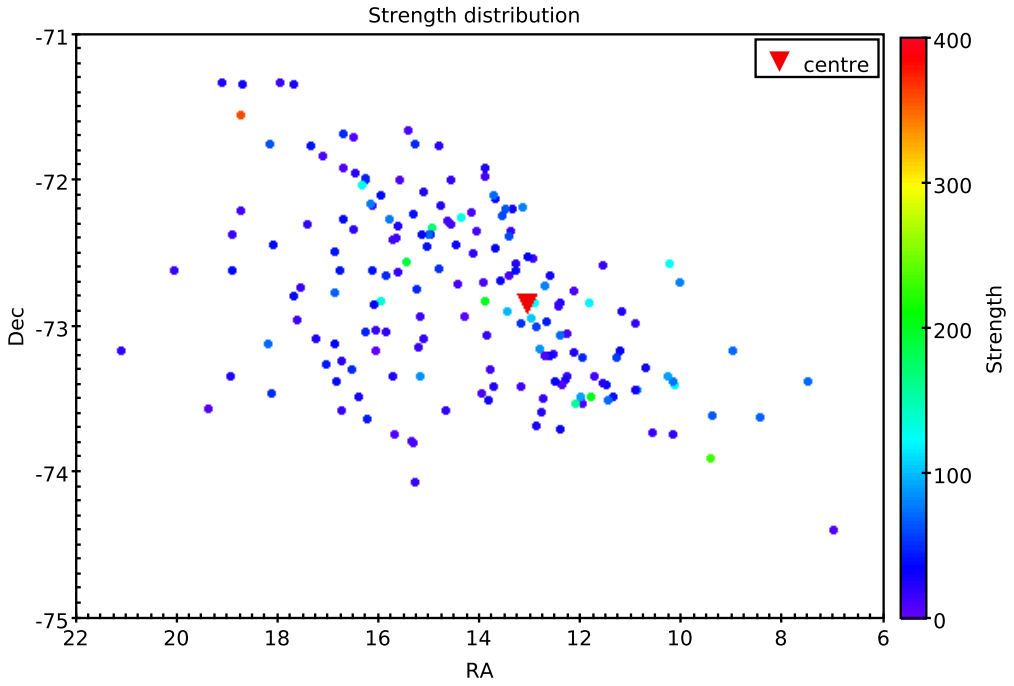

FIGURE 6.5: Spatial distribution of star clusters in the SMC as a function of cluster strength.

close to the bar. We notice that there are two clusters with strength more than 200, located in the South-Western (SW) and NE end of the SMC. We do not find any kind of hierarchical distribution of clusters in the SMC based on their strength, similar to that found in the LMC. We notice the presence of only low mass clusters in the Eastern SMC which is predominantly affected by the tidal forces (Besla *et al.* 2010, 2012).

6.1.5 Age distribution

Age distribution of various groups of SMC clusters is shown in Figure 6.6. We have used a bin width of 0.25 in log scale which is same as the error associated with the age estimation. The figure shows that very poor clusters are distributed over a large age range (log(t) = 6.75 - 9.00) with peak at ∼130 Myr (log(t) =

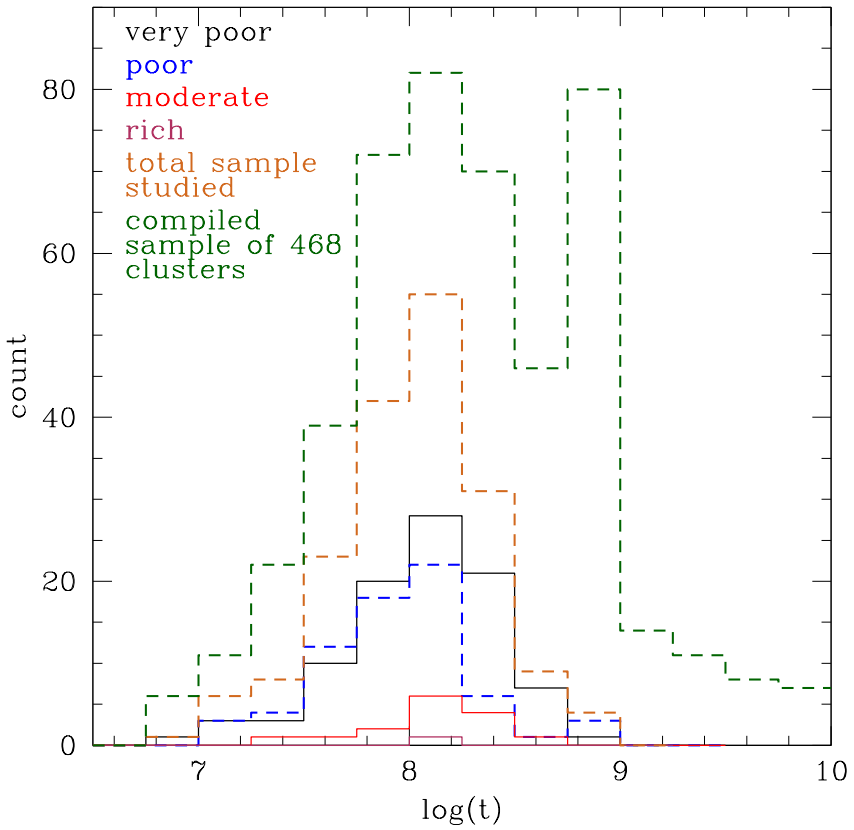

FIGURE 6.6: Age distribution of very poor (black), poor (blue), moderate (red), and rich (maroon) clusters. Distributions of all the four groups of clusters peak in the range of log(t)=8.00-8.25. Combined age distribution of all the studied clusters (chocolate) shows a peak at $\sim$ 130 $\pm$ 35 Myr. Age distribution of the compiled sample of 468 clusters peaks at $\sim$ 130 and $\sim$ 750 Myr.

8.00-8.25). The poor clusters show two peaks : a younger peak at 130 Myr (log(t) = 8.00-8.25) and an older peak at 750 Myr (log(t) = 8.75-9.00). The moderately rich and rich clusters also show peak at 130 Myr (log(t) = 8.00-8.25), similar to the very poor and poor clusters. Therefore, the clusters are mainly distributed between 30 Myr to 300 Myr (log(t) = 7.5 - 8.5). The combined distribution of all the studied SMC clusters peaks at $\sim$ 130 Myr, which is almost same as that we identified in the LMC. The fact that the cluster formation peaked at $\sim$ 130 Myr in both the MCs could suggest that it is due to a common triggering event. We suggest that the recent interaction ($\sim$ 100-250 Myr ago; Besla *et al.* (2012); Diaz and Bekki (2011)) between the LMC and SMC might have triggered the cluster

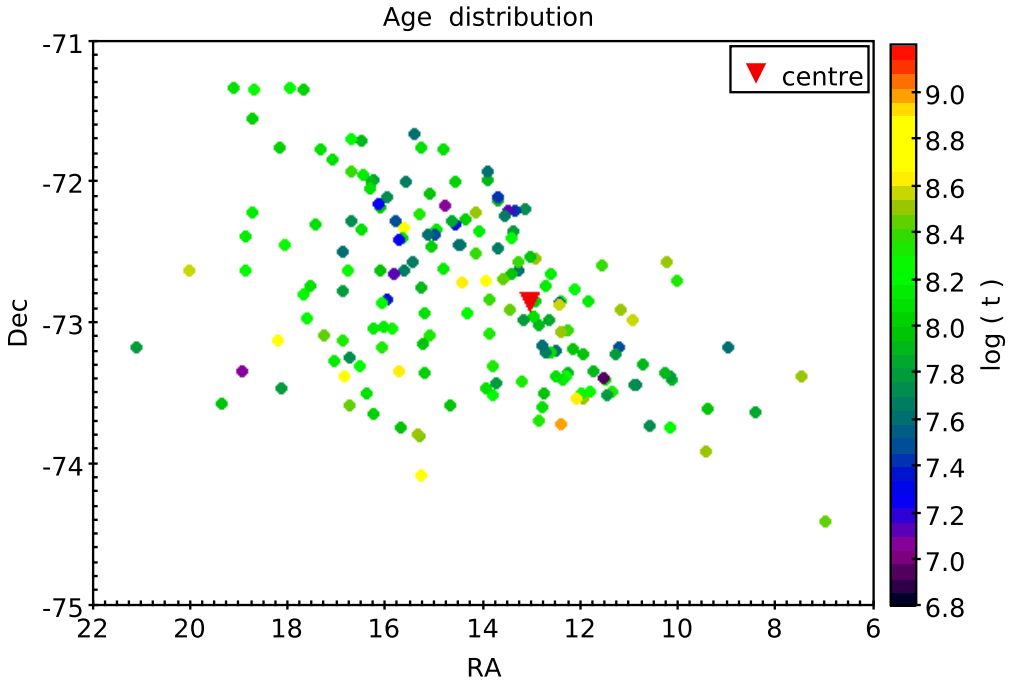

FIGURE 6.7: Spatial distribution of star clusters in the SMC as a function of age.

formation during the above mentioned age range. PU99 found the peak of cluster formation at around 30 Myr, whereas C06 found two peaks of cluster formation at 8 Myr and 90 Myr. G10 found two peaks of cluster formation at 160 and 630 Myr. The younger peak shown in G10 is not very different from our younger peak.

The spatial distribution of age is shown in Figure 6.7. The figure shows that clusters with age around 100 Myr are distributed all over the SMC region. Western and South-Eastern (SE) parts show older clusters. The central part consists of clusters with a relatively larger age range. The SMC stretches out from SW to NE direction and younger clusters are found in specific places, slightly North from the central region. Older clusters are mostly located in Southern part of the SMC and Northern part consists of relatively younger clusters. This is suggestive of preferential location of clusters as a function of age. This needs to be confirmed with a more complete sample of parameterized clusters.

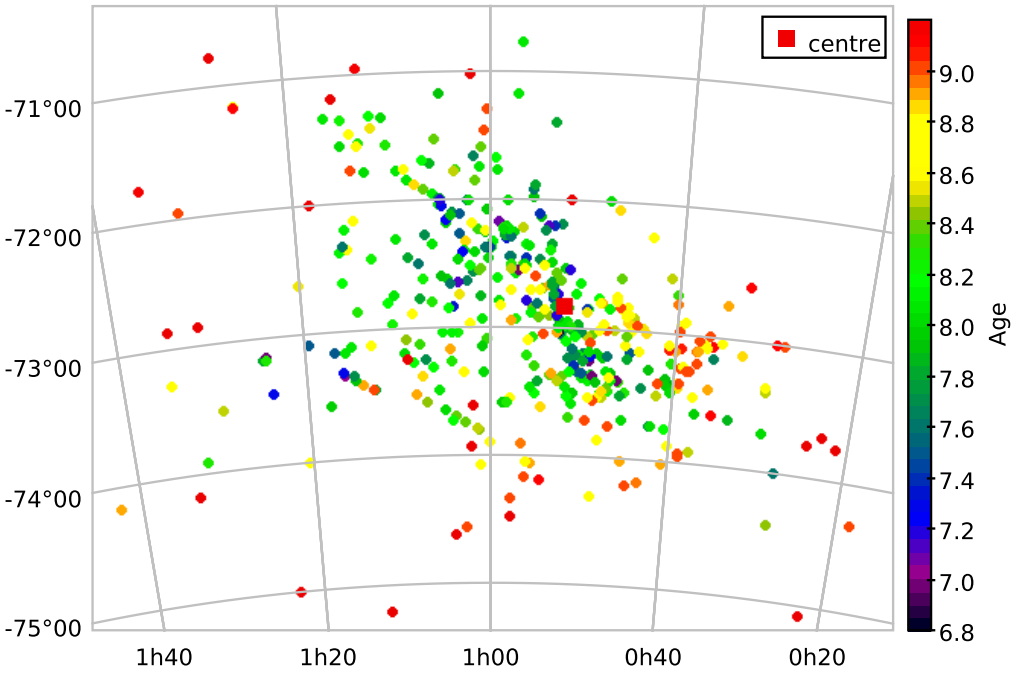

FIGURE 6.8: Spatial distribution of the compiled sample of 468 star clusters in the SMC as a function of age.

We have therefore added 289 clusters from the previous studies which are not common to our catalogue. The clusters and their parameters are taken from G10, PU99, C06, Piatti *et al.* (2005, 2007b,a,c, 2008, 2011); Piatti (2011a); Maia *et al.* (2012); Piatti (2012a); Mighell *et al.* (1998b); Glatt *et al.* (2008); Girardi *et al.* (2013); Crowl *et al.* (2001); Parisi *et al.* (2014); Crowl *et al.* (2001); Dias *et al.* (2014); Piatti *et al.* (2015b); Dias *et al.* (2016). As there are a large number of studies, we use a common reference, ′other-studies′, to indicate all the studies other than G10, PU99, and C06. The addition of clusters from previous studies not only increased the cluster sample but also the coverage of the SMC. The total sample of 468 clusters is large enough to study the spatio-temporal distribution of clusters, which is discussed in the next section. This is the largest parameterized sample of clusters in the SMC. The age distribution of this compiled sample of 468 clusters is also shown in Figure 6.6. The distribution shows two peaks (130 and 750 Myr) of cluster formation. The younger peak is found to be same as that

estimated from our sample.

Spatial distribution of the compiled sample as a function of age is shown in Figure 6.8. The centre of the SMC is denoted by solid red square. The distribution suggests that older clusters are mostly located at the Southern and Western part of the SMC, whereas, the younger clusters are found in the inner SMC along with a few clusters in the East. The clusters with ages $\sim$ 100 Myr are distributed all over the SMC. The distribution also suggests that the SMC is stretched out from SW to NE along the bar, which could be due to the interaction between the MCs. We find that the North-West quadrant of the Fig. 6.8 is devoid of clusters. We suggest that the reasons could be either due to lack of available photometric data in that region resulting in no parameterized clusters, or due to genuine lack of clusters in this part of the SMC. It is important to fill this gap in the spatial distribution of SMC clusters. A genuine lack of clusters in this region could put constraints on the cluster formation as well as gas distribution in the SMC.

6.1.6 Spatio-temporal distribution

To understand the spatio-temporal distribution, the spatial location of clusters in various age range is shown in Figure 6.9. The ages of the clusters are in the range of log(t) = 6.8 to 9.1. The black points in the figure denote the clusters from our catalogue, the red small circles are the clusters from G10, the blue points are from C06 and PU99, and the clusters from ′other-studies′ are denoted as cyan points. The green triangle indicates the centre of the SMC. As shown in Figure 6.9(d), clusters in the age range 630 Myr - 1.25 Gyr are mostly found in the Southern and Western parts of the SMC including the central region. Very few clusters are found in the Northern and Eastern regions during this period. During the period 250 - 630 Myr (Figure 6.9(c)), the clusters are found mostly in the central region,

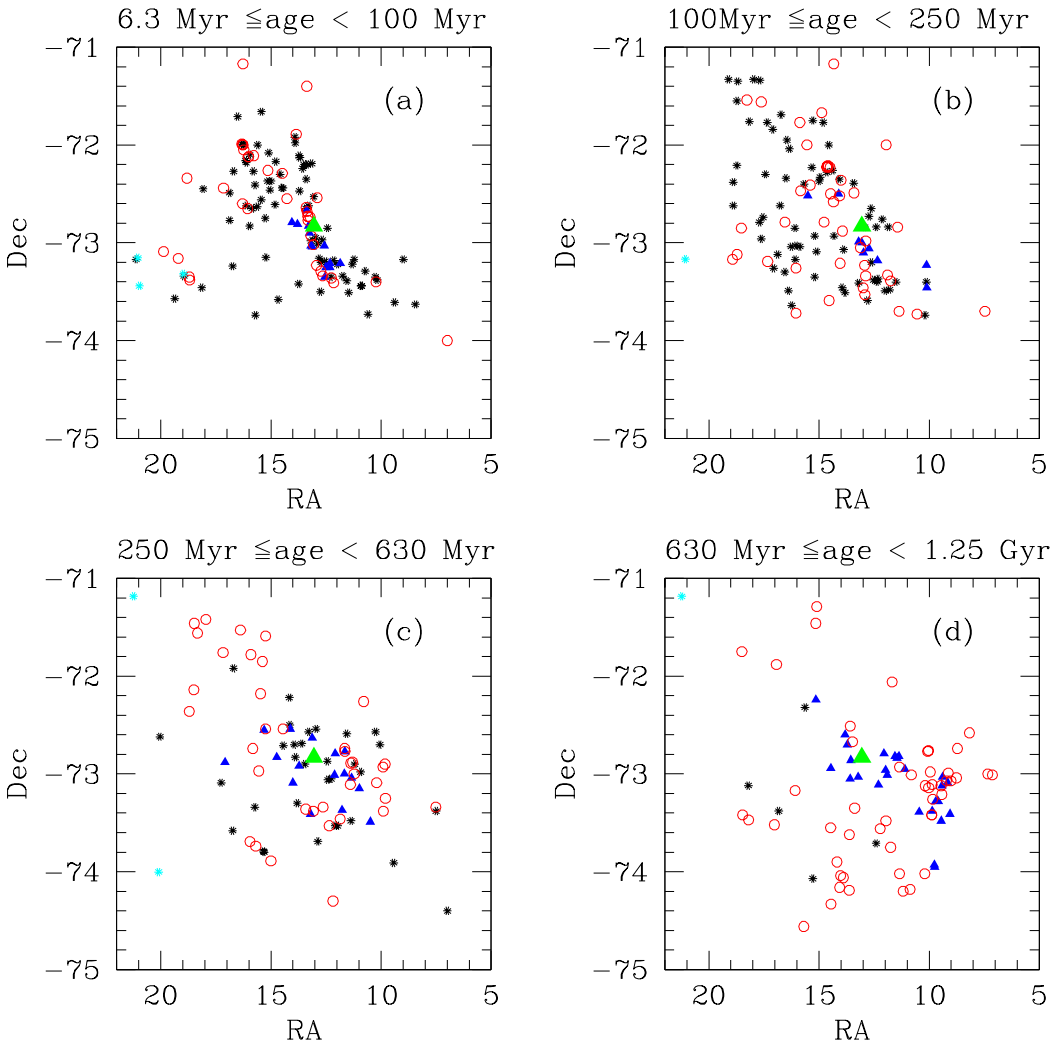

FIGURE 6.9: Spatial location of the SMC clusters at different epochs in each panel, where the clusters are taken from our catalogue (black), by G10 (red circle), C06 and PU99 (blue), 'other-studies' (cyan). The green triangle indicates the centre of the SMC.

along with a group of clusters in the NE region. On the other hand, the Western and the Southern regions are devoid of clusters.

In the age range 100 - 250 Myr (Figure 6.9(b)), most of the clusters are found in the Eastern and NE regions along with the central SMC. The Western and Southern regions continue to be devoid of clusters during this period. We also find that the extent of the NE region is maximum during this period. Figure 6.9(a)

shows the location of clusters formed in the last 100 Myr. These are found to be mostly in the NE region and the central SMC. We notice a specific pattern in the distribution of clusters; different from the other three panels.

Figure 6.9(a) and (d) show the distribution of clusters in two extreme epochs. The spatial distribution can be seen to be distinctly different with no co-relation between the two epochs. Most of the clusters in the older epoch are in the Southern part, whereas the ones in the younger epoch are mostly found in the Northern and central region. The panels Figure 6.9(b) and (c) show the shift of clusters from South to North. Similar shift was found in star formation during the same period by Harris and Zaritsky (2004) (their Fig. 6). Figure 6.9 also suggests that the central region of the SMC is actively forming clusters from $\sim$ 1 Gyr till today. We suggest that a close interaction between the LMC and the SMC 1.2 Gyr ago (Diaz and Bekki (2011)) may be the reason for triggering cluster formation in the Southern and the Western part of the SMC (Figure 6.9(d)). We also suggest that the recent interaction at $\sim$250 Myr (Diaz and Bekki 2011) caused cluster formation in the last 100 Myr, resulting in the spatial distributions as shown in Figure 6.9(a). Figure 13 of Besla *et al.* (2012) showed that the SMC made close passages around the LMC at $\sim$ 900 Myr and 100 Myr ago, which supports the above observation. The spatial distribution of clusters presented in Fig.6.9 could give important clues regarding the details of the interactions.

We made two videos (available online only) to understand the spatio-temporal distribution in detail. In the video-1, we have shown the cluster distribution from older to younger age, and video-2 shows vice-versa. In the videos, we have used the same color notations as in Figure 6.9. The two videos clearly demonstrate the change in location of clusters as a function of age. The details of spatio-temporal distribution of this largest cluster sample will provide important details of cluster formation history in the SMC. The distribution shown in Figure 6.9 are in fact snapshots from the videos for specific epochs. Many such snapshots can be created

for various epochs as required using these videos.

In the case of the LMC (Chapter 4), we identified an outside to inside propagation of cluster formation. On the other hand, in the SMC, we identify a progressive shifting of cluster location from the South to the North during the last 600 Myr. The clusters older than 1.25 Gyr are found to be distributed in the outskirts of the SMC. We identified both the MCs to have a peak in cluster formation at $\sim$ 130 Myr. This is suggestive of a common cluster formation trigger, which is most likely to be the recent interaction between the MCs. The details of spatio-temporal distribution of SMC clusters presented in this chapter together with distribution of LMC clusters (presented in Chapter 4) can be used as a tool to constrain details of the recent LMC-SMC interactions.

6.1.7 Mass-radius relation

In order to understand the structure of the SMC clusters, we have plotted radius of clusters (log(r)) against the strength (log(n_m)) for our studied sample (filled circle) in Figure 6.10. There are five clusters with $n_m > 400$ (categorized as rich clusters), which we excluded for parameterisation, which are also shown in this figure. To compare the structure of the SMC clusters with that of the LMC, we have over-plotted the LMC clusters data (open box). Clusters with different classification are denoted in different color. The figure shows that there is linear relation between radius and strength in logarithmic scale for both the MCs. The figure also suggests that though there is a spread in the radius of clusters with similar strength for both the MCs, the SMC clusters tend to have systematically larger radii than LMC clusters with similar strength. This points to the possibility of compactness of the LMC clusters when compared to the SMC clusters. In order to shed more light on this, it is necessary to estimate the nature of relation between cluster mass and radius.

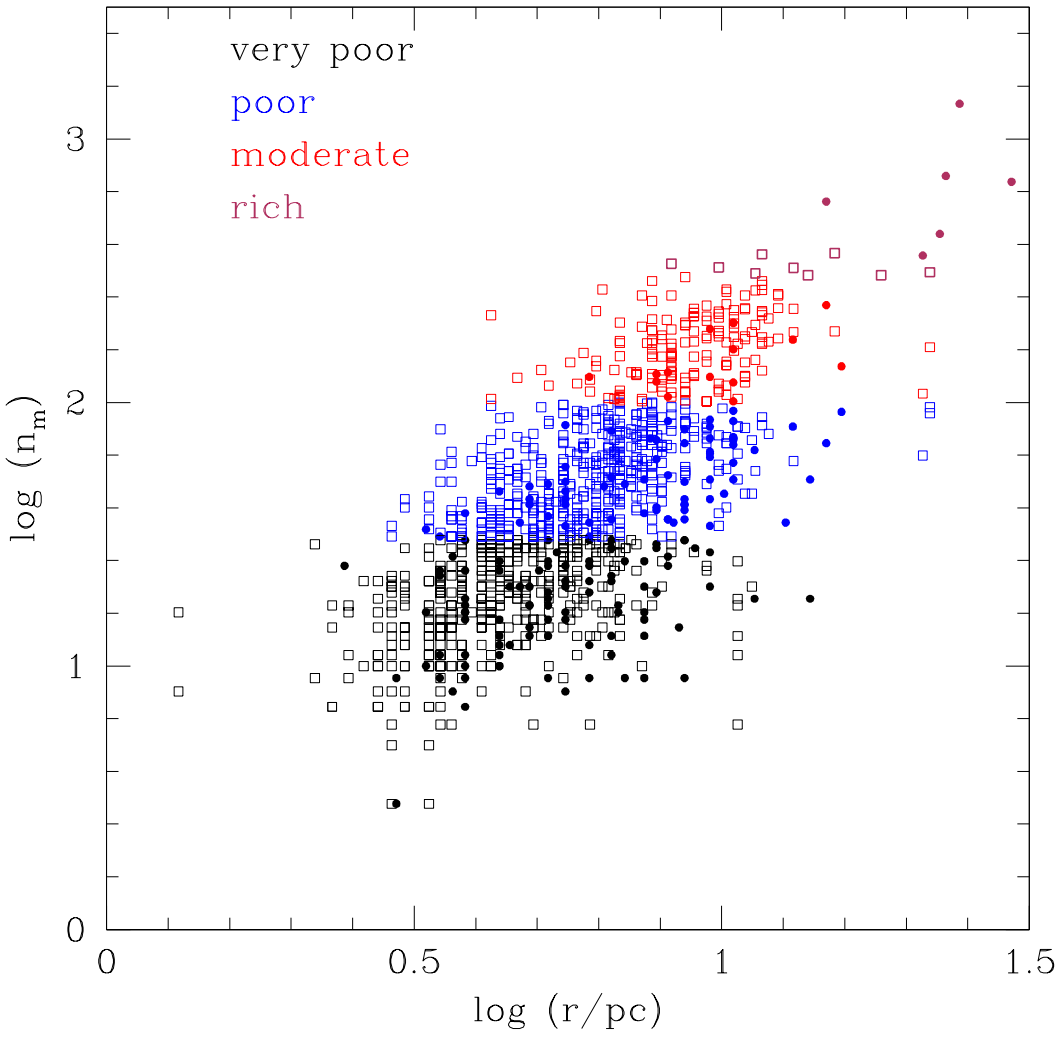

FIGURE 6.10: Relation between radius and strength of clusters in the LMC (open box) and the SMC (filled circle). Clusters of different classification are denoted by different colors.

Figure 6.11 shows the relation between radius (log(r)) and mass (log M) of clusters in the SMC. We took an average of mass range of clusters and average radius of clusters for different groups (I - V) to estimate the co-relation between them. The data points of the LMC and SMC are marked as blue and black respectively. Straight lines fitted to the data points give slopes of 2.10 ($\pm$0.24) and 1.68 ($\pm$0.43) for the LMC and the SMC respectively. The difference in slope if of the order of 1-σ, hence the result is only indicative. There is an indication that the clusters with similar mass occupy smaller radius in the case of the LMC than in the SMC,

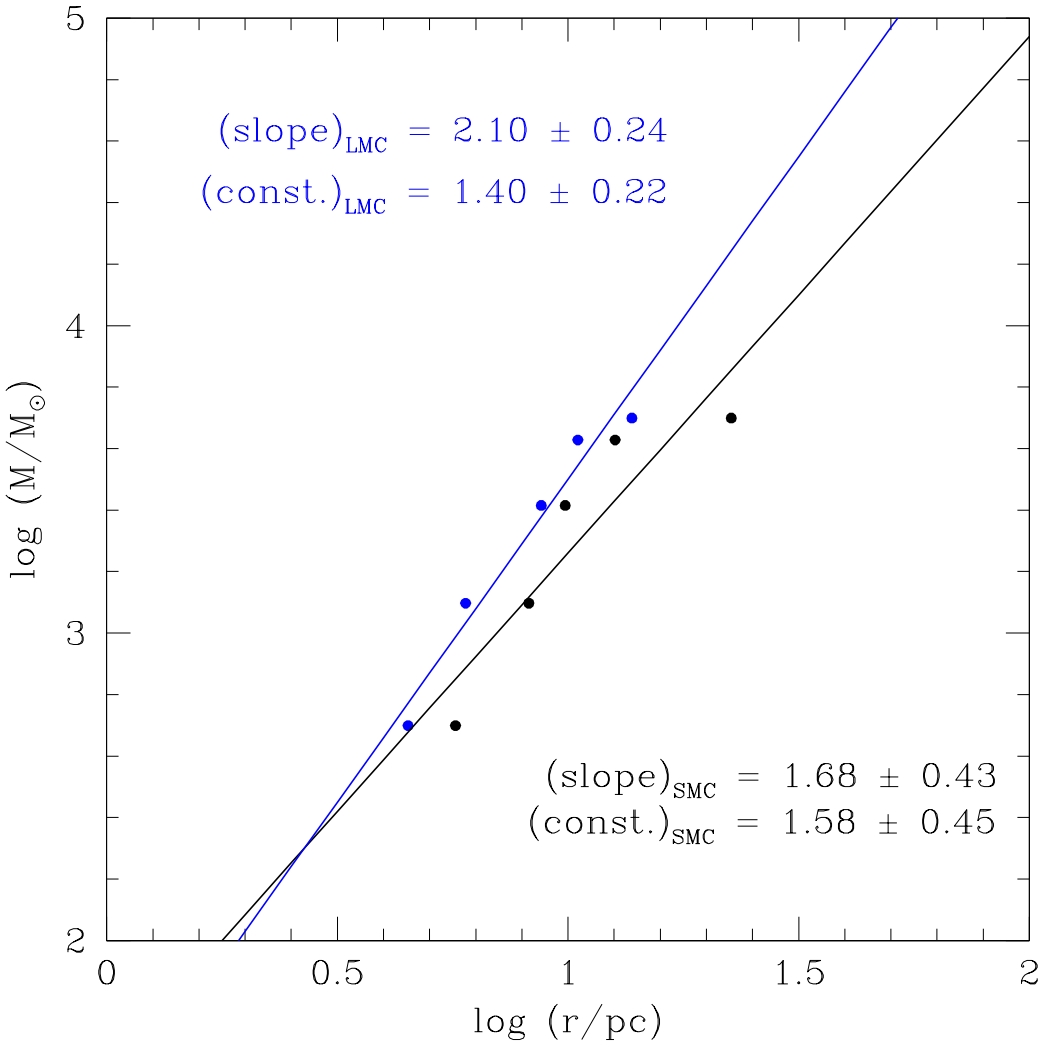

FIGURE 6.11: Relation between average radius and average mass of clusters of different groups. The blue data points correspond to the LMC and the black ones correspond to the SMC. The slope and y-intercept of linear fit are also mentioned in the figure.

indicating that the SMC clusters are loosely bound when compared to those in the LMC. Pfalzner *et al.* (2016) derive a similar relation for star clusters in the solar neighbourhood using the relation $M_c = C_m \times R^{\gamma}$. They find the value of γ as 1.7±0.2 for a large range of cluster mass. They also mention that it is necessary to find out if there exists a universal relation between mass and radius of clusters. We find that the values of γ are similar for the SMC and the Galaxy, whereas it is marginally higher for the LMC. This suggests that cluster formation environment

in the SMC is similar to that of our Galaxy in the solar neighbourhood. Our study shows that there is a tentative evidence for tighter clusters in the LMC, when compared to those in the Galaxy and the SMC. This needs to be verified with the help of better data including individual mass and radii estimates of clusters.

6.2 Summary

1. We have estimated the age and reddening of 179 star clusters in the SMC using OGLE III data and presented a catalog (available online[‡]). Out of 179, 16 clusters are parameterized for the first time. The newly parameterized clusters belong to either very poor or poor group.

2. Field star decontaminated CMDs of all the 179 clusters, fitted with isochrones of estimated age and corrected for reddening are available in online[§] version.

3. The SMC star clusters are classified based on their mass and richness in four groups for the first time.

4. It has been found that 90 % of our studied sample has mass < 1700 $M_{\odot}$, which suggests that the SMC is dominated by low mass clusters. The lower mass limit of the SMC star clusters is found to be very similar to that of the open clusters in the Galaxy. We have also found a tentative evidence for tighter clusters in the LMC, when compared to the SMC and our Galaxy.

5. Combining our sample with previous studies, we compiled age information of 468 clusters to study their spatio-temporal distribution. The age distribution in the SMC peaks at 130 ± 35 Myr, similar to the LMC. We suggest that this could

[‡]http://vizier.cfa.harvard.edu/viz-bin/VizieR?-source=J/A+A/616/A187
[§]available in the appendix of the paper Nayak *et al.* (2018)

be due to the most recent LMC-SMC interaction ($\sim$ 100-250 Myr ago; Besla *et al.* (2012); Diaz and Bekki (2011)).

6. The clusters with age 630 Myr - 1.25 Gyr are found to be located preferentially in the South and West of the SMC, whereas the clusters younger than 100 Myr are found in the North and Eastern regions, suggesting a shift in the location of cluster formation. The central SMC shows a continuous formation of clusters in the last 1 Gyr. The details of this spatio-temporal shift are presented in two videos (available online[¶]).

[¶]https://www.aanda.org/articles/aa/olm/2018/08/aa32227-17/aa32227-17.html

TABLE 6.1: Sample of the complete catalogue[‖] is presented. The table contains the name of the cluster, central coordinates (RA and Dec) as given in B08, size of the cluster taken from B08, estimated reddening and age, in columns 1-6 respectively. Columns 7-9 contain the earlier estimations of ages by G10 ($\log(t_{G10})$), PU99 ($\log(t_{PU99})$) and ($\log(t_{C06})$). The last column contains the designated group number (I-V).

Star cluster	Ra (h m s)	DEC (^{o} $'$ $''$)	Radius ($'$)	E(V−I)	log(t)	$\log(t_{G10})$	$\log(t_{PU99})$	$\log(t_{C06})$	Group
B6*	0 27 57	-74 24 02	0.30	0.10	8.25	–	–	–	I
K9	0 30 00	-73 22 45	0.60	0.17	8.60	8.70	–	–	II
HW8	0 33 46	-73 37 59	0.85	0.11	7.90	8.00	–	–	II
NGC176	0 35 58	-73 09 58	0.60	0.12	7.64	8.20	–	–	II
HW11	0 37 33	-73 36 43	0.65	0.15	8.20	8.50	8.4	8.4	II
L19	0 37 42	-73 54 30	0.85	0.16	8.70	–	>9.0	8.9	IV
B14	0 38 37	-73 48 21	0.26	0.10	8.25	8.65	–	7.9	I
HW12	0 38 51	-73 22 27	0.40	0.09	8.45	8.70	–	8.7	I
H86-48	0 38 56	-73 24 32	0.22	0.07	8.30	–	–	8.0	I
SOGLE6	0 39 33	-73 10 37	0.40	0.17	8.70	8.65	–	–	I

Chapter 7

UVIT-HST-*Gaia*-VISTA study of stellar populations in the star cluster Kron 3

7.1 Introduction

A good number of massive intermediate-age ($\sim$ a few Gyr old) metal-poor star clusters in the Magellanic Clouds show extended main-sequence turn-off (MSTO), that can not be explained by photometric uncertainties or stellar binarity. Age spread within the cluster and effect due to stellar rotation are suggested for the observed extended MSTO. Kron 3 is one such cluster, located in the western region of the main body of the SMC. In this chapter, we plan to investigate the possible reasons behind the observed spread in the MS of Kron 3. Shapley and Wilson (1925a) catalogued this cluster for the first time in the Harvard Circular No. 276 (H.C. 276/81) using observations from a 15-inch telescope at Harvard College Observatory and estimated the cluster diameter as 9.2 pc. Later Gascoigne

and Kron (1952) presented the integrated color and magnitude of this cluster. Kron (1956a) also identified this cluster and estimated its diameter (30 pc) and luminosity (Kron 1956b). The cluster was named after him and appears as number three in his catalog (Kron 1956a). Gascoigne (1966) first presented the CMD of Kron 3 and reported it to be an intermediate-age (∼2 Gyr) cluster. Gascoigne (1980) estimated the age of the cluster as 3 Gyr (limiting magnitude is V=21 mag). Comparing its CMD with theoretical stellar evolutionary model, Hodge (1982) reported metallicity and age of Kron3 as [Fe/H] = −1.3 (±0.3) and 1 Gyr (±0.4) respectively.

The observational data used in above mentioned studies were not deep enough to reveal the MS of the cluster Kron 3. Rich *et al.* (1984) detected the MSTO for the first time (limiting magnitude R=23 mag), using observations from the CTIO 4m telescope and found that Kron 3 hosts multiple populations with a spread in age (age = 5-8 Gyr). The observations were carried out in B and R bands with a seeing of 0″.95. They observed the eastern part of the cluster avoiding the central crowded region. A part of field region was also covered to estimate field stars contamination in the cluster region. The authors estimated the radius of the cluster as ∼2′.4 (42 pc) using the distribution of star counts around the cluster center. They also showed that stars outside the cluster radius belong to a younger population than in the inner region. Fitting isochrones (Vandenberg and Bell 1985) to the CMDs, Alcaino *et al.* (1996) showed that age of Kron 3 ranges from 8-10 Gyr with a DM value of 18.75 mag. They suggested that estimate of a higher DM could be the reason for getting younger ages in previous studies. They questioned the previous estimation of radius by Rich *et al.* (1984). Alcaino *et al.* (1996) showed that stars located in a field outside 2.′0 (35 pc) radius of the cluster center could reproduce cluster red giant branch (RGB) and red clump (RC) in the CMD, along with a rich population of MSTO stars. Therefore, they claimed that radius of the cluster is bigger (∼ 6′ or 105 pc) than previous estimation (∼ 2′.4 or 42 pc) by Rich *et al.* (1984). On the other hand, the recent study by Bica *et al.*

(2008) suggested the radius of the cluster as 1.′7 (30 pc).

With the help of archival Hubble Space Telescope (HST) Wide Field Planetary Camera 2 (WFPC2) observations in F450W (B) and F555W (V) bands, Mighell *et al.* (1998a) estimated age of the cluster as 4.7(±0.6)Gyr. The most recent study by Glatt *et al.* (2008) using HST/ACS data suggests the age to be 6.5 Gyr, with a metallicity of Z=0.001. Hence, there are a range of age (1-10 Gyr) and radius ($\sim$ 30-105 pc) suggested for this cluster.

Metallicity of this cluster is also a source of debate. Gascoigne (1980) estimated the metallicity to be [Fe/H] = −0.6 using the spectra (range 3700-6300 Å) acquired from Anglo-Australian Telescope (AAT), whereas the broad-band Canterna photometry of individual giants resulted in a metallicity of [Fe/H] = −1.5. Studies by Hodge (1982); Rich *et al.* (1984); Alcaino *et al.* (1996); Glatt *et al.* (2008) suggest that metallicity (Z) of the cluster is 0.001 ([Fe/H]=−1.3), whereas Dias *et al.* (2010) reported the metallicity of the cluster as Z=0.0002 by comparing the integrated spectra of the cluster with single stellar population models, suggesting it to be a very metal poor cluster. Alcaino *et al.* (1996) noticed an increase in RGB slope in the CMD with increasing radius of cluster and proposed that a wide range in metallicity could be the reason for this behavior. Danziger (1973) used 11-color intermediate band integrated light photometric system to study the chemical abundances in LMC clusters but including Kron 3. They found that Kron 3 had excessively strong CN index, suggesting higher nitrogen abundance with respect to the other elements. Recent study by Hollyhead *et al.* (2018) confirmed the spectroscopic evidence of nitrogen enhanced stars among the RGB stars. Presence of higher elemental abundance indicates that Kron 3 host stars with multiple populations. As the UV region is more sensitive to metallicity, due to the presence of a large number of absorption lines, it is important to study the UV properties of this cluster, which has not yet been explored.

In this study, we focus on the following aspects of the cluster : (a) estimate the radius of the cluster and (b) study the age and metallicity spread in the cluster using multi-wavelength data. In order to achieve the above aims, firstly, it is important to have a large area coverage as the HST studies have primarily used the central region and the ground based studies have used only the outer regions. Secondly, it is important to have a large coverage in the wavelength including the UV for the cluster as well as the field. We combine our UV observations of this cluster taken with UVIT with HST (for the central regions of the cluster), and *Gaia* and VISTA observations (for the outer regions of the cluster). The superior resolution of UVIT compare to GALEX* in the near-UV and the large area coverage are the advantages of this study.

7.2 Photometry of UVIT data and estimation of cluster radius

Kron 3 was observed in FUV (F148W) and NUV (F242W) filters of the UVIT. In the Chapter 2 we have discussed the generation of science ready images after correcting for satellite drift and distortion using the software CCDLAB (Postma and Leahy 2017). Due to the crowding of stars in the cluster region, a model PSF was generated using isolated stars for both the science ready FUV and NUV images. Then PSF photometry was performed on the images to estimate PSF magnitude of stars as discussed in detail in Chapter 2. We used IRAF package to carry out above task. The FWHM of the model PSF for FUV and NUV filters are 1.″65 and 1.″24 respectively. We applied aperture correction and saturation correction to PSF magnitudes and calculated the final magnitude of the detected stars in corresponding bands.

*The Galaxy Evolution Explorer (GALEX) is an orbiting ultraviolet space telescope launched on April 28, 2003, and operated until early 2012

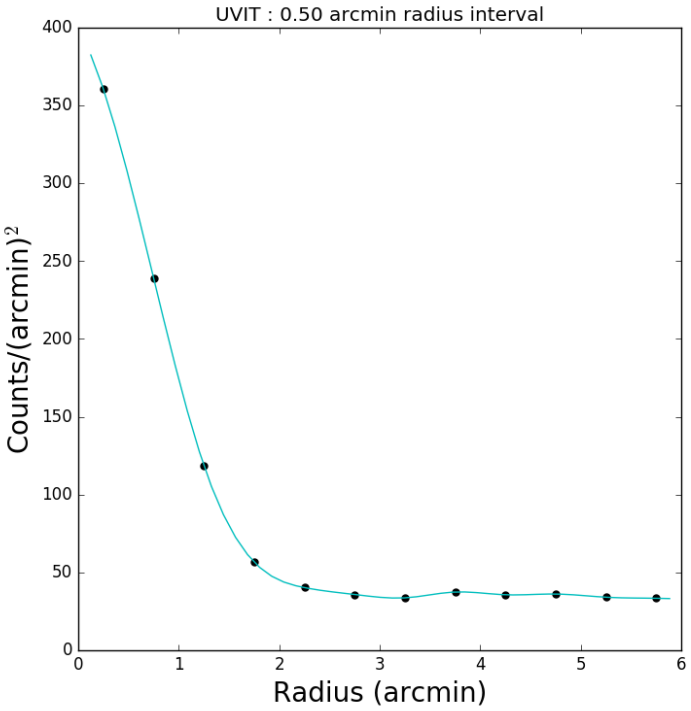

FIGURE 7.1: The radial distribution of star density estimated from UVIT data. The profile suggests that cluster radius is $\sim 2.0'$.

From Figure 2.5, we have seen that there are only a few FUV detections in the central part of Kron 3. Therefore, we used NUV data to estimate cluster radius. We counted the number of stars present in each bin of $0.'5$ in radius around cluster center and normalized with the area of corresponding annuli to determine the number density in each annulus. We plotted number density of stars as a function of radius in Figure 7.1 and fitted it with a cubic spline function. The fitted curve suggests that density of stars within cluster region merges with field star density at $\sim 2.'0$. We therefore considered the radius of the cluster to be $2.'0$ (34.9 pc) and used it in our further analysis. In Figure 7.2, we have plotted photometric error of stars within cluster radius against PSF magnitude for NUV (black points) and FUV (red points) bands. This suggests that photometric error is ≤ 0.3 in both the bands at $\sim$24 magnitude.

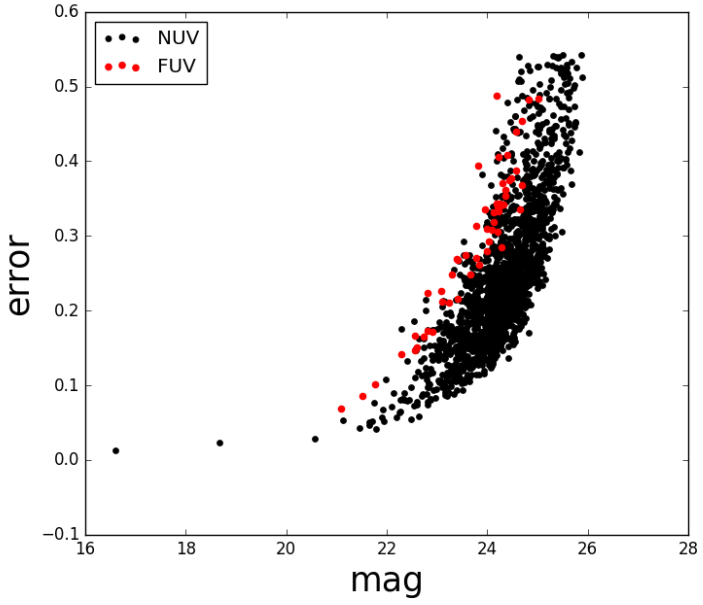

FIGURE 7.2: The photometric error of stars within the cluster radius (2.0′) as a function of magnitude in both NUV and FUV bands.

7.3 Color Magnitude Diagram (CMD)

7.3.1 UV-Optical CMD using UVIT and HST data

We detect only 54 stars in FUV band, but 1623 stars in the NUV within cluster radius of 2′.0, making it hard to make FUV−NUV CMD in order to study cluster properties. On the other hand, it will be quite powerful tool to study cluster properties if we combine NUV data with the data obtained in optical or near-IR filters. We will get a broader color range for the various evolutionary sequences of the cluster, particularly near the MSTO region which is used to estimate the fundamental parameters of the cluster (i.e. age and reddening). We used optical data in F555W (∼V) and F814W(∼I) filters obtained from Hubble Legacy Archive (HLA), which covers the central region of the cluster. We considered stars brighter than 22.5 mag in V filter while cross-matching with NUV data, as we noticed from the isochrone (see Figure 7.3) that we do not detect stars fainter than MSTO

magnitude of Kron 3 (V $\sim$ 22.5) in the UVIT images at the distance of the SMC. Not considering stars fainter than 22.5 magnitude in V band also helped to reduce the crowding in the central part of the cluster, making it easy to cross-match with NUV data. We cross-matched NUV detections with HLA data by considering a maximum separation of 1.″0. In our analysis, we also excluded those findings, where we got multiple HLA detections within 1.″0 radius of one NUV stars. There are 165 such findings. Number of multiple detection increases rapidly for separation more than 1.″0. Using above mentioned criteria, we found 749 common detection in both the data sets.

In the top left panel of Figure 7.3, we plotted V vs (V−I) CMD of full HLA data of Kron 3. We noticed a large spread in the MS as well as MSTO region. We also over-plotted an isochrone (cyan line) of age 7 Gyr for metallicity 0.001 on the CMD, after correcting for reddening of E(V−I) = 0.033 mag and distance modulus (DM) of 19.1 mag. We took the age, reddening and metallicity values from Glatt *et al.* (2008). The above mentioned reddening and DM are used throughout this study to fit the CMDs. In the top right panel we over-plotted V vs (V−I) CMD of the cross-matched stars (black points) on full HLA data (grey points). The cross-matched RC stars are denoted as red points. The bottom right panel shows V vs (NUV−V) CMD of only cross matched stars (black points) and RC stars, which are highlighted in red. We fitted an isochrone after correcting for reddening, extinction and DM. We can see that the clump is no longer a clump in UV-optical CMD, instead gets stretched along the color axis. The extension of RC stars towards bluer color indicates that the RC stars have a range in NUV magnitude. We also notice that the sub-giant branch (SGB), RGB and a part of MS stars are not fitted well by the single isochrone, while these are fitted well in the case of optical CMD. The spread in the MSTO region noticed in the V vs (V−I) CMD becomes even larger in the V vs (NUV−V) CMD. We find that a few SGB, RGB and MS stars get brighter in NUV and appear bluer in V vs (NUV−V) CMD. In the bottom left panel we plotted NUV vs (NUV−V) CMD for cross-matched stars

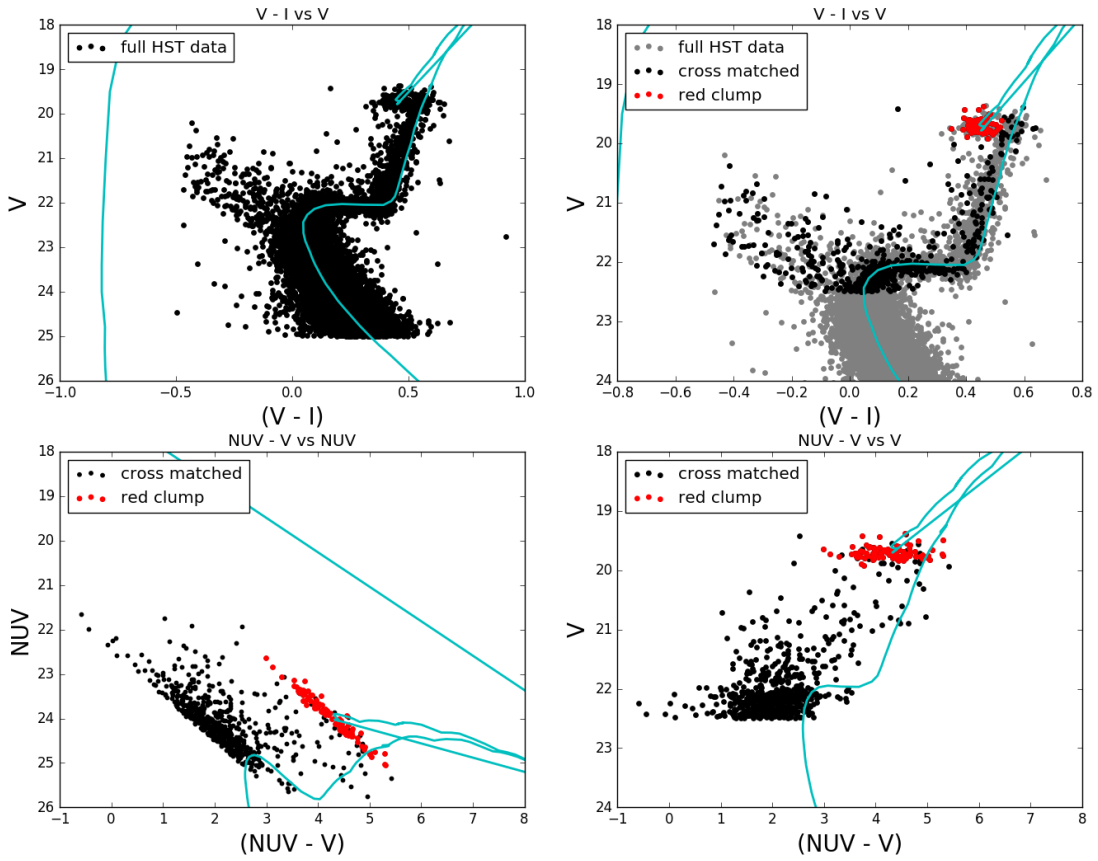

FIGURE 7.3: The top left panel represents the optical CMD of Kron 3, obtained from HLA data. Optical CMD of Kron 3, cross-matched with NUV data is over-plotted (black points) on full HLA data (gray points) in the top right panel. Cross-matched red clump stars are marked as red points in the plot. V vs (NUV−V) CMD is shown in the bottom left panel. We see that red clump stars (red points) get stretched along the color axis. The bottom left panel shows NUV vs (NUV−V) CMD for cross-matched stars. In all the panels, an isochrone (cyan line) of 7Gyr age and metallicity of 0.001 is fitted to the CMD, after correcting for distance modulus and reddening.

and highlighted the RC stars in red. An isochrone of age 7 Gyr and metallicity 0.001 was over-plotted. In this plot we can clearly notice that RC stars extend more than two magnitude in both color (NUV−V) and magnitude axis. We also notice that UVIT reaches its detection limit near the MSTO region, and SGB and part of RGB becomes fainter than MSTO in NUV band. The photometric error is also relatively large near the detection limit. The bottom of the RGB even exceeds the detection limit of the UVIT. Therefore, the stars near the bottom of the RGB in the NUV-optical CMDs not fitted by the isochrone could be due to

lack of detection in NUV. Henceforth we have focused on the evolved population, mainly RC stars which are detected in NUV with less error.

Figure 7.3 suggests that only NUV bright stars located in the MS, SGB and RGB are detected in UVIT images. One possibility is that these bright stars are part of the field star contamination, hence not members of the cluster. In order to ensure whether these bright stars are cluster members or not, it is important to remove field stars from CMD. As the HST data covers only the central part of the cluster, it is not possible to get rid of the distribution of field stars in optical or UV-optical CMD. Hence, we used the recently released *Gaia* data to isolate the field star contamination in cluster CMD, as described in the following subsection.

7.3.2 UV-Optical CMD using UVIT and *Gaia* data

We used the *Gaia* DR2 catalog and considered detection within $15'$ radius around the cluster center to study the field star distribution and its effect on the cluster properties. *Gaia* has large astrometric error in crowded fields such as central regions of dense clusters, which is measured by astrometric_excess_noise parameter (Lindegren *et al.* 2012, 2018). Zero value for the parameter indicates that astrometric solution is most reliable, higher value increases the unreliability in the astrometric solution. Median value of astrometric_excess_noise is 1.3 milli-arcsec at G=19 mag and increases to higher values for fainter sources in the crowded region (Lindegren *et al.* 2018). Hence, we selected stars with astrometric_excess_noise less than 1.3 milli-arcsec. A large fraction ($\sim$70%) of stars is removed by this condition within the central radius $\sim 0.'5$ of the cluster. Hence, *Gaia* data is not useful to study the core of this cluster.

We have also used *Gaia* data to determine the radius of the cluster. We calculated the radial density of stars (number of stars/area) with a bin width of $0.'5$ and

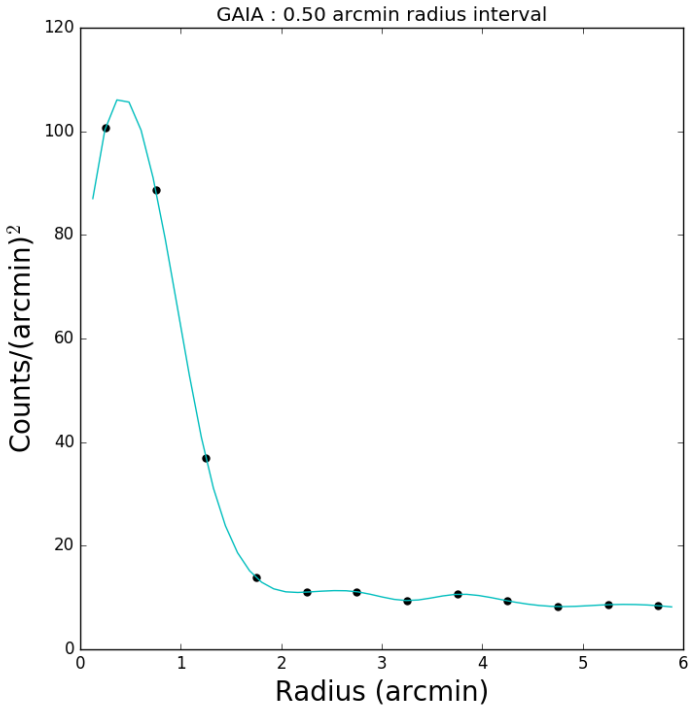

FIGURE 7.4: The radial density profile of Kron 3 using *Gaia* DR2 data, fitted with cubic spline function (cyan).

plotted it against radius in Figure 7.4. We fitted the data points (black dots) with cubic spline (cyan line) and found that density of stars decreased with radius and became equal to field density at $\sim 2.'0$. We observe a dip in the distribution within $0.'5$ radius of the cluster, which is due to the exclusion of stars with large astrometric error. Therefore, the radial distribution of star density suggests that radius of the cluster is $\sim 2.'0$, similar to the value obtained from the UVIT-NUV data.

We cross-matched the NUV data from UVIT with *Gaia* data of $15'$ radius around the cluster center, to investigate the distribution of field stars in the CMD. While cross-matching the two data sets, we considered maximum separation between the same star detected in two bands to be less than or equal to $1.''3$. We excluded four cross-matches, where one star showed more than one cross-match between the two catalogs. We were able to cross-match 238 stars.

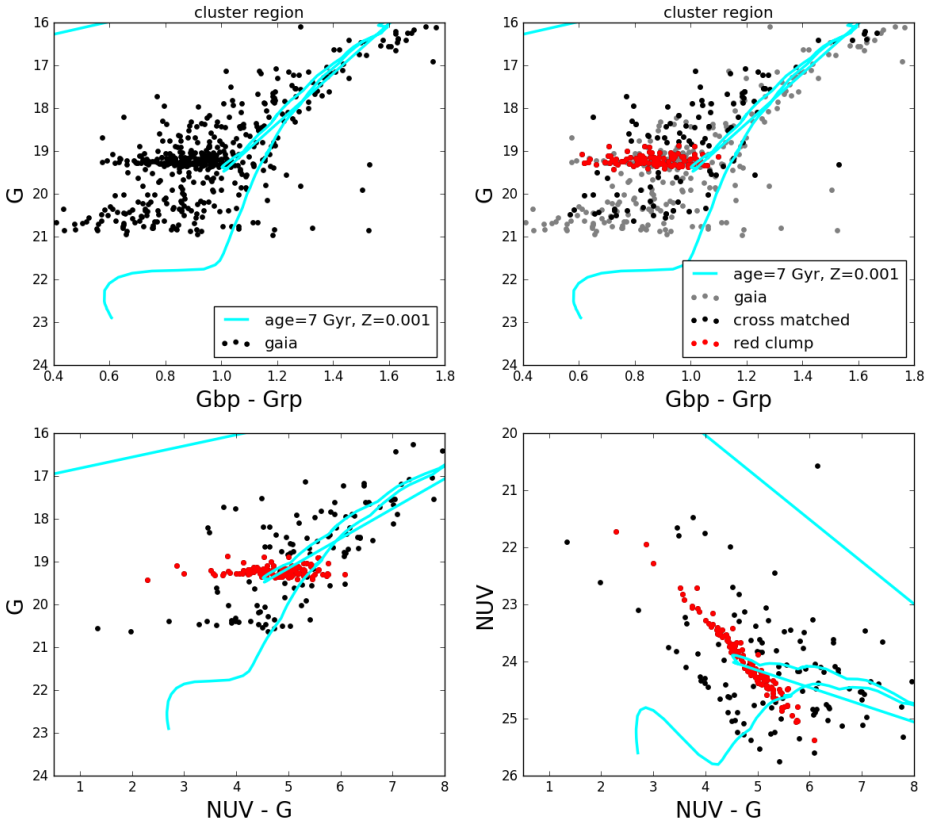

FIGURE 7.5: The top left figure shows G vs (G_{bp}− G_{rp}) CMD of the cluster region using *Gaia* data. In the top right panel we have over-plotted the G vs (G_{bp}− G_{rp}) CMD of *Gaia*-NUV cross-matched data (black points) on full *Gaia* data (gray points) of the cluster region. Red points indicate the red clump stars of cross-matched data, same for other two CMDs also. The bottom right figure shows G vs (NUV−G) CMD of *Gaia*-NUV cross-matched data. The bottom left panel represents NUV vs (NUV−G) CMD for cross-matched data.

In the top left panel of Figure 7.5 we plotted G vs (G_{bp}−G_{rp}) CMD for cluster region (stars within a radius of 2.′0 around the center). An isochrone of age 7 Gyr and metallicity 0.001 was also fitted to the CMD after making correction for earlier values of DM and reddening. In the right panel of Figure 7.5, we over-plotted G vs (G_{bp}−G_{rp}) CMD for cross-matched *Gaia* stars in cluster region (black points) on top of the CMD of *Gaia* stars in cluster region (grey points). RC stars are marked as red. An isochrone was also fitted to the CMDs, similar to previous panel. We can see that RC stars are extended over 0.4 magnitude along the color

axis in both these figures, unlike their distribution in (V, V−I) CMD. The bottom left panel of Figure 7.5 represents G vs (NUV−G) CMD of cross-matched stars with an extended red clump spread over two magnitudes in color, highlighted in red. The similar extension was also found in V vs (NUV−V) CMD (Figure 7.3). The bottom right panel shows NUV vs (NUV−G) CMD for cross-matched stars within cluster region. The figure also exhibits the extension of RC stars over two magnitudes in both color and magnitude axes. Thus, a single isochrone is not able to fit the color extension of RC stars. To investigate whether the extension is due to field star contamination, we performed a statistical technique to decontaminate the field stars.

7.3.3 Removal of field star contamination from cluster CMDs

To carry out the statistical process, we considered that the field stars are uniformly distributed in the sky over a few arcmin around the cluster. An annular field region of area same as the cluster region was chosen outside the cluster radius to carry out the process with an inner radius of 3.′0. We first constructed G vs (NUV−G) CMD for cluster and field region. The field stars within the cluster region are then removed by considering each star in the field CMD and finding its nearest counterpart in the cluster CMD. We considered a grid of [magnitude, color] bins with different sizes, starting with [ΔG , Δ(NUV − G)] = [0.02, 0.01] up to a maximum of [0.5, 0.25], where the units are in magnitude. A similar procedure was used earlier in Chapter 3 to decontaminate field stars in the CMDs of star clusters in the MCs.

In the top left panel of Figure 7.6, we have plotted G vs (NUV−G) CMD for cluster (black) and field region (cyan). Red points indicate RC stars in the cluster region. The top right panel shows the field star decontaminated CMD (G vs NUV−G) of the cluster region. We notice the presence of extended RC stars even

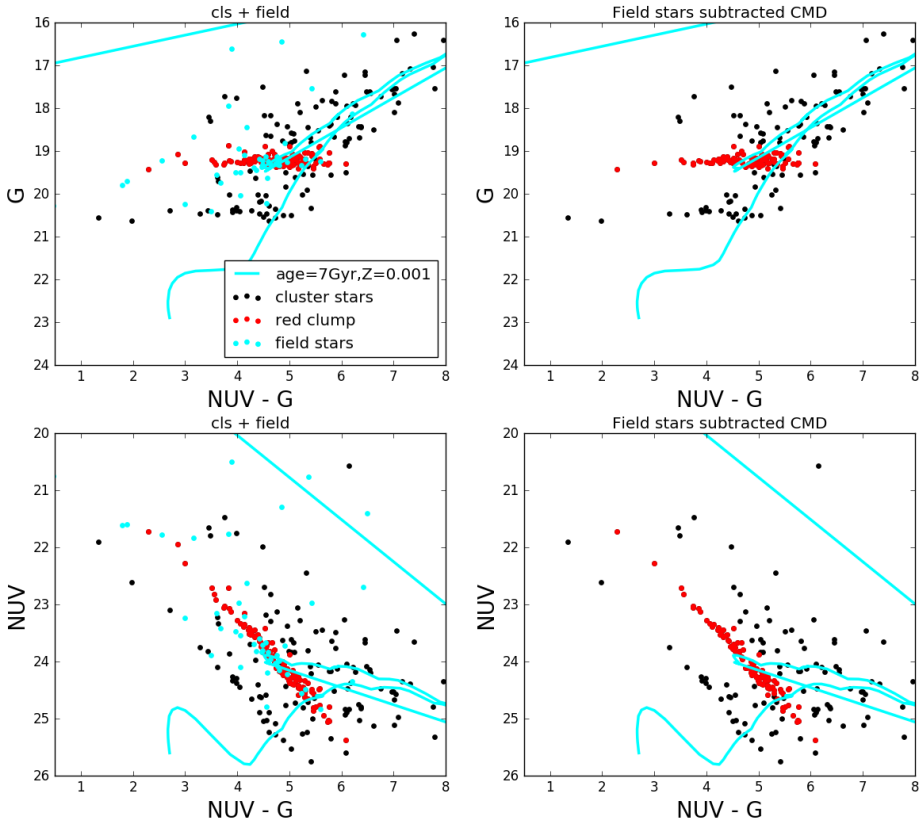

FIGURE 7.6: Top left panel shows G vs$G_{bp} - G_{rp}$ CMD of cluster region (black points) and red clump stars are marked as red points. Fields star CMD (cyan points) is over-plotted on the cluster CMD. The top right panel shows field star decontaminated CMD. The bottom two panels show the same as above but for NUV vs$G_{bp} - G_{rp}$ CMD. We over-plotted an isochrone of 7Gyr age and metallicity of 0.001 to each CMD in this figure.

after the removal of field stars. The bottom left panel of Figure 7.6 shows NUV vs (NUV−G) CMD of cluster (black) and field region (cyan). RC stars are marked as red points. The bottom right panel shows field stars decontaminated NUV vs (NUV−G) CMD for cluster region. The figure suggests that the extension of RC stars is not due to field contamination, rather it is an intrinsic property of the cluster. Now, it is essential to check whether age spread or metallicity spread in the cluster can explain the extended RC present in Kron 3.

7.4 Age and metallicity spread in Kron 3

7.4.1 Isochrones:

To study the age and metallicity spread in Kron 3, we used HLA-UVIT cross-matched data. In Figure 7.7 we plotted V vs (V−I), V vs (NUV−V) and NUV vs (NUV−V) CMDs in the respective panel from left to right and highlighted the RC stars. Then we over-plotted isochrones on each CMD with ages ranging from 2.5 Gyr to 8 Gyr, keeping the metallicity value same as Z=0.001, after correcting for DM and reddening. The figure suggests that though age spread can explain the broad MS in the V vs (V−I) CMD, it is unable to fit the MS spread in both the V vs (NUV−V) and NUV vs (NUV−V) CMDs. The optical CMD (V vs V−I) suggests that the cluster has a spread in the age from 6 to 8 Gyr. However, this spread is not able to explain the extended RC stars. RC points of all the isochrones are located almost at the same part of the RC location, without covering the observed stretch.

In Figure 7.8, we plotted V vs (V−I), V vs (NUV−V) and NUV vs (NUV−V) CMDs in three panels. A set of isochrones of same age 7 Gyr, but with different metallicity values ranging from Z=0.0002 to 0.0190 are over-plotted on each CMD. The figures show that isochrones of different metallicity fit the extended RC. We suggest that the cluster is likely to exhibit a range of metallicities from Z=0.0002 to 0.002 and likely to have a relatively small age spread.

In Figure 7.9, we plotted the distribution of RC stars against color. The upper panel of the figure shows the histogram of (V−I) color of RC stars with a bin size of 0.04 magnitude for full HLA data of Kron 3 and HLA-UVIT cross-matched data, denoted in blue and green color respectively. Both distribution peaks at 0.44 magnitude. Red arrow indicates that the values of (V−I) of RC corresponding to

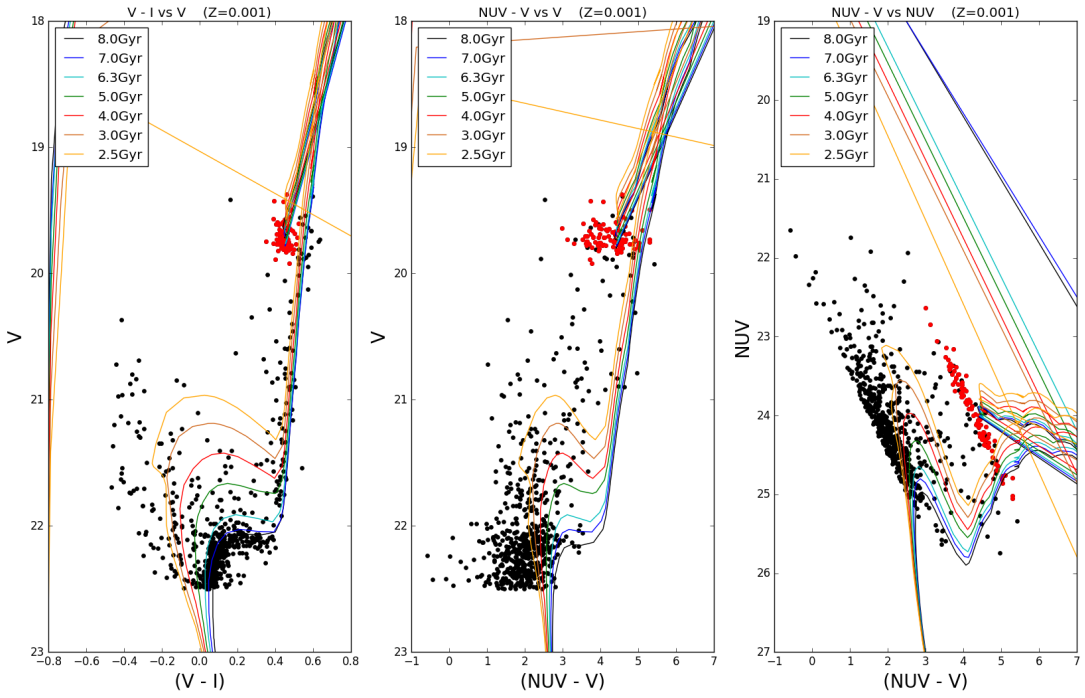

FIGURE 7.7: The V vs (V−I), V vs (NUV−V) and NUV vs (NUV−V) CMDs are shown in three panels respectively from left to right. Red points denote the red clump stars. Isochrones for a range of ages (2.5-8 Gyr, marked with different color) are over-plotted on each CMD, keeping the metallicity value fixed at 0.001. Red clump point of different isochrones merge together in all the three panels.

the isochrones of age range 2.5-8 Gyr for Z=0.001 fall within the peak bin of the distribution. The values of (V−I) of RC corresponding to the isochrones of age 7 Gyr and metallicities Z=0.0002 and 0.002 are shown with black arrows. The lower panel represents the distribution of (NUV−V) color of cross-matched RC stars with a bin size of 0.4 magnitude. The distribution peaks at ∼4.4 magnitude in (NUV−V) color. The arrows indicate the same as mentioned for upper panel. The black arrows in both the plots clearly indicate that broadening of the RC stars can be explained with the presence of metallicity range in the cluster.

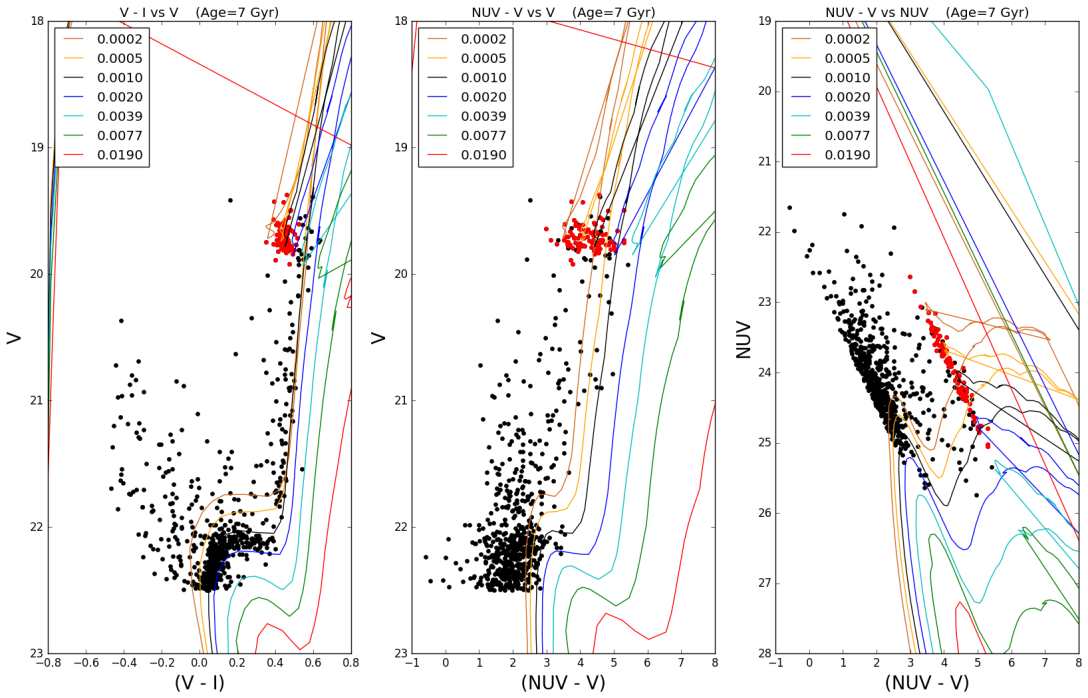

FIGURE 7.8: The V vs (V−I), V vs (NUV−V) and NUV vs (NUV−V) CMDs are shown in three panels respectively from left to right. Red points denote the red clump stars. Keeping the age value fixed at 7Gyr, we have over-plotted isochrones for metallicity ranges from 0.0002 to 0.0190, denoted in different color.

7.4.2 Color of RC stars from model spectra

If there is a metallicity gradient among the RC stars, then the NUV flux of metal poor stars should be higher than that for the metal rich stars. It is therefore necessary to calculate the expected flux for RC stars in different bands from theoretical synthetic spectra and to check whether one can get excess flux in NUV for above mentioned metallicity range. We used Kurucz models (Castelli *et al.* 1997) synthetic spectra obtained from Virtual Observatory SED Analyzer (VOSA; Bayo *et al.* (2008)) tool to estimate flux in different bands.The model spectra cover a large range of the following parameters: range in metallicity is [Fe/H]=-2.5 to 0.5, log(g) ranges from 0 to 5.0 and T_{eff} range is 3500 - 50000 K. [Fe/H] and log(g) have a resolution of 0.5 whereas T_{eff} has a resolution of 250K. From the isochrone table we found that RC stars have a surface gravity value log(g) $\sim$ 2.5 which does

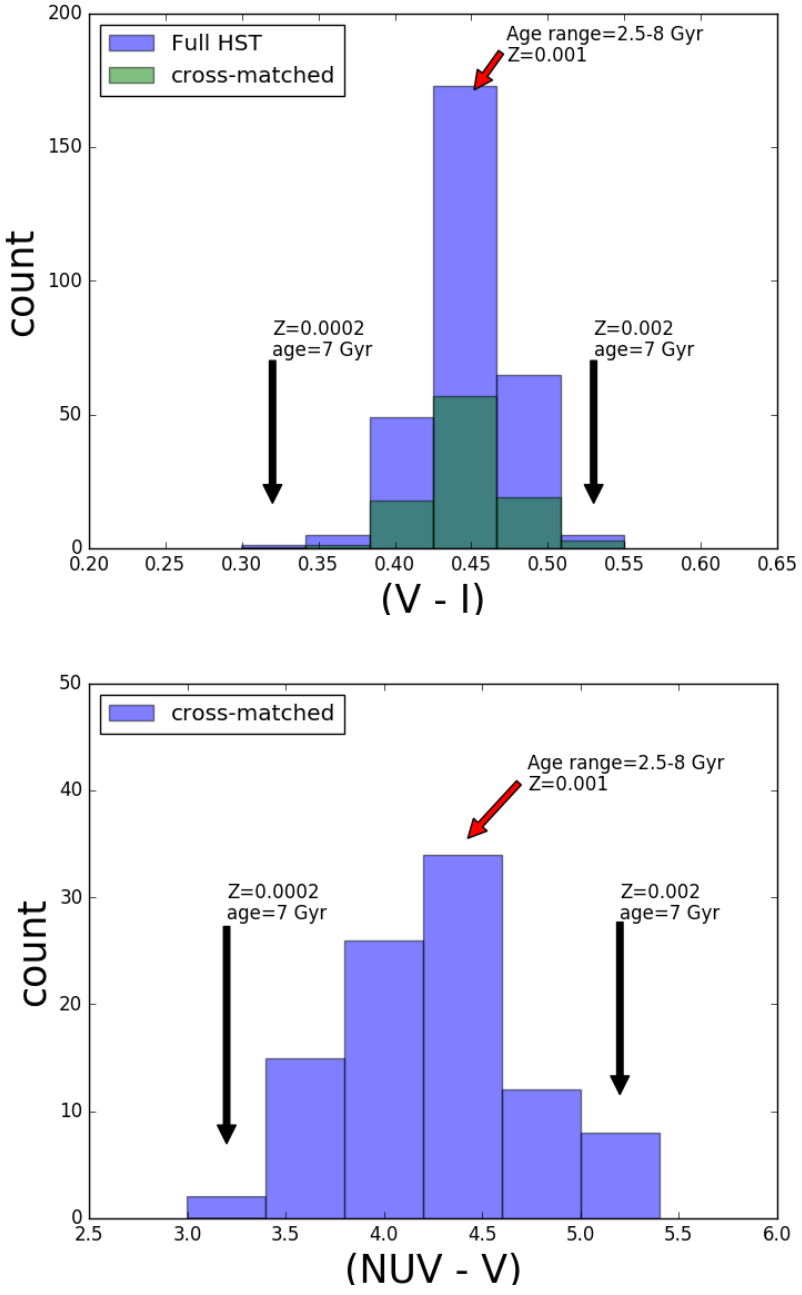

FIGURE 7.9: Figure shows the distribution of red clump stars as a function of color. The upper panel shows the distribution of RC stars against (V−I) color for full HLA data (in blue) and HLA-UVIT cross-matched data (in green). Both distribution peak at ∼0.44 mag. The black arrows indicate values of (V−I) color of RC of a 7 Gyr old isochrone for metallicities Z=0.0002 and Z=0.002. The red arrow indicates the (V−I) values of RC, for isochrones of age range 2.5-8 Gyr with metallicity Z=0.001 lie within the peak bin. The lower panel shows the distribution of RC stars against (NUV−V) color for cross-matched data. The arrows indicate the same as upper panel.

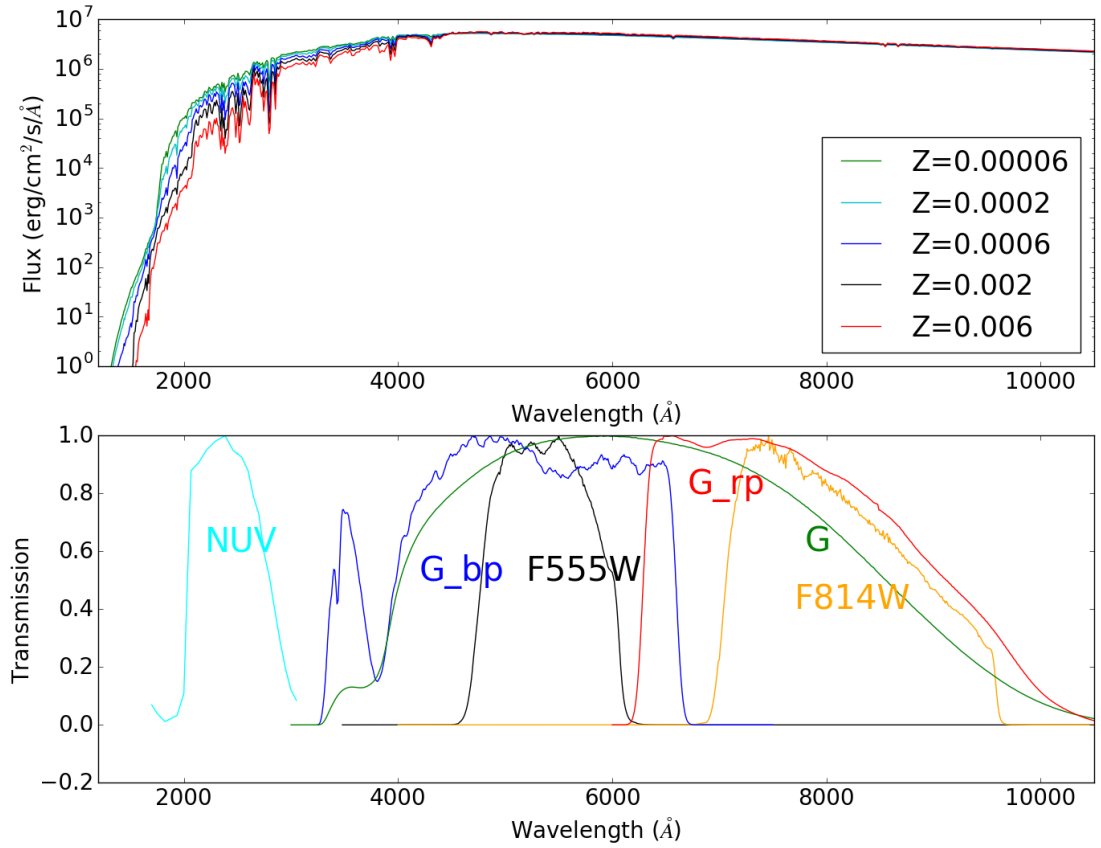

FIGURE 7.10: Model spectra for metallicity range Z = 0.0002 to 0.006 (marked in different color) are presented in the upper panel, for a fixed value of temperature (5250K) and log(g) (2.5). In the lower panel the plot shows response curves for pass bands used in this study, marked in different color. The name of the pass bands are noted in the plot.

not change much with respect to age, metallicity or temperature. From the table we also found that RC stars have a temperature range 5100-5600 K for a metallicity range 0.002 - 0.0002 with an age of 7 Gyr. At first we plotted model spectra in Figure 7.10 for different metallicity, for a fixed value of temperature and log(g) as 5250 K and 2.5 respectively, to check the variation in flux over the wavelength range. Figure 7.10 clearly shows that there is a significant difference in flux for different metallicity for wavelength below 4000 Å, which is not prominent at longer wavelength. In the lower panel of the figure we have shown normalized response curves for different filters used in this study. The names of the filters are noted in the figure. We can see that NUV (N242W) filter falls within the region where variation in flux is noticeable. The zoomed version of this region is shown in Figure

7.11, to highlight the flux variation in the above mentioned metallicity range. It is seen that the continuum flux reduces to almost half when metallicity changes from 0.0002 to 0.002 at 5250 K. Reduction of flux to half of its initial value corresponds to 0.75 magnitude. We also noticed that absorption spectral lines get deeper with increase in metallicity and causes reduction in flux. Figures 7.10 & 7.11 suggest that UV region is more sensitive to metallicity than optical/IR. As most of the absorption lines due to metals appear in the UV, the higher the metallicity the more will be the absorption by metals present at the surface of stars which will make it fainter. As there are more metallic lines present in the UV region than optical or IR, variation in the flux due to metallicity is more in the UV region. This could be one of the reasons for some of the RC stars getting brighter in NUV due to low metallicity, which makes an extended RC distribution in NUV-optical CMDs but not in optical CMDs.

To get a quantitative estimation of expected flux in all the bands, we convolved the filter responses with the model spectra for different temperature and metallicity using VOSA tool. We chose a temperature range 5000-5500 K and an [Fe/H] range -2.5 to -0.5, to estimate fluxes in different pass bands. After estimating the flux, we scaled it to a distance of 10 pc by multiplying it with a scaling factor $(R_c/D)^2$ to calculate absolute flux value, where R_c is average radius of RC stars and D is the distance (10 pc). This absolute flux was converted to absolute magnitude (M) using standard relation : M = -2.5 $\log(F_*/F_0)$, where F_* is the flux of the star and F_0 is the value of zero point flux in respective filter. The zero point flux values were taken from the Spanish Virtual Observatory (SVO) filter profile service. In Figure 7.12 we over-plotted the model generated magnitude of RC stars after correcting for DM and reddening. The green points indicate the magnitude obtained for different metallicity at temperature 5500 K. The blue and orange points denote the same for temperatures 5250 and 5000 K respectively. We also over-plotted isochrones for a range of metallicity but for a fixed age (7 Gyr), marked in different colors. The observed RC clump stars are marked as red.

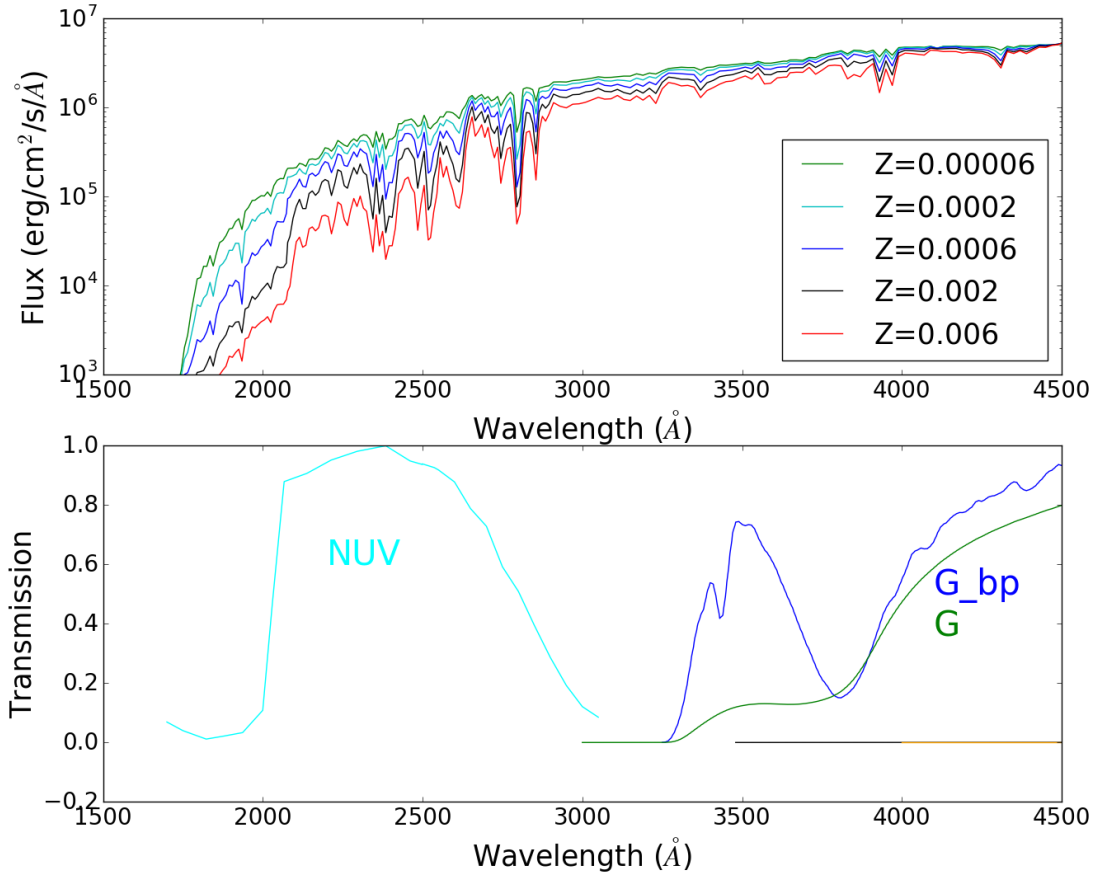

FIGURE 7.11: Figure represents the zoom version of Fig.7.10 to show the absorption lines and flux variation prominently below 4000 Å for different metallicities. The notations in the plots are same as Fig.7.10.

The left panel shows the optical CMD (V vs V−I) using HLA data. The figure also shows that model generated magnitudes are clumped together for a constant temperature, suggesting that the RC population is not stretched in either color or magnitude axis, due to metallicity variation. On the other hand, model generated magnitudes get stretched in color in the V vs (NUV−V) CMD (middle panel) for a constant temperature and show a small variation in the magnitude axis. The middle panel shows that the range of temperature 5250 to 5500K, and metallicity can describe the extension of RC stars, which gets more prominent in the NUV vs (NUV−V) CMD (right panel). In the right panel, the extension of RC stars in both color and magnitude axes are fitted well by the theoretical points for the considered range of temperature and metallicity. This analysis is able to support

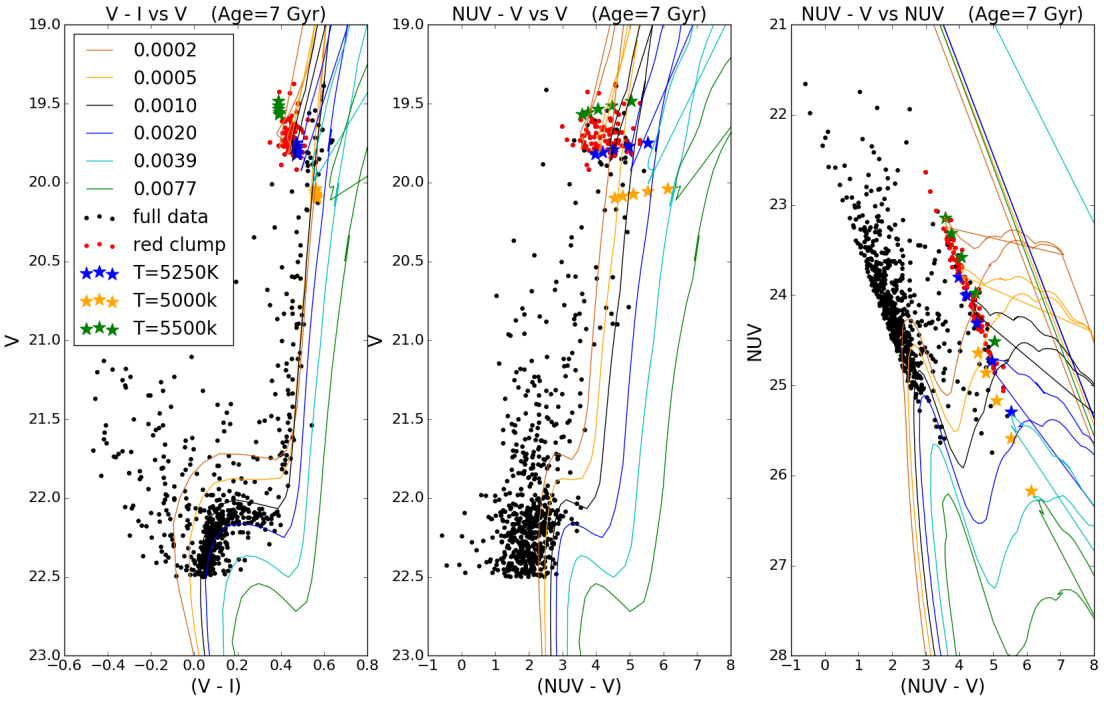

FIGURE 7.12: The V vs (V−I), V vs (NUV−V) and NUV vs (NUV−V) CMDs are shown in three panels respectively from left to right. Red points denote the red clump stars. Keeping the age value fixed at 7Gyr, we have over-plotted isochrones for metallicity values from 0.0002 to 0.0077, denoted in different color. We have also over-plotted the expected colors and magnitudes for RC stars for different temperature and metallicity range after correcting for DM and reddening. Expected color and magnitudes for temperatures 5500, 5250 and 5000K are denoted as green, blue and orange points. The metallicity values used to calculate the expected magnitudes are 0.00006, 0.0002, 0.0006, 0.002, 0.006.

and strengthen the suggestion that Kron 3 hosts stars with a range of metallicity.

7.4.3 Spectral Energy Distribution (SED) of extended RC stars

It is also important that we estimate values of temperature and metallicity for a few RC stars in order to verify the above claim. For this, we constructed spectral energy distribution (SED) for RC stars and fitted them with theoretical model spectra using VOSA tool. The tool performs multiple iterations to fit the observed

flux distribution with the theoretical model flux for different combination of T_{eff}, log(g), [Fe/H] and M_d values, and gives the best fitted parameters after performing a χ^2 minimization. The scaling factor (M_d) is used to scale the model flux to match the observed flux and is defined as $(R_c/D)^2$ where R_c is radius of the star and D is distance to it. We considered the distance to the cluster as 60 kpc. We note that fixing this value does not impact the SED fits, as it affects only the R_c values, which are not considered here. We provided the extinction value of the cluster, $A_V = 0.082$ (Glatt *et al.* 2008) as an input parameter to the VOSA tool. In this study we determined reduced χ^2, which is defined as

$$\chi^2_{reduced} = \frac{1}{N-n} \sum_{k=1}^{N} \frac{(F_{o,k} - M_d \times F_{m,k})^2}{{\sigma_{o,k}}^2} \tag{7.1}$$

Where, N is the number of photometric data points, n is the number of input free parameters, $F_{o,k}$ is observed flux, $F_{m,k}$ is the model flux. To obtain a better estimation of parameters, it is necessary to have more data points covering a wider range of wavelength, while generating the SED and comparing with theoretical model. Therefore we included the VISTA survey data for Magellanic Clouds (VMC; Cioni *et al.* (2011)), to obtain flux values of RC stars in IR regions. Then we looked for the RC stars which are detected in all the four observations by UVIT, HLA, *Gaia* and VMC. We found 18 such RC stars. We used the UVIT, *Gaia* and VMC data to generate the SED after converting magnitude to flux value and fitted with Kurucz model spectra for all the 18 stars. The *Gaia*, UVIT and VISTA fluxes were fitted well with spectra, whereas a small shift was found in the HST flux. As the HST wavelength is covered by the *Gaia* pass bands, we excluded the HST fluxes in the fits. Initially we set all the input parameters ([Fe/H], log(g) and temperature) as a free value to get the best fit parameters. All the stars are fitted with a single spectrum. We found that for most of the stars, fitted parameters lie between -2.5 to -0.5 for [Fe/H] and 5 to 0 for log(g). For two stars [Fe/H] was found to be solar. Temperatures of all the stars were found to lie between 5250 to 5500 K. In Figure

7.13 & 7.14, we have shown model fitted SEDs for two stars. In both figures observed and expected model fluxes are denoted in blue and red points respectively, plotted on the best fitting theoretical spectrum (grey). In Figure 7.13 the observed fluxes of the RC star in different bands are fitted with model spectrum of [Fe/H], log(g) and T_{eff} value -2.5, 1.0 and 5250K respectively. In Figure 7.14 the fitted model spectrum gives the value of [Fe/H], log(g) and T_{eff} as -0.5, 4.5 and 5500K respectively. Both figures suggest that expected model fluxes are matching well within the error of observed fluxes. In the bottom panel of both figures we have also plotted the residual ((observed flux - model flux)/observed flux) for all the filters which clearly indicates that the residue is close to zero. $\chi^2_{reduced}$ values for the fitted SEDs presented in Figure 7.13 & 7.14 are found to be 18.1 and 10.6. The model fitted SEDs of rest of the 16 stars are presented in Figures 7.16 and 7.17 at the end of this chapter. The values of model fitted parameters are noted in those figures.

From the isochrone model we found that log(g) value of RC stars is $\sim$2.5 and does not change much with respect to age and above mentioned metallicity range (-2.5 to 0). Therefore, we tried to fit SED keeping log(g) value fixed at 2.5 and set [Fe/H] & T_{eff} as free parameters. We found that the RC stars are fitted with model spectrum for a relatively smaller metallicity range, -1.5 to 0. We obtained similar temperature range as before. We noticed that $\chi^2_{reduced}$ values did not show much variation with respect to the previous estimates except for two stars. Hence, SED analysis also supports the suggestion that Kron 3 hosts multiple stellar populations with a wide range in metallicity. In Figure 7.15, we have shown the distribution of [Fe/H] derived using SED fitting for 18 stars. Blue histogram represents the distribution of [Fe/H] when all the input parameters are kept free, whereas the green histogram shows the distribution of [Fe/H] while the input values of [Fe/H] and T_{eff} are kept as free but for a fixed value of log(g) = 2.5. The distribution suggests that metallicities are almost equally distributed in a wider range from -2.5 to 0 if we do not fix the log(g). Fixing the value of log(g)

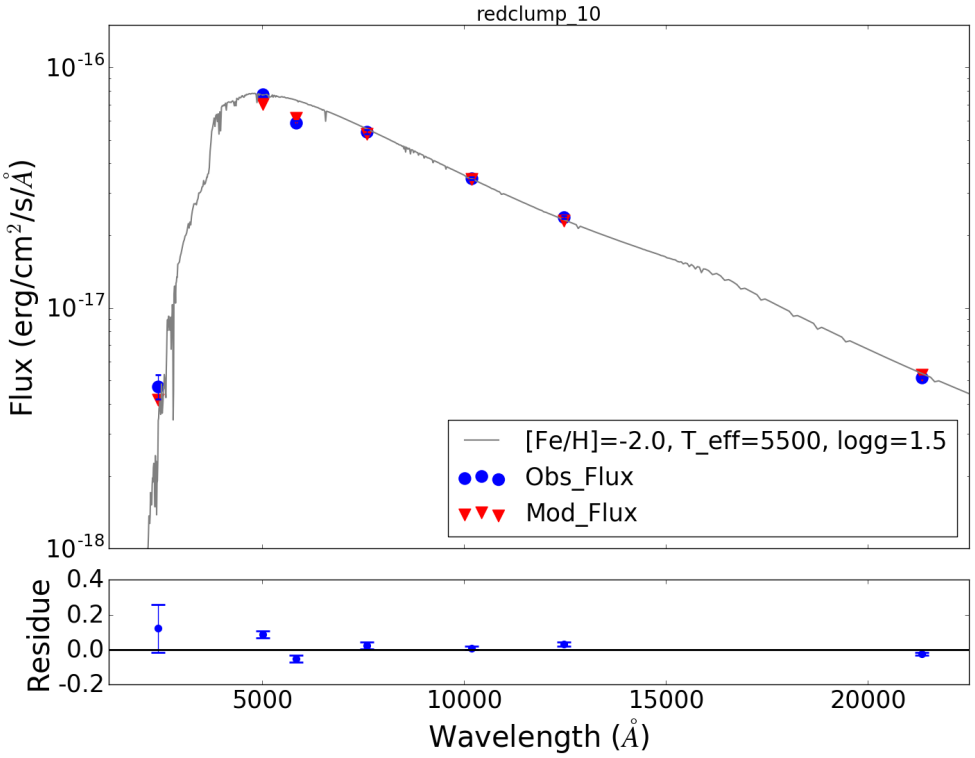

FIGURE 7.13: The upper panel shows spectral energy distribution (SED) of a RC star. The blue and red points represent the observed and expected flux respectively in different pass bands. The synthetic model spectrum (grey) is over-plotted on observed flux. Parameters of the fitted model spectrum are noted the plot. The lower panel shows the residual of fluxes, represent the amount of excess or lack of flux observed in various pass bands for the RC star.

gives a relatively small range in metallicity from -1.5 to 0.0 with a peak at -1.0.

7.5 Discussion

In general, multiple populations due to large variation in the elemental abundance are found in Galactic globular clusters, which were once thought to be chemically homogeneous. Variation in metallicity has been recently found in a few clusters in the SMC, which are in the age range of $\sim$ 6-8 Gyr (Lindsay 1, NGC 416, NGC 339 and Kron 3). These are therefore the youngest clusters where elemental abundance

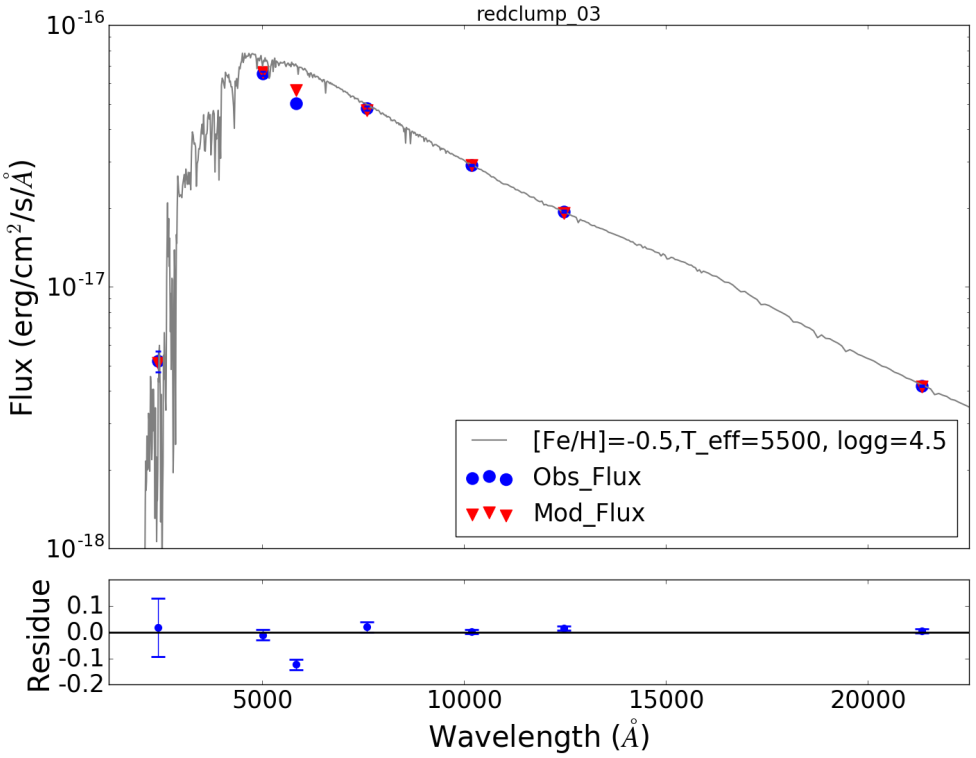

FIGURE 7.14: The Figure represents the same as Figure 7.13, but for another RC star.

variations are found. The results are based on the spectroscopy of giants in the clusters. The morphology of RC stars in these clusters are not studied so far. Here we present the first detailed analysis of the RC stars in Kron 3.

Our UVIT images in NUV are able to detect RC stars in Kron 3 with good photometry. We demonstrate that Kron 3 exhibits an extended RC in UV-Optical CMDs. This extension of RC stars could be due to contamination by field stars, age spread in the cluster, metallicity gradient or variable mass loss among the stars. We investigated some of the above mentioned aspects to explain the extended RC. We noticed that decontamination of field stars is not able to curtail the extension of RC stars, which suggests that it is an intrinsic property of the cluster.

We have also examined whether the extension is due to multiple stellar populations

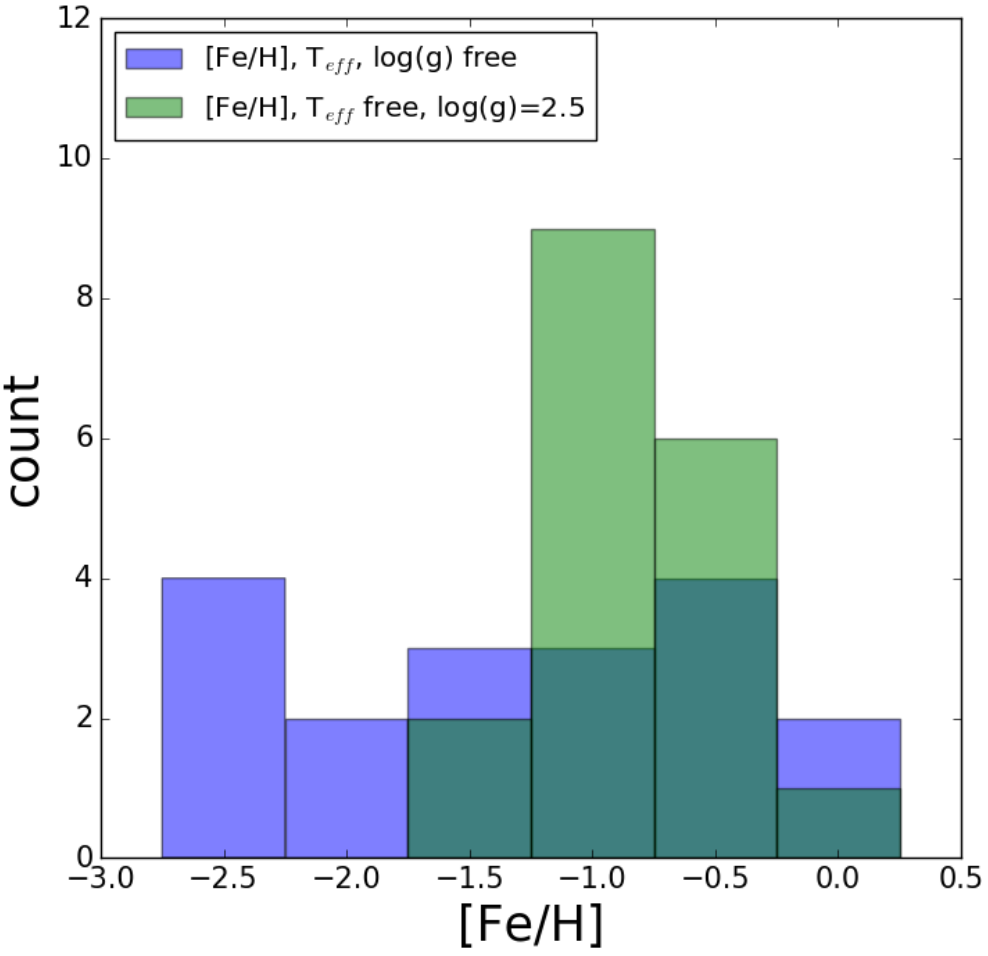

FIGURE 7.15: Figure shows the distribution of metallicity values obtained by fitting SEDs. The blue histogram represents the distribution of [Fe/H] while all input parameters ([Fe/H], log(g) & T_{eff}) are set as free, whereas the green histogram indicates the distribution for a fixed value of log(g) = 2.5 but with other two input parameters kept as free.

arising out of age or metallicity variations. With the help of isochrones, we found that an age spread is unable to fit the extended RC distribution. Theoretical isochrones revealed that color of RC stars is independent of age. We suggest that the cluster has a small range in age, though we are unable to quantify.

We used three methods to check whether a range in metallicity can reproduce the observations. These are (1) isochrones, (2) color from model spectra and (3) SEDs.

Figure 7.8 shows that isochrones of different metallicities for age 7 Gyr are able to explain the extended RC. We found that Kron 3 has a range of metallicities from Z=0.0002 to 0.002. The lower metallicity RC stars appear hotter and brighter in UV-optical CMD, while higher metallicity RC stars appear relatively fainter and cooler.

The color estimated from model spectra with temperature and log(g) corresponding to the RC stars and a metallicity of the above range, were found to remarkably fit the RC distribution in the observed CMD. We show that the spectral features which fall within the NUV pass band is found to be sensitive to metallicity. This is reflected in the range in model generated colors for a range in metallicity. Thus we also demonstrate that NUV pass band is ideal to study variation in metallicity among the RC population.

To get the actual range in temperature as well as metallicity of the RC stars we have constructed SEDs and fitted with model spectrum. We have used a large wavelength coverage for the SED, from NUV to IR. The best fitted model spectrum suggest that RC stars have a large metallicity range between Z=0.00006 to solar metallicity with temperature range 5250 to 5500K. We find that a smaller metallicity range is obtained if we fix the log(g) value to that of the RC stars.

All the three methods suggest that the RC stars have a wide range in metallicity. This is probably the first cluster where the RC stars are suspected to have a large range in metallicity. A spectroscopic abundance study of RC stars in this cluster has not been performed so far. A recent spectroscopic study of RGB stars in Kron 3 by Hollyhead *et al.* (2018) suggested that a sub-population of nitrogen enhanced stars are present in Kron 3. They studied the CN band at 3938 $\mathring{A}$ and found variation in its strength with respect to the CH band. Thus variation in nitrogen could be contributing to the metallicity variation that we find among the RC stars. Dias *et al.* (2010) estimated the metallicity of Kron 3 as Z=0.0004,

which falls within metallicity range found in this study. It is thus important to perform a spectroscopic study of the RC stars in this cluster to understand the elemental variation among these stars. Our study thus supports that Kron 3 is indeed a young cluster of age 7 Gyr with multiple populations due to variation in metallicity.

7.6 Summary

We summarize the results of our study of Kron 3 cluster in the SMC, below:

1. We present the analysis of UVIT-HST-*Gaia*-VISTA data for the intermediate age cluster Kron 3 in the SMC. For the first time, we report the identification of NUV bright RC stars and the extension of RC stars in the CMD. This study thus demonstrates the power of UVIT-HST-*Gaia* combination to study clusters in the Magellanic Clouds.

2. We take advantage of the resolution of HST in the central region of the cluster and *Gaia* for the field coverage, to combine with the UVIT data. We find that the extended RC is an intrinsic property of the cluster and not due to contamination from the field stars. We estimated the radius of the cluster as $2.'0$ (35 pc) from the UVIT and *Gaia* data.

3. We suggest that the cluster exhibits multiple stellar populations with a small age range of 6-8 Gyr and a large metallicity range. All the three methods used in this study suggest a large spread in metallicity among the RC stars.

4. We suggest that the spread in elemental abundance found among the RGB

stars of this cluster (Hollyhead *et al.* 2018) could be contributing to the observed spread in metallicity among the RC stars. This claim needs to be verified using a high resolution spectroscopic study of the RC stars.

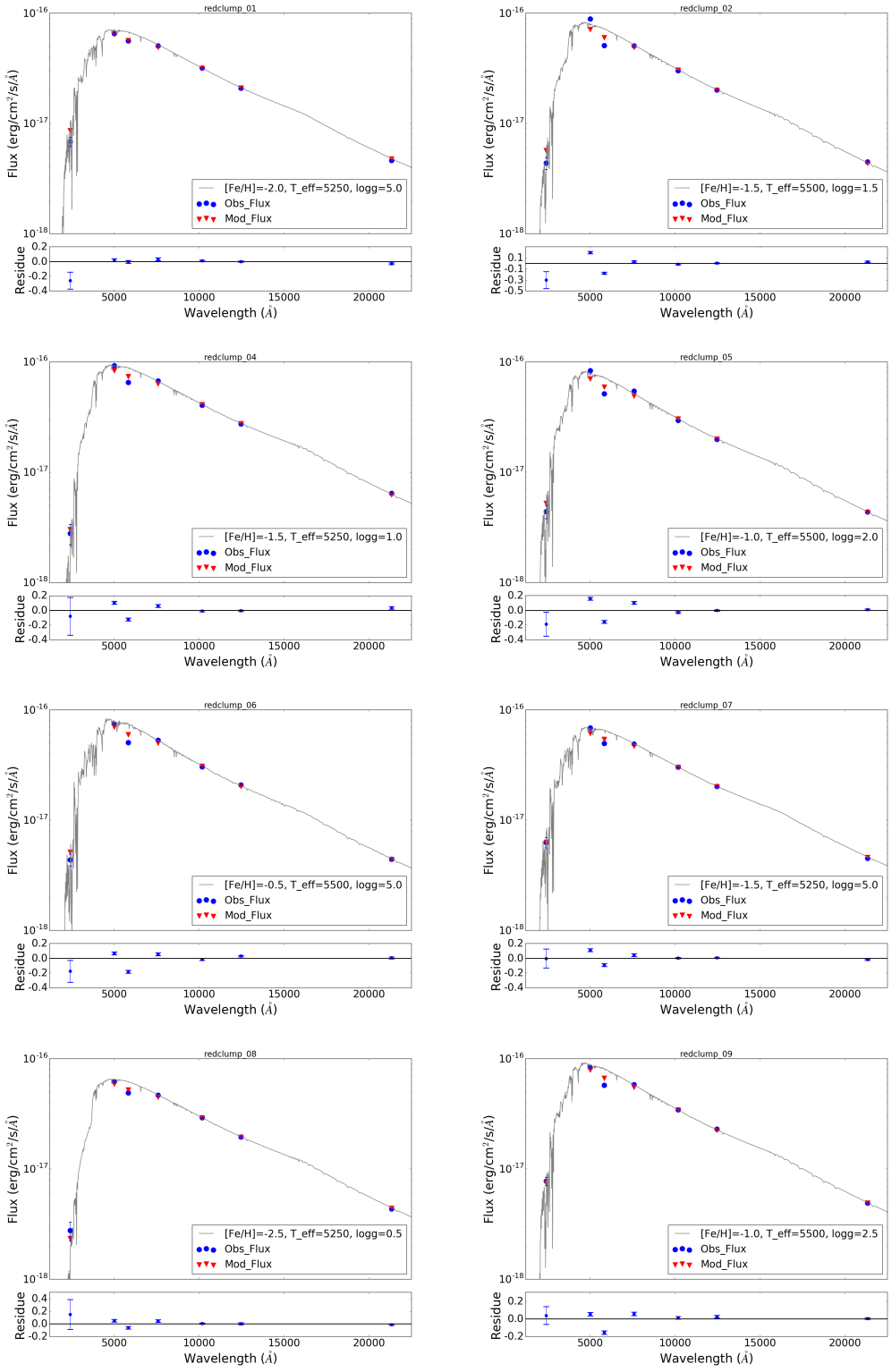

FIGURE 7.16: The Figure represents the same as Figure 7.13, but for eight different RC star.

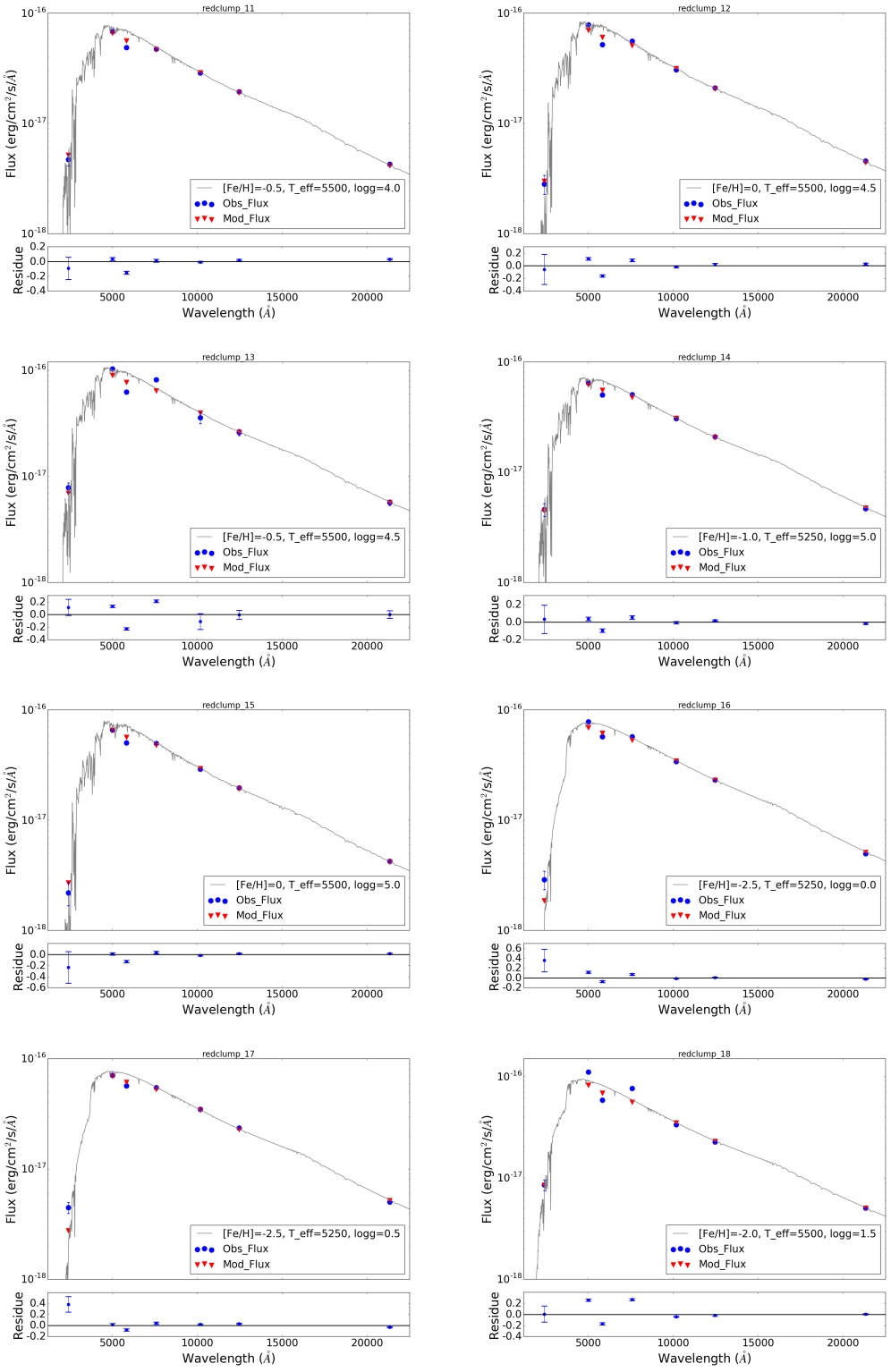

FIGURE 7.17: The Figure represents the same as Figure7.13, but for eight different RC star.

Chapter 8

Conclusions and Future Work

In this thesis, we studied the star cluster population in the Magellanic Clouds (MCs). In the first part we did a comprehensive study to parameterize and classify star clusters located in the LMC and SMC. In the second part we focused on a detailed study of an intermediate age SMC cluster (Kron 3) using multi-wavelength data. In this chapter we summarize the results and conclusions obtained in this thesis work. We also discuss a few potential future projects.

8.1 Summary

The cluster parameters are generally estimated by a manual fitting of isochrones to the CMD. Here, we developed a semi-automated quantitative method and implemented on large survey data OGLE III to estimate the age and reddening of star clusters in the MCs. We have estimated 1072 star clusters in the LMC and 179 in the SMC. We are thus able to homogeneously estimate the parameters for a large number of clusters without any subjective variation from cluster to cluster.A

visual inspection of the CMDs with overlaid isochrones corresponding to the estimated parameters suggests that our method was performed successfully for more than 80% of total sample of clusters. We have parameterize 308 LMC clusters and 16 SMC clusters for the first time.

We present the full catalog of LMC* and SMC† clusters with the relevant and estimated parameters and classification as an online catalog. Field star decontaminated CMDs of all the cataloged clusters fitted with isochrones of estimated age and corrected for reddening and distance are also made available as an online version‡ §.

Star clusters in the MCs are divided into five groups (I - V) based on their richness (n_m). Clusters belongs to group I have cluster members between 6 to 30, group II has $30 < n_m \leq 100$, group III has $100 < n_m \leq 200$, group IV has $200 < n_m \leq 300$, group V has $300 < n_m \leq 400$ member stars. We also estimated mass range corresponding to each group and for the first time, the star clusters in the MCs are classified based on their mass, the fundamental parameter of a cluster. The clusters are classified as very poor (<800 $M_\odot$), poor (800 - 1700 $M_\odot$), moderate (1700 - 5000 $M_\odot$) and rich (>5000 $M_\odot$) clusters.

Our study revealed that in both the clouds cluster formation peaks at the same time at 125 Myr. We suggest that the most recent interaction the clouds as the possible reason for this peak of cluster formation. The distribution of reddening E(V−I) peaks between 0.1 - 0.3 magnitude for all the four classification of clusters in the LMC. In the case of SMC distribution peaks between 0.1 - 0.2 magnitude. The bar region of the LMC was active in cluster formation in recent past during 60-250 Myr. We also noticed that the cluster formation propagated from ends of

*http://vizier.cfa.harvard.edu/viz-bin/VizieR?-source=J/MNRAS/463/1446
†http://vizier.cfa.harvard.edu/viz-bin/VizieR?-source=J/A+A/616/A187
‡LMC: https://academic.oup.com/mnras/article/463/2/1446/2892427#supplementary-data
§SMC: available in the appendix of the paper Nayak *et al.* (2018)

the bar to the central region during above mentioned period.

From age distribution of LMC clusters for different groups, we noticed that very poor clusters are distributed all over studied LMC region, whereas the poor clusters are located in the inner LMC and delineate the bar clearly. The moderately rich clusters are found to be located preferentially in the inner LMC and along the bar. The distribution also suggests that old clusters are formed in the outer region of the LMC, whereas the inner region have younger cluster. This trend is noticed in all the distribution of different groups, suggesting a quenching of cluster formation from outside to inside of the LMC. Therefore, we noticed a hierarchical formation of clusters shifting towards the LMC center from low to high mass clusters and for older to younger age clusters.

We have added 289 clusters in our catalog of SMC clusters from previous study in order to increase the sample of parameterized clusters in the SMC. Age distribution of total 468 SMC clusters demonstrate two extreme epochs of cluster formation in the SMC. The clusters in the older epoch (630 Myr - 1.25 Gyr) are mostly located in the Southern and South-Western (SW) part, whereas the younger clusters with age range 10 - 630 Myr are mostly found in the Northern and North-Eastern part along with central region of the SMC. Therefore, we propose that there is a propagation of cluster formation from South to Northern SMC in last 600 Myr. We made two videos (available online[¶]) to demonstrate the propagation of cluster formation in the SMC. We suggest that interaction between the Clouds at ∼1.2 Gyr (Diaz and Bekki 2011) caused the cluster formation in the South and SW part of the SMC, whereas the recent interaction at ∼250 Myr (Diaz and Bekki 2011) caused the cluster formation in the NE part of the SMC. The clusters older than 1.25 Gyr are found to be located in the outskirt of the SMC.

We found that 90% SMC clusters belong to very poor or poor group with mass

[¶]https://www.aanda.org/articles/aa/olm/2018/08/aa32227-17/aa32227-17.html

$<$ 1700 $M_\odot$, whereas the fraction is relatively less ($\sim$80%) in the LMC. We found that radius and mass of the clusters are connected with a power law relation : $M_c = C_m \times R^\gamma$. The values of γ are 2.1 ($\pm$0.24) and 1.68 ($\pm$0.43) for LMC and SMC clusters respectively. For the open clusters in the solar neighborhood the similar relation with a γ value of 1.71. Therefore, star clusters in the LMC are found to be more tightly packed when compared to the those in the SMC or the MW.

Relation between the radius and estimated age of the clusters indicates that there is no dissolution effect found in both the clouds, not even in the poor group of clusters. This could be an artifact as the most of studied clusters are younger than 500 Myr. The relation between estimated age and reddening provides information about the timescale required for complete dispersal of left over gas and dust in a cluster. It takes $\sim$40 Myr for very poor and poor clusters in the LMC, whereas, slightly longer time ($\sim$60 Myr) is required for moderately rich clusters.

We estimated the stellar mass function slope and total mass of 66 star clusters in the LMC and most of the estimates are done for the first time. LMC clusters are found to have a large range in slope of stellar mass function ranging from -1.5 to -3.0. Stellar mass function slope of LMC clusters peaks at -2.26, which is very similar to the IMF value obtained by Salpeter (1955) and the mean by Kumar *et al.* (2008) for the LMC clusters. We estimate a rather large deviation with respect to the peak, which needs further attention. We found that most of the moderately rich clusters in the LMC are distributed within the mass range of 1500 to 5000 $M_\odot$. Mass distribution of moderately rich star clusters in the LMC peaks between 2500-3000 $M_\odot$. The slope of cluster mass function in the LMC is found to be -1.66 ± 0.08, matches with the previous estimation (between -1.5 to -1.6) by Popescu *et al.* (2012).

We present the analysis of UVIT-HST-*Gaia*-VISTA data for the intermediate age cluster Kron 3 in the SMC. For the first time, we report the identification of

NUV bright RC stars and the extension of RC stars in the CMD. This study thus demonstrates the power of UVIT-HST-*Gaia* combination to study clusters in the Magellanic Clouds. We find that the extended RC is an intrinsic property of the cluster and not due to contamination from the field stars. We estimated the radius of the cluster as 2.′0 (34.9 pc) from the UVIT and *Gaia* data. We suggest that the cluster exhibits multiple stellar population with a small age range of 6-8 Gyr and a large metallicity range. We used three methods to fit the observed RC population and all three methods suggest a large spread in metallicity among the RC stars. We suggest that the spread in elemental abundance found among the RGB stars of this cluster (Hollyhead *et al.* 2018) from spectroscopic studies, could be contributing the the observed spread in metallicity among the RC stars. This claim needs to be verified using a high resolution spectroscopic study of the RC stars.

8.2 Conclusions

The highlights of this thesis are:
The thesis uses a large amount of survey data by OGLE III, public data from HST and proprietary data from UVIT and VISTA. A new tool is developed and implemented to characterize $\sim$ 1200 star clusters in the MCs, useful to age-date huge number of star clusters when large survey data of MCs get published in the future. This study demonstrated the value of near-UV window in addressing metallicity differences among stars in a cluster, by identifying a large spread in metallicity among the red clump (RC) stars in the SMC cluster, Kron 3.

1. The first objective of this thesis is achieved by the parameterisation and classification of 1250 clusters in the MCs, which is performed using a semi-automated method. The method worked relatively better in the LMC, when compared to

the SMC. This is due to several factors, such as, the fraction of poor clusters in the SMC being relatively large, variation in the field star distribution, differential reddening and large depth of the SMC.

2. The classification of clusters is MCs was done for the first time. The classification brought out the important aspect that both Clouds have a large number of star clusters which are similar to the open cluster like systems in our Galaxy. This is one of the important conclusions of this study.

3. The location, age and distribution of clusters in the MCs give insights to their cluster formation histories. Our study detects that both the clouds had gone through a recent burst of cluster formation at $\sim$125 Myr. The most recent LMC-SMC interaction around 100-250 Myr could have triggered the cluster formation.

4. The LMC is found to show an outside to inside cluster formation. The relatively more massive, moderate clusters are preferentially found in the inner regions, while the less massive poor and very poor clusters show a much wider distribution.

5. The LMC bar, which is presently does not show active star formation was active with cluster formation, 60 Myr ago. We find that the bar region of the LMC is found to be active in cluster formation during the period 60 - 250 Myr. We also suggest a progression of cluster formation from the ends of the bar to the central region of the bar during the above period. This could tentatively suggest a flow of gas from the outer to the central region of the active bar.

6. In the SMC, we detect a South-West to North-East propagation of cluster formation as a function of age. The clusters with age 630 Myr - 1.25 Gyr are found to be located preferentially in the South and West of the SMC, whereas the clusters younger than 100 Myr are found in the North and Eastern regions, suggesting a shift in the location of cluster formation. The central SMC shows

a continuous formation of clusters in the last 1 Gyr. These cluster formation patterns are signatures of the two interactions between the LMC and the SMC in the last few Gyr (∼250 Myr and ∼1.25 Gyr ago).

7. The mass range of the clusters in the MW, LMC and the SMC were to have a similar range. The LMC clusters were found to have smaller sizes when compared to those in the MW and the SMC. The size of the clusters could be directly connected to the environment as the LMC has a relatively less tidal environment when compared to our Galaxy and the SMC.

8. The estimated stellar mass function slope of 66 clusters in the LMC suggest that the peak of the distribution matches well with the Salpeter's value for the Solar neighborhood. The large spread in the values about the peak value could be partially true and requires further attention. The total mass of the clusters derived here suggest that their masses are similar to those of OCs. These suggest that there are clusters in the LMC have properties similar to those in our MW.

9. We have demonstrated the power of combining UVIT, HST, *Gaia* and VISTA to study the rich clusters in the SMC. As the flux in the NUV band of the UVIT turns out to be sensitive to the variation in elemental abundance of stars, the extended range of NUV−V colours of the RC stars reveal the presence of a large range in metallicity among them. This is the first time a convincingly extended RC is detected in the RC of Kron 3. We also argue and establish the range in metallicity causing the RC extension in colour. Kron 3 is thus confirmed to be one of the relatively young (∼7 Gyr old) clusters to show multiple populations due to abundance variation. It is thus important to study the RC colour distribution among the rich clusters of similar age, in the SMC. Thus the second objective of this thesis is achieved by this study.

8.3 Future Work

We have developed a semi-automated quantitative method and successfully executed on optical data from the large OGLE III survey to parameterize more than 1000 clusters in MCs. Hence, the method is now well established to execute on larger upcoming survey data, which will help us to probe the cluster formation history in great detail in regions outside the area of this study. We plan to apply this method on upcoming major survey data, like OGLE IV, DECAM, VISTA, LSST. OGLE IV survey covers a larger area in the MCs than OGLE III, apart from the Magellanic Bridge (MB) region. Therefore, OGLE IV data will have a very large number star clusters to study and hence not possible to parameterize manually. Our tool will be ideal to perform the parameterization, the results of which can put more constraint on the details of cluster formation as well as interactions.

In this thesis work, we have excluded 358 LMC clusters and 155 SMC clusters from parameterization, as those clusters are located in crowded field regions. We have inspected the CMDs of those clusters and found that ∼250 LMC clusters and ∼70 SMC clusters show prominent cluster features after decontamination of field stars. Most of the clusters are found to have member strength less than 100, and thus belong to very poor or poor category of clusters. We plan to estimate the parameters of those clusters as a follow up study. This work will help to add more parameterized very poor or poor clusters in the Clouds.

The estimated stellar mass function slopes of 66 clusters need to be checked for effects due to mass segregation, incompleteness of stars as well as stochasticity due to field star contamination. We plan to perform all of the above to firm up our estimations of the MF slopes. As our study has a large number of unstudied clusters, a robust estimation of their MF slopes will be a significant contribution to our understanding of stellar MF in star clusters.

Our study suggests that the intermediate age SMC cluster Kron 3 hosts multiple population of stars with a large range in metallicity. Spectroscopy study of RC stars having different (NUV-V) colour is needed to confirm the metallicity range present in the cluster. The spectroscopy study will also help us to understand the evolutionary history of stars in the Kron 3.

In the UVIT observed tile of Kron 3, another red (van den Bergh 1981), intermediate age (Kontizas 1980; Mould *et al.* 1992; Dias *et al.* 2010) SMC cluster Lindsay 11 is present. The CMD of Lindsay 11 also shows extended RC similar to Kron 3 in both (NUV−G) color as well as (G_{bp} − G_{rp}) color. The previous study by Mould and Aaronson (1982) suggested that Lindsay 11 hosts carbon AGB stars (Buttress *et al.* 1988). Using Simple Stellar Population (SSP) model Dias *et al.* (2010) suggested that Lindsay 11 has a metallicity range between −0.8 to −0.5, which supports the metallicity estimation by Da Costa and Hatzidimitriou (1998) using Ca II triplet spectroscopy of six red giant stars. As Lindsay 11 falls near the outer region of our UVIT tile, extra care is needed to perform photometry and calibration. We plan to analyze a part of the cluster using UVIT and *Gaia* data to study the behaviour of RC stars.

As the extended RC distribution in young star clusters in the SMC is yet to be understood, we plan to study similarly old clusters which are found to host multiple population, such as NGC 416, NGC 339 and Lindsay 1, using *Gaia* data. As demonstrated by our analysis of Kron 3, the cluster CMD based on *Gaia* data itself is capable of bringing out the nature of RC distribution. All intermediate age clusters in the SMC can be studied using *Gaia* for the existence of multiple population among the RC stars.

Bibliography

Alcaino, G., Liller, W., Alvarado, F., Kravtsov, V., Ipatov, A., Samus, N. and Smirnov, O., 1996, "Multicolor CCD Photometry of the SMC Cluster Kron 3", *Astron. J.*, **112**, 2004. [DOI], [ADS]

Alcock, C., Allsman, R. A., Alves, D. R., Axelrod, T. S., Becker, A. C., Bennett, D. P., Bersier, D. F., Cook, K. H., Freeman, K. C., Griest, K., Guern, J. A., Lehner, M., Marshall, S. L., Minniti, D., Peterson, B. A., Pratt, M. R., Quinn, P. J., Rodgers, A. W., Stubbs, C. W., Sutherland, W., Tomaney, A., Vandehei, T. and Welch, D. L., 1999, "The MACHO Project LMC Variable Star Inventory. VIII. The Recent Star Formation History of the Large Magellanic Cloud from the Cepheid Period Distribution", *Astron. J.*, **117**, 920–926. [DOI], [ADS], [astro-ph/9811240]

Anderson, J., Piotto, G., King, I. R., Bedin, L. R. and Guhathakurta, P., 2009, "Mixed Populations in Globular Clusters: Et Tu, 47 Tuc?", *Astrophys. J. Lett.*, **697**, L58–L62. [DOI], [ADS], [arXiv:0904.1626 [astro-ph.GA]]

Bagheri, G., Cioni, M.-R. L. and Napiwotzki, R., 2013, "The detection of an older population in the Magellanic Bridge", *Astron. Astrophys.*, **551**, A78. [DOI], [ADS], [arXiv:1209.0216]

Ballesteros-Paredes, J. and Hartmann, L., 2007, "Remarks on Rapid vs. Slow Star Formation", , **43**, 123–136. [ADS], [arXiv:astro-ph/0605268 [astro-ph]]

Bastian, N., Kamann, S., Cabrera-Ziri, I., Georgy, C., Ekström, S., Charbonnel, C., de Juan Ovelar, M. and Usher, C., 2018, "Extended main sequence turnoffs in open clusters as seen by Gaia - I. NGC 2818 and the role of stellar rotation", *Mon. Not. Roy. Astron. Soc.*, **480**(3), 3739–3746. [DOI], [ADS], [arXiv:1807.10779 [astro-ph.SR]]

Baumgardt, H., Parmentier, G., Anders, P. and Grebel, E. K., 2013, "The star cluster formation history of the LMC", *Mon. Not. Roy. Astron. Soc.*, **430**, 676–685. [DOI], [ADS], [arXiv:1207.5576]

Bayo, A., Rodrigo, C., Barrado Y Navascués, D., Solano, E., Gutiérrez, R., Morales-Calderón, M. and Allard, F., 2008, "VOSA: virtual observatory SED analyzer. An application to the Collinder 69 open cluster", *Astron. Astrophys.*, **492**, 277–287. [DOI], [ADS], [arXiv:0808.0270]

Bekki, K., 2009, "Formation of the off-centre bar in the Large Magellanic Cloud: a collision with a dark satellite?", *Mon. Not. Roy. Astron. Soc.*, **393**, L60–L64. [DOI], [ADS], [arXiv:0811.3279]

Belokurov, V., Erkal, D., Deason, A. J., Koposov, S. E., De Angeli, F., Evans, D. W., Fraternali, F. and Mackey, D., 2017, "Clouds, Streams and Bridges. Redrawing the blueprint of the Magellanic System with Gaia DR1", *Mon. Not. Roy. Astron. Soc.*, **466**, 4711–4730. [DOI], [ADS], [arXiv:1611.04614]

Bertelli, G., Bressan, A., Chiosi, C., Fagotto, F. and Nasi, E., 1994, "Theoretical isochrones from models with new radiative opacities", *Astron. Astrophys. Suppl.*, **106**. [ADS]

Besla, G., Kallivayalil, N., Hernquist, L., van der Marel, R. P., Cox, T. J. and Kereš, D., 2010, "Simulations of the Magellanic Stream in a First Infall Scenario", *Astrophys. J. Lett.*, **721**, L97–L101. [DOI], [ADS], [arXiv:1008.2210]

Besla, G., Kallivayalil, N., Hernquist, L., van der Marel, R. P., Cox, T. J. and Kereš, D., 2012, "The role of dwarf galaxy interactions in shaping the Magellanic

System and implications for Magellanic Irregulars", *Mon. Not. Roy. Astron. Soc.*, **421**, 2109–2138. [DOI], [ADS], [arXiv:1201.1299]

Bica, E., Bonatto, C., Dutra, C. M. and Santos, J. F. C., 2008, "A general catalogue of extended objects in the Magellanic System", *Mon. Not. Roy. Astron. Soc.*, **389**, 678–690. [DOI], [ADS], [arXiv:0806.3049]

Bica, E., Santiago, B., Bonatto, C., Garcia-Dias, R., Kerber, L., Dias, B., Barbuy, B. and Balbinot, E., 2015, "Bridge over troubled gas: clusters and associations under the SMC and LMC tidal stresses", *Mon. Not. Roy. Astron. Soc.*, **453**, 3190–3202. [DOI], [ADS], [arXiv:1507.07725]

Bok, B. J., 1966, "Magellanic Clouds", *Ann. Rev. Astron. Astrophys.*, **4**, 95. [DOI], [ADS]

Bonatto, C., Lima, E. F. and Bica, E., 2012, "Unveiling hidden properties of young star clusters: differential reddening, star-formation spread, and binary fraction", *Astron. Astrophys.*, **540**, A137. [DOI], [ADS], [arXiv:1202.3626 [astro-ph.GA]]

Bressan, A., Marigo, P., Girardi, L., Salasnich, B., Dal Cero, C., Rubele, S. and Nanni, A., 2012, "PARSEC: stellar tracks and isochrones with the PAdova and TRieste Stellar Evolution Code", *Mon. Not. Roy. Astron. Soc.*, **427**, 127–145. [DOI], [ADS], [arXiv:1208.4498 [astro-ph.SR]]

Brocato, E., Di Carlo, E. and Menna, G., 2001, "Large Magellanic Cloud stellar clusters. I. 21 HST colour magnitude diagrams", *Astron. Astrophys.*, **374**, 523–539. [DOI], [ADS]

Burki, G., 1977, "Observational tests on star formation. III - Variation of the upper mass spectrum with the size of very young clusters", *Astron. Astrophys.*, **57**, 135–140. [ADS]

Buttress, J., Cannon, R. D. and Griffiths, W. K., 1988, "The SMC Cluster Lindsay 11", in *The Harlow-Shapley Symposium on Globular Cluster Systems in Galaxies*, (Eds.) Grindlay, J. E., Philip, A. G. D., IAU Symposium, 126, [ADS]

Castelli, F., Gratton, R. G. and Kurucz, R. L., 1997, "Notes on the convection in the ATLAS9 model atmospheres.", *Astron. Astrophys.*, **318**, 841–869. [ADS]

Chandar, R., Fall, S. M. and Whitmore, B. C., 2010, "New Tests for Disruption Mechanisms of Star Clusters: The Large and Small Magellanic Clouds", *Astrophys. J.*, **711**, 1263–1279. [DOI], [ADS], [arXiv:1002.0779]

Chiosi, E., Vallenari, A., Held, E. V., Rizzi, L. and Moretti, A., 2006, "Age distribution of young clusters and field stars in the Small Magellanic Cloud", *Astron. Astrophys.*, **452**, 179–193. [DOI], [ADS], [astro-ph/0604166]

Choudhury, S., Subramaniam, A. and Piatti, A. E., 2015, "Deep Washington Photometry of Inconspicuous Star Cluster Candidates in the Large Magellanic Cloud", *Astron. J.*, **149**, 52. [DOI], [ADS], [arXiv:1410.7198]

Cioni, M.-R. L., van der Marel, R. P., Loup, C. and Habing, H. J., 2000, "The tip of the red giant branch and distance of the Magellanic Clouds: results from the DENIS survey", *Astron. Astrophys.*, **359**, 601–614. [ADS], [astro-ph/0003223]

Cioni, M.-R. L., Clementini, G., Girardi, L., Guandalini, R., Gullieuszik, M., Miszalski, B., Moretti, M.-I., Ripepi, V., Rubele, S., Bagheri, G., Bekki, K., Cross, N., de Blok, W. J. G., de Grijs, R., Emerson, J. P., Evans, C. J., Gibson, B., Gonzales-Solares, E., Groenewegen, M. A. T., Irwin, M., Ivanov, V. D., Lewis, J., Marconi, M., Marquette, J.-B., Mastropietro, C., Moore, B., Napiwotzki, R., Naylor, T., Oliveira, J. M., Read, M., Sutorius, E., van Loon, J. T., Wilkinson, M. I. and Wood, P. R., 2011, "The VMC survey. I. Strategy and first data", *Astron. Astrophys.*, **527**, A116. [DOI], [ADS], [arXiv:1012.5193]

Cordoni, G., Milone, A. P., Marino, A. F., Di Criscienzo, M., D'Antona, F., Dotter, A., Lagioia, E. P. and Tailo, M., 2018, "Extended Main-sequence Turnoff as a Common Feature of Milky Way Open Clusters", *Astrophys. J.*, **869**(2), 139. [DOI], [ADS], [arXiv:1811.01192 [astro-ph.SR]]

Crowl, H. H., Sarajedini, A., Piatti, A. E., Geisler, D., Bica, E., Clariá, J. J. and Santos, Jr., J. F. C., 2001, "The Line-of-Sight Depth of Populous Clusters in

the Small Magellanic Cloud", *Astron. J.*, **122**, 220–231. [DOI], [ADS], [astro-ph/0104227]

Da Costa, G. S. and Hatzidimitriou, D., 1998, "Ca II Triplet Spectroscopy of Giants in Small Magellanic Cloud Star Clusters: Abundances, Velocities, and the Age-Metallicity Relation", *Astron. J.*, **115**, 1934–1945. [DOI], [ADS], [astro-ph/9802008]

Dalton, G. B., Caldwell, M., Ward, A. K., Whalley, M. S., Woodhouse, G., Edeson, R. L., Clark, P., Beard, S. M., Gallie, A. M., Todd, S. P., Strachan, J. M. D., Bezawada, N. N., Sutherland, W. J. and Emerson, J. P., 2006, "The VISTA infrared camera", in *Society of Photo-Optical Instrumentation Engineers (SPIE) Conference Series*, *Proc. SPIE*, 6269, [DOI], [ADS]

D'Antona, F., Bellazzini, M., Caloi, V., Pecci, F. F., Galleti, S. and Rood, R. T., 2005, "A Helium Spread among the Main-Sequence Stars in NGC 2808", *Astrophys. J.*, **631**, 868–878. [DOI], [ADS], [astro-ph/0505347]

Danziger, I. J., 1973, "A photometric study of the integrated light of clusters in the Magellanic Clouds and the Fornax dwarf galaxy", *Astrophys. J.*, **181**, 641. [DOI], [ADS]

de Boer, K. S., 1998, "Bow Shock Induced Star Formation in the LMC: a Large Scale View", in *Magellanic Clouds and Other Dwarf Galaxies*, [ADS]

de Grijs, R. and Anders, P., 2006, "How well do we know the age and mass distributions of the star cluster system in the Large Magellanic Cloud?", *Mon. Not. Roy. Astron. Soc.*, **366**, 295–307. [DOI], [ADS], [astro-ph/0511305]

de Grijs, R., Goodwin, S. P. and Anders, P., 2013, "No compelling evidence of significant early star cluster disruption in the Large Magellanic Cloud", *Mon. Not. Roy. Astron. Soc.*, **436**, 136–149. [DOI], [ADS], [arXiv:1308.3296]

Deason, A. J., Belokurov, V., Erkal, D., Koposov, S. E. and Mackey, D., 2017, "The Clouds are breaking: tracing the Magellanic system with Gaia DR1

Mira variables", *Mon. Not. Roy. Astron. Soc.*, **467**, 2636–2647. [DOI], [ADS], [arXiv:1611.04600]

Dias, B., Coelho, P., Barbuy, B., Kerber, L. and Idiart, T., 2010, "Age and metallicity of star clusters in the Small Magellanic Cloud from integrated spectroscopy", *Astron. Astrophys.*, **520**, A85. [DOI], [ADS], [arXiv:1002.4301 [astro-ph.SR]]

Dias, B., Kerber, L. O., Barbuy, B., Santiago, B., Ortolani, S. and Balbinot, E., 2014, "Self-consistent physical parameters for five intermediate-age SMC stellar clusters from CMD modelling", *Astron. Astrophys.*, **561**, A106. [DOI], [ADS], [arXiv:1311.4579 [astro-ph.SR]]

Dias, B., Kerber, L., Barbuy, B., Bica, E. and Ortolani, S., 2016, "SMC west halo: a slice of the galaxy that is being tidally stripped?. Star clusters trace age and metallicity gradients", *Astron. Astrophys.*, **591**, A11. [DOI], [ADS], [arXiv:1604.03086]

Diaz, J. and Bekki, K., 2011, "Constraining the orbital history of the Magellanic Clouds: a new bound scenario suggested by the tidal origin of the Magellanic Stream", *Mon. Not. Roy. Astron. Soc.*, **413**, 2015–2020. [DOI], [ADS], [arXiv:1101.2500]

Diaz, J. D. and Bekki, K., 2012, "The Tidal Origin of the Magellanic Stream and the Possibility of a Stellar Counterpart", *Astrophys. J.*, **750**, 36. [DOI], [ADS], [arXiv:1112.6191]

Elmegreen, B. G., 2000a, "Modeling a High-Mass Turn-Down in the Stellar Initial Mass Function", *Astrophys. J.*, **539**, 342–351. [DOI], [ADS], [astro-ph/0005455]

Elmegreen, Bruce G., 2000b, "Star Formation in a Crossing Time", *Astrophys. J.*, **530**(1), 277–281. [DOI], [ADS], [arXiv:astro-ph/9911172 [astro-ph]]

Emerson, J., McPherson, A. and Sutherland, W., 2006, "Visible and Infrared Survey Telescope for Astronomy: Progress Report", *The Messenger*, **126**, 41–42. [ADS]

Gascoigne, S. C. B., 1965, "H-R diagrams for globular cluster in the Magellanic Clouds", in *Magellanic Clouds*, (Eds.) Hindman, J. V., Westerlund, B. E., [ADS]

Gascoigne, S. C. B., 1966, "Colour-magnitude diagrams for nine globular-like clusters in the Magellanic Clouds", *Mon. Not. Roy. Astron. Soc.*, **134**, 59. [DOI], [ADS]

Gascoigne, S. C. B., 1980, "The older clusters in the Magellanic Clouds", in *Star Clusters*, (Ed.) Hesser, J. E., IAU Symposium, 85, [ADS]

Gascoigne, S. C. B. and Kron, G. E., 1952, "Colors and Magnitudes of Some Star Clusters in the Magellanic Clouds", *Pub. Astron. Soc. Pac.*, **64**, 196. [DOI], [ADS]

Girardi, L., Chiosi, C., Bertelli, G. and Bressan, A., 1995, "Age distribution of LMC clusters from their integrated UBV colors: history of star formation.", *Astron. Astrophys.*, **298**, 87. [ADS]

Girardi, L., Bertelli, G., Bressan, A., Chiosi, C., Groenewegen, M. A. T., Marigo, P., Salasnich, B. and Weiss, A., 2002, "Theoretical isochrones in several photometric systems. I. Johnson-Cousins-Glass, HST/WFPC2, HST/NICMOS, Washington, and ESO Imaging Survey filter sets", *Astron. Astrophys.*, **391**, 195–212. [DOI], [ADS], [astro-ph/0205080]

Girardi, L., Goudfrooij, P., Kalirai, J. S., Kerber, L., Kozhurina-Platais, V., Rubele, S., Bressan, A., Chandar, R., Marigo, P., Platais, I. and Puzia, T. H., 2013, "An extended main-sequence turn-off in the Small Magellanic Cloud star cluster NGC 411", *Mon. Not. Roy. Astron. Soc.*, **431**, 3501–3509. [DOI], [ADS], [arXiv:1303.1361]

Glatt, K., Grebel, E. K., Sabbi, E., Gallagher, III, J. S., Nota, A., Sirianni, M., Clementini, G., Tosi, M., Harbeck, D., Koch, A., Kayser, A. and Da Costa, G., 2008, "Age Determination of Six Intermediate-Age Small Magellanic Cloud Star Clusters with HST/ACS", *Astron. J.*, **136**, 1703-1727. [DOI], [ADS], [arXiv:0807.3744]

Glatt, K., Grebel, E. K. and Koch, A., 2010, "Ages and luminosities of young SMC/LMC star clusters and the recent star formation history of the Clouds", *Astron. Astrophys.*, **517**, A50. [DOI], [ADS], [arXiv:1004.1247]

González-Fernández, C., Hodgkin, S. T., Irwin, M. J., González-Solares, E., Koposov, S. E., Lewis, J. R., Emerson, J. P., Hewett, P. C., Yoldaș, A. K. and Riello, M., 2018, "The VISTA ZYJHKs photometric system: calibration from 2MASS", *Mon. Not. Roy. Astron. Soc.*, **474**(4), 5459–5478. [DOI], [ADS], [arXiv:1711.08805 [astro-ph.IM]]

Gossage, Seth, Conroy, Charlie, Dotter, Aaron, Cabrera-Ziri, Ivan, Dolphin, Andrew E., Bastian, Nate, Dalcanton, Julianne J., Goudfrooij, Paul, Johnson, L. Clifton, Williams, Benjamin F., Rosenfield, Philip, Kalirai, Jason and Fouesneau, Morgan, 2019, "Combined Effects of Rotation and Age Spreads on Extended Main Sequence Turn Offs", *arXiv e-prints*, arXiv:1907.11251. [ADS], [arXiv:1907.11251 [astro-ph.SR]]

Grocholski, A. J., Cole, A. A., Sarajedini, A., Geisler, D. and Smith, V. V., 2006, "Ca II Triplet Spectroscopy of Large Magellanic Cloud Red Giants. I. Abundances and Velocities for a Sample of Populous Clusters", *Astron. J.*, **132**, 1630–1644. [DOI], [ADS], [astro-ph/0607052]

Harris, J., 2007, "The Magellanic Bridge: The Nearest Purely Tidal Stellar Population", *Astrophys. J.*, **658**, 345–357. [DOI], [ADS], [astro-ph/0612107]

Harris, J. and Zaritsky, D., 2004, "The Star Formation History of the Small Magellanic Cloud", *Astron. J.*, **127**, 1531–1544. [DOI], [ADS], [astro-ph/0312100]

Harris, J. and Zaritsky, D., 2009, "The Star Formation History of the Large Magellanic Cloud", *Astron. J.*, **138**, 1243–1260. [DOI], [ADS], [arXiv:0908.1422]

Hartmann, Lee, Ballesteros-Paredes, Javier and Bergin, Edwin A., 2001, "Rapid Formation of Molecular Clouds and Stars in the Solar Neighborhood", *Astrophys. J.*, **562**(2), 852–868. [DOI], [ADS], [arXiv:astro-ph/0108023 [astro-ph]]

Hindman, J. V., Kerr, F. J. and McGee, R. X., 1963, "A Low Resolution Hydrogen-line Survey of the Magellanic System. II. Interpretation of Results", *Australian Journal of Physics*, **16**, 570. [DOI], [ADS]

Hodge, P. W., 1982, "The billion-year-old clusters of the Magellanic Clouds", *Astrophys. J.*, **256**, 447–451. [DOI], [ADS]

Hollyhead, K., Lardo, C., Kacharov, N., Bastian, N., Hilker, M., Rejkuba, M., Koch, A., Grebel, E. K. and Georgiev, I., 2018, "Kron 3: a fourth intermediate age cluster in the SMC with evidence of multiple populations", *Mon. Not. Roy. Astron. Soc.*, **476**, 114–121. [DOI], [ADS], [arXiv:1801.09670]

Hunter, D. A., Elmegreen, B. G., Dupuy, T. J. and Mortonson, M., 2003, "Cluster Mass Functions in the Large and Small Magellanic Clouds: Fading and Size-of-Sample Effects", *Astron. J.*, **126**, 1836–1848. [DOI], [ADS], [astro-ph/0306528]

Indu, G. and Subramaniam, A., 2011, "The recent star-formation history of the Large and Small Magellanic Clouds", *Astron. Astrophys.*, **535**, A115. [DOI], [ADS], [arXiv:1109.1061]

Jacyszyn-Dobrzeniecka, A. M., Skowron, D. M., Mróz, P., Skowron, J., Soszyński, I., Udalski, A., Pietrukowicz, P., Kozłowski, S., Wyrzykowski, Ł., Poleski, R., Pawlak, M., Szymański, M. K. and Ulaczyk, K., 2016, "OGLE-ing the Magellanic System: Three-Dimensional Structure of the Clouds and the Bridge Using Classical Cepheids", *Acta Astron.*, **66**, 149–196. [ADS], [arXiv:1602.09141]

Kallivayalil, N., van der Marel, R. P., Alcock, C., Axelrod, T., Cook, K. H., Drake, A. J. and Geha, M., 2006, "The Proper Motion of the Large Magellanic Cloud Using HST", *Astrophys. J.*, **638**, 772–785. [DOI], [ADS], [astro-ph/0508457]

Kallivayalil, N., van der Marel, R. P., Besla, G., Anderson, J. and Alcock, C., 2013, "Third-epoch Magellanic Cloud Proper Motions. I. Hubble Space Telescope/WFC3 Data and Orbit Implications", *Astrophys. J.*, **764**, 161. [DOI], [ADS], [arXiv:1301.0832]

Kawamura, Akiko, Mizuno, Yoji, Minamidani, Tetsuhiro, Filipović, Miroslav D., Staveley-Smith, Lister, Kim, Sungeun, Mizuno, Norikazu, Onishi, Toshikazu, Mizuno, Akira and Fukui, Yasuo, 2009, "The Second Survey of the Molecular Clouds in the Large Magellanic Cloud by NANTEN. II. Star Formation", *Astrophys. J. Suppl.*, **184**(1), 1–17. [DOI], [ADS], [arXiv:0908.1168 [astro-ph.CO]]

Kerr, F. J., 1957, "A Magellanic effect on the galaxy.", *Astron. J.*, **62**, 93–93. [DOI], [ADS]

Kim, S., Dopita, M. A., Staveley-Smith, L. and Bessell, M. S., 1999, "H I Shells in the Large Magellanic Cloud", *Astron. J.*, **118**, 2797–2823. [DOI], [ADS]

King, I., 1962, "The structure of star clusters. I. an empirical density law", *Astron. J.*, **67**, 471. [DOI], [ADS]

Kjeldsen, H. and Frandsen, S., 1991, "Stellar photometric stability. II - Ages and distances for 13 open clusters with time series observations", *Astron. Astrophys. Suppl.*, **87**, 119–152. [ADS]

Kontizas, M., 1980, "Preliminary colour-magnitude diagrams of 20 star clusters and their adjoining fields in the small Magellanic Cloud", *Astron. Astrophys. Suppl.*, **40**, 151–189. [ADS]

Kontizas, M., Danezis, E. and Kontizas, E., 1982, "Observed radii and structural parameters of clusters in the SMC", *Astron. Astrophys. Suppl.*, **49**, 1–12. [ADS]

Kontizas, M., Morgan, D. H., Hatzidimitriou, D. and Kontizas, E., 1990, "The cluster system of the Large Magellanic Cloud", *Astron. Astrophys. Suppl.*, **84**, 527–547. [ADS]

Kron, G. E., 1956a, "Star Clusters in the Small Magellanic Cloud: I. Identification of 69 Clusters", *Pub. Astron. Soc. Pac.*, **68**, 125. [DOI], [ADS]

Kron, G. E., 1956b, "Star Clusters in the Small Magellanic Cloud: II. Their Dimensions and Luminosities", *Pub. Astron. Soc. Pac.*, **68**, 230. [DOI], [ADS]

Kumar, B., Sagar, R. and Melnick, J., 2008, "CCD photometric and mass function study of nine young Large Magellanic Cloud star clusters", *Mon. Not. Roy. Astron. Soc.*, **386**, 1380–1397. [DOI], [ADS], [arXiv:0801.1068]

Lamers, H. J. G. L. M., Gieles, M., Bastian, N., Baumgardt, H., Kharchenko, N. V. and Portegies Zwart, S., 2005, "An analytical description of the disruption of star clusters in tidal fields with an application to Galactic open clusters", *Astron. Astrophys.*, **441**, 117–129. [DOI], [ADS], [astro-ph/0505558]

Larson, R. B., 1998, "Early star formation and the evolution of the stellar initial mass function in galaxies", *Mon. Not. Roy. Astron. Soc.*, **301**, 569–581. [DOI], [ADS], [astro-ph/9808145]

Lejeune, T. and Schaerer, D., 2001, "Database of Geneva stellar evolution tracks and isochrones for $(UBV)_J(RI)_C$ JHKLL'M, HST-WFPC2, Geneva and Washington photometric systems", *Astron. Astrophys.*, **366**, 538–546. [DOI], [ADS], [astro-ph/0011497]

Li, Chengyuan, Sun, Weijia, de Grijs, Richard, Deng, Licai, Wang, Kun, Cordoni, Giacomo and Milone, Antonino P., 2019, "Extended Main-sequence Turnoffs in the Double Cluster h and χ Persei: The Complex Role of Stellar Rotation", *Astrophys. J.*, **876**(1), 65. [DOI], [ADS], [arXiv:1904.02005 [astro-ph.SR]]

Lim, Beomdu, Rauw, Gregor, Nazé, Yaël, Sung, Hwankyung, Hwang, Narae and Park, Byeong-Gon, 2019, "Extended main sequence turn-off originating from a

broad range of stellar rotational velocities", *Nature Astronomy*, **3**, 76–81. [DOI], [ADS], [arXiv:1811.01593 [astro-ph.SR]]

Lindegren, L., Lammers, U., Hobbs, D., O'Mullane, W., Bastian, U. and Hernández, J., 2012, "The astrometric core solution for the Gaia mission. Overview of models, algorithms, and software implementation", *Astron. Astrophys.*, **538**, A78. [DOI], [ADS], [arXiv:1112.4139 [astro-ph.IM]]

Lindegren, L., Hernández, J., Bombrun, A., Klioner, S., Bastian, U., Ramos-Lerate, M., de Torres, A., Steidelmüller, H., Stephenson, C., Hobbs, D., Lammers, U., Biermann, M., Geyer, R., Hilger, T., Michalik, D., Stampa, U., McMillan, P. J., Castañeda, J., Clotet, M., Comoretto, G., Davidson, M., Fabricius, C., Gracia, G., Hambly, N. C., Hutton, A., Mora, A., Portell, J., van Leeuwen, F., Abbas, U., Abreu, A., Altmann, M., Andrei, A., Anglada, E., Balaguer-Núñez, L., Barache, C., Becciani, U., Bertone, S., Bianchi, L., Bouquillon, S., Bourda, G., Brüsemeister, T., Bucciarelli, B., Busonero, D., Buzzi, R., Cancelliere, R., Carlucci, T., Charlot, P., Cheek, N., Crosta, M., Crowley, C., de Bruijne, J., de Felice, F., Drimmel, R., Esquej, P., Fienga, A., Fraile, E., Gai, M., Garralda, N., González-Vidal, J. J., Guerra, R., Hauser, M., Hofmann, W., Holl, B., Jordan, S., Lattanzi, M. G., Lenhardt, H., Liao, S., Licata, E., Lister, T., Löffler, W., Marchant, J., Martin-Fleitas, J.-M., Messineo, R., Mignard, F., Morbidelli, R., Poggio, E., Riva, A., Rowell, N., Salguero, E., Sarasso, M., Sciacca, E., Siddiqui, H., Smart, R. L., Spagna, A., Steele, I., Taris, F., Torra, J., van Elteren, A., van Reeven, W. and Vecchiato, A., 2018, "Gaia Data Release 2. The astrometric solution", *Astron. Astrophys.*, **616**, A2. [DOI], [ADS], [arXiv:1804.09366 [astro-ph.IM]]

Mackey, A. D. and Gilmore, G. F., 2003, "Surface brightness profiles and structural parameters for 10 rich stellar clusters in the Small Magellanic Cloud", *Mon. Not. Roy. Astron. Soc.*, **338**, 120–130. [DOI], [ADS], [astro-ph/0209046]

Mackey, A. D., Broby Nielsen, P., Ferguson, A. M. N. and Richardson, J. C., 2008, "Multiple Stellar Populations in Three Rich Large Magellanic Cloud Star Clusters", *Astrophys. J. Lett.*, **681**, L17. [DOI], [ADS], [arXiv:0804.3475]

Maia, F., Piatti, A. E. and Santos, Jr., J. F. C., 2012, "Astrophysical parameters of Small Magellanic Cloud star clusters", *Boletin de la Asociacion Argentina de Astronomia La Plata Argentina*, **55**, 111–115. [ADS]

Maia, F. F. S., Piatti, A. E. and Santos, J. F. C., 2014, "Mass distribution and structural parameters of Small Magellanic Cloud star clusters", *Mon. Not. Roy. Astron. Soc.*, **437**, 2005–2016. [DOI], [ADS], [arXiv:1310.5934]

Marigo, P., Girardi, L., Bressan, A., Groenewegen, M. A. T., Silva, L. and Granato, G. L., 2008, "Evolution of asymptotic giant branch stars. II. Optical to far-infrared isochrones with improved TP-AGB models", *Astron. Astrophys.*, **482**, 883–905. [DOI], [ADS], [arXiv:0711.4922]

Marino, A. F., Milone, A. P., Casagrande, L., Przybilla, N., Balaguer-Núñez, L., Di Criscienzo, M., Serenelli, A. and Vilardell, F., 2018, "Discovery of Extended Main Sequence Turnoffs in Galactic Open Clusters", *Astrophys. J. Lett.*, **863**(2), L33. [DOI], [ADS], [arXiv:1807.05888 [astro-ph.SR]]

Martocchia, S., Niederhofer, F., Dalessandro, E., Bastian, N., Kacharov, N., Usher, C., Cabrera-Ziri, I., Lardo, C., Cassisi, S., Geisler, D., Hilker, M., Hollyhead, K., Kozhurina-Platais, V., Larsen, S., Mackey, D., Mucciarelli, A., Platais, I. and Salaris, M., 2018, "The search for multiple populations in Magellanic Cloud clusters - IV. Coeval multiple stellar populations in the young star cluster NGC 1978", *Mon. Not. Roy. Astron. Soc.*, **477**, 4696–4705. [DOI], [ADS], [arXiv:1804.04141 [astro-ph.SR]]

Mateo, Mario, 1988, "Main-Sequence Luminosity and Initial Mass Functions of Six Magellanic Cloud Star Clusters Ranging in Age from 10 Megayears to 2.5 Gigayears", *Astrophys. J.*, **331**, 261. [DOI], [ADS]

Mighell, K. J., Sarajedini, A. and French, R. S., 1998a, "WFPC2 Observations of Star Clusters in the Magellanic Clouds. II. The Oldest Star Clusters in the Small Magellanic Cloud", *Astron. J.*, **116**, 2395–2414. [DOI], [ADS], [astro-ph/9808091]

Mighell, K. J., Sarajedini, A. and French, R. S., 1998b, "WFPC2 Observations of Star Clusters in the Magellanic Clouds. II. The Oldest Star Clusters in the Small Magellanic Cloud", *Astron. J.*, **116**, 2395–2414. [DOI], [ADS], [astro-ph/9808091]

Milone, A. P., Bedin, L. R., Piotto, G., Anderson, J., King, I. R., Sarajedini, A., Dotter, A., Chaboyer, B., Marín-Franch, A., Majewski, S., Aparicio, A., Hempel, M., Paust, N. E. Q., Reid, I. N., Rosenberg, A. and Siegel, M., 2008, "The ACS Survey of Galactic Globular Clusters. III. The Double Subgiant Branch of NGC 1851", *Astrophys. J.*, **673**, 241–250. [DOI], [ADS], [arXiv:0709.3762]

Milone, A. P., Bedin, L. R., Piotto, G. and Anderson, J., 2009, "Multiple stellar populations in Magellanic Cloud clusters. I. An ordinary feature for intermediate age globulars in the LMC?", *Astron. Astrophys.*, **497**, 755–771. [DOI], [ADS], [arXiv:0810.2558]

Milone, A. P., Bedin, L. R., Cassisi, S., Piotto, G., Anderson, J., Pietrinferni, A. and Buonanno, R., 2013, "Multiple stellar populations in Magellanic Cloud clusters. II. Evidence also in the young NGC 1844?", *Astron. Astrophys.*, **555**, A143. [DOI], [ADS], [arXiv:1302.1240 [astro-ph.SR]]

Milone, A. P., Bedin, L. R., Piotto, G., Marino, A. F., Cassisi, S., Bellini, A., Jerjen, H., Pietrinferni, A., Aparicio, A. and Rich, R. M., 2015, "Multiple stellar populations in Magellanic Cloud clusters - III. The first evidence of an extended main sequence turn-off in a young cluster: NGC 1856", *Mon. Not. Roy. Astron. Soc.*, **450**, 3750–3764. [DOI], [ADS], [arXiv:1504.03252 [astro-ph.SR]]

Milone, A. P., Marino, A. F., D'Antona, F., Bedin, L. R., Da Costa, G. S., Jerjen, H. and Mackey, A. D., 2016, "Multiple stellar populations in Magellanic Cloud clusters - IV. The double main sequence of the young cluster NGC 1755", *Mon.*

Not. Roy. Astron. Soc., **458**, 4368–4382. [DOI], [ADS], [arXiv:1603.03493 [astro-ph.SR]]

Milone, A. P., Marino, A. F., D'Antona, F., Bedin, L. R., Piotto, G., Jerjen, H., Anderson, J., Dotter, A., di Criscienzo, M. and Lagioia, E. P., 2017, "Multiple stellar populations in Magellanic Cloud clusters - V. The split main sequence of the young cluster NGC 1866", *Mon. Not. Roy. Astron. Soc.*, **465**, 4363–4374. [DOI], [ADS], [arXiv:1611.06725 [astro-ph.SR]]

Mould, J. and Aaronson, M., 1982, "The extended giant branches of intermediate age globular clusters in the Magellanic Clouds. III", *Astrophys. J.*, **263**, 629–638. [DOI], [ADS]

Mould, J. R., Jensen, J. B. and Da Costa, G. S., 1992, "The age of the Small Magellanic Cloud cluster Lindsay 11", *Astrophys. J. Suppl.*, **82**, 489–494. [DOI], [ADS]

Muraveva, T., Subramanian, S., Clementini, G., Cioni, M.-R. L., Palmer, M., van Loon, J. T., Moretti, M. I., de Grijs, R., Molinaro, R., Ripepi, V., Marconi, M., Emerson, J. and Ivanov, V. D., 2018, "The VMC survey - XXVI. Structure of the Small Magellanic Cloud from RR Lyrae stars", *Mon. Not. Roy. Astron. Soc.*, **473**, 3131–3146. [DOI], [ADS], [arXiv:1709.09064 [astro-ph.SR]]

Nayak, P. K., Subramaniam, A., Choudhury, S., Indu, G. and Sagar, R., 2016, "Star clusters in the Magellanic Clouds - I. Parametrization and classification of 1072 clusters in the LMC", *Mon. Not. Roy. Astron. Soc.*, **463**, 1446–1461. [DOI], [ADS], [arXiv:1608.06389]

Nayak, P. K., Subramaniam, A., Choudhury, S. and Sagar, R., 2018, "Star clusters in the Magellanic Clouds. II. Age-dating, classification, and spatio-temporal distribution of the SMC clusters", *Astron. Astrophys.*, **616**, A187. [DOI], [ADS], [arXiv:1804.00635]

Nidever, D. L., Majewski, S. R., Butler Burton, W. and Nigra, L., 2010, "The 200° Long Magellanic Stream System", *Astrophys. J.*, **723**, 1618–1631. [DOI], [ADS], [arXiv:1009.0001]

Nidever, D. L., Monachesi, A., Bell, E. F., Majewski, S. R., Muñoz, R. R. and Beaton, R. L., 2013, "A Tidally Stripped Stellar Component of the Magellanic Bridge", *Astrophys. J.*, **779**, 145. [DOI], [ADS], [arXiv:1310.4824]

Niederhofer, F., Bastian, N., Kozhurina-Platais, V., Larsen, S., Hollyhead, K., Lardo, C., Cabrera-Ziri, I., Kacharov, N., Platais, I., Salaris, M., Cordero, M., Dalessandro, E., Geisler, D., Hilker, M., Li, C., Mackey, D. and Mucciarelli, A., 2017a, "The search for multiple populations in Magellanic Cloud clusters - II. The detection of multiple populations in three intermediate-age SMC clusters", *Mon. Not. Roy. Astron. Soc.*, **465**, 4159–4165. [DOI], [ADS], [arXiv:1612.00400 [astro-ph.SR]]

Niederhofer, F., Bastian, N., Kozhurina-Platais, V., Larsen, S., Salaris, M., Dalessandro, E., Mucciarelli, A., Cabrera-Ziri, I., Cordero, M., Geisler, D., Hilker, M., Hollyhead, K., Kacharov, N., Lardo, C., Li, C., Mackey, D. and Platais, I., 2017b, "The search for multiple populations in Magellanic Cloud clusters - I. Two stellar populations in the Small Magellanic Cloud globular cluster NGC 121", *Mon. Not. Roy. Astron. Soc.*, **464**, 94–103. [DOI], [ADS], [arXiv:1609.01595 [astro-ph.SR]]

Nikolaev, S., Drake, A. J., Keller, S. C., Cook, K. H., Dalal, N., Griest, K., Welch, D. L. and Kanbur, S. M., 2004, "Geometry of the Large Magellanic Cloud Disk: Results from MACHO and the Two Micron All Sky Survey", *Astrophys. J.*, **601**, 260–276. [DOI], [ADS]

Oke, J. B., 1974, "Absolute Spectral Energy Distributions for White Dwarfs", *Astrophys. J. Suppl.*, **27**, 21. [DOI], [ADS]

Olsen, K. A. G., Zaritsky, D., Blum, R. D., Boyer, M. L. and Gordon, K. D., 2011, "A Population of Accreted Small Magellanic Cloud Stars in the Large Magellanic Cloud", *Astrophys. J.*, **737**, 29. [DOI], [ADS], [arXiv:1106.0044]

Olszewski, E. W., Schommer, R. A., Suntzeff, N. B. and Harris, H. C., 1991, "Spectroscopy of giants in LMC clusters. I - Velocities, abundances, and the age-metallicity relation", *Astron. J.*, **101**, 515–537. [DOI], [ADS]

Palma, T., Gramajo, L. V., Clariá, J. J., Lares, M., Geisler, D. and Ahumada, A. V., 2016, "Catalogue of Large Magellanic Cloud star clusters observed in the Washington photometric system", *Astron. Astrophys.*, **586**, A41. [DOI], [ADS], [arXiv:1511.05451 [astro-ph.SR]]

Pancino, Elena, Ferraro, Francesco R., Bellazzini, Michele, Piotto, Giampaolo and Zoccali, Manuela, 2000, "New Evidence for the Complex Structure of the Red Giant Branch in ω Centauri", *Astrophys. J. Lett.*, **534**(1), L83–L87. [DOI], [ADS], [arXiv:astro-ph/0003222 [astro-ph]]

Parisi, M. C., Grocholski, A. J., Geisler, D., Sarajedini, A. and Clariá, J. J., 2009, "Ca II Triplet Spectroscopy of Small Magellanic Cloud Red Giants. I. Abundances and Velocities for a Sample of Clusters", *Astron. J.*, **138**, 517–532. [DOI], [ADS], [arXiv:0808.0018]

Parisi, M. C., Geisler, D., Carraro, G., Clariá, J. J., Costa, E., Grocholski, A. J., Sarajedini, A., Leiton, R. and Piatti, A. E., 2014, "Age Determination of 15 Old to Intermediate-age Small Magellanic Cloud Star Clusters", *Astron. J.*, **147**, 71. [DOI], [ADS], [arXiv:1402.1687 [astro-ph.SR]]

Pfalzner, S., Kirk, H., Sills, A., Urquhart, J. S., Kauffmann, J., Kuhn, M. A., Bhandare, A. and Menten, K. M., 2016, "Observational constraints on star cluster formation theory. I. The mass-radius relation", *Astron. Astrophys.*, **586**, A68. [DOI], [ADS], [arXiv:1512.00334 [astro-ph.SR]]

Piatti, A. E., 2011a, "New candidate intermediate-age star clusters in the Small Magellanic Cloud", *Mon. Not. Roy. Astron. Soc.*, **416**, L89–L93. [DOI], [ADS]

Piatti, A. E., 2011b, "New insights on the bursting formation of star clusters in the Large Magellanic Cloud", *Mon. Not. Roy. Astron. Soc.*, **418**, L40–L44. [DOI], [ADS]

Piatti, A. E., 2012a, "Identification of a New Relatively Old Star Cluster in the Small Magellanic Cloud", *Astrophys. J. Lett.*, **756**, L32. [DOI], [ADS], [arXiv:1207.7301]

Piatti, A. E., 2012b, "Washington photometry of 26 moderately young small angular size clusters in the Large Magellanic Cloud", *Astron. Astrophys.*, **540**, A58. [DOI], [ADS]

Piatti, A. E., 2012c, "The star field age-metallicity relationship of the Small Magellanic Cloud", *Mon. Not. Roy. Astron. Soc.*, **422**, 1109–1121. [DOI], [ADS]

Piatti, A. E., 2014, "Disentangling the physical reality of star cluster candidates projected towards the inner disc of the Large Magellanic Cloud", *Mon. Not. Roy. Astron. Soc.*, **440**, 3091–3099. [DOI], [ADS], [arXiv:1403.3561]

Piatti, A. E. and Geisler, D., 2013, "The Age-Metallicity Relationship of the Large Magellanic Cloud Field Star Population from Wide-field Washington Photometry", *Astron. J.*, **145**, 17. [DOI], [ADS], [arXiv:1208.3899]

Piatti, A. E., Sarajedini, A., Geisler, D., Bica, E. and Clariá, J. J., 2002, "Constraining the LMC cluster age gap: Washington photometry of NGC 2155 and SL 896 (LW 480)", *Mon. Not. Roy. Astron. Soc.*, **329**, 556–566. [DOI], [ADS]

Piatti, A. E., Bica, E., Geisler, D. and Clariá, J. J., 2003a, "Fundamental parameters of the LMC clusters NGC 1836, NGC 1860, NGC 1865, SL 444, LW 224 and SL 548", *Mon. Not. Roy. Astron. Soc.*, **344**, 965–977. [DOI], [ADS]

Piatti, A. E., Geisler, D., Bica, E. and Clariá, J. J., 2003b, "Young star clusters immersed in intermediate-age fields in the Large Magellanic Cloud bar", *Mon. Not. Roy. Astron. Soc.*, **343**, 851–862. [DOI], [ADS]

Piatti, A. E., Sarajedini, A., Geisler, D., Seguel, J. and Clark, D., 2005, "Tracing the formation history of intermediate-age star clusters in the Small Magellanic Cloud", *Mon. Not. Roy. Astron. Soc.*, **358**, 1215–1230. [DOI], [ADS]

Piatti, A. E., Sarajedini, A., Geisler, D., Clark, D. and Seguel, J., 2007a, "Young star clusters immersed in intermediate-age fields in the Small Magellanic Cloud", *Mon. Not. Roy. Astron. Soc.*, **377**, 300–316. [DOI], [ADS]

Piatti, A. E., Sarajedini, A., Geisler, D., Gallart, C. and Wischnjewsky, M., 2007b, "Five young star clusters in the outer region of the Small Magellanic Cloud", *Mon. Not. Roy. Astron. Soc.*, **382**, 1203–1212. [DOI], [ADS]

Piatti, A. E., Sarajedini, A., Geisler, D., Gallart, C. and Wischnjewsky, M., 2007c, "Two newly identified, relatively old star clusters in the Small Magellanic Cloud", *Mon. Not. Roy. Astron. Soc.*, **381**, L84–L88. [DOI], [ADS]

Piatti, A. E., Geisler, D., Sarajedini, A., Gallart, C. and Wischnjewsky, M., 2008, "Seven young star clusters in the inner region of the Small Magellanic Cloud", *Mon. Not. Roy. Astron. Soc.*, **389**, 429–440. [DOI], [ADS]

Piatti, A. E., Geisler, D., Sarajedini, A. and Gallart, C., 2009, "Washington photometry of five star clusters in the Large Magellanic Cloud", *Astron. Astrophys.*, **501**, 585–593. [DOI], [ADS]

Piatti, A. E., Clariá, J. J., Bica, E., Geisler, D., Ahumada, A. V. and Girardi, L., 2011, "Washington photometry of 14 intermediate-age to old star clusters in the Small Magellanic Cloud", *Mon. Not. Roy. Astron. Soc.*, **417**, 1559–1575. [DOI], [ADS]

Piatti, A. E., Guandalini, R., Ivanov, V. D., Rubele, S., Cioni, M.-R. L., de Grijs, R., For, B.-Q., Clementini, G., Ripepi, V., Anders, P. and Oliveira, J. M., 2014, "The VMC Survey. XII. Star cluster candidates in the Large Magellanic Cloud", *Astron. Astrophys.*, **570**, A74. [DOI], [ADS], [arXiv:1407.5471]

Piatti, A. E., de Grijs, R., Ripepi, V., Ivanov, V. D., Cioni, M.-R. L., Marconi, M., Rubele, S., Bekki, K. and For, B.-Q., 2015a, "The VMC survey - XVI. Spatial variation of the cluster formation activity in the innermost regions of the Large Magellanic Cloud", *Mon. Not. Roy. Astron. Soc.*, **454**, 839–848. [DOI], [ADS], [arXiv:1509.00827]

Piatti, A. E., de Grijs, R., Rubele, S., Cioni, M.-R. L., Ripepi, V. and Kerber, L., 2015b, "The VMC survey - XV. The Small Magellanic Cloud-Bridge connection history as traced by their star cluster populations", *Mon. Not. Roy. Astron. Soc.*, **450**, 552–563. [DOI], [ADS], [arXiv:1503.06656]

Pietrzynski, G. and Udalski, A., 1999, "Erratum: The Optical Gravitational Lensing Experiment. Age of Star Clusters from the SMC", *Acta Astron.*, **49**, 435. [ADS]

Pietrzynski, G. and Udalski, A., 2000, "The Optical Gravitational Lensing Experiment. Ages of about 600 Star Clusters from the LMC", *Acta Astron.*, **50**, 337–354. [ADS], [astro-ph/0010360]

Piotto, G., 2009, "Observations of multiple populations in star clusters", in *The Ages of Stars*, (Eds.) Mamajek, E. E., Soderblom, D. R., Wyse, R. F. G., IAU Symposium, 258, [DOI], [ADS]

Piotto, G., Bedin, L. R., Anderson, J., King, I. R., Cassisi, S., Milone, A. P., Villanova, S., Pietrinferni, A. and Renzini, A., 2007, "A Triple Main Sequence in the Globular Cluster NGC 2808", *Astrophys. J. Lett.*, **661**, L53–L56. [DOI], [ADS], [astro-ph/0703767]

Piskunov, A. E., 1977, "Star formation in open clusters. Observational approach.", *Nauchnye Informatsii*, **37**, 47–62. [ADS]

Piskunov, A. E., Kharchenko, N. V., Schilbach, E., Röser, S., Scholz, R.-D. and Zinnecker, H., 2008, "The initial luminosity and mass functions of the Galactic open clusters", *Astron. Astrophys.*, **487**, 557–566. [DOI], [ADS], [arXiv:0806.2217]

Popescu, B., Hanson, M. M. and Elmegreen, B. G., 2012, "Age and Mass for 920 Large Magellanic Cloud Clusters Derived from 100 Million Monte Carlo Simulations", *Astrophys. J.*, **751**, 122. [DOI], [ADS], [arXiv:1203.6124]

Postma, J. E. and Leahy, D., 2017, "CCDLAB: A Graphical User Interface FITS Image Data Reducer, Viewer, and Canadian UVIT Data Pipeline", *Pub. Astron. Soc. Pac.*, **129**(11), 115 002. [DOI], [ADS]

Putman, M. E., Staveley-Smith, L., Freeman, K. C., Gibson, B. K. and Barnes, D. G., 2003, "The Magellanic Stream, High-Velocity Clouds, and the Sculptor Group", *Astrophys. J.*, **586**, 170–194. [DOI], [ADS], [astro-ph/0209127]

Rich, R. M., Da Costa, G. S. and Mould, J. R., 1984, "Main-sequence photometry of the SMC globular cluster Kron 3", *Astrophys. J.*, **286**, 517–528. [DOI], [ADS]

Ripepi, V., Cioni, M.-R. L., Moretti, M. I., Marconi, M., Bekki, K., Clementini, G., de Grijs, R., Emerson, J., Groenewegen, M. A. T., Ivanov, V. D., Molinaro, R., Muraveva, T., Oliveira, J. M., Piatti, A. E., Subramanian, S. and van Loon, J. T., 2017, "The VMC survey - XXV. The 3D structure of the Small Magellanic Cloud from Classical Cepheids", *Mon. Not. Roy. Astron. Soc.*, **472**, 808–827. [DOI], [ADS], [arXiv:1707.04500]

Rubele, S., Girardi, L., Kerber, L., Cioni, M.-R. L., Piatti, A. E., Zaggia, S., Bekki, K., Bressan, A., Clementini, G., de Grijs, R., Emerson, J. P., Groenewegen, M. A. T., Ivanov, V. D., Marconi, M., Marigo, P., Moretti, M.-I., Ripepi, V., Subramanian, S., Tatton, B. L. and van Loon, J. T., 2015, "The VMC survey - XIV. First results on the look-back time star formation rate tomography of the Small Magellanic Cloud", *Mon. Not. Roy. Astron. Soc.*, **449**, 639–661. [DOI], [ADS], [arXiv:1501.05347 [astro-ph.SR]]

Rubele, S., Pastorelli, G., Girardi, L., Cioni, M.-R. L., Zaggia, S., Marigo, P., Bekki, K., Bressan, A., Clementini, G., de Grijs, R., Emerson, J., Groenewegen, M. A. T., Ivanov, V. D., Muraveva, T., Nanni, A., Oliveira, J. M., Ripepi, V., Sun, N.-C. and van Loon, J. T., 2018, "The VMC survey - XXXI: The spatially

resolved star formation history of the main body of the Small Magellanic Cloud", *Mon. Not. Roy. Astron. Soc.*, **478**, 5017–5036. [DOI], [ADS], [arXiv:1805.04516]

Ruprecht, J., 1966, "Classification of open star clusters", *Bulletin of the Astronomical Institutes of Czechoslovakia*, **17**, 33. [ADS]

Sagar, R., 1987, "Study of interstellar extinction in some young open clusters", *Mon. Not. Roy. Astron. Soc.*, **228**, 483–499. [DOI], [ADS]

Sagar, R., 1995, "Star clusters in the Magellanic Clouds.", *Bulletin of the Astronomical Society of India*, **23**, 433–441. [ADS]

Sagar, R. and Cannon, R. D., 1995, "A deep UBVRI CCD photometric study of the moderately young southern open star cluster NGC 4755 = κ Crucis.", *Astron. Astrophys. Suppl.*, **111**, 75. [ADS]

Sagar, R. and Qian, Z. Y., 1993, "Intracluster extinction in young open star clusters", *Bulletin of the Astronomical Society of India*, **21**, 565–568. [ADS]

Sagar, R. and Richtler, T., 1991, "Mass functions of five young Large Magellanic Cloud star clusters", *Astron. Astrophys.*, **250**, 324–339. [ADS]

Sagar, R., Piskunov, A. E., Miakutin, V. I. and Joshi, U. C., 1986, "Mass and age distributions of stars in young open clusters", *Mon. Not. Roy. Astron. Soc.*, **220**, 383–403. [DOI], [ADS]

Saha, A., Olszewski, E. W., Brondel, B., Olsen, K., Knezek, P., Harris, J., Smith, C., Subramaniam, A., Claver, J., Rest, A., Seitzer, P., Cook, K. H., Minniti, D. and Suntzeff, N. B., 2010, "First Results from the NOAO Survey of the Outer Limits of the Magellanic Clouds", *Astron. J.*, **140**, 1719–1738. [DOI], [ADS], [arXiv:1008.3727]

Salpeter, E. E., 1955, "The Luminosity Function and Stellar Evolution.", *Astrophys. J.*, **121**, 161. [DOI], [ADS]

Scalo, J. M., 1986, "The stellar initial mass function", *Fundamentals of Cosmic Physics*, **11**, 1–278. [ADS]

Schneider, F. R. N., Ramírez-Agudelo, O. H., Tramper, F., Bestenlehner, J. M., Castro, N., Sana, H., Evans, C. J., Sabín-Sanjulián, C., Simón-Díaz, S., Langer, N., Fossati, L., Gräfener, G., Crowther, P. A., de Mink, S. E., de Koter, A., Gieles, M., Herrero, A., Izzard, R. G., Kalari, V., Klessen, R. S., Lennon, D. J., Mahy, L., Maíz Apellániz, J., Markova, N., van Loon, J. Th., Vink, J. S. and Walborn, N. R., 2018a, "The VLT-FLAMES Tarantula Survey. XXIX. Massive star formation in the local 30 Doradus starburst", *Astron. Astrophys.*, **618**, A73. [DOI], [ADS], [arXiv:1807.03821 [astro-ph.SR]]

Schneider, F. R. N., Sana, H., Evans, C. J., Bestenlehner, J. M., Castro, N., Fossati, L., Gräfener, G., Langer, N., Ramírez-Agudelo, O. H., Sabín-Sanjulián, C., Simón-Díaz, S., Tramper, F., Crowther, P. A., de Koter, A., de Mink, S. E., Dufton, P. L., Garcia, M., Gieles, M., Hénault-Brunet, V., Herrero, A., Izzard, R. G., Kalari, V., Lennon, D. J., Maíz Apellániz, J., Markova, N., Najarro, F., Podsiadlowski, Ph., Puls, J., Taylor, W. D., van Loon, J. Th., Vink, J. S. and Norman, C., 2018b, "An excess of massive stars in the local 30 Doradus starburst", *Science*, **359**(6371), 69–71. [DOI], [ADS], [arXiv:1801.03107 [astro-ph.SR]]

Searle, L., Wilkinson, A. and Bagnuolo, W. G., 1980, "A classification of star clusters in the Magellanic Clouds", *Astrophys. J.*, **239**, 803–814. [DOI], [ADS]

Shapley, H. and Wilson, H. H., 1925a, "The Magellanic Clouds, VI. Positions and Descriptions of 170 Nebulae in the Small Cloud.", *Harvard College Observatory Circular*, **276**, 1–4. [ADS]

Shapley, H. and Wilson, H. H., 1925b, "The Magellanic Clouds, IV. The Absolute Magnitudes of Nebulae, Clusters, and Peculiar Stars in the Large Cloud.", *Harvard College Observatory Circular*, **271**, 1–8. [ADS]

Stetson, Peter B., 1987, "DAOPHOT: A Computer Program for Crowded-Field Stellar Photometry", *Pub. Astron. Soc. Pac.*, **99**, 191. [DOI], [ADS]

Storm, J., Carney, B. W., Gieren, W. P., Fouqué, P., Latham, D. W. and Fry, A. M., 2004, "The effect of metallicity on the Cepheid Period-Luminosity relation from a Baade-Wesselink analysis of Cepheids in the Galaxy and in the Small Magellanic Cloud", *Astron. Astrophys.*, **415**, 531–547. [DOI], [ADS], [astro-ph/0401211]

Subramaniam, A., Tandon, S. N., Hutchings, J., Ghosh, S. K., George, K., Girish, V., Kamath, P. U., Kathiravan, S., Kumar, A., Lancelot, J. P., Mahesh, P. K., Mohan, R., Murthy, J., Nagabhushana, S., Pati, A. K., Postma, J., Rao, N. K., Sankarasubramanian, K., Sreekumar, P., Sriram, S., Stalin, C. S., Sutaria, F., Sreedhar, Y. H., Barve, I. V., Mondal, C. and Sahu, S., 2016, "In-orbit performance of UVIT on ASTROSAT", in *Space Telescopes and Instrumentation 2016: Ultraviolet to Gamma Ray*, *Proc. SPIE*, 9905, [DOI], [ADS], [arXiv:1608.01073 [astro-ph.IM]]

Subramanian, S. and Subramaniam, A., 2009, "Depth estimation of the Large and Small Magellanic Clouds", *Astron. Astrophys.*, **496**, 399–412. [DOI], [ADS], [arXiv:0809.4362]

Subramanian, S. and Subramaniam, A., 2012, "The Three-dimensional Structure of the Small Magellanic Cloud", *Astrophys. J.*, **744**, 128. [DOI], [ADS], [arXiv:1109.3980]

Subramanian, S. and Subramaniam, A., 2013, "Structure of the Large Magellanic Cloud from near infrared magnitudes of red clump stars", *Astron. Astrophys.*, **552**, A144. [DOI], [ADS], [arXiv:1301.7538]

Subramanian, S., Rubele, S., Sun, N.-C., Girardi, L., de Grijs, R., van Loon, J. T., Cioni, M.-R. L., Piatti, A. E., Bekki, K., Emerson, J., Ivanov, V. D., Kerber, L., Marconi, M., Ripepi, V. and Tatton, B. L., 2017, "The VMC Survey - XXIV. Signatures of tidally stripped stellar populations from the inner Small

Magellanic Cloud", *Mon. Not. Roy. Astron. Soc.*, **467**, 2980–2995. [DOI], [ADS], [arXiv:1701.05722]

Sun, Weijia, de Grijs, Richard, Deng, Licai and Albrow, Michael D., 2019, "Stellar Rotation and the Extended Main-sequence Turnoff in the Open Cluster NGC 5822", *Astrophys. J.*, **876**(2), 113. [DOI], [ADS], [arXiv:1904.03547 [astro-ph.SR]]

Taff, L. G., 1974, "The luminosity function of the zero-age main sequence.", *Astron. J.*, **79**, 1280–1286. [DOI], [ADS]

Tandon, S. N., Hutchings, J. B., Ghosh, S. K., Subramaniam, A., Koshy, G., Girish, V., Kamath, P. U., Kathiravan, S., Kumar, A., Lancelot, J. P., Mahesh, P. K., Mohan, R., Murthy, J., Nagabhushana, S., Pati, A. K., Postma, J., Rao, N. K., Sankarasubramanian, K., Sreekumar, P., Sriram, S., Stalin, C. S., Sutaria, F., Sreedhar, Y. H., Barve, I. V., Mondal, C. and Sahu, S., 2017a, "In-orbit Performance of UVIT and First Results", *Journal of Astrophysics and Astronomy*, **38**, 28. [DOI], [ADS], [arXiv:1612.00612 [astro-ph.IM]]

Tandon, S. N., Subramaniam, A., Girish, V., Postma, J., Sankarasubramanian, K., Sriram, S., Stalin, C. S., Mondal, C., Sahu, S., Joseph, P., Hutchings, J., Ghosh, S. K., Barve, I. V., George, K., Kamath, P. U., Kathiravan, S., Kumar, A., Lancelot, J. P., Leahy, D., Mahesh, P. K., Mohan, R., Nagabhushana, S., Pati, A. K., Kameswara Rao, N., Sreedhar, Y. H. and Sreekumar, P., 2017b, "In-orbit Calibrations of the Ultraviolet Imaging Telescope", *Astron. J.*, **154**, 128. [DOI], [ADS], [arXiv:1705.03715 [astro-ph.IM]]

Trumpler, R. J., 1930, "Preliminary results on the distances, dimensions and space distribution of open star clusters", *Lick Observatory Bulletin*, **14**, 154–188. [DOI], [ADS]

Udalski, A., 2003, "The Optical Gravitational Lensing Experiment. Real Time Data Analysis Systems in the OGLE-III Survey", *Acta Astron.*, **53**, 291–305. [ADS], [astro-ph/0401123]

Udalski, A., Szymanski, M., Stanek, K. Z., Kaluzny, J., Kubiak, M., Mateo, M., Krzeminski, W., Paczynski, B. and Venkat, R., 1994, "The Optical Gravitational Lensing Experiment. The Optical Depth to Gravitational Microlensing in the Direction of the Galactic Bulge", *Acta Astron.*, **44**, 165–189. [ADS], [astro-ph/9407014]

Udalski, A., Szymanski, M., Kubiak, M., Pietrzynski, G., Wozniak, P. and Zebrun, K., 1998a, "The Optical Gravitational Lensing Experiment. BVI Maps of Dense Stellar Regions. I. The Small Magellanic Cloud", *Acta Astron.*, **48**, 147–174. [ADS], [astro-ph/9806313]

Udalski, A., Szymanski, M., Kubiak, M., Pietrzynski, G., Wozniak, P. and Zebrun, K., 1998b, "VizieR Online Data Catalog: OGLE SMC BVI photometry (Udalski+ 1998)", *VizieR Online Data Catalog*, **1204**. [ADS]

Udalski, A., Szymanski, M., Kubiak, M., Pietrzynski, G., Soszynski, I., Wozniak, P. and Zebrun, K., 2000, "The Optical Gravitational Lensing Experiment. BVI Maps of Dense Stellar Regions. II. The Large Magellanic Cloud", *Acta Astron.*, **50**, 307–335. [ADS], [astro-ph/0010150]

Udalski, A., Soszynski, I., Szymanski, M. K., Kubiak, M., Pietrzynski, G., Wyrzykowski, L., Szewczyk, O., Ulaczyk, K. and Poleski, R., 2008a, "The Optical Gravitational Lensing Experiment. OGLE-III Photometric Maps of the Large Magellanic Cloud", *Acta Astron.*, **58**, 89–102. [ADS], [arXiv:0807.3889]

Udalski, A., Soszyński, I., Szymański, M. K., Kubiak, M., Pietrzyński, G., Wyrzykowski, Ł., Szewczyk, O., Ulaczyk, K. and Poleski, R., 2008b, "The Optical Gravitational Lensing Experiment. OGLE-III Photometric Maps of the Small Magellanic Cloud", *Acta Astron.*, **58**, 329. [ADS]

van den Bergh, S., 1981, "UBV observations of globular clusters in the Magellanic Clouds", *Astron. Astrophys. Suppl.*, **46**, 79–87. [ADS]

van den Bergh, S., 1991, "Star clusters in the clouds of Magellan", *Astrophys. J.*, **369**, 1–12. [DOI], [ADS]

van der Marel, R. P., 2001, "Magellanic Cloud Structure from Near-Infrared Surveys. II. Star Count Maps and the Intrinsic Elongation of the Large Magellanic Cloud", *Astron. J.*, **122**, 1827–1843. [DOI], [ADS], [astro-ph/0105340]

van der Marel, R. P. and Kallivayalil, N., 2014, "Third-epoch Magellanic Cloud Proper Motions. II. The Large Magellanic Cloud Rotation Field in Three Dimensions", *Astrophys. J.*, **781**, 121. [DOI], [ADS], [arXiv:1305.4641]

van der Marel, R. P., Kallivayalil, N. and Besla, G., 2009, "Kinematical structure of the Magellanic System", in *The Magellanic System: Stars, Gas, and Galaxies*, (Eds.) Van Loon, J. T., Oliveira, J. M., IAU Symposium, 256, [DOI], [ADS], [arXiv:0809.4268]

Vandenberg, D. A. and Bell, R. A., 1985, "Theoretical isochrones for globular clusters with predicted BVRI and Stromgren photometry", *Astrophys. J. Suppl.*, **58**, 561–621. [DOI], [ADS]

Westerlund, B. E., 1997, "Book Review: The Magellanic Clouds / Cambridge U Press, 1997", *The Observatory*, **117**, 317. [ADS]

Wozniak, P. and Szymanski, M., 1998, "Stellar Variability Background in OGLE-I Microlensing Search", *Acta Astron.*, **48**, 269–288. [ADS], [astro-ph/9804193]

Zaritsky, D., Harris, J., Thompson, I. B., Grebel, E. K. and Massey, P., 2002, "The Magellanic Clouds Photometric Survey: The Small Magellanic Cloud Stellar Catalog and Extinction Map", *Astron. J.*, **123**, 855–872. [DOI], [ADS], [astro-ph/0110665]

Zaritsky, D., Harris, J., Thompson, I. B. and Grebel, E. K., 2004, "The Magellanic Clouds Photometric Survey: The Large Magellanic Cloud Stellar Catalog and Extinction Map", *Astron. J.*, **128**, 1606–1614. [DOI], [ADS], [astro-ph/0407006]

Zhao, H. and Evans, N. W., 2000, "The So-called "Bar" in the Large Magellanic Cloud", *Astrophys. J. Lett.*, **545**, L35–L38. [DOI], [ADS], [astro-ph/0009155]